

Mechanism of ubiquitin transfer by RING E3 ligases

Hao Dou (M.Sc)

Submitted in fulfillment of the requirements for the Degree
of
Doctor of Philosophy

Beatson Institute for Cancer Research
School of Medicine
College of Medical, Veterinary and Life Sciences
University of Glasgow

October 2013

Supervisor: Dr. Danny T Huang

© Hao Dou, 2013

Abstract

In ubiquitin (Ub) system, E3 ligases have a central role in mediating substrate ubiquitination and triggering substrate degradation or other signalling transductions. RING E3s are the largest family of E3s and they promote direct Ub transfer from E2's active site to substrate. Some RING E3s require dimerization for their activity, but structural evidence on the importance of dimerization and the mechanism of Ub transfer are lacking. I report the structure of the human dimeric RING domain from BIRC7 (also called MLIAP or Livin) in complex with the E2 UbcH5B covalently linked to Ub (UbcH5B~Ub; ~ refers to thioester or oxyester linkage). This 2.18 Å complex structure reveals extensive Ub interactions with UbcH5B and both subunits of the RING domain dimer that stabilize the globular body and C-terminal tail of Ub. Mutations that disrupt these noncovalent interactions or RING dimerization reduce E2~Ub binding affinity and ubiquitination activity. My results provide structural insights into how dimeric RING E3s recruit E2~Ub and optimize the donor Ub configuration for transfer.

CBL family proteins (CBLs) are monomeric RING E3s that negatively regulate receptor tyrosine kinase (RTK) signalling pathway. Precise control of CBLs E3 activity is crucial for many cellular functions. My structural and biochemical data show that the RING domain of c-CBL adopts an autoinhibited conformation, where the E2-binding surface of the RING domain is blocked by the tyrosine kinase-binding domain (TKBD). CBLs can be activated by phosphorylation of a conserved tyrosine residue on the linker helix region (LHR; Tyr371 in c-CBL and Tyr363 in CBL-B). This activation is required for RTK ubiquitination. I report a crystal structure of Tyr363-phosphorylated human CBL-B, bound to a stabilized Ub-linked E2 (UbcH5B–Ub; – is used to separate components of a complex, in this case, also refers to isopeptide linkage). This 2.21 Å complex structure reveals that the pTyr363 of CBL-B contacts Ub's Ile36 surface. Using kinetic analyses, I demonstrate that this interaction is crucial in Ub transfer. Together, my results suggest that both monomeric and dimeric RING E3s use a similar mechanism in optimizing the Ub conformation and activating E2~Ub thioester for transfer, although the Ub-stabilizing components may vary in different RING E3s.

Acknowledgements

First, I would like to thank my supervisor, Dr. Danny Huang for all his support, guidance, and encouragement throughout my PhD study. He also gave me good advice on my thesis writing and job-hunting. I am grateful to my advisor Dr. Andrew Pannifer, panel reviewer Prof. Mike Olson and previous advisor Prof. Frank Kozielski for their advice and discussion about my projects. I would like to thank my thesis examiners Prof. Ronald Hay and Dr. Nick Morrice for their thoughtful and valuable comments. I would like to thank Lori Buetow for her support in the lab and thoughtful discussion, without which I will not be able to achieve these results within 3.5 years. I would also like to thank Gary Sibbet and our collaborators Andreas Hock (R15) and Kenneth Cameron (DDP) for their input for my projects and our papers. Thanks also go to other members of R04 group: Marta Klejnot, Gabriele Marcano, Mads Gabrielsen, and Alexander Schüttelkopf (DDP) for their valuable help and friendship. I am very thankful to my MSc supervisors, Prof. Malcome Walkinshaw and Prof. Linday Sawyer (University of Edinburgh), who introduced me to X-ray crystallography and inspired my interest.

A very big thank to my husband Zhewei Wang, who travelled to Glasgow from China twice a year for accompanying me. His love, encouragement, support, and trust overcame long distance and allowed me to continue my studies. I would like to thank my parents, Shuyun Liu and Benyan Dou for the love and support they have given me.

I am very lucky to have some friends in Glasgow, Edinburgh, and China. Thank you all for your friendship to make my experience enjoyable and memorable and a special mention to Emma Liu for her interesting conversations during lunch at Beatson.

I would like to thank the Beatson services, including Molecular Technology Services, Proteomics Facility, and Central Services for their enormous help. I would also like to thank Diamond Light Source (DLS), the European Synchrotron Radiation Facility (ESRF) for beamtime and assistance in data collection. Finally yet importantly, I am very grateful to Cancer Research UK (CRUK) for funding my studies and our research.

Author's Declaration

I declare that I am the sole author of this thesis and the work presented here is entirely my own, except where acknowledged to others. This thesis does not include work that has been submitted for consideration for another degree in this or any other university.

Table of Contents

| | |
|--|----|
| Abstract | 2 |
| Acknowledgements | 3 |
| Author's Declaration | 4 |
| Table of Contents | 5 |
| List of Figures | 10 |
| List of Tables | 12 |
| Abbreviations | 13 |
| Chapter 1 | 18 |
| Introduction | 18 |
| 1 Introduction..... | 19 |
| 1.1 Overview of ubiquitin system..... | 19 |
| 1.1.1 Ub conjugation..... | 19 |
| 1.1.2 E1s..... | 22 |
| 1.1.3 E2s..... | 23 |
| 1.1.4 RING E3s..... | 24 |
| 1.1.4.1 Categories of RING E3s | 25 |
| 1.1.4.2 RING E3-E2 interface..... | 27 |
| 1.1.4.3 RING E3-substrate interface..... | 28 |
| 1.1.4.4 RING E3-mediated Ub transfer | 29 |
| 1.2 BIRC family proteins (IAPs)..... | 29 |
| 1.2.1 Apoptosis | 29 |
| 1.2.2 BIRC family proteins (IAPs) | 30 |
| 1.2.2.1 E3 activity | 32 |
| 1.2.2.2 Other functions..... | 32 |
| 1.2.3 Available structures of IAPs (BIRC family proteins)..... | 33 |
| 1.3 CBL proteins..... | 35 |
| 1.3.1 CBL family proteins (CBLs) | 35 |
| 1.3.1.1 E3 activity | 37 |
| 1.3.1.2 Other functions..... | 38 |
| 1.3.2 Available structures of CBL proteins | 39 |
| 1.4 Objectives of the thesis | 43 |

| | |
|--|----|
| Chapter 2 | 44 |
| Material and Methods | 44 |
| 2 Material and Methods | 45 |
| 2.1 Molecular cloning of recombinant plasmids..... | 45 |
| 2.1.1 Plasmid source | 45 |
| 2.1.2 Primer design | 45 |
| 2.2 Expression and purification of proteins | 46 |
| 2.2.1 Purification of BIRC7 RING for crystallization..... | 47 |
| 2.2.2 Purification of c-CBL fragment for crystallization..... | 47 |
| 2.2.3 Purification of pCBL-B fragment for crystallization | 48 |
| 2.2.4 Purification of UbcH5B~Ub variants for crystallization | 48 |
| 2.2.4.1 The generation of UbcH5B _{RAS} ~Ub (developed by Danny Huang) 48 | |
| 2.2.4.2 The generation of UbcH5B _{RK} ~Ub (developed by Danny Huang) 49 | |
| 2.2.5 Protein purification for assays | 49 |
| 2.3 Crystallization | 50 |
| 2.3.1 Structure of BIRC7 _{239-C} ~UbcH5B _{RAS} ~Ub complex | 50 |
| 2.3.2 Native structure of c-CBL..... | 51 |
| 2.3.3 Structure of pCBL-B~UbcH5B _{RK} ~Ub~ZAP-70 peptide complex 51 | |
| 2.4 Data collection and processing | 51 |
| 2.5 Structure determination and refinement..... | 52 |
| 2.5.1 Structure of BIRC7 _{239-C} ~UbcH5B~Ub complex | 52 |
| 2.5.2 Native structure of c-CBL..... | 53 |
| 2.5.3 Structure of pCBL-B~UbcH5B _{RK} ~Ub~ZAP-70 peptide complex 53 | |
| 2.6 In vitro assays | 54 |
| 2.6.1 Assays to validate the structure of BIRC7 _{239-C} ~UbcH5B _{RAS} ~Ub complex 54 | |
| 2.6.2 Assays to validate c-CBL structure..... | 54 |
| 2.6.3 Assays to validate pCBL-B~UbcH5B _{RK} ~Ub~ZAP-70 peptide structure 55 | |
| 2.7 Kinetics assay on DiUb formation..... | 56 |

| | | |
|------------------|--|-----------|
| 2.7.1 | Kinetics validation of BIRC7 _{239-C} -UbcH5B _{RAS} -Ub complex structure | 56 |
| 2.7.2 | Kinetics validation of pCBL-B-UbcH5B _{RK} -Ub-ZAP-70 peptide structure..... | 57 |
| 2.8 | Verify the crystallized complex by SDS-PAGE..... | 57 |
| 2.9 | Surface plasmon resonance (SPR) assay | 58 |
| Chapter 3 | | 59 |
| | Mechanism of Ub transfer by a dimeric RING E3, BIRC7 (ML-IAP)..... | 59 |
| 3 | Mechanism of Ub transfer by a dimeric RING E3, BIRC7 (ML-IAP) | 60 |
| 3.1 | Aims and objectives..... | 60 |
| 3.2 | Results..... | 62 |
| 3.2.1 | Strategies..... | 62 |
| 3.2.2 | Structure of BIRC7 _{239-C} -UbcH5B _{RAS} -Ub complex | 64 |
| 3.2.3 | Detailed interactions and validation..... | 67 |
| 3.2.3.1 | UbcH5B-Ub's Ile44 patch interactions..... | 67 |
| 3.2.3.2 | UbcH5B-Ub's tail interactions | 72 |
| 3.2.3.3 | BIRC7 RING-Ub's Ile36 patch interactions..... | 75 |
| 3.2.4 | Dimerization required for RING E3 activity | 76 |
| 3.2.5 | The cross-dimer arrangement required for Ub transfer | 79 |
| 3.2.6 | Kinetic validation of the BIRC RING-E2~Ub model..... | 81 |
| 3.2.6.1 | Kinetic assay design..... | 81 |
| 3.2.6.2 | BIRC RING domain sequence and structural alignments | 83 |
| 3.2.6.3 | Kinetic validation using BIRC3 RING domain..... | 85 |
| 3.3 | Discussion..... | 87 |
| 3.3.1 | Structural comparison with RNF4-UbcH5A-Ub complex | 87 |
| 3.3.2 | RING E3s stabilize donor Ub configuration in solution..... | 89 |
| 3.3.3 | Models for RING dimers | 90 |
| Chapter 4 | | 92 |
| | Structural and functional study of c-CBL, a monomeric RING E3..... | 92 |
| 4 | Structural and functional study of c-CBL, a monomeric RING E3..... | 93 |
| 4.1 | Aims and objectives..... | 93 |
| 4.2 | Results..... | 94 |
| 4.2.1 | Strategies..... | 94 |
| 4.2.2 | Structure of c-CBL reveals an autoinhibited conformation..... | 95 |

| | | |
|--|--|------------|
| 4.2.3 | c-CBL adopts a closed conformation in solution..... | 98 |
| 4.2.4 | Interactions in the closed RING conformation | 101 |
| 4.2.4.1 | Probing RING-TKBD interactions | 104 |
| 4.2.4.2 | The RING-TKBD interaction competes against E2 binding 105 | |
| 4.2.4.3 | The RING-TKBD interaction reduces E3 activity..... | 106 |
| 4.3 | Discussion..... | 108 |
| 4.3.1 | Autoinhibition of c-CBL..... | 108 |
| 4.3.2 | Phosphorylation-dependent activation of c-CBL..... | 110 |
| 4.3.3 | Model for autoinhibition and phosphorylation-dependent activation of c-CBL..... | 112 |
| Chapter 5 | | 113 |
| Mechanism of Ub transfer by a monomeric RING E3, pTyr363-CBL-B..... | | 113 |
| 5 | Mechanism of Ub transfer by a monomeric RING E3, pTyr363-CBL-B | 114 |
| 5.1 | Aims and objectives..... | 114 |
| 5.2 | Results..... | 115 |
| 5.2.1 | Strategies..... | 115 |
| 5.2.2 | Structure of pCBL-B-UbcH5B _{RK} -Ub-ZAP-70 peptide complex 117 | |
| 5.2.3 | pCBL-B adopts an active RING conformation..... | 120 |
| 5.2.4 | Detailed interactions and validation..... | 122 |
| 5.2.5 | Kinetics validation | 125 |
| 5.2.5.1 | Kinetic assay design..... | 125 |
| 5.2.5.2 | Kinetic validation using CBL-B _{LRR} | 126 |
| 5.2.6 | The model of unphosphorylated CBL _{LRR} -UbcH5B _{RK} -Ub..... | 128 |
| 5.3 | Discussion..... | 131 |
| 5.3.1 | The donor Ub configuration poised for transfer | 131 |
| 5.3.2 | Additional element outside the RING domain may be required for other monomeric RING E3 activity | 133 |
| 5.3.3 | Implications for cancer-linked mutations | 134 |
| Chapter 6 | | 137 |
| Conclusion and Future directions | | 137 |
| 6 | Conclusion and Future directions | 138 |
| 6.1 | Mechanisms of Ub transfer by RING E3s | 138 |

| | | |
|------------------|--|-----|
| 6.2 | Regulations of RING E3 activity | 139 |
| 6.3 | Characterization of CBL and BIRC family proteins..... | 140 |
| Chapter 7 | | 142 |
| Appendix | | 142 |
| 7 | Appendix..... | 143 |
| 7.1 | Appendix 1. Construct list | 143 |
| 7.2 | Appendix 2. Contribution list | 145 |
| 7.3 | Appendix 3. Enzyme kinetics | 146 |
| 7.3.1 | Brief introduction..... | 146 |
| 7.3.2 | Kinetic data process | 147 |
| 7.3.3 | Autoradiogram representation | 149 |
| 7.4 | Appendix 4. The purity of full-length c-CBL variants | 150 |
| 7.5 | Appendix 5. Published papers and structures | 151 |
| 8 | Bibliography | 152 |

List of Figures

| | |
|--|----|
| Figure 1-1. Schematic of the Ub system..... | 20 |
| Figure 1-2. Structures of Ub E1 (Uba1) and in complex with E2 (Ubc4)..... | 22 |
| Figure 1-3. Interacting surfaces in E2 UbcH5B..... | 23 |
| Figure 1-4. Structure of the RING domain..... | 25 |
| Figure 1-5. Schematic of RING E3 families..... | 26 |
| Figure 1-6. The RING E3-E2 interfaces are highly conserved..... | 28 |
| Figure 1-7. Schematic representation of the human IAP family proteins with C-terminal RING domains..... | 31 |
| Figure 1-8. Crystal structures of the BIR3 and the RING domain of cIAP2..... | 34 |
| Figure 1-9. Schematic representation of the CBL family proteins..... | 36 |
| Figure 1-10. The TKBD of c-CBL..... | 40 |
| Figure 1-11. The structure of c-CBL N-terminal fragment in complex with UbcH5B and ZAP-70 peptide..... | 41 |
| Figure 3-1. Sequence alignment of RING domains from BIRC family..... | 62 |
| Figure 3-2. The purity of BIRC7 RING domain (BIRC7 _{239-C}) and crystals of BIRC7 _{239-C} -UbcH5B _{RAS} ~Ub..... | 63 |
| Figure 3-3. Complex structure of BIRC7 _{239-C} -UbcH5B _{RAS} ~Ub..... | 66 |
| Figure 3-4. Ub adopts multiple conformations in E2~Ub complex structures.... | 67 |
| Figure 3-5. Detailed interactions of the E2-Ub's Ile44 surface..... | 68 |
| Figure 3-6. Lysine-discharge reactions to validate the E2-Ub interfaces..... | 69 |
| Figure 3-7. Autoubiquitination of BIRC7 occurs in Smac ubiquitination assays..... | 70 |
| Figure 3-8. Assays of BIRC7 autoubiquitination and Smac ubiquitination <i>in vitro</i> | 71 |
| Figure 3-9. Detailed interactions on the E2-Ub's tail surface..... | 72 |
| Figure 3-10. Detailed interactions between UbcH5B's loop 114-119 and Ub's tail..... | 74 |
| Figure 3-11. Detailed interactions on the E3-Ub's Ile36 surface..... | 75 |
| Figure 3-12. <i>In vitro</i> ubiquitination assay to validate the E3-Ub's Ile36 patch interface..... | 76 |
| Figure 3-13. The BIRC7 _{239-C} dimer interface..... | 77 |

| | |
|--|-----|
| Figure 3-14. BIRC7 dimerization. | 78 |
| Figure 3-15. The cross-dimer arrangement is required for E3 activity..... | 80 |
| Figure 3-16. Initial kinetics reactions under certain conditions..... | 82 |
| Figure 3-17. Wild-type BIRC7 _{239-C} kinetic data. | 83 |
| Figure 3-18. BIRC3 RING is a good substitution of BIRC7 RING for kinetic assay..... | 84 |
| Figure 3-19. Kinetic validation on the BIRC3 RING-UbcH5B~Ub model..... | 85 |
| Figure 3-20. The E2-Ub's tail interfaces from dimeric E3-E2-Ub structures.... | 88 |
| Figure 3-21. Structures or models of dimeric E3-UbcH5~Ub complexes..... | 91 |
| Figure 4-1. The purity of c-CBL fragment and crystals of c-CBL fragment..... | 94 |
| Figure 4-2. Structural alignment of the TKBD..... | 96 |
| Figure 4-3. Structure of c-CBL fragment compared with c-CBL-UbcH7-ZAP70 complex..... | 97 |
| Figure 4-4. Locations of Arg139 and Asp435 in different c-CBL structures..... | 98 |
| Figure 4-5. Disulfide formation observed by SDS-PAGE..... | 99 |
| Figure 4-6. CBL variants disulfide bond formation tested by thrombin cleavage. | 101 |
| Figure 4-7. Detailed interactions to stabilize the closed RING conformation... | 102 |
| Figure 4-8. Superposition of RING domains from the structures of c-CBL fragment and c-CBL-UbcH7-ZAP70 peptide complex. | 103 |
| Figure 4-9. Sequence alignment of CBL protein or CBL homolog from different species. | 104 |
| Figure 4-10. Probing RING-TKBD interaction with disulfide crosslinking assay. | 105 |
| Figure 4-11. The RING-Met222 interaction plays an inhibitory role in the E3 activity of c-CBL. | 107 |
| Figure 4-12. Four states of c-CBL's RING domain. | 109 |
| Figure 4-13. Novel LHR-RING interactions in pTyr371-c-CBL-UbcH5B-ZAP- 70 peptide..... | 111 |
| Figure 4-14. Model for autoinhibition and phosphorylation-dependent activation of c-CBL. | 112 |
| Figure 5-1. Sequence alignment of N-terminal fragments from CBL family.... | 115 |
| Figure 5-2. The purity of pCBL-B and crystals of pCBL-B-UbcH5B _{RK} -Ub complex..... | 117 |

| | |
|---|-----|
| Figure 5-3. Overall structure of pCBL-B-UbcH5B _{RK} -Ub-ZAP-70 peptide. ... | 119 |
| Figure 5-4. pCBL-B adopts an active RING conformation. | 120 |
| Figure 5-5. The LHR-binding surface in pCBL-B-UbcH5B _{RK} -Ub-ZAP-70 peptide structure. | 121 |
| Figure 5-6. Lysine-discharge reactions on unphosphorylated and phosphorylated CBL-B variants. | 122 |
| Figure 5-7. Detailed donor Ub interactions. | 123 |
| Figure 5-8. Effects of UbcH5B and Ub mutations on Ub transfer by pCBL-B _{LRR} | 124 |
| Figure 5-9. Kinetics reactions within initial rate under certain conditions. | 126 |
| Figure 5-10. Effects of pTyr363-Ub interface on the Ub transfer kinetics. | 127 |
| Figure 5-11. Lysine-discharge assay on unphosphorylated CBL-B _{LRR} | 130 |
| Figure 5-12. Comparison of E3-E2-Ub/SUMO complexes. | 132 |
| Figure 5-13. Sequence alignment of RING or U-box domains. | 134 |
| Figure 5-14. Locations of cancer mutations on c-CBL structures. | 136 |

List of Tables

| | |
|---|-----|
| Table 3-1. Dissociation constants (K_d) for interactions between RING E3s, UbcH5B and UbcH5B _S ~Ub variants. | 61 |
| Table 3-2. Data collection and refinement statistics. | 64 |
| Table 3-3. BIRC3 RING kinetics of DiUb formation assay. | 86 |
| Table 4-1. Data collection and refinement statistics. | 95 |
| Table 4-2. The RING-Met222 interaction competes against E2 binding by SPR analysis. | 106 |
| Table 5-1. Data collection and refinement statistics. | 118 |
| Table 5-2. CBL-B _{LRR} kinetics of DiUb formation assay. | 128 |
| Table 5-3. Selected cancer mutations in c-CBL. | 135 |

Abbreviations

| | |
|------------|--|
| AML | Acute myeloid leukaemia |
| BIR domain | Baculovirus IAP Repeat domain |
| BIRC | Baculoviral IAP repeat-containing |
| BIRC7 | Baculoviral IAP repeat-containing 7 |
| BSA | Bovine serum albumin |
| CBL | Casitas B-lineage lymphoma |
| cIAP1/2 | Cellular inhibitor of apoptosis protein 1/2 |
| CIN85 | CBL-interacting protein of 85kDa |
| CMML | Chronic myelomonocytic leukaemia |
| CSPs | Chemical shift perturbations |
| CUL | Cullin family proteins |
| iCys | The c-CBL mutant (R139C/D435C) |
| DiUb | Two Ub monomers covalently linked through an isopeptide bond, between a lysine residue of one Ub and the C-terminal glycine residue of another |
| DUB | Deubiquitinase |
| E1 | Ubiquitin activating enzyme |
| E2 | Ubiquitin conjugating enzyme |
| E3 | Ubiquitin ligase |
| EDTA | Ethylenediaminetetraacetic acid |
| EGFR | Epidermal growth factor receptor |
| IAP | Inhibitors of apoptosis |
| IPTG | Isopropyl β -D-thiogalactopyranoside |
| JMML | Juvenile myelo-monocytic leukaemia |
| K_{cat} | Catalytic constant |
| K_d | Dissociation constant |
| K_m | Michaelis-Menten constant |
| LHR | Linker helix region in CBL |
| LRR | Linker helix region and the RING domain in CBL |
| MAPK | Mitogen-activated protein kinase |
| MLIAP | Melanoma inhibitor of apoptosis |

| | |
|---------------------------|---|
| NaTT | Sodium tetrathionate |
| NEM | N-ethylmaleimide |
| NF- κ B | Nuclear factor κ B |
| NMR | Nuclear magnetic resonance |
| PDB | Protein Data Bank |
| PI3K | Phosphatidylinositol-3-kinase |
| PMSF | Phenylmethylsulfonyl fluoride |
| PTK | Protein tyrosine kinase |
| RBR | RING between RING fingers |
| RING domain | Really Interesting New domain |
| RTK | Receptor tyrosine kinase |
| SDS-PAGE | Sodium dodecyl sulfate polyacrylamide gel electrophoresis |
| SH2 | Src Homology 2 domain |
| SH3 | Src Homology 3 domain |
| Smac/DIABLO | Second mitochondriaderived activator of caspases / Direct IAP binding protein with low pI |
| SPR | Surface plasmon resonance |
| Syk | Spleen tyrosine kinase |
| TC | Thrombin cleavage |
| TEV | Protease found in the tobacco etch virus |
| TKBD | Tyrosine kinase-binding domain |
| Ub | Ubiquitin |
| Ubl | Ubiquitin like protein |
| UBA domain | Ubiquitin associated domain |
| UbcH5B _{RAS} ~Ub | Mutant UbcH5B (S22R/N77A/C85S) covalently linked to Ub |
| UbcH5B _{RK} -Ub | Mutant UbcH5B (S22R/C85K) covalently linked to Ub |
| UbcH5B _S ~Ub | Mutant UbcH5B (C85S) covalently linked to Ub |
| Ubl | Ubiquitin-like protein |
| XIAP | X-linked inhibitor of apoptosis |
| ZAP-70 | Zeta chain associated protein kinase 70 |

| | |
|------------------|----------------------------|
| Å | Ångström |
| A ₆₀₀ | Absorbance at 600 nm |
| kDa | Kilodaltons |
| M | Molar |
| mg | Milligram |
| mg/ml | Milligram per millilitre |
| min | Minutes |
| ml | Millilitre |
| mM | Millimolar |
| pmol | Picomole |
| r.m.s.d | Root-mean-square deviation |
| s | Seconds |
| µg | Microgram |
| µl | Microlitre |

For my family

Chapter 1

Introduction

1 Introduction

1.1 Overview of ubiquitin system

1.1.1 Ub conjugation

In eukaryotes, most cellular proteins are degraded by proteasomes when their activity is no longer needed. The selective degradation is carried out by a series of enzymes in the ubiquitin (Ub) system. In this system, proteins destined for degradation (also called substrate) are covalently modified by Ub. The basic functions of Ub and the mechanism of Ub conjugation were first discovered by Aaron Ciechanover, Avram Hershko, and Irwin Rose in 1980. They named the process of Ub conjugation as ubiquitination and they were awarded the Nobel Prize in Chemistry in 2004 [1, 2]. Over the decades, numerous cellular processes have been found to be related to ubiquitination including cell cycle regulation, endocytosis, inflammation, DNA transcription, and DNA repair [3-6]. Defects in ubiquitination often lead to cellular disorders, which have been implicated in various human diseases including cancer [7].

Ub is an 8.5 kDa protein comprising 76 amino residues and evolutionally conserved from yeast to human. Ub is covalently linked to substrates by a cascade of enzymes, including Ub activating enzyme (E1), Ub conjugating enzyme (E2) and Ub ligase (E3). In this cascade, the C-terminal tail of Ub, Gly76 is first activated by an E1 in the presence of ATP. The activation consists of forming an intermediate Ub adenylate and a thioester-linked Ub to the active site cysteine of the E1 with the release of PPI and AMP. Activated Ub is then transferred to the active site cysteine of E2 to form an E2~Ub thioester (~ refers to thioester linkage). Finally, an E3 catalyses the Ub transfer from E2~Ub to a substrate. The C-terminal Gly76 of Ub is conjugated to the ϵ -amino group of a lysine residue on the substrate via an isopeptide linkage (**Figure 1-1**).

Proteins that are similar to Ub are called ubiquitin like proteins (Ubls). Most Ubls can be conjugated to substrate via similar enzymatic process to ubiquitination [8]. Among all the Ubls, Nedd8 has the closest sequence to Ub (58% identity) [8] and plays a role in cell cycle control [9]. The conjugation of Nedd8 to substrate is called neddylation. The best-studied Nedd8 substrates are Cullin family proteins (CUL) [10].

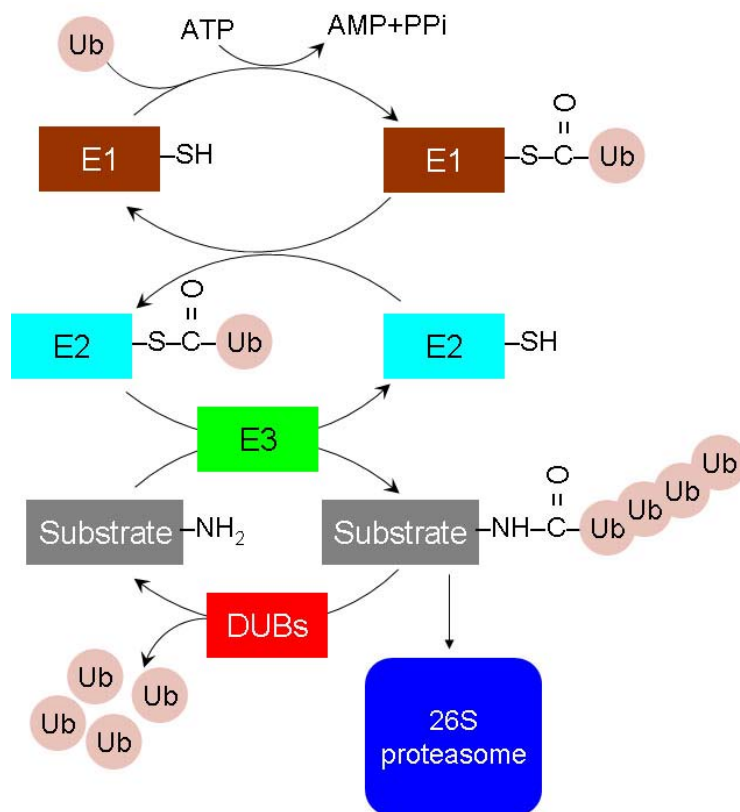


Figure 1-1. Schematic of the Ub system.

Ub is activated by an E1, and transferred to an E2. The E3 binds both E2 and substrate and promotes the Ub transfer from E2 to substrate. Ubiquitinated substrate can be either targeted to 26S proteasome for degradation or deubiquitinated by DUBs.

In Ub system, there are currently 2 E1s, about 30 E2s, and at least 600 E3s identified in human [11]. Two major families of E3s are classified: E3s with HECT (homologous to the E6-AP carboxyl terminus) domain and E3s with RING (really interesting new gene) or RING-like domain (e.g., U-Box domain). HECT domain is characterized by N- and C-lobes, where N-lobe recruits E2~Ub and C-lobes contains a catalytic cysteine residue that attacks the E2~Ub thioester linkage to form an E3~Ub thioester. Ub is then transferred to a substrate lysine. The largest family of E3s are RING E3s. RING E3s generally contain a RING domain and a substrate-binding domain. RING E3s do not have a catalytic cysteine like HECT E3s, thus they do not form E3~Ub intermediate. Instead, the RING domain recruits E2~Ub to facilitate Ub transfer from E2~Ub to substrate.

Ub contains 7 surface lysine residues (Lys6, Lys11, Lys27, Lys29, Lys33, Lys48 and Lys63), each of which can be isopeptide-linked by another Ub's C-terminal Gly76 to form different types of Ub linkages [12]. The linkages can be divided into two

classes: monoubiquitination and polyubiquitination. Monoubiquitination referring to the attachment of a single Ub to the substrate is involved in membrane protein internalization, trafficking, lysosomal degradation, and histone function [13-15]. A well-known monoubiquitinated protein is epidermal growth factor (EGF) receptor pathway substrate clone 15 (Eps15), a phosphorylation substrate of epidermal growth factor receptor (EGFR) [16]. HECT E3 Nedd4 and RING-between-RING (RBR) E3 parkin have been shown to monoubiquitinate Eps15 [17, 18]. Monoubiquitination of Eps15 seems to prevent it from interacting with ubiquitinated EGFR and promote EGFR endocytosis [18, 19]. Polyubiquitination, alternatively, means multiple Ub are linked via a specific lysine residue of Ub. The most studied types of polyubiquitination are Lys48-linked Ub chains and Lys63-linked Ub chains. It is widely accepted that Lys48-linked ubiquitination are involved in proteasomal degradation [20] and Lys63-linked ubiquitination is mostly related to DNA damage repair, intracellular signalling and endosomal trafficking to the lysosome [12, 21, 22], however much remain unclear. The types of ubiquitination seem to depend on the different combinations of E2 and E3 enzymes during *in vitro* reactions [12]. For example, E3 breast cancer susceptibility gene 1 (BRCA1) interacts with UbcH6 and Ube2e2 to catalyse monoubiquitination, whereas BRCA1 interacts with UbcH5C to form polyubiquitination [12]. A combination of Ube2w with Ubc13-Mms2 and Ube2K catalyse Lys 63- or Lys 48-linked chain formation with BRCA1, respectively [23]. Certain pair of E2 and E3 is able to mediate different types of ubiquitination. For example, UbcH5 and CHIP can catalyse all types of polyubiquitination on substrate *in vitro* [24]. It remains unclear whether the E2/E3 pairs decide the types of ubiquitination *in vivo*.

Protein degradation is an irreversible process, where at least four ubiquitin molecules must be attached to the Lys48 residue from the substrate in order to be recognized by the 26S proteasome, a large multi-catalytic protease complex [20]. Ub molecules are first cleaved off the substrate proteins immediately prior to destruction by 19S particle and are recycled for further use. Then substrate proteins are rapidly degraded into small peptides (usually 3-24 amino acid residues in length) in the 20S particle [25]. In contrast to protein degradation, protein ubiquitination is a reversible process. The deconjugation of Ub molecules is performed by deubiquitinating enzymes (DUBs), which catalyse the removal of Ub from native conjugates, poly-ubiquitin chains, or

protein promoter [26]. In addition to the reversal of ubiquitination, DUBs are involved in processing of the Ub precursors, Ub recycling and Ub chains editing [27]. Hence, DUBs may function as negative or positive regulators of the Ub system.

1.1.2 E1s

Ub E1s (Uba1 and Uba6) as the initiator of ubiquitination are monomeric enzymes containing two active sites. The adenylation active site is involved in binding ATP·Mg²⁺ and activating Ub's C-terminus. The catalytic cysteine site then attacks the Ub adenylate to form an E1~Ub thioester. These two active sites are distal to each other [28-30] (**Figure 1-2**). Previous studies suggested domains in E1s undergo rotations for the thioester formation [31, 32]. Recent structures of Uba1~Ub~ATP·Mg and in complex with E2 reveal that further conformational changes are required in E1s to enable Ub transfer to E2's active site [33] (– is used to separate components of a complex).

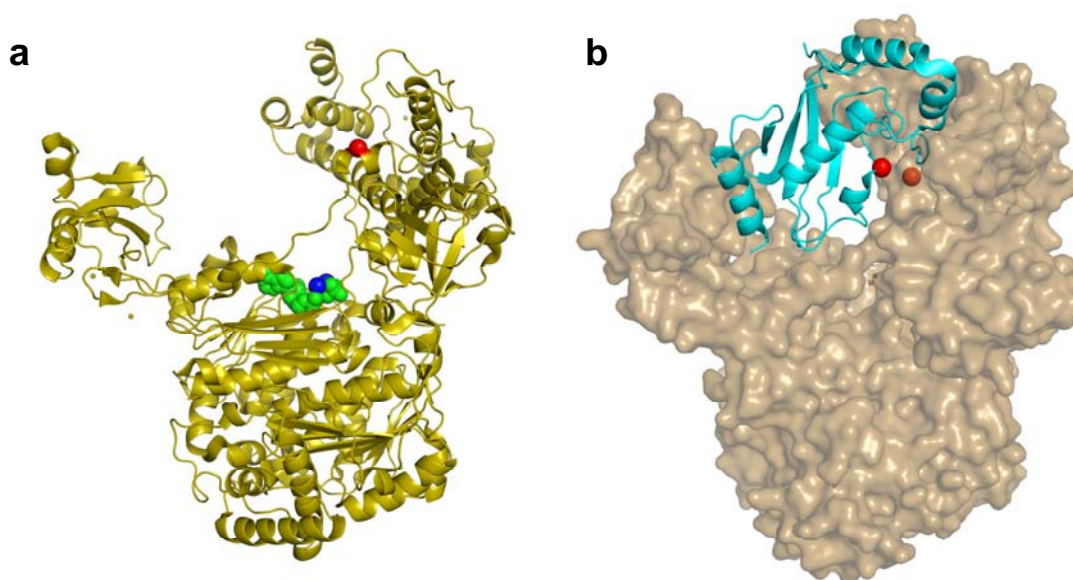


Figure 1-2. Structures of Ub E1 (Uba1) and in complex with E2 (Ubc4).

(a) The portion of E1 from the structure of Uba1~Ub~ATP·Mg (PDB 4II3 [33]). E1 Uba1 is coloured sand. The catalytic cysteine, ATP and Mg²⁺ are shown as spheres and coloured as red, green, and blue respectively.

(b) Surface representation of E1 in complex with E2 from the structure of Uba1~Ubc4~Ub~ATP·Mg (PDB 4II2 [33]). E1 is coloured as in a. E2 is shown as cartoon and coloured cyan. The active site cysteines of E1 and E2 are shown as red spheres.

1.1.3 E2s

E2s as the connectors between E1s and E3s have highly conserved Ub conjugating domains (Ubc domains), which are consisted of five α -helices and four β -sheets (**Figure 1-3a**). The residues that interact with either E1s or E3s are mostly overlapped [34, 35], indicating that E2s cannot simultaneously bind both E1s and E3s. Near the active sites, there are three residues known as HPN motif (**Figure 1-3b**). The histidine and proline may support the protein structure around the active site. The asparagine has been shown to be essential for stabilizing the oxyanion intermediate and isopeptide bond formation [36].

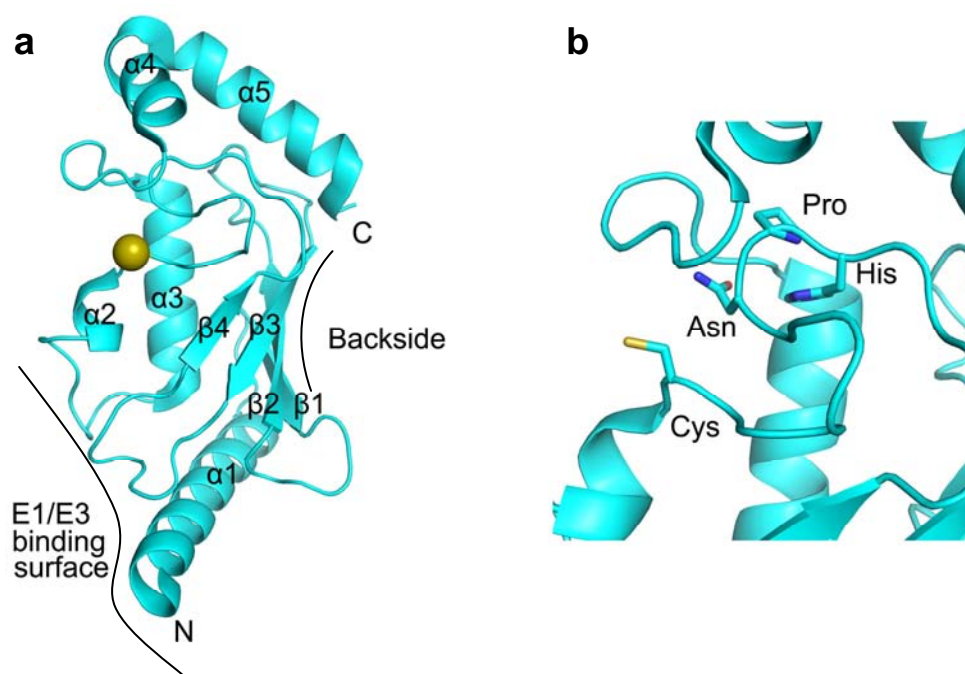


Figure 1-3. Interacting surfaces in E2 UbcH5B.

(a) Structure of E2 UbcH5B from PDB 3EB6 [37]. UbcH5B is coloured in cyan with catalytic cysteine shown in olive sphere. α -helices ($\alpha1$ to $\alpha5$) and β -sheets ($\beta1$ to $\beta4$) are labelled. The E1/E3 binding surface and the backside of E2 are indicated.

(b) Key residues at E2's active site and HPN motif are shown as sticks with N atoms blue, O atoms red and S atoms yellow.

On the opposite side from the active site (backside region), some E2s can interact non-covalently with an Ub's hydrophobic patch formed by Leu8, Ile44 and Val70 (also called Ub's Ile44 patch) [38, 39]. This surface of Ub is also commonly recognized by ubiquitin-association (UBA) domains [40]. Similarly, yeast E2 Ubc4

interacts with Ubl Nedd8 via its backside [41]. The Ub-E2 backside interactions have low affinity (K_d of about 300 μ M) but it is essential in polyubiquitination [39].

In addition to association with Ub/Ubl, the backsides of E2s were reportedly able to bind certain RING E3s. For example, Ube2g2-binding region (G2BR) domain of E3 gp78 binds to the E2 Ube2g2 with high affinity (about 20 nM) [42]. Rad18 possesses a Rad6 binding domain (R6BD) to recruit E2 Rad6 through its backside, thus competes with Ub's backside binding to Rad6, and inhibits polyubiquitination [38]. A recent study also suggests the interactions between the backside of E2 Ubc7p and a transmembrane protein Cue1p. This recruitment activates Ubc7p's active site and improves E3 binding [43].

1.1.4 RING E3s

RING E3s commonly contain a RING domain (about 40-60 amino acids) that coordinates two zinc ions (Zn). The RING domain was originally described as cysteine-rich sequence motif by Freemont and colleagues in 1991 [44]. RING domain was first identified as the protein product of the human RING1 gene – Really Interesting New Gene 1 [45] but the function of RING domains was not clear. They were known to be involved in protein-protein interactions, including oncogenesis, signal transduction and viral replication [46]. Until 1999, the function of the RING domain was clarified as E3 ligases. c-CBL [47-49] and Ubr1p [50] were shown to bind E2s through their RING domains and promote substrate ubiquitination for proteasomal degradation. Subsequently, more and more RING domain proteins were discovered to have E3 activity.

In the RING motif, also called the C3HC4 motif, one Zn is bound to four cysteines, and the other Zn is bound to three cysteines and a histidine. The basic sequence of the canonical RING is Cys-X(2)-Cys-X(9-39)-Cys-X(1-3)-His-X(2-3)-Cys-X(2)-Cys-X(4-48)-Cys-X(2)-Cys, where X can be any amino acid, and the bracketed numbers refer to the lengths of the intervening sequences [51] (**Figure 1-4a**). The structure of the RING domain reveals that the conserved cysteine and histidine residues that are

involved in binding ions are buried within the core of the RING domain (**Figure 1-4b**).

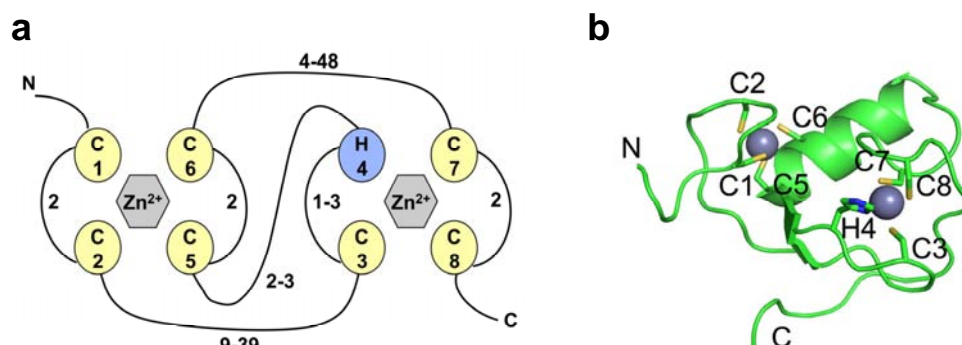


Figure 1-4. Structure of the RING domain.

(a) Schematic presentation of the structure of the RING domain. The Zn^{2+} binding ligands, and cysteine (C) or histidine (H) are shown as numbered spheres. Two pairs of ligands coordinate one Zn^{2+} atom (gray hexagon) referred to as a “cross-brace” motif. The numbers next to the loops indicate the minimum and maximum number of residues to connect the Zn^{2+} binding ligands.

(b) Structure of the RING domain of c-CBL from PDB 1FBV [52]. RING domain is coloured green. Zn^{2+} -binding ligands are shown as sticks with N atoms blue and S atoms yellow. Zn^{2+} atoms are shown as gray spheres.

1.1.4.1 Categories of RING E3s

RING E3s can be divided into monomers, dimers or multi-subunit complexes (**Figure 1-5**). Monomeric RING E3s (also called single-subunit RING E3s) is functional on its own. Example includes c-CBL that targets EGFR for degradation [53]. In dimeric RING E3s, dimerization generally occurs between the RING domain and surrounding regions with their homo- or hetero-partners. Homodimeric RING E3s include IAPs (the inhibitor of apoptosis proteins, also called BIRCs) [37] and RNF4 (ring finger protein 4) [54]. Heterodimeric RING E3s include MDM2/MDMX (also known as HDM2/HDMX in human)[55], BRCA1/BARD1 (breast cancer 1/BRCA1-associated RING domain 1) [56] and RNF2/BMI1 (RING finger protein 2/Polycomb RING finger oncogene) [57]. In heterodimers, one RING domain (MDMX, BARD1, BMI1) often lacks E3 activity but might play a role in stabilizing the other active RING domain, thereby enhancing dimeric E3 activity [23, 58, 59]. Multi-subunit RING E3 complex make up the largest family of RING E3s. The most studied one is the family of Cullin RING Ligase (CRL), which is characterized by scaffold proteins (such as

CUL1, 2, 3, 4A, 4B, 5, 7), RING domain proteins (such as RBX1, Rbx2, Hrt1), and substrate binding proteins (such as F-box, SOCS/BC-box, BTB). Some CRLs contain adaptor proteins (such as Skp1) [60]. CRLs that commonly contain CUL1 are named SCF complexes, a best-understood family involved in cell cycle [61]. SCF complexes generally contain components CUL1, Skp1, RBX1 and variable F-box proteins for diverse substrate recognition [62]. Another example of CRLs is anaphase-promoting complex/cyclosome (APC/C), which contain 13 core components and are structurally similar to the SCF complex [63]. Despite the structural and biochemical similarities, cellular functions of the SCF complex and the APC/C are different. The SCF complex is active mainly in G1, S, and early M phases, whereas APC/C regulates mitosis and G1 phase [64].

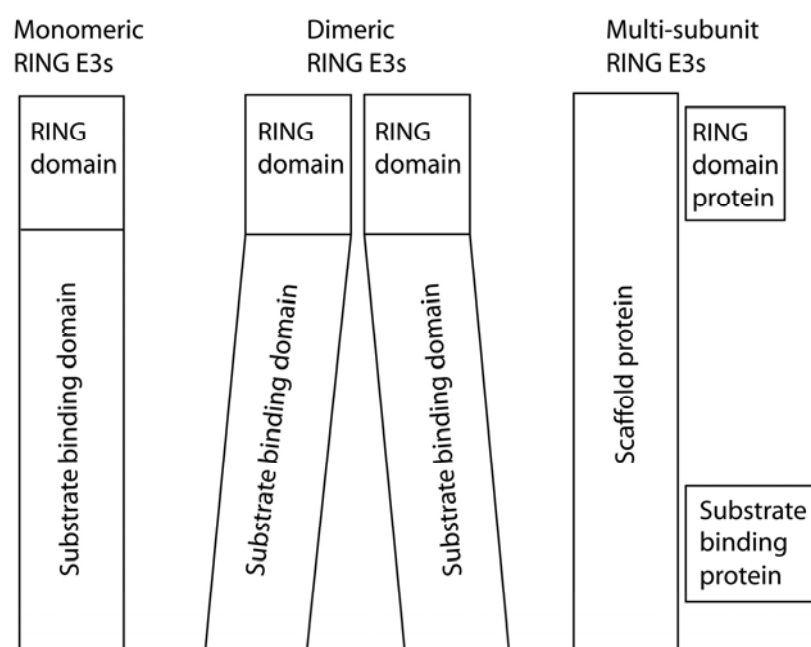


Figure 1-5. Schematic of RING E3 families.

Functional domains or components in different families of RING E3s are indicated.

Certain proteins contain domains that are structurally similar to the RING domains. For example, UFD2-homology domain (U-box domain) resembles the RING domain without coordinating Zn^{2+} atoms. Some U-box proteins also have E3 activity. The available structures of U-box CHIP and Prp19 reveal a similar dimer interface as homodimeric RING E3s [65, 66]. Plant homeo domain (PHD domain) shares a similar sequence of cysteine and histidine residues to the RING domain. Some PHD containing proteins function as E3s [67, 68]. Finally, there are E3s that contain at least

one RING domain, such as RING-between-RING-type E3 (RBR). They use the first RING domain (RING1, RING-like) to bind an E2 and the second RING domain (RING2, HECT-like) to conjugate Ub to its active site cysteine for subsequent Ub transfer [69]. A well-known protein from this family is Parkin. Mutations in Parkin have been linked to Parkinson's disease [70].

1.1.4.2 RING E3-E2 interface

RING E3s were thought to function as scaffold to connect E2s and substrates to facilitate Ub transfer. The RING domain plays an important role in E2~Ub recruitment. The detailed RING-E2 interactions were first illustrated by the crystal structure of c-CBL bound to E2 UbcH7, where two UbcH7 loops (L1 and L2) interact with the two zinc-binding loops of the RING domain (RING loops) [52] (**Figure 1-6a**). These loops are structurally conserved among E2s and RING domains [52], therefore, similar RING-E2 interactions are observed in other RING E3 complexes, such as UbcH5B–cIAP2 and Ubc13/Mms2–RNF8 complexes [37, 71] (**Figure 1-6b**).

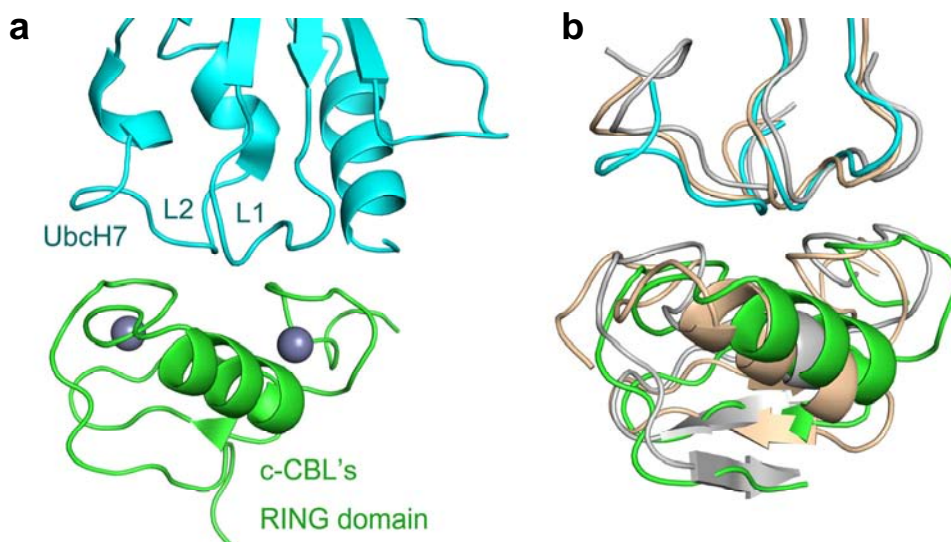


Figure 1-6. The RING E3-E2 interfaces are highly conserved.

(a) The portion of c-CBL's RING domain and E2 Ubch7 from PDB 1FBV [52] reveals the interacting surface between the canonical RING domain and Ubch7. Ubch7 is coloured cyan and c-CBL's RING domain green. Zn^{2+} atoms are shown as gray spheres. The L1 and L2 of E2 are labelled.

(b) Structural alignments of the RING E3-E2 interface from different complexes. The E2 and the RING domain from c-CBL-Ubch7-ZAP-70 peptide complex (PDB 1FBV [52]) are coloured as in a. The E2 loops and the RING domains in Ubch5B-cIAP2 (PDB 3EB6 [37]) and Ubch13/Mms2-RNF8 (PDB 4EPO [71]) are coloured gray and wheat, respectively, and aligned to the ones in c-CBL-Ubch7-ZAP-70 peptide complex.

1.1.4.3 RING E3-substrate interface

In contrast to the conserved E2-RING interactions, the modes of substrate recognition by RING E3s are highly varied. Many RING E3s contain specific domains for binding their substrates [11]. For example, CBL family proteins contain Src homology 2 (SH2) domain that recognizes tyrosine-phosphorylated substrates. Mdm2/MdmX uses an N-terminal domain to bind p53 and hence mediates p53 ubiquitination. IAPs recruit caspases through their baculovirus inhibitor of apoptosis protein repeat (BIR) domains and promote caspases ubiquitination [72, 73]. CRLs utilize diverse substrate binding proteins for substrate recognition [60]. The best examples are the F-box proteins, which recruit various signal proteins [74]. Further investigations are required to explore the selectivity, specificity, and regulation in the mechanisms of substrate recognition by RING E3s.

1.1.4.4 RING E3-mediated Ub transfer

RING E3s lack a catalytic cysteine to form E3~Ub intermediate. Over the last decade, numerous studies have been focused on understanding how RING E3s function to promote Ub transfer. Several studies showed that some E2s display an E3-independent activity in Ub transfer, for examples Ube2S [75], Cdc34 [76], Ubc13/Mms2 [71], and UbcH5C [69]. Interestingly, in the presence of RING E3s, Ub transfer is greatly enhanced [71, 77], indicating a catalytic role of RING E3s in Ub transfer. However, existing structures show that the E2-E3 binding interface is distal from the E2's active site cysteine [37, 52] suggesting that RING E3s may not facilitate Ub transfer through direct interactions. Due to the instability of E2~Ub thioester linkage, there is no structure that captured a RING E3 bound to E2~Ub intermediate, thus it remains unclear how RING E3 enhances Ub transfer.

1.2 BIRC family proteins (IAPS)

1.2.1 Apoptosis

Apoptosis refers to the process of programmed cell death and may occur in many cellular organisms. In 1842, Carl Vogt discovered this kind of cell death, but the word 'apoptosis' is first used by John F.R. Kerr at University of Queensland [78]. In the early stage of apoptosis, cell shrinks, resulting in dense cytoplasm, tightly packed organelles, and visible pyknosis. Shrunken cell is then broken into apoptotic bodies, which can be engulfed and destroyed by phagocytic cells [79]. In general, apoptosis presents advantages to organisms, for example, the apoptosis of the finger cells in mammalian embryos causes the differentiation of fingers and toes. Apoptosis does not only exist in higher organisms. In 2002, Sydney Brenner, Robert Horvitz and John Sulston discovered the apoptosis in *C.elegans*, for which they shared the Nobel Prize for Physiology or Medicine [80]. Their findings suggest that the basic pathways of apoptosis are evolutionary conserved.

Apoptosis is accurate and controlled cell death by a diverse range of cell signals without causing an inflammatory reaction. Unlike apoptosis, necrosis is a form of

unregulated cell death that is caused by external factors, such as injury, poison, or infection and often associated with severe tissue damage and inflammation [81]. Autophagy is another kind of programmed cell death. Unlike apoptosis, autophagy is normally induced without the activation of caspases, but associated with the accumulation of autophagic vesicles [82].

Apoptosis can be induced by two principle pathways. The extrinsic pathway is triggered by groups of death receptors located in the plasma membrane of the cell upon stimulation with extracellular ligands [83]. The key enzymes to execute apoptosis are the cysteine aspartic acid proteases called caspases. Fas (also called Apo-1 or CD95) and tumor-necrosis factor receptor (TNF-R) recruit caspase-8 or -10 (initiator caspases) to the death inducing signalling complex (DISC), where initiator caspases are activated. Initiator caspases are then capable to activate effector caspases, such as caspase-3 or -7 involved in degrading cellular targets. The second pathway to regulate apoptosis is intrinsic pathway [84]. This pathway is activated by intracellular stress signals, including oxidative stress and treatment with cytotoxic drugs. In response to apoptotic stimuli, Bcl-2 protein family become activated and act on the mitochondria to release cytochrome c, which is followed by apoptosome formation and caspase activation. In this pathway, cytochrome c recruits and activates caspase-9, the initiator caspase of the apoptosome. Subsequently, caspase-9 activates effector caspase, caspase-3, for the cleavage of the cellular substrates needed for apoptosis. Additionally, activation of the intrinsic pathway can also occur following the activation of the extrinsic pathway via the caspase-8 cleavage of Bid, a Bcl-2 family member to its activated form [85].

1.2.2 BIRC family proteins (IAPs)

To maintain the cell population within organisms, apoptosis somehow needs to be regulated [86, 87]. A family of proteins called the inhibitors of apoptosis (IAP) proteins were first discovered in baculoviruses named Cp-IAP (Cydia pomonella granulosis virus) and Op-IAP (Orgyia pseudotsugta nuclear polyhedrosis virus) [88], thus IAP proteins are also called baculoviral IAP repeat-containing proteins (BIRC

proteins). They were found to rescue the loss function of p35, a baculoviral anti-apoptosis protein [89, 90]. These IAPs all contain at least one copy of the BIR domain (Baculovirus IAP Repeat (BIR) domains). The BIR domain is a zinc-coordinated domain with a core sequence C(X)₂C(X)₆W(X)₃D(X)₅H(X)₆C, where X is any amino acid and is usually about 80 amino acid long [91]. Since then, many proteins containing BIR domains have been identified in other eukaryotic cells, from yeast to human. The first human IAP identified was the neuronal apoptosis inhibitory protein (NAIP, also called BIRC1), involved in spinal muscular atrophy (SMA), a neurodegenerative disorder [92, 93]. Further human IAPs such as cIAP1/BIRC2, cIAP2/BIRC3, XIAP/BIRC4, survin/BIRC5, and MLIAP/BIRC7 were subsequently identified by sequence homology and examined for their anti-apoptotic activity [94]. So far, 8 mammalian IAP family members all contain one or more copies of BIR domains for protein-protein interactions, but not all of them have a C-terminal RING domain (**Figure 1-7**). For IAPs that have E3 activity, the RING domains are required for regulating autoubiquitination and substrate degradation [95, 96]. Some IAPs, such as cIAP1 and cIAP2, contain a caspase recruitment (CARD) domain [97]. Recently, an Ub associated (UBA) domain was reported in IAPs. The UBA domain is located between the BIR3 domain and the CARD in cIAP1 and cIAP2, or between the BIR3 domain and the RING domain in XIAP [98, 99].

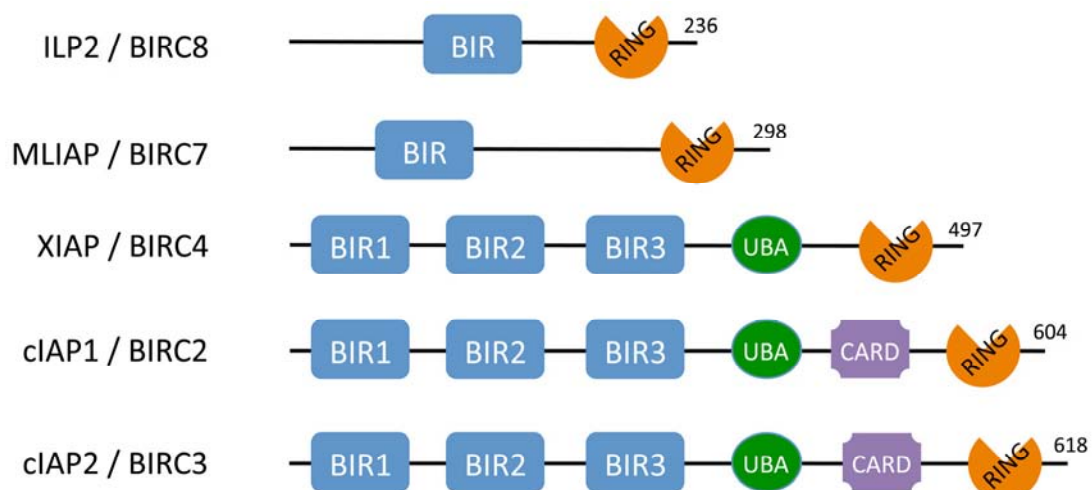


Figure 1-7. Schematic representation of the human IAP family proteins with C-terminal RING domains.

The number of residues of each IAP and their functional domains are shown.

1.2.2.1 E3 activity

IAPs are dimeric RING E3s. The E3 activity of IAPs is associated with their anti-apoptotic functions. For example, XIAP has been shown to inhibit apoptosis by ubiquitinating caspase-3 and targeting it for proteasomal degradation [72, 73]. cIAPs reportedly ubiquitinate caspase-3 and caspases-7 and promote proteasomal degradation of these caspases [100]. IAPs were also reported to regulate apoptosis by mediating ubiquitination of second mitochondria derived activator of caspases (Smac, also called DIABLO) and target Smac for degradation [101]. The expression level of IAPs can be regulated by autoubiquitination, which targets IAPs for proteasomal degradation and may play an important role in the regulation of apoptosis [95].

In IAPs, RING domain dimerization has been reported to be essential for their E3 activity [102, 103]. The RING domain of cIAP1 was found to form a heterodimer with the RING domain of XIAP, which appears to promote XIAP ubiquitination and degradation by the proteasome [104]. cIAPs were reported to remain monomeric via autoinhibition, whereas BIR-antagonist binding induces conformational rearrangements to enable RING dimerization and activation [105].

IAPs use multiple BIR domains for precise substrate recognition. Early studies showed that the linker region between the BIR1 and BIR2 domains of XIAP recruits caspase-3 or caspase-7 [106]. The BIR2 domain contributes to additional contacts with caspases [107, 108]. The BIR3 domain is involved in caspase-9 or Smac interactions [109, 110].

1.2.2.2 Other functions

Despite E3 activity, IAPs execute their anti-apoptotic functions via protein-protein interactions. XIAP was reported to inhibit caspase by blocking the active sites of caspase-3 and caspase-7 [106]. It was also suggested to trap caspase-9 in an inactive (monomeric) state by preventing caspase-9 dimerization [109]. Smac and caspases share an N-terminal IAP binding motif (IBM), thus Smac binding prevents caspase

from binding to IAPs and induces apoptosis [111, 112]. Rather than by direct interaction with caspases, cIAPs were shown to sequester Smac from XIAP, allowing XIAP to inhibit caspases [113]. MLIAP might also be responsible in binding Smac and preventing it from antagonizing XIAP, thereby regulating apoptosis [114].

IAPs are also indicated to function as either positive or negative regulators in NF- κ B activation [115]. For example, cIAPs mediate ubiquitination of receptor-interacting protein kinase (RIP1/RIPK1), which is essential to recruit other signal proteins for NF- κ B activation [116]. cIAPs also negatively regulate NF- κ B signalling via ubiquitination and degradation of NF- κ B-inducing kinase (NIK) [117].

IAPs are differentially overexpressed in many tumour tissues. For example, high level of XIAP is found in patients with melanoma and liver cancer [118, 119]. MLIAP is frequently overexpressed in tumours including melanoma and bladder cancer [120, 121]. Overexpression of cIAPs results in liver tumor formation and growth in mice [122]. High expression levels of IAPs, particularly XIAP are associated with a poor prognosis and overall survival in patients [123].

1.2.3 Available structures of IAPs (BIRC family proteins)

Domains commonly shared in IAPs are the BIR domain and the RING domain. The structure of the BIR domain shows that it forms a globular Zn-cooperation structure, which consists of four or five α -helices and a variable number of anti-parallel β -sheets [124] (**Figure 1-8a**). The RING domains in IAPs function as a dimer. Existing structures reveal the dimer interface formed between the core and the N-terminal helices of the RING domains [37] (**Figure 1-8b**).

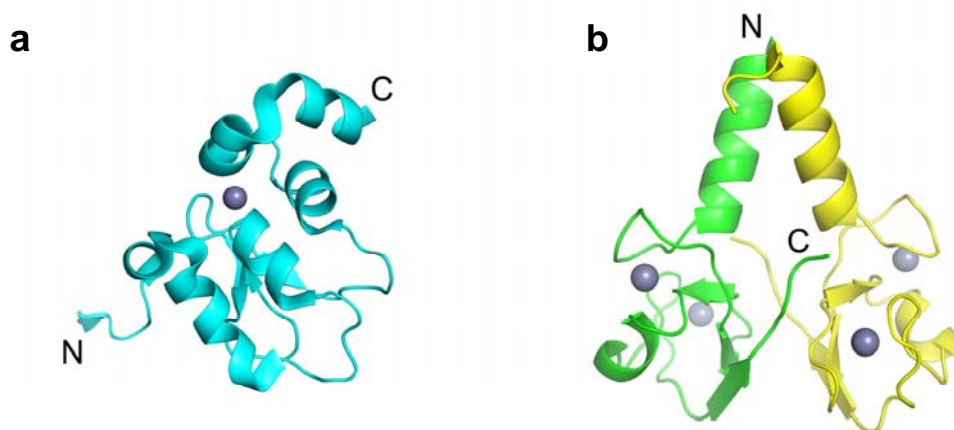


Figure 1-8. Crystal structures of the BIR3 and the RING domain of cIAP2.

(a) Cartoon representation of the structure of the BIR3 from cIAP2 coloured in cyan (PDB: 2UVL) [124]. The Zn^{2+} atom is shown in sphere.

(b) The structure of the RING domain from cIAP2 (PDB: 3EB5) [37] with one subunit in green and the other in yellow. The asymmetric unit consists of one subunit of the dimer. The biological RING dimer is generated by crystallographic symmetry. The Zn^{2+} atoms are shown in spheres.

To date, there are no structures of full-length IAPs, but fragments of IAPs with or without their binding partner or inhibitors have been solved. XIAP that is best studied consists of three BIR domains, BIR1, BIR2 and BIR3 followed by a C-terminal RING domain (**Figure 1-7**). The BIR1 domain from XIAP was shown to dimerize and interact with an adaptor protein TAB1 to induce NF- κ B activation [125]. The linker region between the BIR1 and BIR2 has been shown to recruit caspase-7 [106]. The BIR2 was shown to bind caspase-3 [107] whereas the BIR3 was reported to recruit caspase-9, Smac or Smac mimics [109, 110, 126]. An UBA domain involved in recruiting ubiquitination chain was identified in XIAP and its structure is consistent with the structures of known UBA proteins based on an NMR model [127]. The crystal structure of the RING domain has also been solved recently [128].

In cIAPs, crystal structures demonstrate the detailed interactions between the BIR1 domain and TRAF2 [129]. The BIR3 domain of cIAPs is assumed to interact with caspase-9 and Smac based on structures of the BIR3 in complex with caspase-9 peptide, Smac peptide or other Smac mimetics [130, 131]. A crystal structure of cIAP2 RING domain bound to Ubch5B reveals that the IAP RING-E2 interface resembles other existing RING E3-E2 complexes [37]. The CARD was reported to inhibit the activation of cIAP1's E3 activity by preventing RING dimerization and E2 binding [97]. A recent crystal structure of cIAP1 containing the BIR3, the CARD and

the RING domain demonstrates that cIAP1 adopts an autoinhibited monomeric state where the CARD interacts with the E2 binding surface of the RING domain. Antagonist binding (Smac mimetics or caspase) to the BIR3 domain induces conformational changes to release autoinhibition and enable RING domain dimerization for activation [105].

MLIAP and ILP2 that are less studied, contain only one BIR domain followed by a ~100 amino acid linker and a C-terminal RING domain. So far, only the crystal structures of the BIR have been solved [132, 133].

1.3 CBL proteins

1.3.1 CBL family proteins (CBLs)

CBL (Casitas B-lineage lymphoma) was initially identified as the cellular form of v-CBL, a transforming protein from murine retrovirus that induces early B-lineage lymphoma [134]. The mammalian CBL family proteins include three homologues known as c-CBL, CBL-B and CBL-C. c-CBL and CBL-B are ubiquitously expressed in mammalian cells and primarily in cytoplasm [135]. CBL-C (also called CBL-3) lacks some C-terminal domains, which is primarily expressed in epithelial cells [136]. Additionally, CBL homologues have been identified in non-mammalian species, such as D-CBL in *D. melanogaster* and Sli-1 in *C. elegans*, indicating that CBL family proteins are conserved through evolutionary path [137, 138].

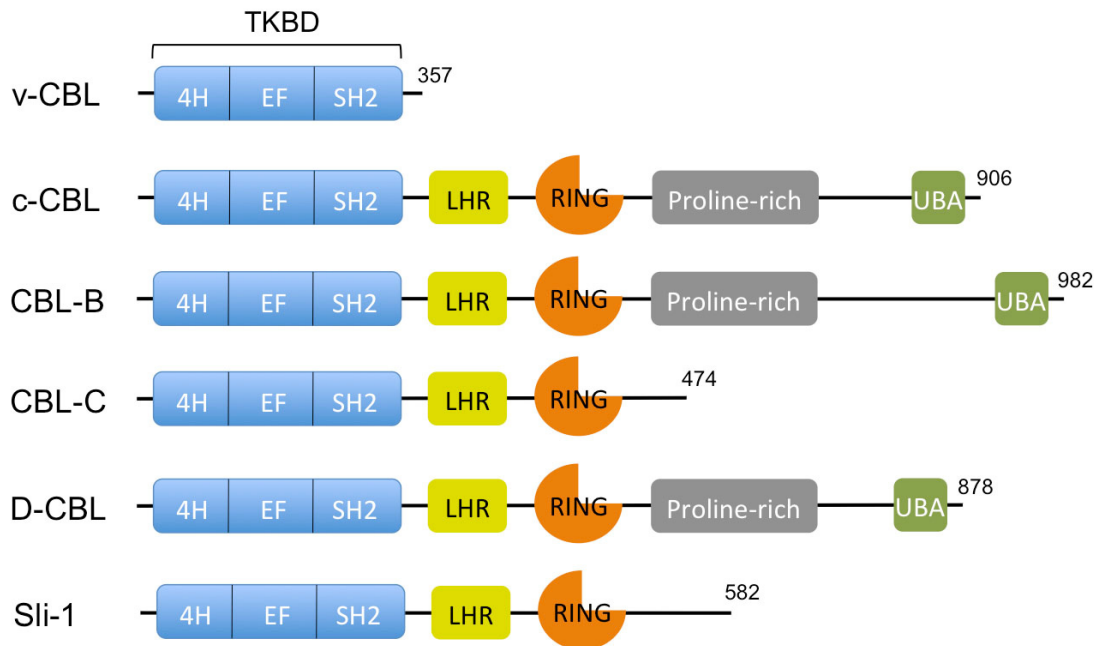


Figure 1-9. Schematic representation of the CBL family proteins.

The number of residues of each CBL protein and their functional domains are shown.

CBL proteins can be divided into several domains (**Figure 1-9**). The highly conserved N-terminal fragment of CBL proteins includes a tyrosine kinase-binding domain (TKBD), a linker helix region (LHR) and a RING domain. The TKBD is comprised of a four-helix bundle (4H), a calcium-binding EF-hand domain (EF) and a SH2 domain [139]. The SH2 domain is capable of binding to phosphotyrosine residues (pTyr) of protein tyrosine kinases (PTKs), both receptor (RTKs) and non-receptor kinases (non-RTKs) [140, 141]. The LHR that displays a loop-helix-loop structure links the TKBD and the RING domain. Phosphorylation on the conserved tyrosine residue from the LHR (Tyr371 in c-CBL, Tyr363 in CBL-B and Tyr341 in CBL-C) has been reported to be crucial for the activation of E3 activity [48]. Some mutations or deletions on this site cause c-CBL to become transforming or oncogenic [142]. Recently, this conserved tyrosine residue has been reported as a ‘hot spot’ for CBL mutations in human myeloid neoplasms [143]. The RING domain that is capable to bind an E2 is important for CBL’s E3 function [49, 144]. CBL proteins have been reported to mediate ubiquitination of PTKs toward degradation [145, 146]. Despite substrate ubiquitination, the RING domain is also involved in autoubiquitination toward proteasomal degradation [49]. Instead of E2 binding, the RING domain can interact with Sprouty proteins. Sprouty2 was reported to compete against E2 binding,

thus inhibits the E3 activity of CBL proteins [147]. The inhibition of the RING domain by Sprouty2 can be released by tyrosine-phosphorylation of Sprouty2. Phosphorylated Sprouty2 can be recruited to the TKBD of c-CBL and targeted for ubiquitination-dependent degradation [148].

CBL proteins have been reported to associate with hundreds of cellular proteins [149]. The C-terminal domains play an important role in diverse substrate recognition. c-CBL, CBL-B and D-CBL contain a proline-rich region followed by the RING domain, which appears to bind proteins containing SH3 domains, such as Src kinase, PI3 kinases [150, 151]. In addition, c-CBL and CBL-B contain several tyrosine residues at the C-terminus. These tyrosines are phosphorylated by protein tyrosine kinases (PTKs). Upon phosphorylation, they serve to recruit SH2 domain-containing proteins [152, 153]. Finally, c-CBL and CBL-B contain an UBA domain at the C-terminus, which appears to be involved in dimerization or binding Ub, but not CBL's E3 activity [154].

1.3.1.1 E3 activity

CBL proteins regulate RTKs or non-RTKs signalling pathways by serving as RING E3s. c-CBL is best-characterized in attenuating EGFR signalling. Upon epidermal growth factor (EGF) binding, EGFR dimerizes and autophosphorylates several tyrosine residues at its C-terminus, resulting in the activation of downstream signalling cascades. EGFR is recruited to clathrin-coated pits that can be internalized into endocytic vesicles. EGFR can either be recycled back to the plasma membrane or directed to lysosomal destruction. It has become increasingly evident that CBL proteins have a key role in EGFR degradation via its E3 activity [49, 155, 156]. Upon EGF stimulation, c-CBL is recruited to activated EGFR via the TKBD interactions with phosphotyrosine 1045 (pY1045) of EGFR [48]. c-CBL can also indirectly bind to activated EGFR through an adaptor protein Grb2. Grb2 was shown to bind to the proline-rich region of c-CBL via its SH3 domain, and also interact with the pY1068 or pY1086 on EGFR through its SH2 domain [157]. Following recruitment to EGFR, c-CBL is phosphorylated by EGFR. Phosphorylation of Tyr371 on the LHR activates

c-CBL's ligase activity. c-CBL recruits E2~Ub and promotes ubiquitination of the receptor at multiple sites [158]. Previously, CBL proteins have been shown to mediate mono- or Lys63-type of ubiquitination on EGFR to direct EGFR through the endocytic pathway [158, 159], but other studies indicate that CBL-mediated ubiquitination of EGFR is not required for ligand-induced internalization of EGFR [160]. Recently, c-CBL has been reported to mediate Lys48-linked ubiquitination on EGFR [161]. Overall, CBL proteins function by specifically targeting activated EGFRs and mediating their lysosomal degradation, thereby regulating EGFR signalling pathway [162, 163].

Additionally, CBL proteins are involved in down-regulation of non-RTKs. It has been shown that c-CBL is essential to promote Src, Lck, Syk and Lyn proteasomal degradation [164-167]. CBLs are also known to bind to the p85 subunit of phosphatidylinositol-3-kinase (PI3K) and ubiquitinate p85 for degradation [168]. c-CBL also associates with arginine-binding protein 2 (ArgBP2), a multi-adaptor protein that links c-Abl kinase to c-CBL. ArgBP2 and c-Abl kinase are then ubiquitinated by c-CBL [169]. Interestingly, CBL proteins also target themselves for proteasomal degradation via autoubiquitination when they are associated with EGFR or Src [164, 170, 171].

1.3.1.2 Other functions

CBL proteins also function as adaptor proteins to trigger or inhibit signal transduction through a diverse array of interactions. The multiple protein-protein interacting modules enable CBL proteins to recruit different substrates for ubiquitination and degradation. In addition, these protein-protein interacting modules also allow CBL proteins to function as adaptor proteins independent of their E3 activity [149]. For example, CBL proteins promote receptor internalization via its interaction with an adaptor protein, CBL-interacting protein of 85kDa (CIN85) [172]. CIN85 binds to c-CBL or CBL-B via its SH3 domain and this interaction is enhanced by EGFR-induced tyrosine phosphorylation of CBL proteins. The proline-rich region of CIN85 interacts with endophilins that are regulatory components of clathrin-coated vesicles (CCVs)

and induces membrane curvature and CCV formation [173]. Activated receptors could be internalized via the recruitment the CBL–CIN85–endophilin complex [174]. In addition, CBL proteins compete with son-of-sevenless (SOS) by binding to Grb2, thus blocks MAPK signalling through the Ras pathway [149]. Conversely, CBL is also involved in the activation of MAP kinases by acting as an adaptor in the activation of ERK and JNK kinases [175]. Furthermore, c-CBL plays a role in PI3K-independent insulin signalling, which is regulated by adapter proteins including adapter containing PH and SH2 domains (APS) and CBL-associated protein (CAP). Upon stimulation, the insulin receptor phosphorylates and recruits c-CBL through APS to form the APS/CBL/CAP complex for the stimulation of glucose transporter type 4 (GLUT4) translocation [176].

Previous studies suggested that CBLs are implicated in regulating T-cell or B-cell receptors (TCR or BCR) [177]. c-CBL promotes ubiquitination of the TCR, thereby negatively regulating T cell development and activation [178]. CBL-B was reported to negatively regulate the BCR signalling by targeting a key protein Syk for ubiquitination and subsequent degradation [179]. A recent study indicated that CBL-B inhibits the activity of Nedd4, a HECT E3, which positively regulates T cell activation [180].

1.3.2 Available structures of CBL proteins

The highly conserved N-terminal fragment of CBL proteins has been widely studied. To date, the crystal structures or NMR models of TKBD from mammalian CBLs have been solved. The native TKBD structure consists of an N-terminal four-helix bundle (4H), a calcium-binding domain with the EF-hand fold, and an unusual SH2 domain (only shares sequence identity of about 11% with other SH2 domains) [139] (**Figure 1-10a**). Previous structures showed that phosphotyrosine peptide binds to the SH2 domain and induces a slight conformational change in this domain (**Figure 1-10b**). However, the conformations of the 4H and EF-hand domains remain unchanged upon phosphotyrosine peptide binding [139].

a

b

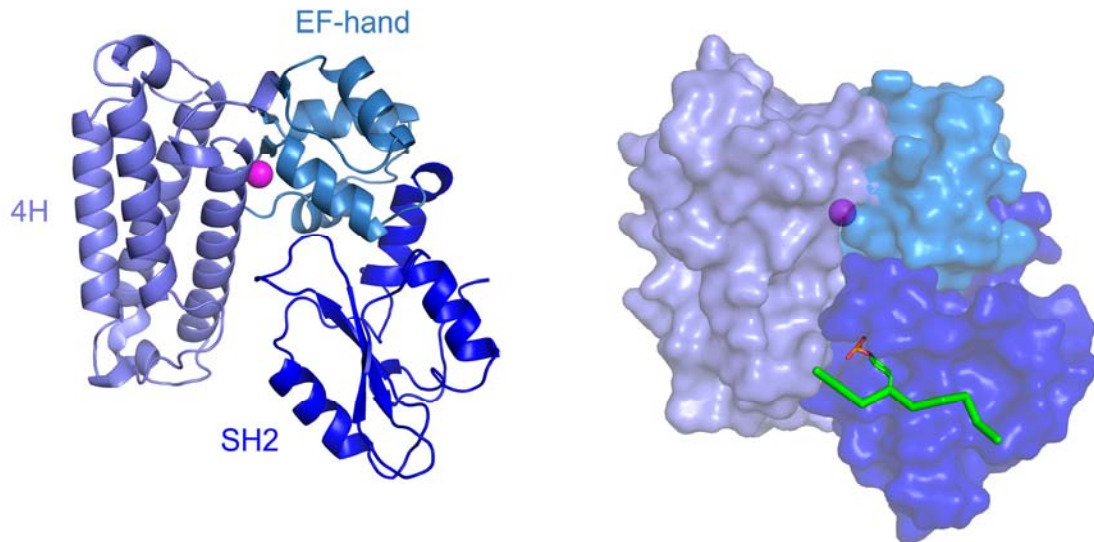


Figure 1-10. The TKBD of c-CBL.

(a) The structure of native TKBD from c-CBL is shown in cartoon representation. The 4H domain is coloured slate, the EF-hand domain marine, and SH2 domain blue. The Ca^{2+} atom is shown as magenta sphere.

(b) Surface view of the TKBD in the presence of a phosphotyrosine peptide. Domains of the TKBD are coloured as in a. The phosphotyrosine peptide is shown as green ribbon. The side chain of phosphotyrosine is shown as stick, with O atoms red, P atom orange. The Ca^{2+} atom is shown as magenta sphere.

To date, the structure of the longest fragment of CBL proteins contains the TKBD, the LHR, and the RING domain from c-CBL. This N-terminal fragment was crystallized in complex with the E2 UbcH7 and ZAP-70 peptide, a phosphotyrosine peptide that comprises the ZAP-70 kinase-binding site on the TBKD [52] (**Figure 1-11a**). This structure was the first to reveal how a RING domain binds an E2. The RING-E2 interactions are stabilized by hydrophobic interactions involving UbcH7's Phe63, Pro97, and Ala98 and c-CBL's Ile383, Trp408, Cys404, Ser407, Pro417 and Phe418 (**Figure 1-11b**). However, this structure raises few questions. First, the E2's catalytic cysteine is distal from the substrate-binding site of c-CBL ($> 70 \text{ \AA}$); therefore, it is unclear how the Ub is transferred to substrate or whether the gap can be bridged by full-length substrates. Second, Tyr371 packs against TKBD and is buried (**Figure 1-11c**). Hence, it remains unknown how this tyrosine residue is phosphorylated by kinases. Notably, in this paper, they predicted that Tyr371 may have a structural role, thus mutations on this residue would likely affect the TKBD-LHR interaction and hence the E2 binding, leading to decrease in E3 activity [52]. This result argued against earlier studies that used Y371F mutant to probe the effects of Tyr371

phosphorylation [142]. Later on, biochemical studies showed that phosphorylated c-CBL N-terminal fragment displayed an enhanced activity over wild type [181].

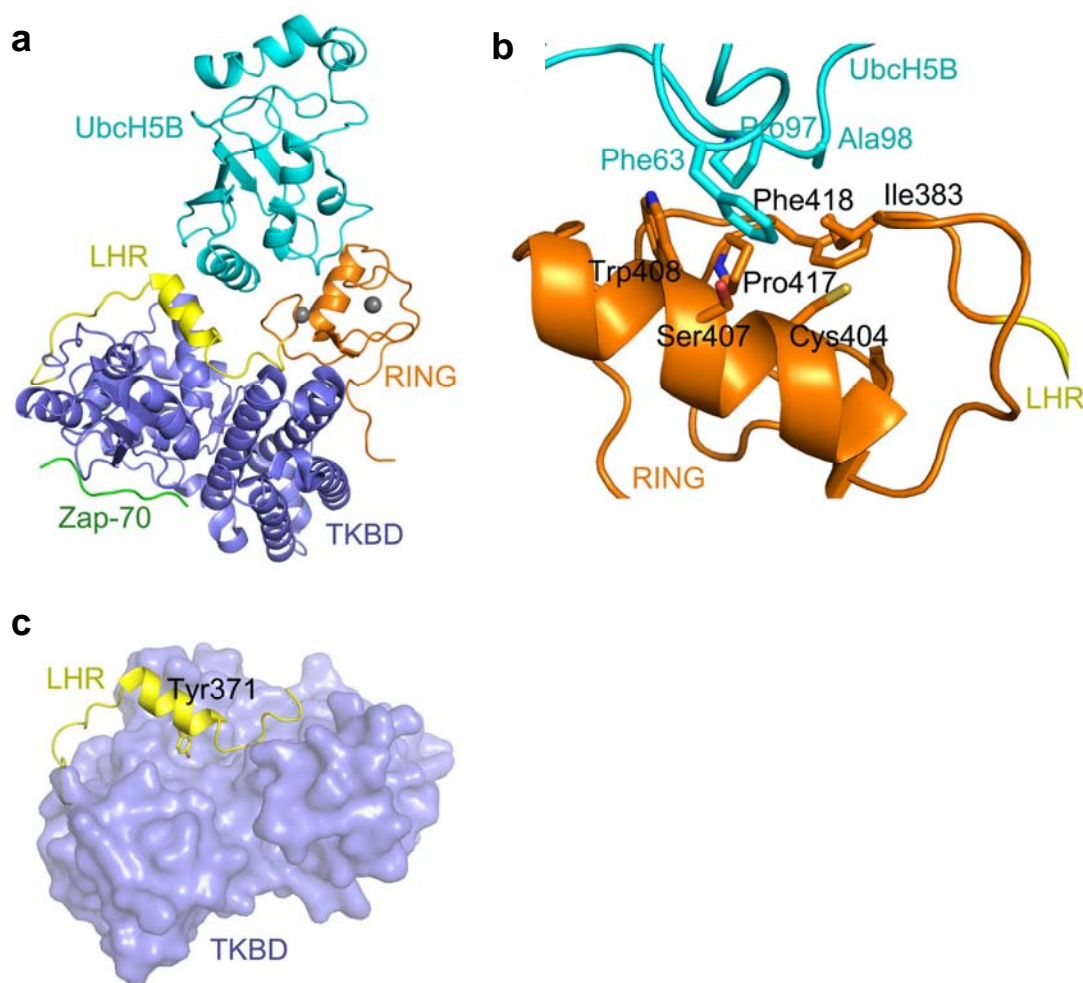


Figure 1-11. The structure of c-CBL N-terminal fragment in complex with UbcH5B and ZAP-70 peptide.

(a) The complex structure of c-CBL bound to UbcH5B and ZAP-70 peptide. The TKBD is coloured slate, the LHR yellow, the RING domain orange, the UbcH5B cyan, and ZAP-70 peptide green. The Zn^{2+} atoms are shown as gray spheres.

(b) The close-up view of the E2-RING interaction. Key residues are shown as sticks, with N atoms blue, O atom red, and S atom yellow.

(c) The surface view of the TKBD with the LHR shown in cartoon representation. The side chain of Tyr371 is displayed as sticks with C atoms yellow, O atom red.

Another region in CBL proteins for recruiting substrates or binding partners is the C-terminal proline-rich region [150, 151]. To date, there are few crystal structures of proteins containing the proline-rich region with more than five $C\alpha$ atoms, possibly because this region is flexible and difficult to crystallize [182]. Existing CBL structure

only contains a peptide sequence of this region bound to the SH3 domain from CIN85 [183]. Both c-CBL and CBL-B have a UBA domain at the C-terminus. These two UBA sequences are highly similarity (75%) and resemble the typical UBA structure [184]. A crystal structure of the UBA domain from CBL-B bound to an Ub was solved [185]. It seems that the UBA from c-CBL does not bind Ub as the one from CBL-B, presumably due to a negatively charged glutamine residue on its Ub binding surface [184].

1.4 Objectives of the thesis

The E3 ligase activity of the RING domain was first identified in 1999. Since then, a great amount of work has been done to identify various RING E3s and to characterize their structures. The structural information gained has helped us in understanding how RING E3s function. However, further investigations are required to fully understand how RING E3s are regulated and how they promote Ub transfer. To this end, the objectives of my thesis are:

- 1) To determine the crystal structure of a dimeric RING E3, BIRC7 RING dimer in complex with a stabilized E2~Ub. This complex structure will hopefully explain how RING E3 activates E2~Ub for transfer
- 2) To determine the crystal structure of the N-terminal fragment of c-CBL. Early studies hinted that c-CBL RING domain alone is more active than the N-terminal TKBD-LHR-RING fragment suggesting that the activity of c-CBL may be regulated [181, 186]. Structure of this fragment will provide insights into how c-CBL is regulated.
- 3) To determine the crystal structure of a monomeric RING E3, phosphorylated CBL-B fragment in complex with a stabilized E2~Ub. Comparison of this structure with the dimeric RING E3–E2~Ub structures will provide insights into how different types of RING E3s recruit and activate E2~Ub.
- 4) To verify the essential interactions observed in the crystal structures by developing an *in vitro* ubiquitination assay or other biochemical assays.
- 5) To develop assay to measure the kinetics constants (K_m and k_{cat}) of RING E3-catalysed reactions. The kinetic constants would allow us to identify the mutational effects in enzyme catalysis and catalytic efficiency of different E3s.

Chapter 2

Material and Methods

2 Material and Methods

2.1 Molecular cloning of recombinant plasmids

2.1.1 Plasmid source

The cDNAs of full-length human BIRC3, BIRC7, c-CBL and CBL-B were purchased from Source BioScience. The pGEX4T1 vector was purchased from GE Healthcare. A modified pGEX4T1 vector was designed by Lori Buetow, yielding hexahistidine-glutathione S-transferase (His-GST) tag. It is termed as xH-pGEX4T1. Constructs were generated by standard polymerase chain reaction (PCR)-ligation techniques and sequences were verified by automated sequencing.

2.1.2 Primer design

Pfu turbo DNA polymerase was used according to the manufacturer's protocol (Stratagene). Fragments or full-length BIRC3, BIRC7, BIRC7, c-CBL and CBL-B were amplified by the following primers (Integrated DNA Technologies):

| Constructs | Primers | Restriction sites |
|--|---|-------------------|
| BIRC3 RING (BIRC3 _{541-C}) | 5' - cgGGATCCgatctaccagtgaagaacaattgc | BamH1 |
| | 3' - cgGAATTCcatgaaagaaatgtacgaactgtacc | EcoR1 |
| BIRC7 RING (BIRC7 _{239-C}) | 5' - cgGGATCCgtggaggcgcagctgcggcg | BamH1 |
| | 3' - cgGAATTCctaggacaggaaggtgcgcac | EcoR1 |
| BIRC7 (full-length) | 5' - cgGGATCCatgggacctaagacagtccaag | BamH1 |
| | 3' - cgGAATTCctaggacaggaaggtgcgcac | EcoR1 |
| c-CBL fragment (c-CBL ₄₇₋₄₃₅) | 5' - cgGGATCCccgccggggacggtggacaagaag | BamH1 |
| | 3' - ccgCTCGAGttaatcaaacggatctaccacgatggg | XhoI |
| CBL-B fragment (CBL-B ₃₆₋₄₂₇) | 5' - gaAGATCTcctaagcaagctgccgcagatc | Bgl II |
| | 3' - ccgCTCGAGgtaatcaaagggatccacgattatgg | XhoI |
| CBL-B RING (CBL-B ₃₄₆₋₄₂₇) | 5' - gaAGATCTgaacctacacctcatgaccatata | Bgl II |
| | 3' - ccgCTCGAGgtaatcaaagggatccacgattatgg | XhoI |

The forward and reverse primers for generating E3 mutants were designed based on available structures and ordered from Integrated DNA Technologies. Other related

plasmids (eg. UbcH5B, Ub, and Smac variants) were cloned by me, Danny Huang and Lori Buetow (**Appendix 1**. Construct list).

The PCR product was then digested with restriction enzymes (NEB), gel purified (Qiagen), and ligated (Quick ligase, NEB) into suitable vectors, followed by a TEV or thrombin protease cleavage site.

2.2 Expression and purification of proteins

For crystallization, plasmids of interest were transformed into *E. coli* BL21 (DE3) Gold competent cells. Bacterial culture (usually 12-24 liters) were grown at 37°C in Terrific Broth (TB) with 100 mg/l ampicillin to an A_{600} of approximately 0.75 and induced with 0.2 mM isopropyl β -D-thiogalactopyranoside (IPTG, ForMedium) overnight at 20°C. Harvested cells were resuspended in suitable buffers (normally the wash buffer used in the first step of purification) with 1 mM phenylmethylsulfonyl fluoride (PMSF), and 15 mg lysozyme per liter of culture. Cells were subjected to one cycle of freeze-thaw. Before sonication, additional 1.5 mM PMSF was added. Sonication was performed using the Vibra-Cell VCX 750 sonicator (Sonics & Materials, Inc.) with a 13 mm probe, at 85 % amplitude and 8 x 8 seconds pulses with an 8-second pause in between each pulse for 2 cycles. Clear lysate was purified by glutathione sepharose (GSH) or Ni^{2+} -affinity chromatography, ion-exchange chromatography, and size-exclusion chromatography. Fractions containing the protein of interest were pooled, frozen in liquid nitrogen, and stored in the running buffer of size-exclusion chromatography at -80°C.

Protein concentrations were determined by Bradford assay [187] with bovine serum albumin (BSA) as standard. The concentration of Ub is measured at A_{280} [188, 189]:

$$Con(mg/ml) = \frac{A_{280} * MW(Da)}{Ext.Co} \approx \frac{A_{280}}{0.16}$$

Buffers that are commonly used in the lab are listed:

| Chromatography | Buffers |
|----------------------------|---|
| GSH-affinity | Wash buffer: 50 mM Tris-HCl pH 7.6, 200 mM NaCl and 1 mM DTT |
| | Elution buffer: 50 mM Tris-HCl pH 8.0, 200 mM NaCl, 5 mM DTT and 10 mM GSH |
| Ni ²⁺ -affinity | Wash buffer: 25 mM Tris-HCl pH 7.6, 150 mM NaCl, 5 mM BME and 15 mM imidazole |
| | Elution buffer: 25 mM Tris-HCl pH 7.6, 150 mM NaCl, 5 mM BME and 200 mM imidazole |
| Size-exclusion | Running buffer: 25 mM Tris-HCl pH 7.6, 150 mM NaCl and 1 mM DTT |

2.2.1 Purification of BIRC7 RING for crystallization

Plasmid of BIRC7 RING (BIRC7_{239-C}) that was cloned in the xH-pGEX4T1 vector was expressed and purified by Ni²⁺- affinity chromatography. It was then treated with TEV protease to cleave the His-GST-tag, and further purified by GSH-affinity pass-back and size-exclusion chromatography (HiLoad 16/600 Superdex 75 followed by Superdex 75, GE). Fractions containing pure BIRC7_{239-C} were pooled with a final concentration of about 4.9 mg/ml, frozen and stored in the running buffer of size-exclusion chromatography at -80°C.

2.2.2 Purification of c-CBL fragment for crystallization

Plasmid of c-CBL fragment (c-CBL₄₇₋₄₃₅) that was cloned in pGEX4T1 vector was expressed and purified by GSH-affinity chromatography, treated with TEV protease to cleave the GST-tag, and further purified by GSH-affinity pass-back and size exclusion chromatography (Superdex 75, GE). Fractions containing pure c-CBL₄₇₋₄₃₅ were pooled with a final concentration of about 12.9 mg/ml, frozen and stored in the running buffer of size-exclusion chromatography at -80°C.

2.2.3 Purification of pCBL-B fragment for crystallization

CBL-B fragment (CBL-B₃₆₋₄₂₇) was cloned in pGEX4T1 vector with a thrombin cleavage site. It was coexpressed with mouse Src₈₄₋₅₂₆, which was cloned in pRSFDuet vector containing an N-terminal His-MBP tag. Bacterial culture were grown at 37°C in TB with 100 mg/l ampicillin and 25 mg/l kanamycin and induced as described in section 2.2. 2 mM sodium vanadate (Sigma) was added before purification to prevent dephosphorylation. pCBL-B₃₆₋₄₂₇ was purified by GSH-affinity chromatography, treated with thrombin protease to cleave the GST-tag, and further purified by GSH-affinity pass-back, anion exchange chromatography (SOURCE Q, GE; pI 6.12; Buffer A and B are listed below; protein eluted at around 20 mS/cm) and size exclusion chromatography (Superdex 75, GE). Fractions containing the protein of pure pCBL-B were pooled and concentrated on an Amicon Ultra centrifugal filter (Millipore), with size-exclusion limit of 30 kDa, to a final concentration of about 3.28 mg/ml, frozen in liquid nitrogen, and stored in the running buffer of size-exclusion chromatography at -80°C.

| Chromatography | Buffers |
|----------------|---|
| Anion exchange | Buffer A: 50 mM Tris-HCl pH 8.5, and 1 mM DTT |
| | Buffer B: 50 mM Tris-HCl pH 8.5, 1 M NaCl, and 1 mM DTT |

2.2.4 Purification of Ubch5B~Ub variants for crystallization

2.2.4.1 The generation of Ubch5B_{RAS}~Ub (developed by Danny Huang)

Wild-type Ub was cloned into pGEX4T1 with an N-terminal GST-tag followed by a TEV cleavage site. Untagged *Arabidopsis thaliana* E1 Uba1 was cloned in pET23d vector. Untagged Ubch5B with S22R/N77A/C85S mutations (Ubch5B_{RAS}) was cloned in pRSF_1b. The lysate of Ub and E1 were first mixed in the presence of 5 mM MgCl₂ and 5 mM ATP for 2h at 4°C (generating E1~GST-Ub). The mixed lysate was then purified by GSH-affinity chromatography (eluted with 25 mM DTT) to yield untagged E1, followed by anion exchange chromatography. GST-Ub was also purified by GSH-affinity chromatography (eluted with GSH elution buffer). Untagged

UbcH5B_{RAS} was first purified by cation exchange chromatography without DTT. All semi-purified proteins were mixed for generating UbcH5B_{RAS}~Ub. TEV protease, 10 mM MgCl₂ and 10 mM ATP were added to the mixture at 19°C for 1 day. The UbcH5B_{RAS}~Ub was then purified by cation exchange chromatography followed by size-exclusion chromatography, and stored in 25 mM HEPES (pH 7.5), 0.2 M NaCl and 1 mM DTT.

2.2.4.2 The generation of UbcH5B_{RK}-Ub (developed by Danny Huang)

Wild-type Ub was cloned into xH-pGEX4T1 with an N-terminal His-GST-tag followed by a TEV cleavage site. His-GST-Ub, untagged *Arabidopsis thaliana* Uba1, and untagged UbcH5B with S22R/C85K mutations (UbcH5B_{RK}) were expressed and purified as described in section 2.2.4.1. Isopeptide-linked UbcH5B-Ub was formed by mixing semi-purified Uba1, UbcH5B_{RK}, and His-GST-Ub in the presence of 10 mM MgCl₂ and 10 mM ATP at 30 °C for 1 day. The UbcH5B_{RK}-Ub was purified by Ni²⁺-affinity chromatography, followed TEV protease cleavage at 19°C. His-GST was removed by Ni²⁺-affinity chromatography and UbcH5B_{RK}-Ub was further purified by cation exchange and size-exclusion chromatography. The UbcH5B_{RK}-Ub was stored in 25 mM HEPES, pH 7.5, 0.2 M NaCl and 1 mM DTT at -80°C.

2.2.5 Protein purification for assays

For ubiquitination assays, RING E3s (BIRC7_{239-C}, BIRC3_{541-C}, c-CBL₄₇₋₄₃₅) variants were cloned in pGEX4T1 vector, expressed and purified as described above except cleavage was performed on GSH beads without the pass-back step.

Full-length c-CBL variants were expressed from pRSFDUET vector containing a N-terminal His-tag with TEV cleavage site. Proteins were purified by Ni²⁺-affinity chromatography, followed by anion exchange (monoQ, GE; pI 6.1; Buffer A and B are listed below; protein eluted at about 22 mS/cm) and size exclusion

chromatography (SD200, GE). Proteins were stored in the running buffer of size-exclusion chromatography at -80°C.

| Chromatography | Buffers |
|---------------------------|---|
| Anion exchange (monoQ) | Buffer A: 50 mM Tris-HCl pH 8.0, and 1 mM DTT |
| | Buffer B: 50 mM Tris-HCl pH 8.0, 1 M NaCl, and 1 mM DTT |

SMAC comprising residues 56-C was expressed from pET23d vector with a C-terminal protein kinase A recognition sequence (RRAVS) and uncleavable His-tag. Proteins were purified by Ni²⁺-affinity chromatography, followed by size-exclusion chromatography (Superdex 75, GE).

Ub variants were expressed in pGEX2TK vector and purified by GSH-affinity chromatography, treated with TEV protease to remove the GST-tag. They were further purified by GSH-affinity pass-back and size exclusion chromatography (Superdex 75, GE). His-tag Ub and His-tag Ub Δ GG (with a deletion of last two glycine residues) were expressed in pRSF1b vector and purified by Ni²⁺-affinity without removing the His-tag, followed by size exclusion chromatography (Superdex 75, GE).

2.3 Crystallization

2.3.1 Structure of BIRC7_{239-C}-Ubch5B_{RAS}~Ub complex

Crystals were obtained by mixing the protein with an equal volume of reservoir solution and grown by hanging drop vapor diffusion at 4 °C. BIRC7_{239-C} (4.7 mg/ml) was mixed with Ubch5B_{RAS}~Ub (25.4 mg/ml) at a 1:1 molar ratio, and crystals were grown in conditions containing 100 mM HEPES, pH 7.0, 17–20% (w/v) PEG 3350 and 0.2 M tri-ammonium citrate. The crystals were flash-frozen in 100 mM HEPES, pH 7.0, 23% (w/v) PEG 3350, 0.2 M tri-ammonium citrate and 20% (v/v) glycerol.

2.3.2 Native structure of c-CBL

Crystals of CBL₄₇₋₄₃₅ (13 mg/ml) were grown by hanging drop vapour diffusion at 8°C by mixing equal volumes of protein and a reservoir solution containing 0.1 M Tris-HCl, pH 9.0-9.5, 3.7-4.0 M sodium formate and 5 mM DTT. Crystals were flash-frozen in 0.1 M Tris-HCl, pH 9.0-9.5, 4.2 M sodium formate, 5 mM DTT, 8% (v/v) glycerol, 8% (v/v) ethylene glycol and 8% (w/v) sucrose.

2.3.3 Structure of pCBL-B-UbcH5B_{RK}-Ub-ZAP-70 peptide complex

Crystals were obtained by hanging-drop vapor diffusion at 4°C. pCBL-B (3.5 mg/ml) was mixed with UbcH5B_{RK}-Ub (20 mg/ml) and ZAP-70 peptide (10 mM, sequence TLNSDG(p)YTPEPA, Alta Bioscience) at a 1:1:1 molar ratio. Crystals were grown in conditions containing 0.1 M bicine, pH 9.0, 8-11% (w/v) PEG3350, and 0.1 M sodium formate. The crystals were flash frozen in 0.1 M bicine, pH 9.0, 13% (w/v) PEG3350, 0.1 M sodium formate, and 30% (v/v) ethylene glycol.

2.4 Data collection and processing

The diffraction data were collected at the European Synchrotron Radiation Facility (ESRF) or Diamond Light Source (DLS). The data were integrated and scaled with HKL2000 [190] or integrated with Mosflm [191] or automated XDS [192] and scaled using the CCP4 program suite [193]. The detailed information is as follows:

| Structures | Synchrotron: beamlines | Images files /xray/Permanent/ | Data process |
|--|----------------------------------|----------------------------------|--------------------------------|
| BIRC7 _{239-C} -UbcH5B _{RAS} ~Ub | DLS: I04, I24 | 572_16_ (2012_02_10) | XDS |
| c-CBL | ESRF: ID14-1 DLS: I02, I03 | JD13_ (2010_03_16) | HKL2000 Mosflm/Scala XDS |
| pCBL-B-UbcH5B _{RK} -Ub-ZAP- 70 peptide | DLS: I04, I24 | 568_6_ (2012_10_15) | XDS |

2.5 Structure determination and refinement

Details of the refinement statistics are shown in **Table 3-2**, **Table 4-1**, and **Table 5-1**. All figure models were generated using PYMOL (Schrödinger) (**Appendix 2**. Contribution list)

2.5.1 Structure of BIRC7_{239-C}-UbcH5B~Ub complex

BIRC7_{239-C}-UbcH5B_{RAS}~Ub complex crystals belong to space group P4₃2₁2 with two molecules in the asymmetric unit. Initial phases of BIRC7_{239-C}-UbcH5B_{RAS}~Ub were obtained by molecular replacement with PHASER [194] using PDB 3EB6 (BIRC3 RING-UbcH5B complex) [37] and PDB 3A33 (UbcH5B~Ub) [195] as the search models, respectively. All models were built in COOT [196] and refined using CCP4 [193], CNS [197] and PHENIX [198].

The structure of BIRC7_{239-C}-UbcH5B_{RAS}~Ub (Chains A-F) was refined at a resolution of 2.18 Å and the final model contained two copies of UbcH5B (Chain A residues 2-147 and Chain D residues 2-147), BIRC7_{239-C} (Chain B residues 242-298 and Chain E residues 242-298), Ub (Chain C residues 1-76 and Chain F residues 2-76). Residues with poor side-chain electron density were stubbed.

2.5.2 Native structure of c-CBL

Native c-CBL crystals belong to space group $C222_1$ with six molecules in the asymmetric unit. Initial phases of CBL were obtained by molecular replacement with PHASER [194] using PDB 1B47 [139] (CBL 47-350) and PDB 2CBL [139] (CBL 47-350 and ZAP-70 peptide 4-12) as the search models. The structure of the RING domain from c-CBL (381-428; PDB 1FBV [52]) was manually moved into the electron densities of native c-CBL. All models were built in COOT [196] and refined using CCP4 [193], CNS [197] and PHENIX [198].

The structure of CBL (Chains A-F) was refined at a resolution of 2.67 Å. The model contained Chain A (residues 47-353 and 359-435), Chain B (residues 47-355 and 360-435), Chain C (residues 47-354 and 359-435), Chain D (residues 47-354 and 359-435), Chain E (residues 47-353 and 360-435), and Chain F (residues 47-353 and 359-435). Atoms from residue side-chains with poor electron density were omitted.

2.5.3 Structure of pCBL-B-UbcH5B_{RK}-Ub-ZAP-70 peptide complex

The crystals of pCBL-B-UbcH5B_{RK}-Ub-ZAP-70 peptide complex belong to space group $P12_11$, containing four molecules in the asymmetric unit. Initial phases were obtained by molecular replacement with PHASER [194] using the TKBD from CBL-B (PDB 3PFV; [199]) and a model of phosphorylated CBL-B LHR-RING bound to UbcH5B that generated from PDBs 2LDR [199] and 4A49 [200]; Ub from PDB 4AUQ [201] as the search models. The r.m.s.d for C α atoms between the molecular replacement models and the four copies in the final model ranged from 0.55-0.59 Å, 1.20-1.22 Å, and 0.41-0.46 Å for the TKBD, pCBL-B LHR-RING-UbcH5B, and Ub, respectively. All models were built in COOT [196] and refined using PHENIX [198].

The complex structure (Chains A-P) was refined at a resolution of 2.21 Å. The final model contained four copies of pCBL-B (Chains A, E, M residues 38-427 and Chain I residues 41-426), ZAP-70 peptide (Chains B and N residues 4-12 and Chains F and J residues 5-12), UbcH5B (Chains C, G, K and O residues 2-147) and Ub (Chains D, H, L and P residues 1-76). Atoms from residue side-chains with poor electron density were omitted.

2.6 *In vitro* assays

2.6.1 Assays to validate the structure of BIRC7_{239-C}-UbcH5B_{RAS}~Ub complex

— *In vitro* ubiquitination assay

E2 UbcH5B (20 μ M) was charged by mouse Uba1 (0.4 μ M) and Ub or 32 P-Ub (40 μ M) in a buffer that contains 50 mM Tris-HCl (pH 7.6), 50 mM NaCl, 5 mM MgCl₂, 5 mM ATP, 1 mM DTT, 0.3 U/ml inorganic pyrophosphatase, 0.3 U/ml creatine kinase, 5 mM creatine phosphate, 1 mg/ml BSA (except for assays detected with SimplyBlue™ SafeStain (Invitrogen)) for 15-30 min at 23 °C. Charging reaction (10 μ l) was stopped by 0.25 U apyrase (Sigma) and 30 mM EDTA for 5 min at 23 °C. The autoubiquitination was initiated by the addition of BIRC7 variants (2 μ M). The SMAC-ubiquitination was started by the addition of a mixture of BIRC7 (0.220 μ M) and 32 P-SMAC (5.6 μ M). Lysine-discharge reactions was performed by adding a mixture of BIRC7 (2 μ M) and L-lysine (150 mM) or a mixture of BIRC3_{541-C} (0.220 μ M) and L-lysine (150 mM). Western blots of DiUb formation assay was carried out by addition of a mixture of BIRC7 (0.220 μ M) and His-Ub (200 μ M). The final UbcH5B~Ub concentration was about 7 μ M for all reactions. Reactions were quenched with 2X SDS loading buffer (with DTT only for the DiUb assays) at the indicated time and loaded onto SDS-PAGE. Results were visualized by SDS-PAGE (stained with SimplyBlue™ SafeStain), autoradiography (32 P-Ub), or western blots (immunoblotted with Ub (P4D1-A11, Millipore) or His-probe (sc-803, Santa Cruz) antibodies). The concentrations in the parentheses indicate the final protein concentrations.

2.6.2 Assays to validate c-CBL structure

— Disulfide crosslinking assay and *in vitro* ubiquitination assay

A mixture of c-CBL variants (30 μ g), UbcH5B (C85S) (100 μ M) and ZAP-70 peptide (20 μ M) was made up to 70 μ l with a buffer that contains 25 mM Tris-HCl (pH 7.6), 150 mM NaCl, and 1mM DTT on ice. 0.8 μ g of sample was removed for zero time point. The formation of disulfide was initiated by removal of DTT using a Zeba spin desalting column (Thermo Scientific) to exchange the buffer to 25 mM Tris-HCl (pH

7.6) and 150 mM NaCl at 23 °C. 0.8 µg of sample was removed at indicated times, quenched with N-ethylmaleimide (NEM; 20 mM) for 10 min and then mixed with 4X SDS loading buffer and monitored by SDS-PAGE. For disulfide strategy assay, sodium tetrathionate (NaTT; 0.1 mM; Sigma) was added to the buffer-exchanged c-CBL variants at 23 °C for 5 min, quenched with NEM for 10 min and mixed with 4X SDS loading buffer. NEM-treated samples were then mixed with thrombin protease at 23 °C for 90 min and stopped with 4X SDS loading buffer. Reduced samples were further prepared by adding 100 mM DTT. Gels were stained with SimplyBlue™ SafeStain (Invitrogen) and scanned on a densitometer (BioRAD GS-800) for quantification. The volumes of the disulfide-bonded (D) and unmodified (U) species were quantified using Quantity One software (BioRAD). The fraction of disulfide bond formed (F) was expressed as $F = D / (D + U)$. Reactions were performed in triplicates. Curves for the fraction of disulfide bond formed over time were generated by Excel.

Varied amounts of UbcH5B were pre-charged as described above. The autoubiquitination of full-length c-CBL was initiated by the addition of c-CBL variants (3 µM). Substrate Syk (71.9 kDa) was purchased from ORIGENE. The Syk ubiquitination was started by a mixture of c-CBL variants (0.1 µM) and Syk (about 4 µg/ml; 50 nM). The reactions were quenched with 4X LDS loading buffer and DTT (100 mM) at 23 °C for 10 min. Samples were then heated at 95 °C for 3 min and loaded onto SDS-PAGE for transferring to nitrocellulose membrane. Syk was detected by Western blotting with Syk antibody (ab60886, abcam). The concentrations in the parentheses indicate the final protein concentrations.

2.6.3 Assays to validate pCBL-B-UbcH5B_{RK}-Ub-ZAP-70 peptide structure

— *In vitro* ubiquitination assay

UbcH5B variants (7 µM) were charged with mouse Uba1 (0.4 µM) and Ub variants (40 µM) for 15 min at 23°C as described above. Charging was stopped by incubating the reaction with 0.25 U apyrase (Sigma) and 30 mM EDTA for 5 min at 23°C. The lysine-discharge reactions were initiated by the addition of a mixture of CBL-B_{LRR} or

pCBL-B_{LRR} (120 nM) and L-lysine (150 mM). The final UbcH5B~Ub variant concentrations were about 1.8 μ M for all reactions. Reactions were quenched with 4X SDS loading buffer at the indicated time, resolved by SDS-PAGE and stained with InstantBlue (Expedeon).

2.7 Kinetics assay on DiUb formation

2.7.1 Kinetics validation of BIRC7_{239-C}-UbcH5B_{RAS}-Ub complex structure

UbcH5B (66 μ M) was charged by mouse UBA1 (2.5 μ M) and ³²P-Ub variant (130 μ M) in a buffer that contains 50 mM HEPES (pH 7.5), 50 mM NaCl, 5 mM MgCl₂, 5 mM ATP, 1 mM DTT, 0.3 U/ml inorganic pyrophosphatase, 0.3 U/ml creatine kinase, and 5 mM creatine phosphate for 15 min at 23 °C. Charging was stopped by incubating the reaction with 0.25 U apyrase (Sigma) and 30 mM EDTA for 5 min at 23°C. Different amounts of pre-charged UbcH5B~³²P-Ub variants were then added to reactions that contain His-Ub (820 μ M) and BIRC7_{239-C} or BIRC3_{541-C} variants with a buffer of 50 mM HEPES (pH 7.5), 50 mM NaCl. Final E3 concentrations are indicated in **Table 3-3**. Reactions were quenched with 2X SDS loading buffer and DTT (100 mM) at 30 s, resolved by SDS-PAGE, dried and exposed to a phosphoimager. Under these conditions, less than 15% of UbcH5B~³²P-Ub variants were transferred to His-Ub, thus representing initial rate. In addition, there was no observable autoubiquitination of BIRC3_{541-C} variants or BIRC7_{239-C}. DiUb bands were quantified using ImageQuant (GE Healthcare). Control reactions lacking E3 at each UbcH5B~³²P-Ub variants concentrations were performed for background subtraction during quantification. All reported kinetic parameters were determined by fitting at least two independent datasets to the Michaelis-Menten equation using SigmaPlot 8.0 (Systat Software Inc.).

2.7.2 Kinetics validation of pCBL-B-UbcH5B_{RK}-Ub-ZAP-70 peptide structure

Varied amounts of UbcH5B were charged independently with mouse Uba1 (1.8 μ M) and 32 P-Ub variants (70 μ M) for 15 min at 23°C as described above. UbcH5B~ 32 P-Ub variants were then added to reactions containing a mixture of His-Ub Δ GG (1 mM) and CBL-B_{LRR} or pCBL-B_{LRR} variants with buffer of 50 mM HEPES (pH 7.5) and 50 mM NaCl. Final E3 concentrations are indicated in **Table 5-2**. After 2 min, reactions were quenched with 2X SDS loading buffer and DTT (100 mM), resolved by SDS-PAGE, and exposed to a phosphoimager. Under these conditions, UbcH5B~ 32 P-Ub variants are continuously regenerated by E1 and less than 0.2% of His-Ub Δ GG is modified by 32 P-Ub at the highest UbcH5B concentration, thus representing an initial rate of reaction. In addition, there was no observable autoubiquitination of CBL-B_{LRR} or pCBL-B_{LRR} variants. DiUb bands were quantified using ImageQuant (GE Healthcare). Control reactions were performed as described above. All reported kinetic parameters were determined by fitting three independent datasets to the Michaelis-Menten equation using SigmaPlot 8.0 (Systat Software Inc.).

2.8 Verify the crystallized complex by SDS-PAGE

To check if the crystals contain the complex of RING E3-E2-Ub, several large crystals were harvested from the crystallization drops with 30 μ l of mother liquor and transferred to a 1.5 ml Eppendorf tube. The crystals were then spun down in the tube and old mother liquor was replaced by fresh mother liquor. This step was repeated for 6-7 times to ensure no layers of original protein solution were present on the surface of crystals. The crystals were transferred again to a fresh Eppendorf tube to get rid of any protein solution stuck to tube walls. Finally, crystals were dissolved in protein loading buffer and loaded onto SDS-PAGE for characterization.

2.9 Surface plasmon resonance (SPR) assay

— E2 binding affinity of c-CBL variants (developed by Gary Sibbet)

c-CBL fragment constructs with N-terminal GST tag (about 2 mg/ml) and UbcH5B at high concentrate (20 mg/ml) were purified for SPR experiment. Binding experiments were conducted by Gary Sibbet at 25°C using a Biacore T100/T200 SPR instrument with a CM-5 chip. GST tagged wild-type c-CBL, mutant M222E and M222F were individually captured by anti-GST antibody which was coupled onto the chip. The response units were around 1,000-2,000. UbcH5B was serially titrated in running buffer (25 mM Tris (pH 7.6), 150 mM NaCl, 0.1 mg/ml BSA, 1 mM DTT and 0.005% (v/v) Tween-20) and floated onto the chip. Purified GST protein was used as a control. The data were analyzed by steady-state affinity analysis using the Biacore T100 and T200 evaluation software package (Biacore Life Sciences).

Chapter 3
Mechanism of Ub transfer by a dimeric RING E3,
BIRC7 (ML-IAP)

3 Mechanism of Ub transfer by a dimeric RING E3, BIRC7 (ML-IAP)

3.1 Aims and objectives

At the start of my PhD, how RING E3 promotes Ub transfer is unclear. Early biochemical studies suggested that RING E3s promote Ub transfer by allosterically activating E2 [36, 202], but this allosteric activation is not evident from available RING-E2 structures. The initial aim of this project is to obtain a crystal structure of a RING E3 bound to an E2~Ub complex. The structural information may provide insights into this process. However, it is challenging to obtain a stable RING E3-E2~Ub complex because E2~Ub with thioester linkage is rapidly dissociated into E2 and Ub in the presence of an E3. Mutating E2's active site cysteine to serine allows the generation of a stable oxyester linkage (UbcH5B_S~Ub), which mimics the thioester linkage. The late Cecile Pickart's group have shown that E2's conserved Asn (Asn77 in UbcH5B) contributes to isopeptide bond formation by stabilizing the oxyanion intermediate during lysine attack from substrate [36]. To increase the stability of E2~Ub for crystallization, we mutated Asn77 to alanine. Furthermore, UbcH5B's Ser22 was mutated to arginine to prevent backside binding with Ub [39].

Several dimeric RING E3s, such as RNF4 and BIRC3, display a higher binding preference for E2~Ub than a free E2 [203, 204]. Using surface plasmon resonance (SPR) analysis, my colleague Gary Sibbet investigated the binding affinity of several dimeric RING E3s for UbcH5B and UbcH5B_S~Ub. He showed that BIRC3, BIRC4, BIRC7 and MDM2/MDMX have a much higher binding affinity for UbcH5B_S~Ub than free UbcH5B (**Table 3-1**). To investigate how RING E3s activate E2~Ub thioester in catalysis and to understand the role of RING dimerization in E3 activity, I attempted to crystallize an E3-E2~Ub complex structure using aforementioned dimeric RING E3s and Ub-linked UbcH5B (S22R/N77A/C85S), termed as UbcH5B_{RAS}~Ub.

Table 3-1. Dissociation constants (K_d) for interactions between RING E3s, UbcH5B and UbcH5B_S~Ub variants.

| GST-immobilized protein | Analyte | K_d (μ M) |
|-------------------------|-------------------------|------------------|
| Various RING dimers | E2 or E2~Ub | |
| BIRC3 | UbcH5B | 300 ± 7 |
| BIRC3 | UbcH5B _S ~Ub | 5 ± 4 |
| BIRC4 | UbcH5B | 151 ± 3 |
| BIRC4 | UbcH5B _S ~Ub | 36 ± 1 |
| BIRC7 | UbcH5B | Not measurable |
| BIRC7 | UbcH5B _S ~Ub | 136 ± 2 |
| MDM2/MDMX | UbcH5B | Not measurable |
| MDM2/MDMX | UbcH5B _S ~Ub | 130 ± 31 |

Note: Due to the weak binding, E2 or E2~Ub concentrations could not be saturated for some of these measurements. Some K_d values were not measurable or were estimated according to the data obtained from steady-state. s.e.m. values are indicated.

In this chapter, I report the crystal structure of BIRC7 RING dimer (BIRC7_{239-C}) in complex with UbcH5B_{RAS}~Ub. Based on the structure, I describe the detailed interactions on E3–E2~Ub interfaces. In addition, I present biochemical analyses to validate the observed interactions. Lastly, I perform kinetic analyses on DiUb formation to gain insights into the molecular mechanism of Ub transfer by dimeric RING E3s.

3.2 Results

3.2.1 Strategies

I cloned and purified several dimeric RING domains from BIRC family (about 6-8 KDa). Sequence alignments show that the RING domains are highly conserved (**Figure 3-1**). Interestingly, BIRC7 RING domain lacks a conserved valine residue. This valine is located near the E2-binding surface based on the structure of BIRC3. It is likely that the absence of this valine residue may be responsible for the observed weak E2 and E2~Ub binding affinities (**Table 3-1**).

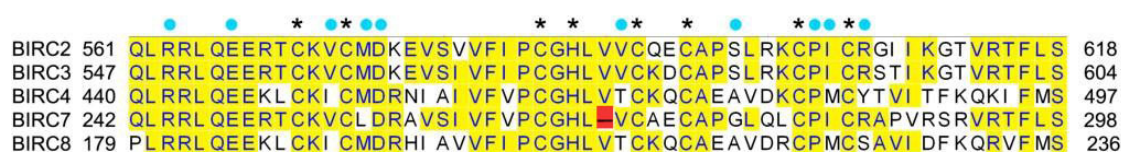


Figure 3-1. Sequence alignment of RING domains from BIRC family.

Proteins sequences were aligned by Clustal W method in MegAlign software. Conserved residues are highlighted in yellow. Residues that contact E2 Ubch5B are predicted based on the structure of Ubch5B–BIRC3 RING [37] and indicated by cyan dots. Asterisks indicate the Zn-binding ligands on the RING domains. Red box with a dash indicates that the conserved valine residue is absent in BIRC7.

Ubch5B_{RAS}~Ub was purified by my supervisor Danny Huang (**Chapter 2**). Purified BIRC RING domains were then mixed with Ubch5B_{RAS}~Ub at 1:1 molar ratio and screened against over 1000 different crystallization conditions. The screening was performed at 4 °C. Crystals were obtained for different BIRC–Ubch5B_{RAS}~Ub complexes. To confirm that crystals contain the BIRC–Ubch5B_{RAS}~Ub complex, the crystals were harvested, washed, and loaded on SDS-PAGE (**Chapter 2**). Despite containing the full complex, some complexes have poor diffraction quality or the Ub moiety was disorder upon solving the structure. After multiple rounds of screening and optimization, I finally obtained good diffracting BIRC7_{239-C}–Ubch5B_{RAS}~Ub crystals. **Figure 3-2a** shows the purity of BIRC7_{239-C} used in the crystallization and **Figure 3-2b** shows that the crystals contain both BIRC7_{239-C} and Ubch5B_{RAS}~Ub with around 1:1 molar ratio. The BIRC7–Ubch5B_{RAS}~Ub crystals have hexagonal shape with thickness (**Figure 3-2c**) and the optimized crystal diffracted to 2.18 Å.

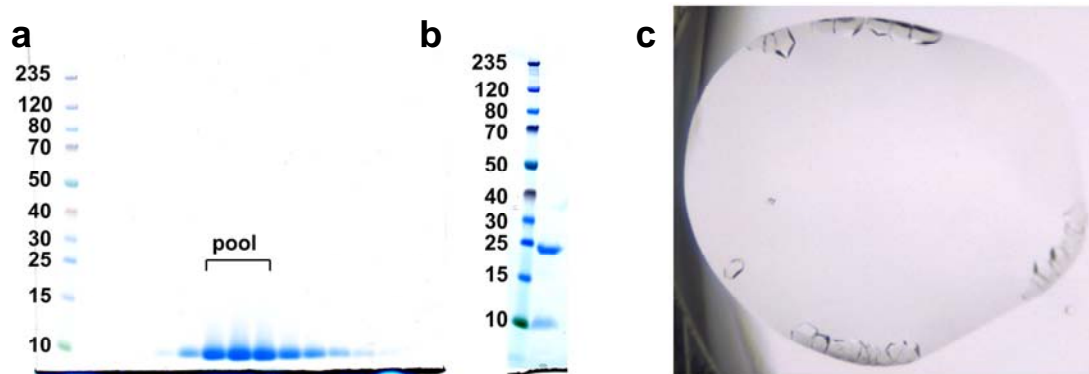


Figure 3-2. The purity of BIRC7 RING domain (BIRC7_{239-C}) and crystals of BIRC7_{239-C}-Ub_{H5}B_{RAS}-Ub.

(a) The RING domain of BIRC7 was purified by series of chromatography described in **Chapter 2**. The gel shows the purity of the protein after the final step, size-exclusion chromatography (SD75). Fractions were pooled as indicated for crystallization trials.

(b) The complex crystals were confirmed to contain Ub_{H5}B_{RAS}-Ub (higher band) and BIRC7_{239-C} (lower band).

(c) The crystals of BIRC7_{239-C}-Ub_{H5}B_{RAS}-Ub complex.

3.2.2 Structure of BIRC7_{239-C}-UbcH5B_{RAS}~Ub complex

The structure of BIRC7_{239-C} in complex with UbcH5B_{RAS}~Ub diffracts to 2.18 Å at synchrotron. The complex crystallized in space group P4₃2₁2 with two copies of BIRC7_{239-C}-UbcH5B_{RAS}~Ub heterotrimer per asymmetric unit. The two heterotrimers are similar to each other (r.m.s.d. of 0.43 Å for C α atoms). Data collection and refinement statistics are shown in **Table 3-2**.

Table 3-2. Data collection and refinement statistics.

| BIRC7 _{239-C} -UbcH5B _{RAS} ~Ub | |
|---|----------------------------------|
| Data Collection | |
| Space group | P4 ₃ 2 ₁ 2 |
| Cell dimensions | |
| a, b, c (Å) | 100.6, 100.6, 123.9 |
| α , β , γ (°) | 90, 90, 90 |
| Resolution (Å) | 30-2.18 (2.29-2.18) |
| R_{sym} (%) | 0.057 (0.621) |
| I/σ | 16.5 (3.3) |
| Completeness (%) | 99.8 (99.8) |
| Redundancy | 6.7 (6.6) |
| Wilson B factor | 45.9 |
| Refinement | |
| Resolution (Å) | 30-2.18 |
| No. reflections | 33958 |
| $R_{\text{free}}/R_{\text{work}}$ | 0.250/0.202 |
| No. atoms | |
| Protein | 4232 |
| Ions | 4 |
| Water | 153 |
| B -factors | |
| Protein | 63.9 |
| Ions | 35.1 |
| Water | 50.7 |
| R.m.s. deviations | |
| Bond length (Å) | 0.009 |
| Bond angles (°) | 1.239 |

Note: Highest-resolution shell is shown in parenthesis. $R_{\text{work}} = \Sigma|F_o - F_c|/\Sigma F_o$. R_{free} is the crossvalidation of R factor, with 5% of the total reflections omitted in model refinement.

The BIRC7_{239-C}-UbcH5B_{RAS}~Ub complex has a compact structure. The BIRC7 RING dimer dimerizes in a similar manner as in BIRC3 [37], and binds to two molecules of UbcH5B_{RAS}~Ub (**Figure 3-3**). The structure of UbcH5B_{RAS} and Ub resembles previously published UbcH5B and Ub structures [195] (r.m.s.d of 0.43 and 0.42,

respectively, for C α atoms). The structure of BIRC7 RING is similar to the BIRC3 RING domain [37] (r.m.s.d of 1.13 for Ca atoms). For discussion purposes, I differentiate molecules from the two heterotrimers with A or B subscripts (e.g. BIRC7_A or Ub_B, **Figure 3-3**). The quality of the electron density was better for subunit A, so I focus on subunit A and the C-terminal tail of BIRC7_B.

To maintain this structure, donor Ub interacts with both E2 and RING dimer. First, Ub_A is linked to UbcH5B_A's active site (Ser85 in my structure) through its C-terminal tail. Second, Ub_A interacts with UbcH5B_A's α 3 helix via its Ile44 surface. Third, the Ile36 surface of Ub_A contacts the RING domain of BIRC7_A. Notably, the C-terminal tail of BIRC7_B packs against Ub_A and the C-terminal tail of BIRC7_A packs against Ub_B (**Figure 3-3**).

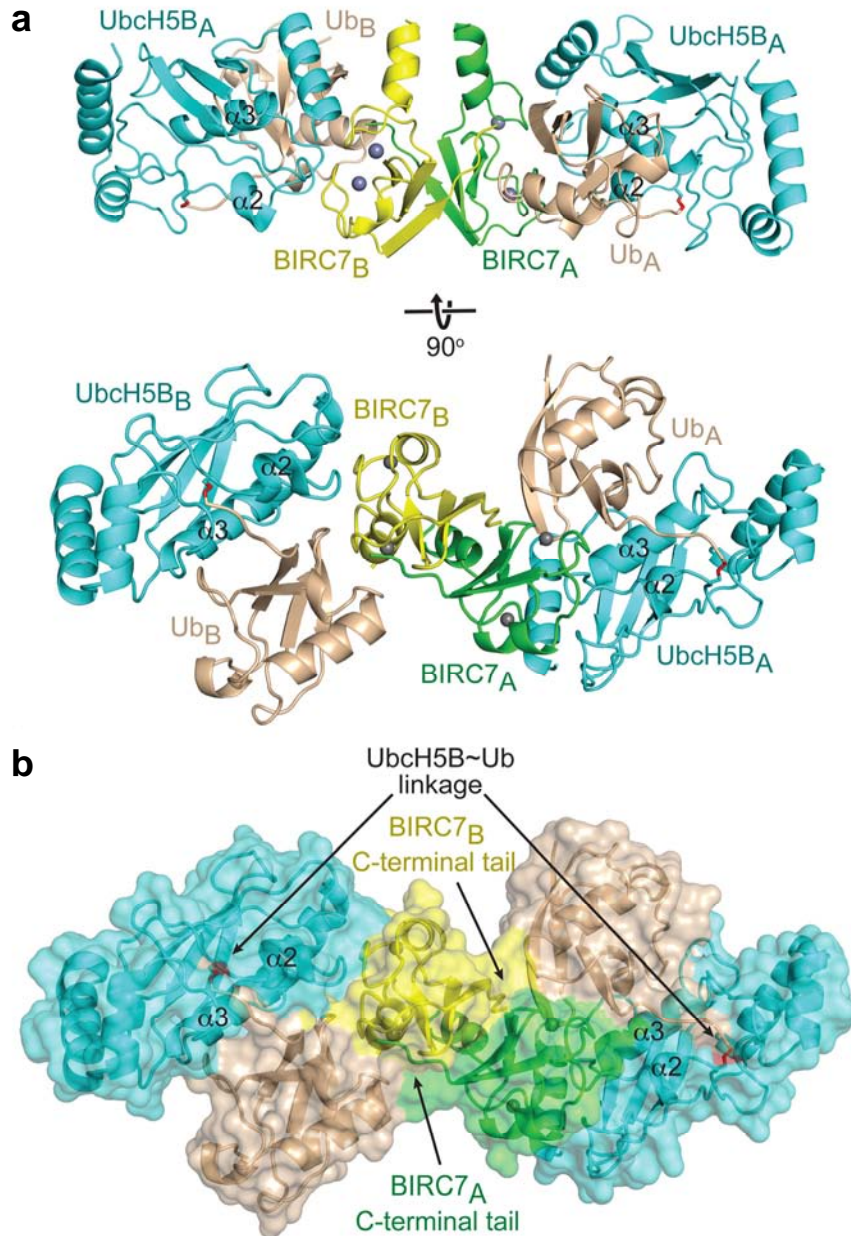


Figure 3-3. Complex structure of BIRC7_{239-C}-UbcH5B_{RAS}-Ub.

(a) Cartoon representation of the complex with two crystallographic trimers differentiated with A or B subscripts. Zn²⁺ atoms are demonstrated as gray spheres; Ub is coloured wheat, BIRC7_A green, BIRC7_B yellow, and UbcH5B cyan with the covalent linkage highlighted in red. Helices α2 and α3 from UbcH5B are labelled. The lower panel is rotated 90° around x-axis from the upper panel.

(b) Surface representation of the complex, coloured and oriented as in the lower panel of a. The oxyester linkages in UbcH5B_{RAS}-Ub and the C-terminal tails of the BIRC7_{239-C} dimer are indicated with arrows.

3.2.3 Detailed interactions and validation

3.2.3.1 UbcH5B-Ub's Ile44 patch interactions

In the Ub system, E2~Ub thioester undergoes lysine attack by substrates, resulting in the formation of an isopeptide bond between the C-terminal tail of Ub and substrate's lysine [205]. Surfaces on Ubs and E2s have been reported to be crucial in Ub transfer. A study on E2 Cdc34 showed that the mutations on Ub's Ile44 surface (I44A or R42E) are defective in Ub transfer. However, these defects, Ub I44A and R42E, can be rescued by Cdc34's $\alpha 3$ mutations, S129 and E133R, respectively, suggesting that the interactions between the Ub's Ile44 patch and E2's $\alpha 3$ are crucial for efficient thioester discharge [76]. The existing structures of E2~Ub demonstrate that the conjugated Ub is able to adopt multiple conformations against E2s (**Figure 3-4**) and does not explain how this interaction is important for Ub transfer.

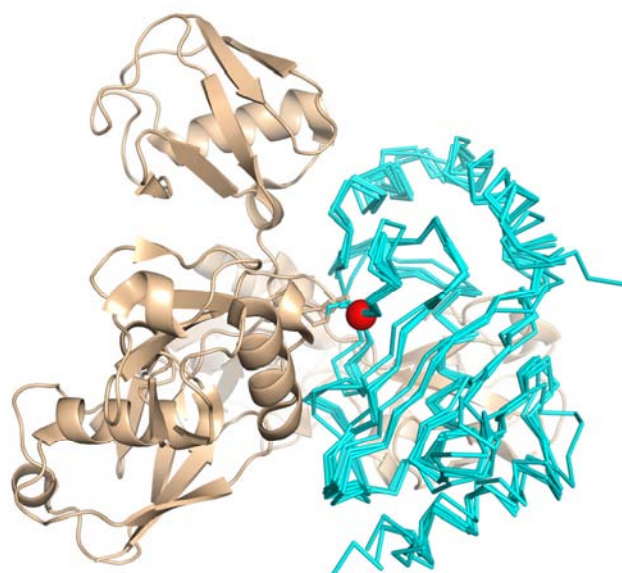


Figure 3-4. Ub adopts multiple conformations in E2~Ub complex structures or NMR models.

E2s from E2~Ub structures, models or E2~Ub portions were aligned and shown in ribbon representation, coloured cyan (PDB ID 3A33 [195], 2GMI [206], 3UGB [207], 1FXT [208], 3JW0 [209]). Covalent linked Ubs are shown in cartoon representation and coloured wheat. The active sites of E2s are shown in red spheres.

In my structure, the conjugated Ub interacts with UbcH5B's $\alpha 3$ via its Ile44 surface, Notably, UbcH5B_{RAS}~Ub conformation and UbcH5B-Ub interactions do not resemble most E2~Ub structures, but is close to a previous NMR model [208]. The UbcH5B-Ub interactions are stabilized by hydrophobic interactions between the side chains of Ub's Ile44 and UbcH5B's Ser108; between the side chains of Ub's His68, Val70, and

UbcH5B's Leu104; between side chains of Ub's Leu8 and UbcH5B's Leu97. Hydrogen bonds are formed between the side chains of Ub's Arg42 and UbcH5B's Asp112 and Ser108; between the side chain of Ub's Lys48 and the backbone oxygen of UbcH5B's Asn; between the backbone oxygen of Ub's Lys6, Leu69 and the side chain of UbcH5B's Lys101 (**Figure 3-5**).

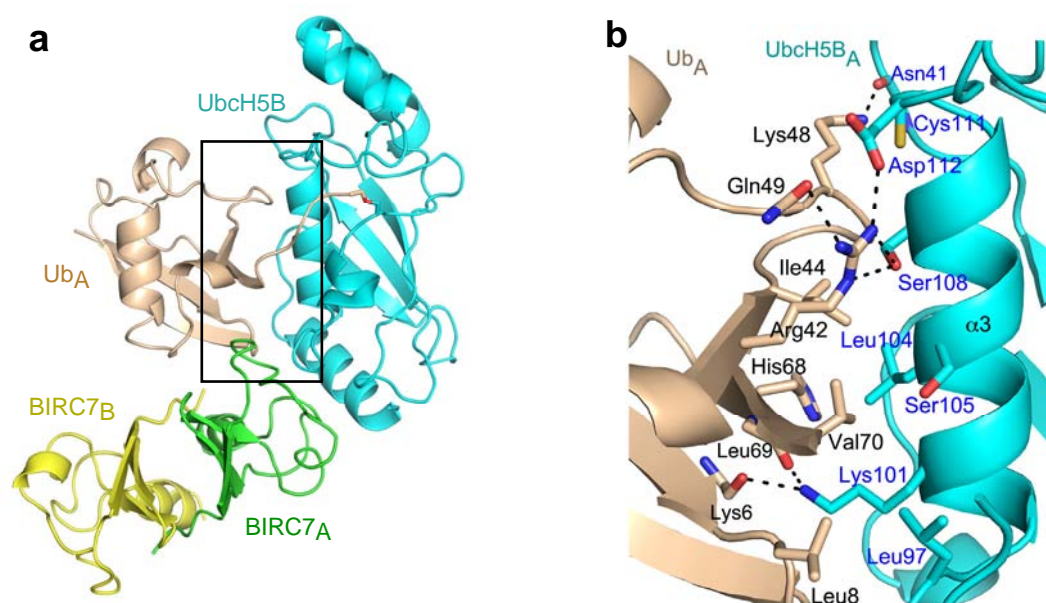


Figure 3-5. Detailed interactions of the E2-Ub's Ile44 surface.

(a) Overall structure of BIRC7 RING dimer bound to UbcH5B~Ub, coloured as in **Figure 3-3a**. The interface of E2-Ub's Ile44 patch is shown inside the rectangle box.

(b) The close-up view of the E2-Ub's Ile44 surface. Key residues are shown as sticks representation and coloured is as in **Figure 3-3**, with N atoms blue, O atoms red, and S atoms yellow. Putative hydrogen bonds are shown as dashed lines.

To assess the importance of the observed interactions, *in vitro* assays were performed including lysine-discharge, BIRC7 autoubiquitination and SMAC ubiquitination assays (**Appendix 2**. Contribution list). Lysine-discharge assay measures the single-turnover Ub transfer from the E2's active site to the free lysine (acceptor) [210]. The reactions were monitored by the disappearance of E2~Ub bands on the SDS-gels. To eliminate mutational effect from E1-catalysed E2~Ub formation, reactions were performed under pulse-chase condition as described in **Chapter 2**. At time zero, over 90% of UbcH5B was charged with Ub observed by SDS-PAGE (**Figure 3-6a**). For UbcH5B mutants, the reactions were performed using ^{32}P -Ub and UbcH5B variants were charged with ^{32}P -Ub equivalently as visualized by autoradiogram (**Figure 3-6b**

and c). In wild-type reactions, almost 90% of UbcH5B~Ub or UbcH5B~³²P-Ub were discharged after 45 second and reactions were complete after 90 second. Mutations on the E2-Ub's Ile44 surface include UbcH5B's K101E, L104A, S108R, D112A and Ub's L8D, R42E, I44A, G47E, Q49E, and H68A/V70A were defective in lysine-discharge assay. UbcH5B's S22R mutation that is distal to the Ub's Ile44 surface, displayed similar activity to wild type (**Figure 3-6**).

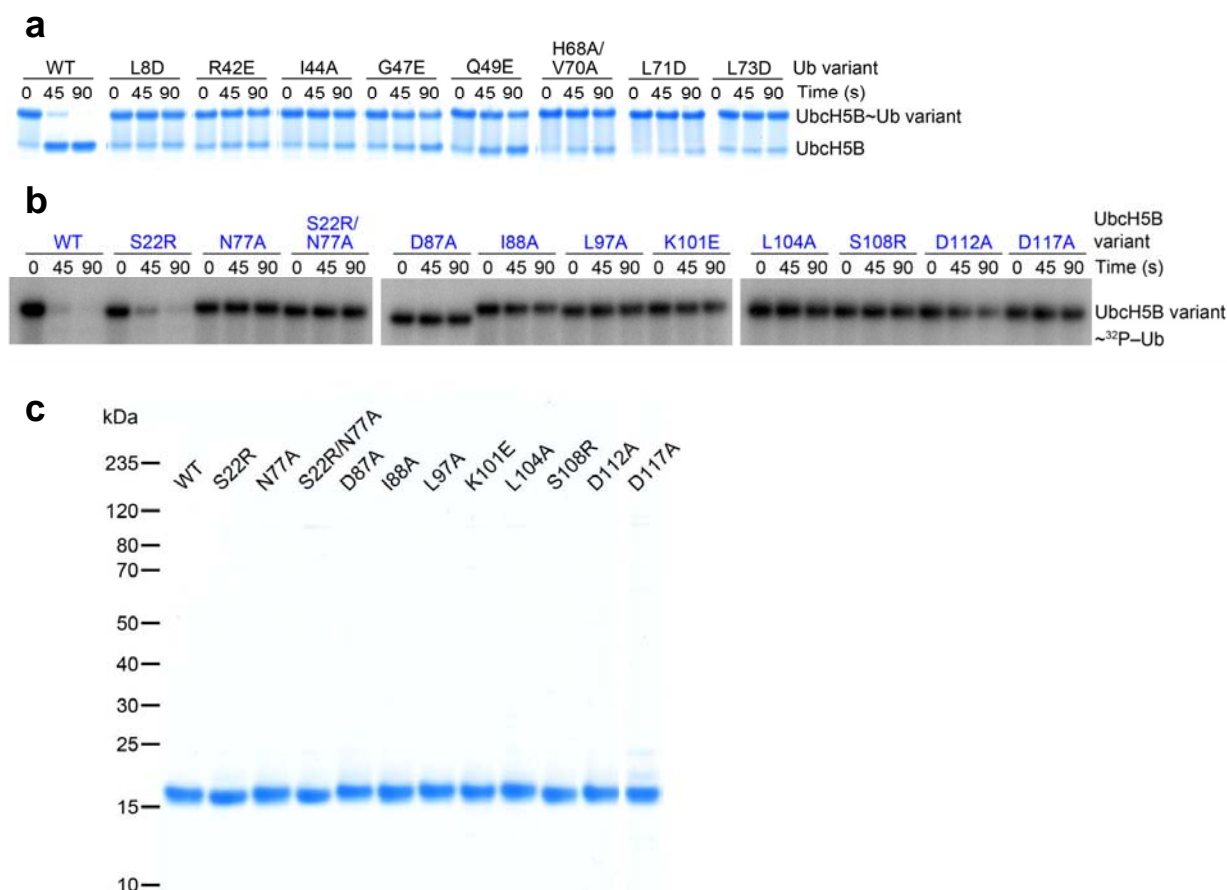


Figure 3-6. Lysine-discharge reactions to validate the E2-Ub interfaces.

(a) Nonreduced SDS-PAGE shows the disappearance of UbcH5B~Ub with full-length BIRC7, L-lysine and Ub variants over time.

(b) As in a but for UbcH5B variants and visualized by autoradiograms of the disappearance of UbcH5B~³²P-Ub.

(c) The purity of UbcH5B variants. 2µg of UbcH5B variants were loaded on SDS-PAGE.

E3s have been reported to undergo autoubiquitination both *in vivo* and *in vitro* [69, 211]. BIRC7 autoubiquitination assay was performed using full-length BIRC7 to investigate mutational defects on poly-Ub chain formation. XIAP has been reported to promote SMAC ubiquitination *in vitro* [101]. I found that BIRC7 also catalyses SMAC ubiquitination, but BIRC7 autoubiquitination also occurred simultaneously

(**Figure 3-7**). To quantify the mutational effects on substrate ubiquitination, radioactively labelled SMAC was used.

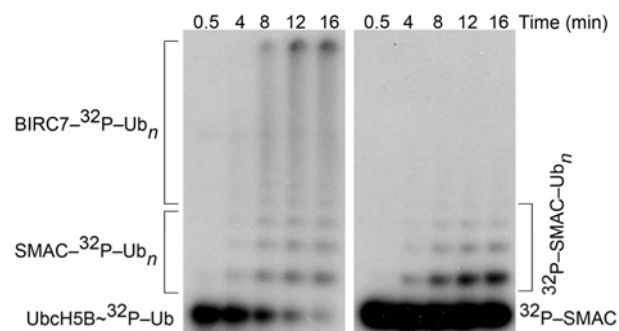


Figure 3-7. Autoubiquitination of BIRC7 occurs in SMAC ubiquitination assays.

Left: Non-reduced autoradiogram of SMAC ubiquitination shows the disappearance of UbcH5B-³²P-Ub, the formation of BIRC7-³²P-Ub_n and the formation of SMAC-³²P-Ub_n over time with wild-type UbcH5B, BIRC7 and ³²P-Ub under pulse-chase conditions.

Right: Non-reduced autoradiogram shows the formation of ³²P-SMAC-Ub_n over time. Reactions were performed under the same conditions as in the left panel but with ³²P-SMAC and unlabeled Ub. Ub_n indicates poly-Ub chain.

Mutations of key residues on UbcH5B's $\alpha 3$ (K101E, L104A, S108R and D112A) and Ub's Ile44 surface (L8D, R42E, I44A, G47E, Q49E and H68A V70A) cause defects in Ub transfer in autoubiquitination and SMAC ubiquitination. Unlike lysine-discharge (**Figure 3-6b**), UbcH5B S22R mutant was defective in autoubiquitination and SMAC ubiquitination, presumably due to the role of Ser22 in poly-ubiquitination (**Figure 3-8**).

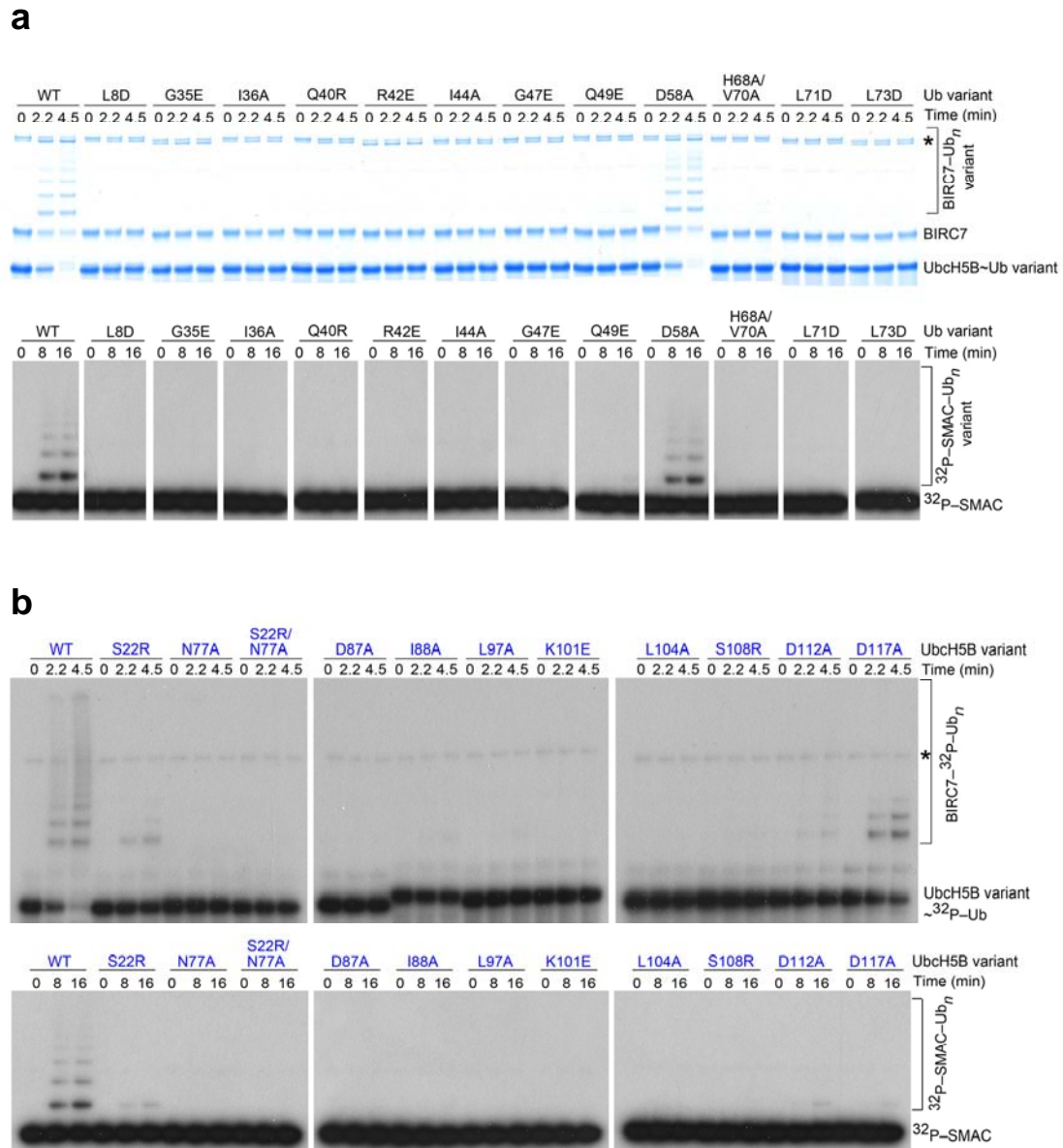


Figure 3-8. Assays of BIRC7 autoubiquitination and SMAC ubiquitination *in vitro*.

(a) Mutational analyses of Ub variants. Upper panel: non-reduced SDS-PAGE of shows the formation of Ub products and disappearance of UbcH5B~Ub with full-length BIRC7 and Ub variants over time. The asterisk indicates the E1~Ub band. Lower panel: non-reduced autoradiogram shows the formation of ^{32}P -SMAC~Ub_n over time with full-length BIRC7, ^{32}P -SMAC and Ub variants.

(b) Mutational analyses of UbcH5B variants. Upper panel: same as in the upper panel of **a**, but with UbcH5B variants. Lower panel: same as in the lower panel of **b**, but with UbcH5B variants. Ub_n indicates poly-Ub chain.

3.2.3.2 UbcH5B-Ub's tail interactions

Ub_A's Gly76 is conjugated to Ser85 of UbcH5B_A and the C-terminal tail of Ub_A is extended and stabilized by residues from UbcH5B_A's $\alpha 2$. Hydrophobic interactions are formed between Ile88 of UbcH5B_A and Leu73 of Ub_A; between Leu97 of UbcH5B_A and Ub_A's Leu8 and Leu71. In addition, hydrogen bonds occur between the side chains of UbcH5B_A's Asp112 and Ub_A's Arg42; between the side chain of UbcH5B_A's Asp87 and the backbone nitrogen of Ub_A's Arg74; and between the backbone nitrogen of UbcH5B_A's Asp87 and the backbone oxygen of Ub_A's Arg74. Furthermore, BIRC7_A's Arg286 also contributes to stabilize the configuration of the Ub's tail. Hydrophobic interaction occurs between BIRC7_A's Arg286 and Leu71 of Ub. Hydrophilic interactions are formed between the side chains of Arg286 and Ub_A's Gln40; and between the side chains of Arg286 and the backbone oxygen of Ub_A's Arg72. BIRC7_A's Arg286 also interacts with the backbone oxygen of UbcH5B_A's Gln92 (**Figure 3-9**).

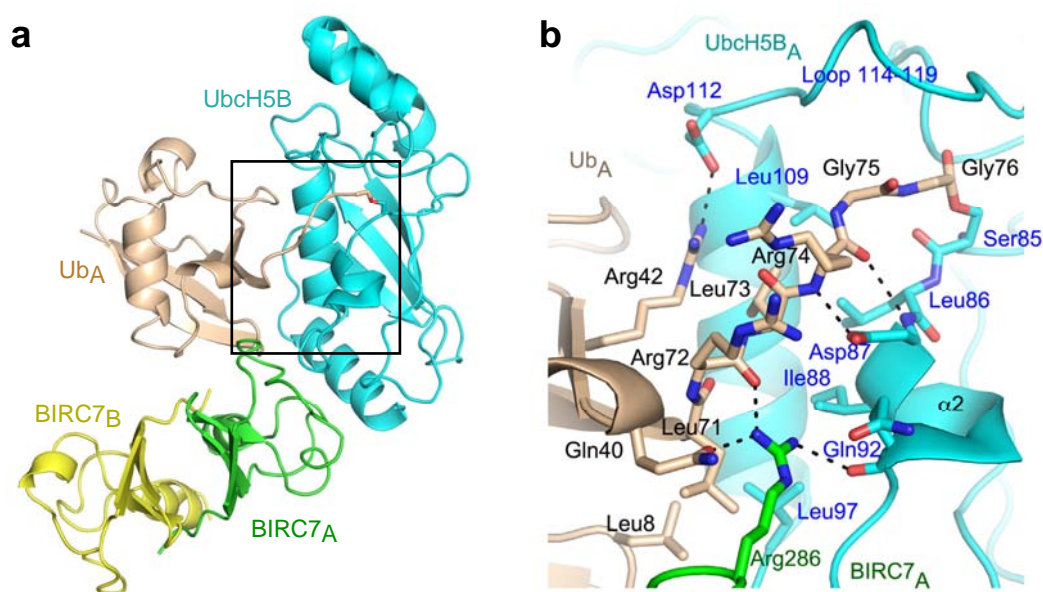


Figure 3-9. Detailed interactions on the E2-Ub's tail surface.

(a) Overall structure of BIRC7 RING dimer bound to UbcH5B~Ub, coloured as in **Figure 3-3a**. The interface of E2-Ub's tail is shown inside the rectangle box.

(b) Detailed interactions of the E2-Ub's tail surface. Key residues are shown as sticks and coloured as in **Figure 3-3**, with N atoms blue and O atoms red. Putative hydrogen bonds are shown as dashed lines.

To verify the importance of these interactions in Ub transfer, several mutants were tested, including UbcH5B's D87A, I88A, L97A and Ub's L71D and L73D. Mutations on the E2-Ub's tail interface caused defects in lysine-discharge, BIRC7 autoubiquitination and SMAC ubiquitination assays (**Figure 3-6 and 3-8**). A conserved asparagine near the E2's active site (eg Asn77 in UbcH5B) is thought to stabilize the oxyanion intermediate that forms during nucleophilic attack [36, 202]. However, in my structure, Asn77 is mutated to Ala. Modelling of an asparagine at this position showed that carbonyl oxygen of Ub's Gly76 is within the hydrogen bond distance of Asn77 side chain. Consistent with the importance of Asn77, UbcH5B N77A mutant was defective in BIRC7-mediated Ub transfer (**Figure 3-6, 3-8**).

Furthermore, loop 114-119 of UbcH5B that is adjacent to the Ub tail appears to be flexible. The electron density for the loop 114-119 is poor. The average B factors for Gly75 and Gly76 of Ub (115 \AA^2) and loop 114-119 of UbcH5B (95.7 \AA^2) are high compared to that of the overall structure, suggesting these regions are not well ordered (**Figure 3-10a**). In existing UbcH5~Ub structures, this loop is stabilized by hydrophilic interactions with Asn77. In this conformation, the side chain of Asp117 interacts with the amide of Ub's Gly76 [207] (**Figure 3-10b**). Thus, the disordered UbcH5B loop 114-119 region in my structure may be due to N77A mutation.

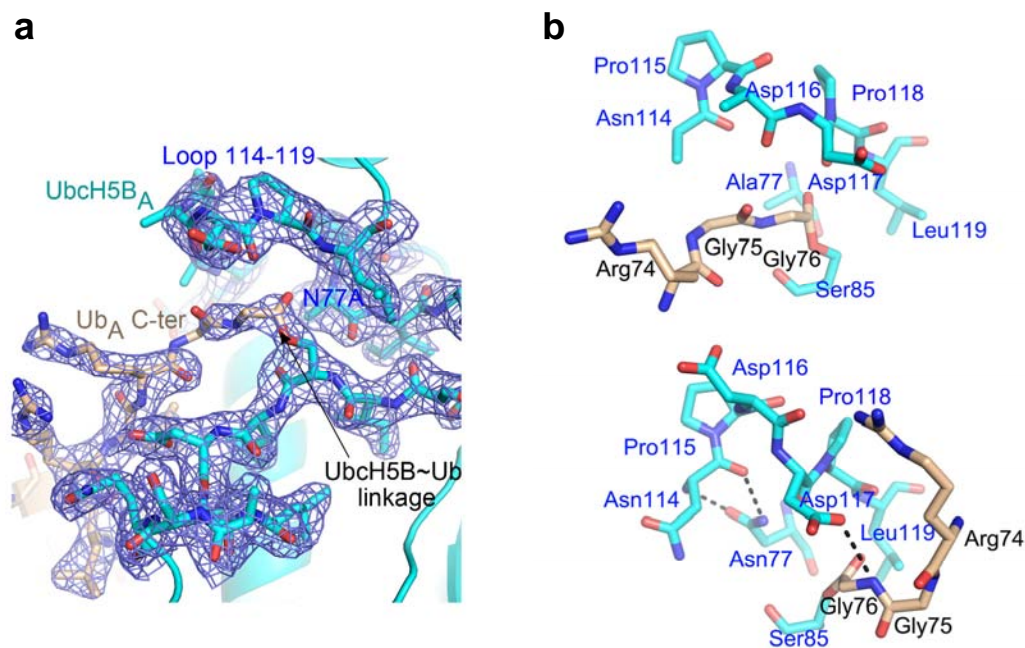


Figure 3-10. Detailed interactions between UbcH5B's loop 114-119 and Ub's tail.

(a) Electron density map of the UbcH5B_A~Ub_A linkage, UbcH5B_A loop 114-119 and Ub_A tail-UbcH5B_A interactions, with key residues shown as sticks and coloured as in **Figure 3-3**, with N atoms blue and O atoms red. 2Fo – Fc electron density (blue) contoured at 1.0 sigma is shown.

(b) Upper panel: key residues on UbcH5B's loop 114-119 and Ub tail from my structure are shown as sticks and coloured as in **Figure 3-3**, with N atoms blue and O atoms red. Lower panel: same as in upper panel but from the structure of UbcH5C~Ub (PDB 3UGB [207]). Putative hydrogen bonds are shown as dashed lines.

3.2.3.3 BIRC7 RING-Ub's Ile36 patch interactions

In addition to E2-Ub's Ile44 patch and E2-Ub's tail interactions, Ub_A's Ile36 patch makes extensive contacts with the BIRC7_A RING domain and BIRC7_B's C-terminal tail, providing the first structural evidence of donor Ub-RING interactions (**Figure 3-11**). Leu8, Thr9, Ile36 and Pro37 on Ub_A form hydrophobic contacts with BIRC7_A's Ile284, His269 and Cys285. Hydrogen bonds occur between the side chains of BIRC7_A's Arg286 and Ub_A's Gln40, and between the side chain of BIRC7_A's His269 and the backbone oxygen of Ub_A's Glu34. The C-terminal tail of BIRC7_B contacts Ub_A via hydrophilic and hydrophobic interactions. Hydrogen bonds are formed between the side chains of BIRC7_B's Arg294 and the side chain and backbone oxygen of Ub_A's Asp32. Hydrophobic interactions occur between BIRC7_B's Phe296 and Ub_A's Gly35; between BIRC7_B's Ser298 and Ub_A's Thr9, Lys11 (**Figure 3-11**).

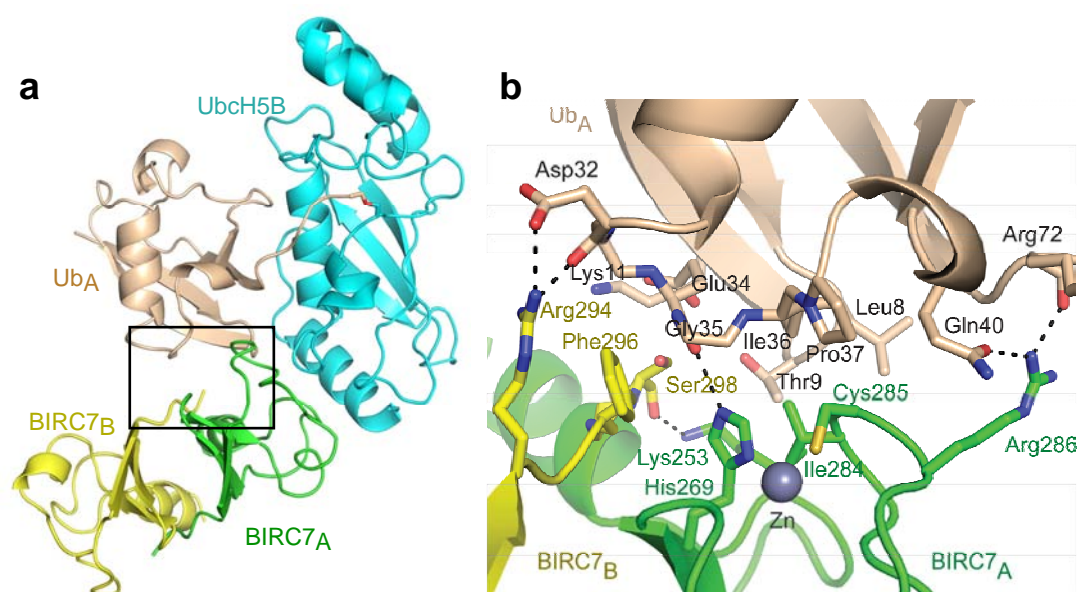


Figure 3-11. Detailed interactions on the E3-Ub's Ile36 surface.

(a) Overall structure of BIRC7 RING dimer bound to UbcH5B~Ub, coloured as in **Figure 3-3**. The interface of E3-Ub's Ile36 is shown inside the rectangle box.

(b) Detailed interactions of the E3-Ub's Ile36 surface. Key residues are shown as sticks representation and coloured as in **Figure 3-3**, with N atoms blue, O atoms red, and S atoms yellow. Putative hydrogen bonds are shown as dashed lines.

These interactions were validated by lysine-discharge and BIRC7 autoubiquitination assays (**Figure 3-12**). Compared to wild-type reactions, Ub mutants on the RING-Ub's Ile36 patch were defective in lysine-discharge assay. Asp58 of Ub is distal from any donor Ub interface, thus D58A displayed similar activity to wild type. BIRC7

mutations that disrupt the E2-binding surface (V254A) or E3-Ub interface (I284A, R286A, F296H) were defective in ubiquitination assay. Mutant with a C-terminal tail deletion was also defective (Δ 296-298).

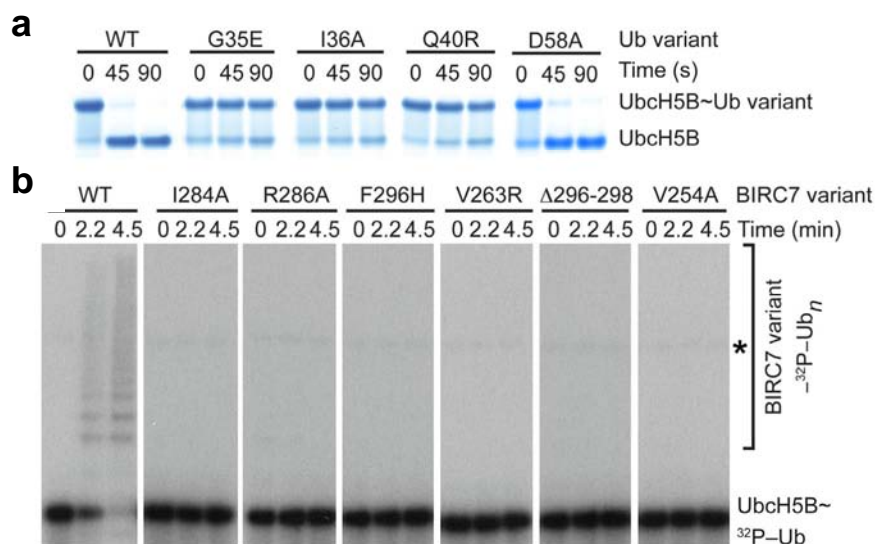


Figure 3-12. *In vitro* ubiquitination assay to validate the E3-Ub's Ile36 patch interface.
(a) Non-reduced SDS-PAGE shows the disappearance of UbcH5B~Ub with full-length BIRC7, L-lysine and Ub variants over time.
(b) Mutational analyses of full-length BIRC7 variants. Non-reduced autoradiogram shows the formation of ^{32}P -Ub products and disappearance of UbcH5B~ ^{32}P -Ub over time with full-length BIRC7 variants. The asterisk indicates the E1~Ub band. Ub_n indicates poly-Ub chain.

3.2.4 Dimerization required for RING E3 activity

The RING domains of BIRC family proteins are highly conserved (**Figure 3-1**). Previous studies showed that the BIRC RING domains form stable dimers in solution [37]. The hydrophobic dimer interface is formed between the C-terminal tail from one subunit and the core of the RING domain from the other; and between the N-terminal helices from both subunits. Moreover, the conserved hydrophilic interactions near the N-terminal helices are present in BIRC dimers (eg. between Arg250 and Glu249 in BIRC7) [37, 128] (**Figure 3-13a**).

Dimerization is required for dimeric RING E3 activity [54, 55]. As shown in **Figure 3-13b**, Val263 is a key residue on the dimer interface. Mutating Val263 to arginine

presumably disrupts this interface. Phe296, Leu297 and Ser298 are the last three residues at the C-terminal tail involved in dimerization, thus a tail deletion mutant ($\Delta 296-298$) may not dimerize. Size-exclusion chromatography showed that these full-length mutants eluted later than wild-type BIRC7, suggesting that they exist as monomers in solution (**Figure 3-14**). BIRC7 autoubiquitination assay showed that monomeric mutants (V263R, $\Delta 296-298$) were defective in Ub transfer (**Figure 3-12b**).

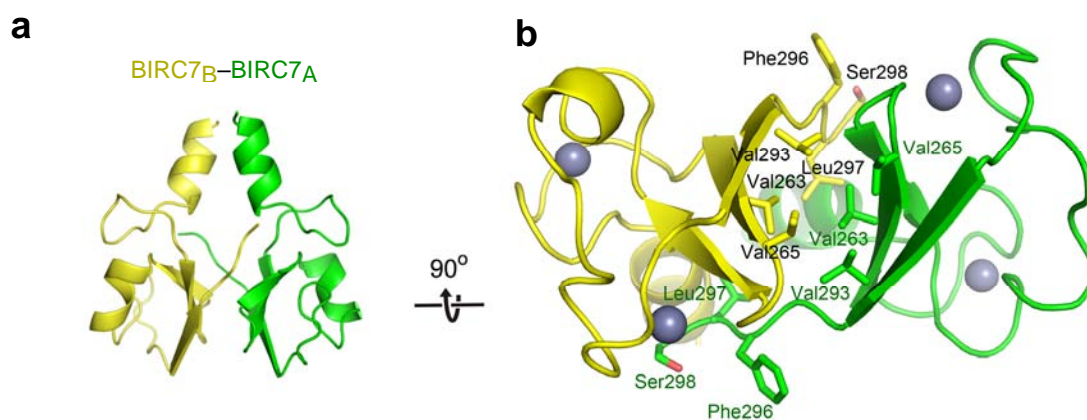


Figure 3-13. The BIRC7_{239-C} dimer interface.

(a) The BIRC7_{239-C} dimer from the structure of BIRC7_{239-C}-Ubch5B_{RAS}~Ub. BIRC7_A is coloured green and BIRC7_B yellow.

(b) Detailed hydrophobic interactions on the dimer interface. Key residues are shown as sticks and coloured as in a. Zn²⁺ atoms are demonstrated as gray spheres.

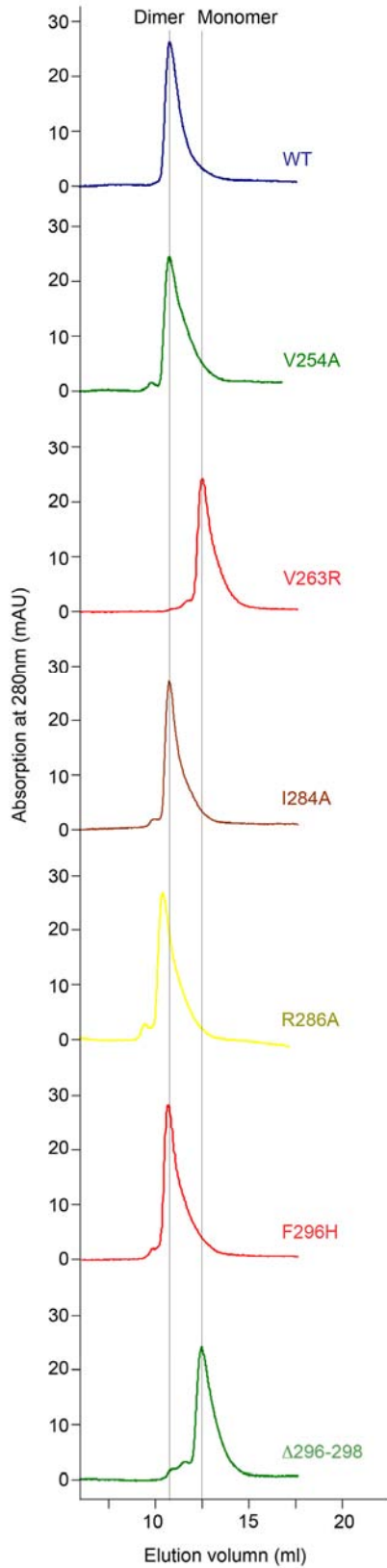


Figure 3-14. BIRC7 dimerization.

Purified full-length BIRC7 variants (120 μ g) were passed over size-exclusion chromatography (SD75 GE).

3.2.5 The cross-dimer arrangement required for Ub transfer

My structure shows that BIRC7_{239-C} dimer recruits two UbcH5B~Ub complexes, but competent binding of a single UbcH5B~Ub complex requires both RING domains. The RING domain of one subunit binds an UbcH5B~Ub and the tail of the other contacts the globular body of Ub, which is termed as the cross-dimer arrangement (**Figure 3-3**).

To probe the importance of cross-dimer arrangement, we hypothesised that a dimer that comprises a subunit with a RING mutation and a second subunit with a tail mutation should be active as it retains the ability of binding an UbcH5B~Ub complex. Val254 is the key residue on the E2-binding surface. Dimeric V254A mutant was defective in Ub transfer (**Figure 3-12b and 3-14**). Based on an early study of RNF4 [203], I generated a tail F296H mutant, which was defective in Ub transfer, but maintained RING dimerization (**Figure 3-12b and 3-14**). Initially, I tried co-expression of these two mutants in *E. coli* cells where one mutant is expressed with a GST-tag and the other with a His-tag. However, due to the dimerization of GST protein, I did not obtain the V254A/F296H heterodimer at 1:1 ratio. Instead, I assumed that BIRC7 RING domain dimer might associate and dissociate in solution. By mixing the V254A and F296H homodimers in solution, I may obtain V254A/F296H heterodimer leading to enhancement in ubiquitination. Indeed, the mixture of purified V254A and F296H homodimers led to an enhancement in ubiquitination (**Figure 3-15**). Therefore, the cross-dimer arrangement is required for UbcH5B~Ub recruitment and dimeric RING E3 activity.

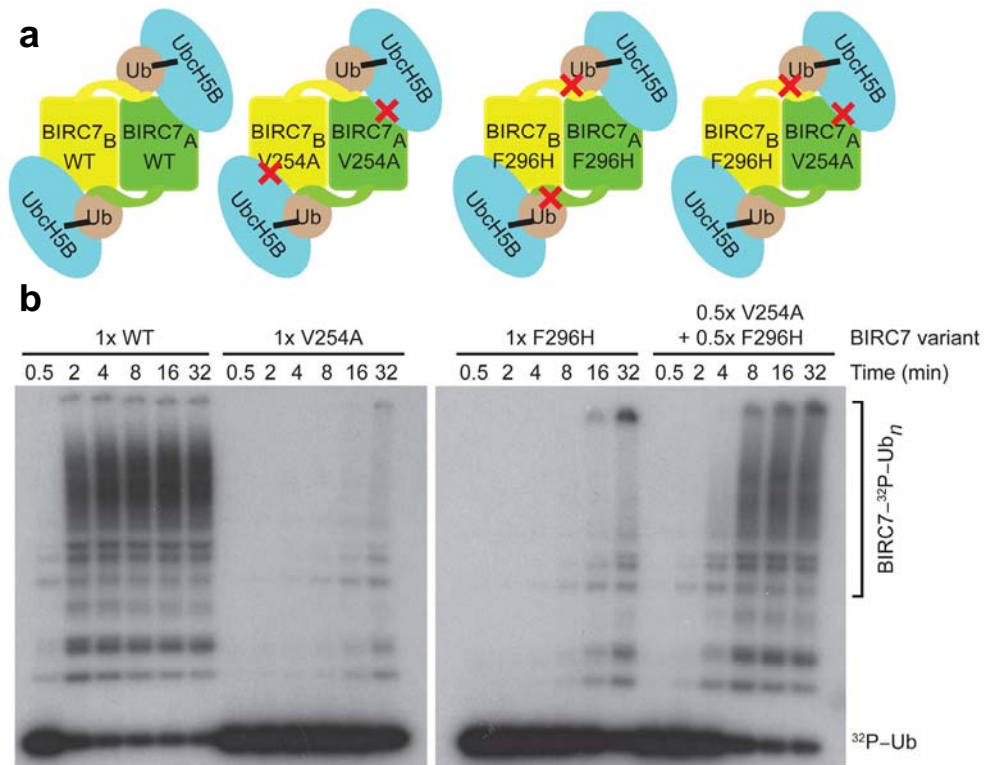


Figure 3-15. The cross-dimer arrangement is required for E3 activity.

(a) Experimental design to validate the interactions between dimeric E3 and Ub. BIRC7 mutants expected to disrupt (red Xs) the BIRC7 RING-UbcH5B interaction (V254A) or the BIRC7 tail-Ub interaction (F296H) are shown. A heterodimer of the RING and tail mutants should be more active than a homodimer of either mutant.

(b) Reduced autoradiograms show the formation of ³²P-Ub products with wild-type UbcH5B, and full-length BIRC7 variants over time.

3.2.6 Kinetic validation of the BIRC RING–E2~Ub model

3.2.6.1 Kinetic assay design

My structure and biochemical data suggest that the cross-dimer arrangement is not only crucial for binding E2~Ub, but is also involved in stabilizing the donor Ub configuration for transfer. Ub's globular body and tail appear to be positioned in an optimal configuration that is poised for transfer. It seems that the position of Ub's globular body has a direct impact on the Ub's C-terminal tail configuration and hence the reactivity of the E2~Ub thioester bond. Thus, mutations in the globular Ub interactions are expected to have an impact on E2~Ub binding (K_m) as well as the tail configuration and therefore resulted in decrease in the rate of Ub transfer (k_{cat}). To verify this hypothesis, kinetic analyses were performed on BIRC7-mediated DiUb formation (a brief introduction of enzyme kinetics refers to **Appendix 3**. Enzyme kinetics). To eliminate BIRC7 autoubiquitination, I used BIRC7_{239-C} instead of full-length BIRC7. The donor Ub was labelled with ³²P-ATP. His-tagged Ub was used as the acceptor Ub, which cannot be radioactively labelled. The DiUb formation reactions can be considered the following scheme:



To determine the kinetic constants, kinetic analyses were performed under initial rate condition. The initial rate condition was determined by performing time courses of product (DiUb) formation under multiple E2~Ub and E3 concentrations (**Figure 3-16**). We assume that the reactions are within the initial rate when less than 10% of E2~³²P-Ub is transferred to His-Ub. This can be determined by the amount of E2~³²P-Ub left and DiUb (³²P-Ub– His-Ub) formed in the assay. Once the initial rate condition is satisfied, the reaction is performed with varying E2~Ub concentrations and then Michaelis-Menten constants can be obtained by plotting the reaction rate against E2~Ub concentration.

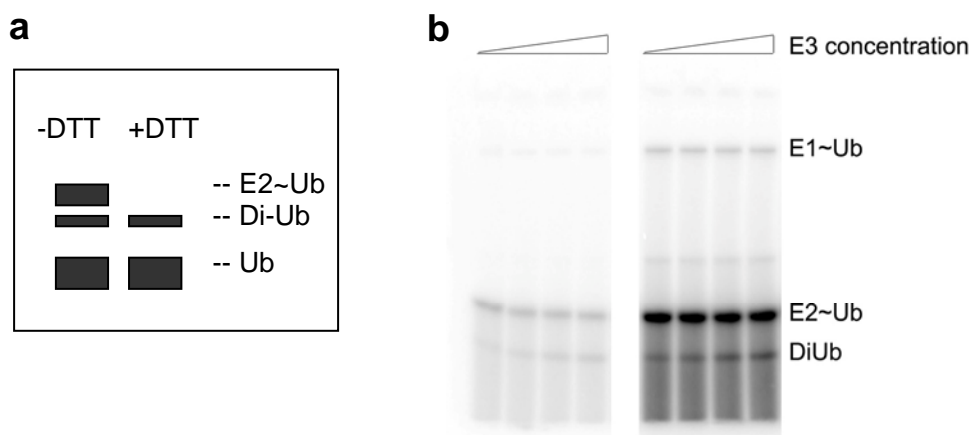


Figure 3-16. Initial kinetics reactions under certain conditions.

(a) Strategy for visualization of DiUb formation with or without DTT.

(b) An example of non-reduced autoradiogram shows the DiUb formation at the lowest (left panel) and highest (right panel) concentrations of UbcH5B~Ub with an increasing concentration of E3. Total product is equal to the amount of UbcH5B~³²P-Ub and DiUb formed. Certain concentration of E3 that catalysed less than 10% product formation is selected for subsequent kinetic analyses.

To minimize mutational effects on E1-catalysed UbcH5B~Ub formation, UbcH5B variants were pre-charged with ³²P-Ub variants and then the reactions were stopped by addition of apyrase and EDTA. UbcH5B~³²P-Ub variants were then diluted to different concentrations and added to a reaction containing His-Ub and E3 variants. His-Ub that does not contain protein kinase A recognition sequence cannot be radioactively labelled, thus it serves as acceptor Ub. The final concentration of His-Ub is 820 μM, which is the highest achievable acceptor Ub concentration that we can add to the reaction mixture. At this concentration, it is unlikely that acceptor Ub will saturate UbcH5B's active site, because the acceptor Ub is not bound to BIRC7_{239-C}. Therefore, any significant change in acceptor Ub concentration during the reaction will have an impact on the kinetic constants. However, under these reaction conditions, less than 0.4% of total His-Ub is converted to DiUb and thus we assume that acceptor Ub is at a fixed concentration during kinetic analyses. By fixing acceptor Ub concentration, I can investigate the effects of BIRC7_{239-C}-UbcH5B~Ub interactions on catalysis. Kinetic data process and original autoradiogram representation are shown in **Appendix 3**.

The kinetic parameters for the reaction catalysed by wild-type BIRC7_{239-C} were first measured using wild-type Ub and UbcH5B. Unfortunately, at 30 μM of UbcH5B~Ub,

BIRC7-catalysed reaction only approached saturation (**Figure 3-17**), presumably due to the weak E2~Ub binding affinity (**Table 3-1**). Defective mutants are likely to have higher K_m values and would be more difficult to achieve saturation. I concluded that BIRC7_{239-C} is not suitable for kinetic analyses.

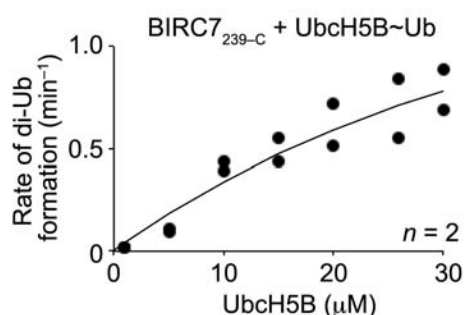


Figure 3-17. Wild-type BIRC7_{239-C} kinetic data.

Single-turnover kinetics of DiUb formation is catalysed by BIRC7_{239-C} (1 μM) under pulse-chase conditions. The rate of DiUb formation is plotted against UbcH5B concentration. *n* indicates the number of replicates.

3.2.6.2 BIRC RING domain sequence and structural alignments

BIRC3 RING domain (BIRC3_{541-C}) binds UbcH5B_S~Ub much tighter than BIRC7_{239-C} (about 25-fold higher) (**Table 3-1**), suggesting that BIRC3_{541-C} may be suitable for kinetic analyses. The RING domain of BIRC3 resembles the one of BIRC7 (r.m.s.d 1.13 Å) and the sequences are 74% identical (**Figure 3-18a and c**). A model of BIRC3_{541-C}-UbcH5B_{RAS}~Ub was built by superposing the RING domain of BIRC3 (PDB 3EB5 [37]) onto BIRC7_{239-C} in my structure (**Figure 3-18b**). In the sequence alignment, the BIRC7 residues that interact with Ub in my structure are identical to those in BIRC3. Besides, all of the BIRC7-Ub interactions observed in my structure are present in the model of BIRC3-UbcH5B~Ub complex. To confirm that the mechanism of Ub transfer catalysed by BIRC3_{541-C} and BIRC7_{239-C} are similar, lysine-discharge assays were performed using the same sets of mutants tested in the BIRC7 assays (**Figure 3-6 and 12**). The activity profiles were identical, where all of the mutants were defective in Ub transfer except UbcH5B's S22R and Ub's D58A (**Figure 3-18d**).

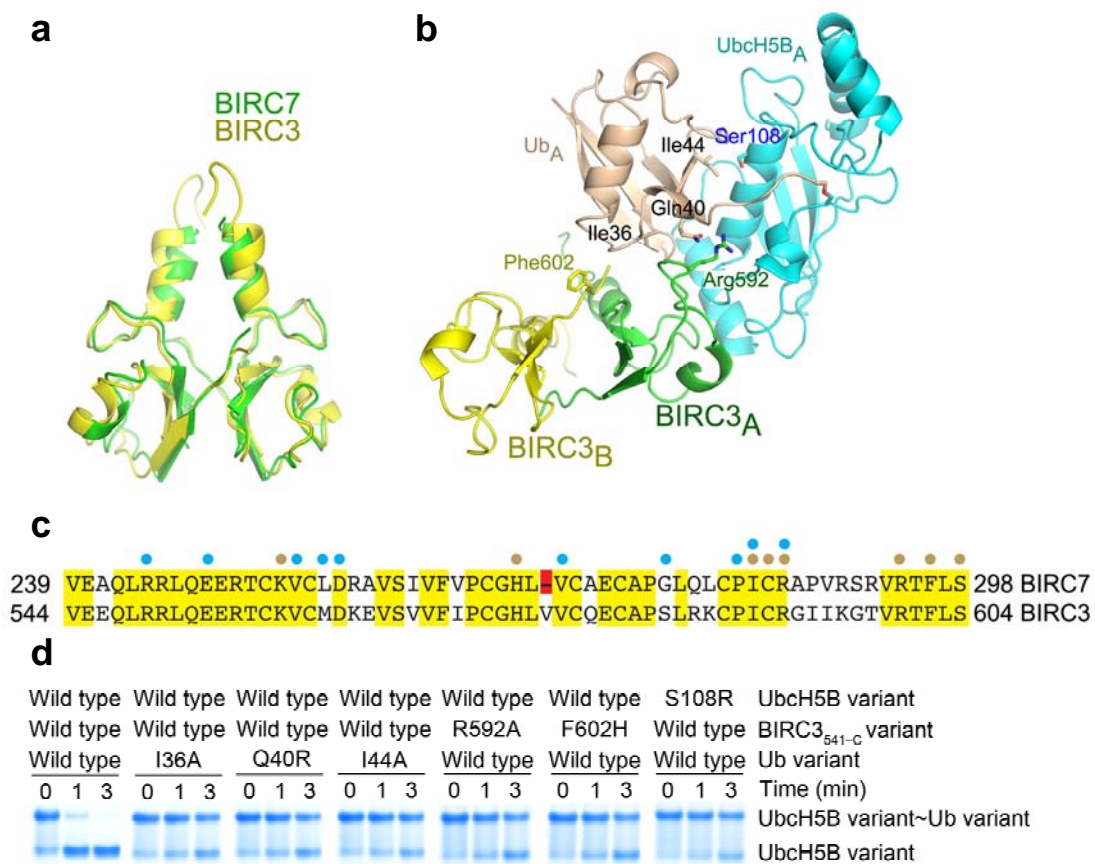


Figure 3-18. BIRC3 RING is a good substitution of BIRC7 RING for kinetic assay.

(a) Superposition of the structure of BIRC3 RING dimer (coloured yellow, PDB 3EB6 [37]) onto BIRC7 RING dimer (coloured green) from my structure. The BIRC3 RING dimer was generated from a symmetry-related molecule.

(b) The model of BIRC3_{541-C}-UbcH5B_{RAS}-Ub. Key residues involved in donor Ub interactions are indicated. Colouring is as described in **Figures 3-3**.

(c) ClustalW sequence alignment of BIRC7 and BIRC3 RING domains. Identical residues are highlighted in yellow. The valine residue absent in BIRC7 is highlighted in red. Cyan and wheat circles indicate BIRC residues involved in contacting UbcH5B and Ub, respectively, as observed in my structure and existing structure (PDB 3EB6 [37]).

(d) Non-reduced SDS-PAGE of pulse-chase lysine-discharge reactions shows the disappearance of UbcH5B~Ub with BIRC3_{541-C}, UbcH5B or Ub variants over time.

3.2.6.3 Kinetic validation using BIRC3 RING domain

Unlike BIRC7_{239-C}, BIRC3_{541-C}-catalysed reaction can be saturated (**Figure 3-19a**). The K_m was well below the highest UbcH5B~Ub concentration (30 μM). Three mutants were selected to validate the BIRC3_{541-C}-UbcH5B_{RAS}~Ub model: Ub's I44A, Ub's I36A and BIRC3's F602H (corresponding to BIRC7's F296H). Ub's Ile44 on the E2-Ub interface contacts with Ser108 on UbcH5B's $\alpha 3$. Ub's Ile36 and BIRC3's Phe602 comprise part of the E3-Ub interface. Each of these mutants increased K_m and decreased k_{cat} as predicted. Incorporation of Ub's I44A resulted in about 80-fold decrease in catalytic efficiency (k_{cat}/K_m), whereas incorporation of Ub's I36A or BIRC3's F602H led to about 15-fold decrease in catalytic efficiency (**Figure 3-19, Table 3-3 and Appendix 3**). Therefore, donor Ub interactions with UbcH5B and the RING domain are crucial for optimal Ub positioning and catalysis.

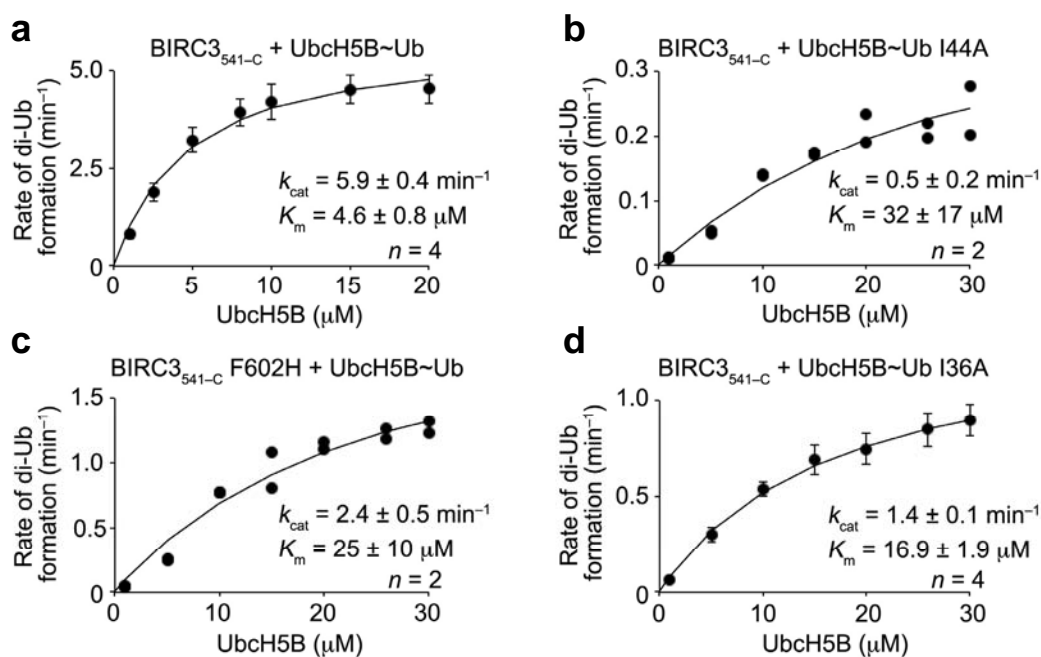


Figure 3-19. Kinetic validation on the BIRC3 RING-UbcH5B-Ub model.

(a) Single-turnover kinetics of DiUb formation was catalysed by wild-type BIRC3_{541-C} under pulse-chase conditions. The rate of DiUb formation was plotted against UbcH5B concentration. Kinetic parameters and number of replicates, n , are indicated. Error bars are shown as standard error (SEM).

(b) As in **a** but performed with ³²P-Ub I44A

(c) As in **a** but performed with BIRC3_{541-C} F602H

(d) As in **a** but performed with ³²P-Ub I36A.

Table 3-3. BIRC3 RING kinetics of DiUb formation assay.

| E3 or Ub variants (final concentration) | k_{cat} (min^{-1}) | K_{m} (μM) | $k_{\text{cat}}/K_{\text{m}}$ ($10^3 \text{ min}^{-1}\text{M}^{-1}$) | Mutational effects |
|--|---|-------------------------------------|---|---------------------------|
| Wild type (200 nM) | 5.9 ± 0.4 | 4.6 ± 0.8 | 1283 | |
| BIRC3's F602H (600 nM) | 2.4 ± 0.5 | 25 ± 10 | 96 | 13-fold defective |
| Ub'I36A (600 nM) | 1.4 ± 0.1 | 16.9 ± 1.9 | 83 | 15-fold defective |
| Ub'I44A (1.5 μM) | 0.5 ± 0.2 | 32 ± 17 | 16 | 80-fold defective |

3.3 Discussion

3.3.1 Structural comparison with RNF4–UbcH5A–Ub complex

In the structure of BIRC7_{239-C}–UbcH5B_{RAS}~Ub complex, the donor Ub adopts in the conformation that appears poised for transfer. Both the globular body and tail of donor Ub are stabilized in this conformation. The Ile44 patch of Ub_A interacts with the UbcH5B_A's α 3. The Ile36 patch of Ub_A contacts BIRC7_A's RING domain and BIRC7_B's C-terminal tail. The tail configuration of Ub_A is maintained by residues from UbcH5B_A's α 2 and Arg286 from BIRC7_A. Biochemical results suggested that disruption of these interactions caused defects in BIRC7-catalysed Ub transfer (**Figure 3-6, 3-8, and 3-12**). Failure in stabilizing the globular body of Ub seems to have a disruptive influence on the tail configuration of Ub. This is confirmed by my kinetic analyses, in which mutations in the globular Ub interactions not only had a reduced E2~Ub binding (K_m), but also resulted in decrease in the rate of Ub transfer (k_{cat}) (**Figure 3-19**). Together, these results suggest that BIRC7 mediates Ub transfer by recruiting UbcH5B~Ub, stabilizing the donor Ub configuration, and positioning the tail of donor Ub in an optimized conformation for transfer.

These findings agree with a previous study on RNF4 by Ronald Hay's group, in which modelling and biochemical analyses predicted that the RING E3 binds directly to both E2 and the donor Ub, thereby optimizing the E2~Ub conformation [203]. Recently, they solved a crystal structure of RNF4 RING domain in complex with isopeptide-linked UbcH5A–Ub to 2.2 Å [212]. The RNF4–UbcH5A–Ub complex structure also adopts a compact architecture with the fused RNF4 dimer bound to two molecules of UbcH5A–Ub. Notably, the fusion in RNF4 has been shown not to affect protein structure and enzyme activity [203]. UbcH5A that belongs to UbcH5 E2 family is similar to UbcH5B with r.m.s.d of 0.445 and 89.1% sequence identity. Based on the RNF4–UbcH5A–Ub structure, the E2-Ub's Ile44 and E3-Ub's Ile36 interactions are similar to that observed in my structure. Furthermore, in their structure UbcH5A's Asn77 is present, because the isopeptide linkage obtained by mutating the catalytic cysteine to a lysine is very stable and does not require additional mutations near E2's active site to stabilize the E2–Ub linkage. The side chain of UbcH5A's Asn77 is hydrogen bonded to the backbone oxygen of Ub's Gly76. Moreover, Asn77 also stabilizes E2's loop 114-117, where Asn114 located on

this loop forms hydrogen bond with the backbone oxygen of Ub's Gly75. Thus, residues from E2's loop 114-117 and $\alpha 3$ seem to lock the tail of Ub in an optimal configuration for transfer (**Figure 3-20a**).

In my structure, the interactions between the tail of Ub and the E2's loop 114-117 are lacking, possibly due to the N77A mutation in UbcH5B that fails to support the E2's loop [207] (**Figure 3-20b**). However, my results from *in vitro* ubiquitination assays suggest that this E2 loop is crucial in Ub transfer (**Figure 3-6 and 3-8**). Together, these results demonstrate the mechanism of Ub transfer by dimeric BIRC7 via the stabilization donor Ub conformation and activation of UbcH5B~Ub linkage. This Ub-priming mechanism also exists in other dimeric RING E3s, such as RNF4.

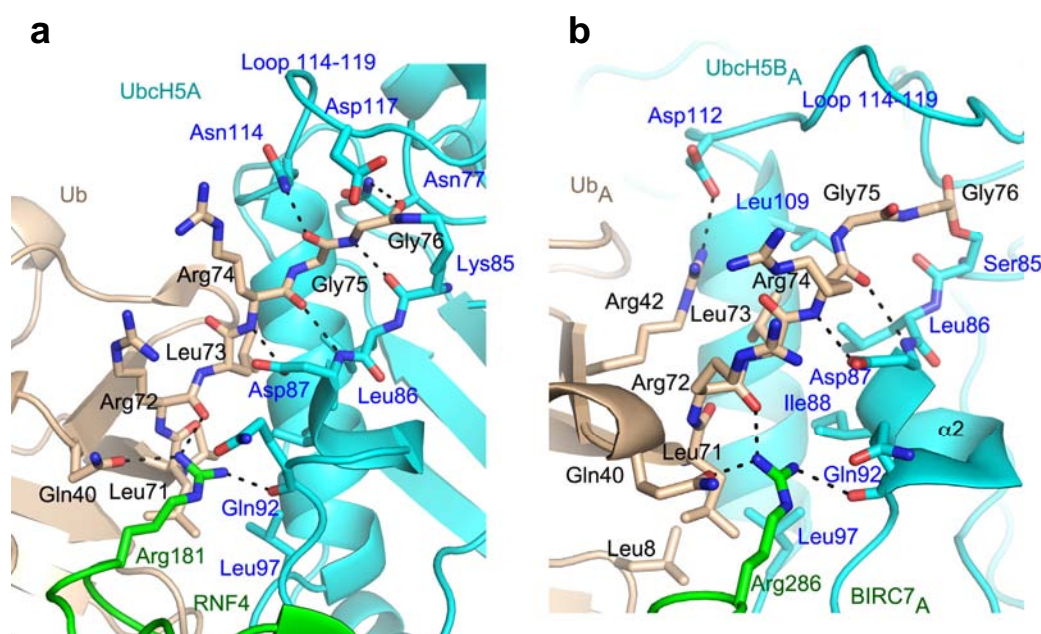


Figure 3-20. The E2-Ub's tail interfaces from dimeric E3-E2-Ub structures.

(a) Detailed interactions of the E2-Ub's tail surface from the RNF4-UbcH5A-Ub structure with UbcH5A mutant S22R/C85K (PDB 4AP4 [212]). Key residues are shown as sticks and coloured as in **Figure 3-3**, with N atoms blue and O atoms red. Putative hydrogen bonds are shown as dashed lines.

(b) Detailed interactions of the E2-Ub's tail surface from the BIRC7_{239-C}-UbcH5B_{RAS}-Ub structure with UbcH5B mutant S22R/N77A/C85S.

3.3.2 RING E3s stabilize donor Ub configuration in solution

My structural and biochemical data suggest that BIRC7 promotes Ub transfer by positioning the donor Ub in an optimal configuration for transfer. This is also supported by my colleague Gary Sibbet's NMR data [201]. He charged the mutant UbcH5B_{RAS} with ¹⁵N-labeled Ub (UbcH5B_{RAS} ~[¹⁵N]Ub) and acquired ¹H-¹⁵N HSQC spectra in the absence and presence of BIRC7 RING domain. He showed that in absence of BIRC7 RING domain, interactions between donor Ub's Ile44 patch and UbcH5B are preferred but donor Ub may sample other conformations in solution, as observed in other UbcH5~Ub NMR models [213, 214]. BIRC7 RING domain binding induces chemical shift perturbations (CSPs) indicating alteration in donor Ub interactions. These CSPs mapped onto the Ub-UbcH5B and Ub-BIRC7 interfaces in my structure. Together, these results suggest that donor Ub can form non-covalent interactions with UbcH5B in the absence of E3, but BIRC7_{239-C} binding promotes the donor Ub interaction observed in my structure, where the donor Ub is poised for transfer [201].

More comprehensive NMR studies were done by Rachel Klevit's group to investigate the interactions between UbcH5C~Ub and two RING/U-box E3s, BRCA1/BARD1 and E4B [215]. Their results showed that E2~Ub are flexible and adopt many inactive ('open') configurations in the absence of an RING/Ubox E3; whereas binding of an RING/Ubox E3 promotes a shift in the dynamic ensemble of UbcH5C~Ub to adopt active ('closed') configurations, which are more reactive for Ub transfer. Thus, RING/U-box E3 ligases allosterically activate E2~Ub conjugates for transfer [215].

3.3.3 Models for RING dimers

Dimerization is required for dimeric RING E3's activity both *in vivo* and *in vitro* [54, 55]. Based on my structure and RNF4-UbcH5A-Ub structure, aromatic residue tyrosine or phenylalanine at the C-terminus of RING dimers is crucial in donor Ub interactions. Previous studies on heterodimer Mdm2/MdmX and homodimer RNF4 have investigated the mutational effects at the C-terminus. Substitutions of aromatic residues on Mdm2 C-terminal tail, such as Y489F and Y489H retained E3 activity in the degradation of p53 *in vivo*, whereas Y489A mutation on Mdm2 is inactive. It indicates that the activity of Mdm2/MdmX presumably relies on aromatic stacking [58]. Furthermore, biochemical studies on RNF4 suggested that tryptophan substitution at Tyr193 of RNF4 retains the ability to dimerize and has a reduced activity in substrate ubiquitination. Although Y193H remains dimeric in solution, results from pull-down assay showed that neither Y193H nor Y193A retains the ability to bind E2~Ub, thus both Y193H and Y193A are defective for ubiquitination assay [203]. A recent study on BIRC4 also demonstrated that the aromatic residues at the C-terminus are not required for dimerization but crucial for Ub transfer [128].

Interestingly, some dimeric E3s contain non-aromatic residues at this point position, such as U-box E3 PRP19's Val54 [66]. Based on structural alignment, we hypothesise that the C-terminal tails of those RING E3s may contact the same hydrophobic Ile36 patch of Ub but the interactions may vary (**Figure 3-21**). Some E3s do not share the cross-dimer interface, such as RNF2/BMI1 [57]. A model of RNF2/BMI1-E2-Ub complex generated using my structure indicates side chain clash between E3 and Ub (**Figure 3-21**). Future studies are required to explore the modes of E2~Ub optimization by other types of dimeric E3s.

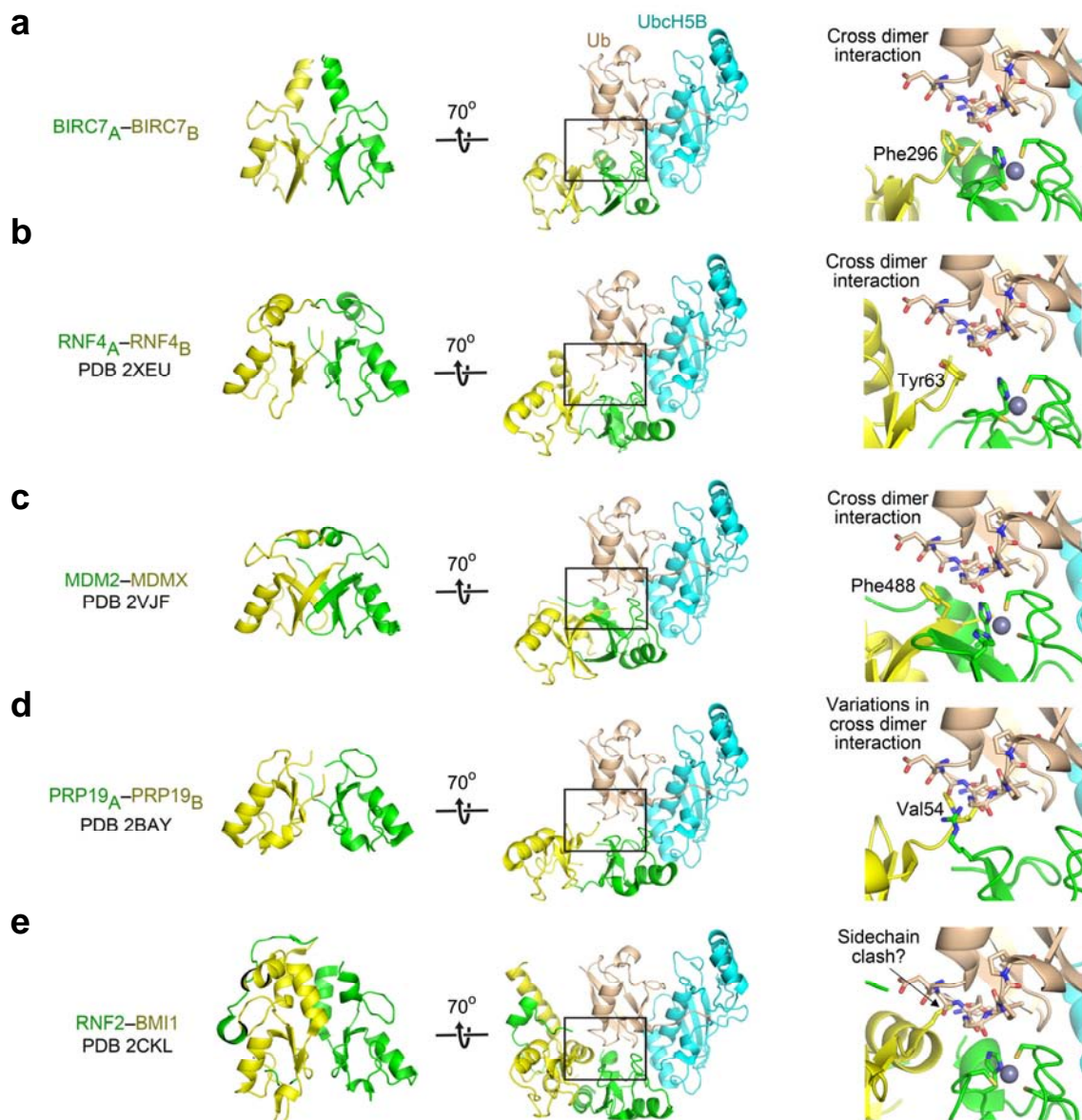


Figure 3-21. Structures or models of dimeric E3-UbcH5-Ub complexes.

(a-b) Structures of dimeric RING E3-UbcH5~Ub complexes. Left panel: cartoon representations of BIRC7 dimer (a) and RNF4 dimer (b). Middle panel: The portion of dimer bound to UbcH5~Ub from BIRC7_{239-C}-UbcH5B_{RAS}-Ub structure and RNF4-UbcH5A-Ub structures, rotated 70° from view of left panel. Right panel: Close-up view of dimer interactions with donor Ub with key residues shown as sticks.

(c-e) Models of dimeric E3-UbcH5B~Ub. Left panel: cartoon representations of E3 dimers, MDM2/MDMX (c), PRP19 (d), and RNF2/BMI1 (e), generated by structural alignment with the BIRC7 dimer. One subunit is coloured green and the second yellow. Middle panel: Models of E3 dimers bound to UbcH5B~Ub. Models were generated by superposing the green subunits onto BIRC7_A. Right panel: Close-up view of E3 dimer interactions with Ub with key residues shown as sticks. Colouring is as described in **Figure 3-3**.

Chapter 4
**Structural and functional study of c-CBL, a
monomeric RING E3**

4 Structural and functional study of c-CBL, a monomeric RING E3

4.1 Aims and objectives

CBL family proteins are single-subunit RING E3s that contain several domains, including the N-terminal TKBD, linker helix region (LHR), the RING domain, and C-terminal extensions. Early studies showed that the N-terminal fragment of CBLs retains the ability to bind E2 and TKBD ligands to mediate substrate ubiquitination [52, 216]. Interestingly, the N-terminal fragment becomes more active upon deletion of the TKBD [181, 186]. It indicates that an inhibitory mechanism may exist for regulating E3 activity. However, existing structures of CBL proteins cannot explain this observation. The aim of this project is to obtain a structure of N-terminal fragment of c-CBL to gain structural insights into how it is regulated.

In this chapter, I report the crystal structure of c-CBL revealing an autoinhibited configuration. Based on the structure, I describe the detailed interactions on the RING-TKBD interface. In addition, I present results from disulfide crosslinking assay and SPR assay to validate this structure. Lastly, I discuss multiple RING conformations based on existing structures of CBL proteins. My results demonstrate an autoinhibitory mechanism of c-CBL via blocking the E2-binding surface. Together with my colleagues' data on phosphorylated c-CBL, we provided molecular insights into CBL's autoinhibition and phosphorylation-dependent activation.

4.2 Results

4.2.1 Strategies

c-CBL N-terminal fragment (residue 47-435) was cloned, expressed and purified as described in **Chapter 2**. The purity of protein for crystallization trials is shown in **Figure 4-1**. c-CBL crystals grew into square plates or half square plates at 8°C.

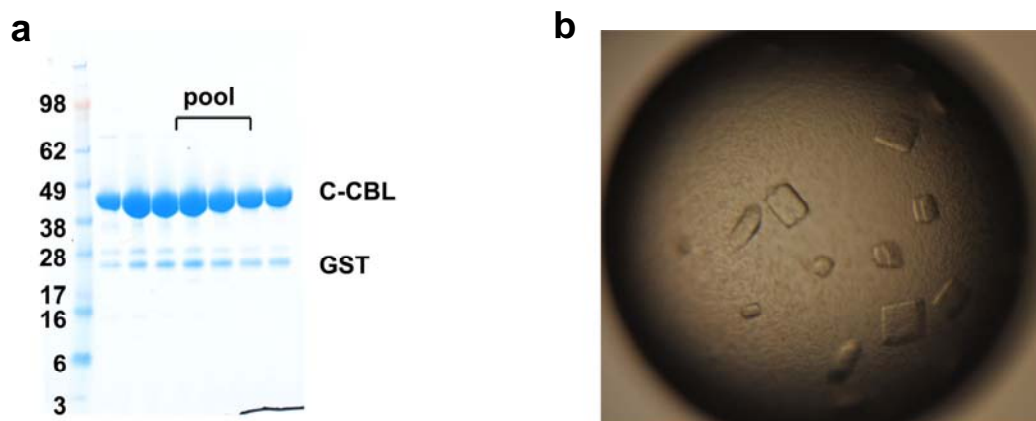


Figure 4-1. The purity of c-CBL fragment and crystals of c-CBL fragment.

(a) c-CBL fragment was purified by series of chromatography described in **Chapter 2**. The gel shows the purity of the protein after the final step, size-exclusion chromatography (SD75 GE). Fractions were pooled as indicated for crystallization trials.

(b) The crystals of c-CBL fragment.

4.2.2 Structure of c-CBL reveals an autoinhibited conformation

The crystal of c-CBL N-terminal fragment diffracts to 2.67 Å resolution with the space group of C222₁ and contains six molecules per asymmetric unit (r.m.s.d between 0.27-0.52 Å for C α atoms) [200]. My discussion focuses on one molecule in the asymmetric unit. Data collection and refinement statistics are shown in **Table 4-1**.

Table 4-1. Data collection and refinement statistics.

| c-CBL N-terminal fragment | |
|-----------------------------------|---------------------|
| Data Collection | |
| Space group | C222 ₁ |
| Cell dimensions | |
| a, b, c (Å) | 146.8, 148.6, 348.2 |
| α , β , γ (°) | 90, 90, 90 |
| Resolution (Å) | 50-2.67 (2.81-2.67) |
| R_{sym} (%) | 0.072 (0.317) |
| I/σ | 11.0 (3.4) |
| Completeness (%) | 97.6 (96.5) |
| Redundancy | 3.4 (3.0) |
| Wilson B factor | 45.9 |
| Refinement | |
| Resolution (Å) | 50-2.67 |
| No. reflections | 101826 |
| $R_{\text{free}}/R_{\text{work}}$ | 0.263/0.218 |
| No. atoms | |
| Protein | 18693 |
| Ions | 18 |
| Water | 121 |
| B -factors | |
| Protein | 57.2 |
| Ions | 56.3 |
| Water | 48.4 |
| R.m.s. deviations | |
| Bond length (Å) | 0.011 |
| Bond angles (°) | 1.35 |

Note: Highest-resolution shell is shown in parenthesis.

The N-terminal fragment of c-CBL consists of the TKBD, the LHR and the RING domain. The TKBD of my structure resembles the structure of TKBD (PDB 1B47; r.m.s.d of 0.456 Å for C α atoms) [139] (**Figure 4-2a**) and the TKBD domain in c-CBL-UbcH7-ZAP-70 peptide complex structure (PDB 1FBV; r.m.s.d of 1.065 Å for C α atoms) [52] (**Figure 4-2b**). The slightly higher r.m.s.d when compared to the TKBD domain in c-CBL-UbcH7-ZAP-70 peptide complex is likely due to the

conformational changes in the substrate-binding domain upon ZAP-70 peptide binding (**Figure 4-2b**).

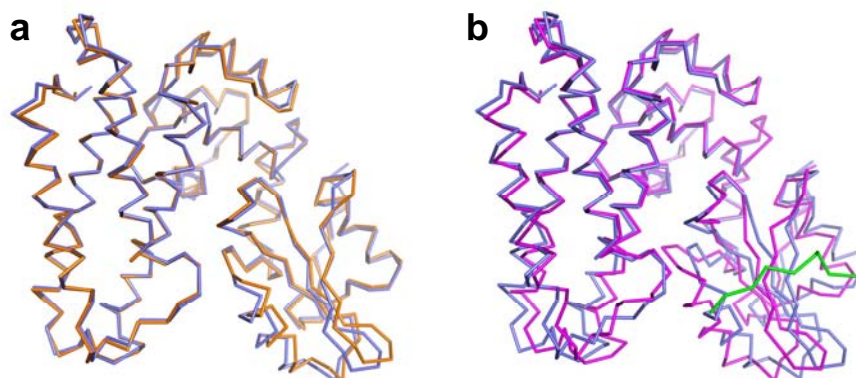


Figure 4-2. Structural alignment of the TKBD.

(a) Structural alignment of the TKBD from c-CBL fragment (coloured slate) and the TKBD structure (PDB 1B47 [139]; coloured orange) shown in ribbon representation.

(b) Structural alignment of the TKBD from c-CBL fragment (coloured slate) and the TKBD portion from c-CBL-UbcH7-ZAP70 complex (PDB 1FBV [52]; coloured magenta) shown in ribbon representation. ZAP-70 peptide is coloured green

The LHR consists of a linker loop 1 (LL1; residues 352-363), linker helix (LH; residues 364-374), and linker loop 2 (LL2; residues 375-380). In comparison to c-CBL-UbcH7-ZAP-70 peptide complex, the TKBD, the LL1 and the LH configuration remain unchanged, but the LL2 and the RING domain undergo rotations. Notably, the RING domain's E2 binding surface contacts the TKBD and the LH, making the overall structure more compact (**Figure 4-3**). The RING domain orientation appears to prevent E2 binding, thereby revealing a closed RING conformation. Conversely, the RING domain in c-CBL-UbcH7-ZAP-70 peptide structure does not pack against TKBD and the E2-binding surface is accessible for E2 binding. Therefore, it is called the open RING conformation.

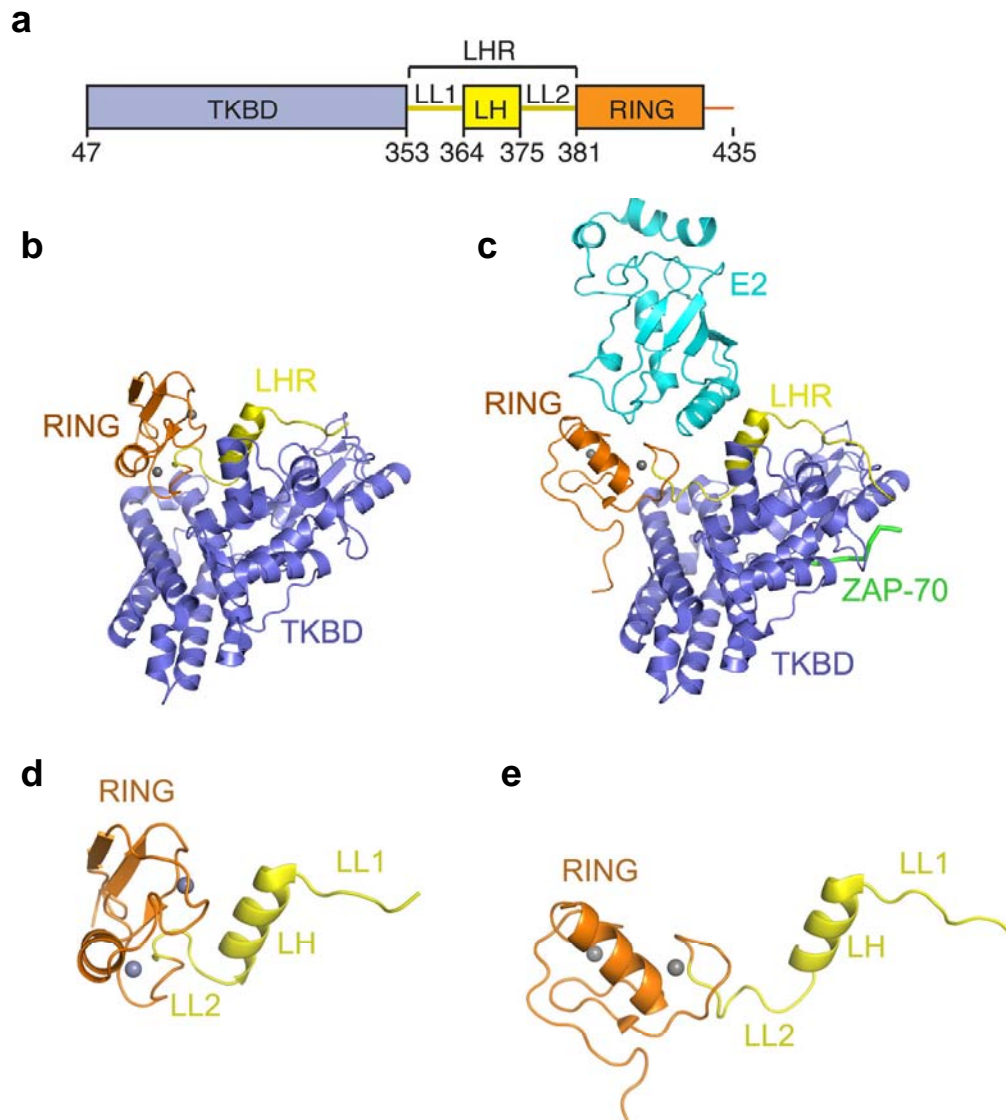


Figure 4-3. Structure of c-CBL fragment compared with c-CBL-UbcH7-ZAP70 complex.

(a) Diagram of the crystallized CBL fragment: the TKBD coloured blue, the LHR (LL1, LH and LL2) yellow and the RING domain orange. Residues encompassing each domain are indicated.

(b) Structure of c-CBL fragment coloured as in a. Zn^{2+} atoms are shown as gray spheres.

(c) Structure of c-CBL-UbcH7-ZAP70 complex (PDB 1FBV [52]) coloured as in a. E2-UbcH7 is coloured cyan. ZAP-70 peptide is shown as green ribbon.

(d,e) The LHR and the RING domain conformations in c-CBL fragment (d) and c-CBL-UbcH7-ZAP70 complex (e) coloured as in a.

4.2.3 c-CBL adopts a closed conformation in solution

To address whether c-CBL adopts the closed RING conformation in solution, I developed a disulfide assay to probe the proximity of the RING domain and the TKBD. I engineered a disulfide pair by mutating one residue at the C-terminus of the RING domain (Asp435) and one residue in the TKBD (Arg139) to cysteine. The distance between their C β s is about 7 Å in the c-CBL fragment structure, but greater than 28 Å in the c-CBL–UbcH7–ZAP-70 peptide structure (**Figure 4-4**). Thus, I expect the disulfide bond to form between the TKBD and RING domain in the native state, but in the presence of E2, the amount of disulfide bond formed will decrease.

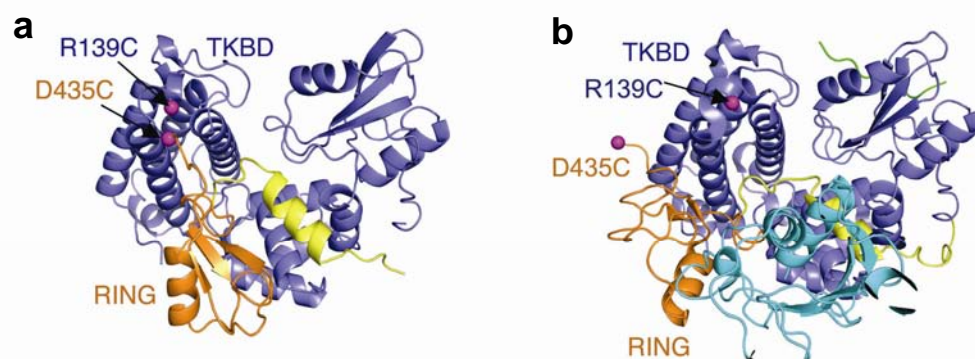


Figure 4-4. Locations of Arg139 and Asp435 in different c-CBL structures.

(a) In the structure of c-CBL fragment, the distance between the C β s of two engineered cysteine mutations (R139C/D435C) is about 7 Å.

(b) The distance between the C β s of engineered R139C and D435C is greater than 28 Å in the structure of c-CBL–UbcH7–ZAP-70 peptide. Colouring is as describe in **Figure 4-3**.

The reaction was initiated by removal of DTT (1 mM) present in the protein buffer using buffer-exchange spin column (Zeba column). The disulfide bond formation was monitored over time at room temperature. The assay was stopped by N-Ethylmaleimide (NEM), which modifies any free cysteine to prevent further disulfide bond formation. c-CBL R139C/D435C mutant (referred to as diCys) migrated as two bands on SDS-PAGE over time (**Figure 4-5**). I speculated that the lower band on the gel came from the disulfide-bonded product. I found that addition of cross-linking reagent sodium tetrathionate (NaTT) facilitated disulfide bond formation (**Figure 4-6**).

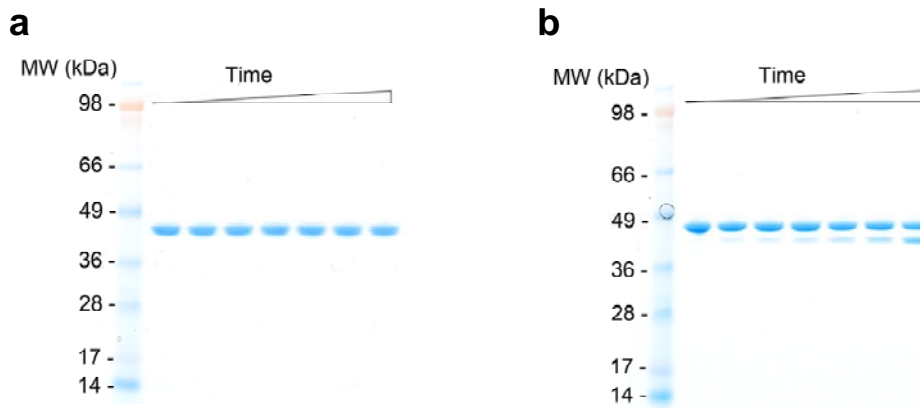


Figure 4-5. Disulfide formation observed by SDS-PAGE.

(a) Wild-type c-CBL fragment runs at about 45 kDa. In the absence of DTT, wild type migrates as a single band on SDS-PAGE over time.

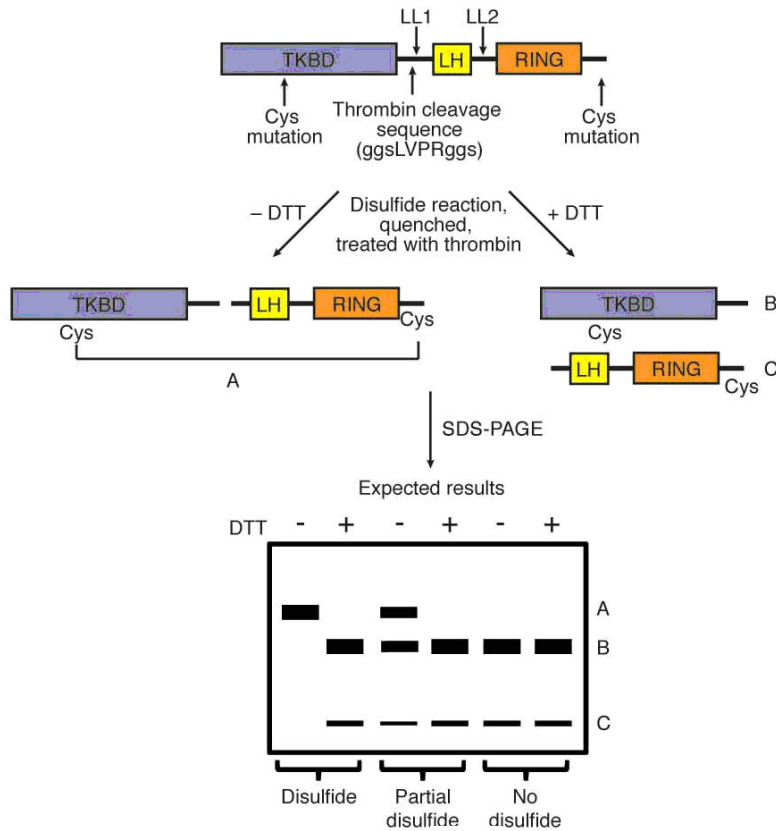
(b) In the absence of DTT, diCys mutant migrates as two bands on SDS-PAGE. The faster migrating band (lower band) is more pronounced over time.

To verify disulfide formation in diCys, I engineered a thrombin cleavage (TC) linker (sequence ggsLVPRggs) between Glu354 and Pro355 in LL1. Thrombin treatment is expected to separate c-CBL into two fragments (bands B and C; **Figure 4-6a**). If disulfide bond is formed, c-CBL remains intact (band A; **Figure 4-6a**), but will dissociate into bands B and C in the presence of 100 mM DTT (**Figure 4-6a**). In theory, complete disulfide bond formation will produce band A, and partial disulfide bond formation will yield bands A, B and C in the absence of DTT. If no disulfide bond is formed, bands B and C are expected in the presence and absence of DTT (**Figure 4-6a**).

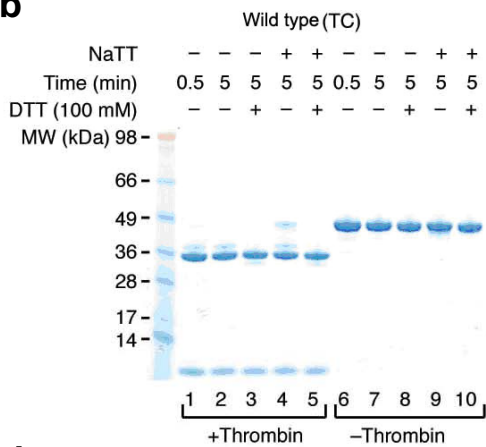
As predicted, wild type (TC) construct did not form disulfide bond and diCys (TC) formed partial disulfide in the absence of NaTT and more in the presence of NaTT (**Figure 4-6b and c**). This disulfide-bonded product can be reduced by DTT (**Figure 4-6c** lane 2 versus lane 3 or lane 4 versus lane 5). Interestingly, in the absence of thrombin treatment, lanes 2 and 4 in **Figure 4-6c** contained disulfide-bonded species migrated as two bands (**Figure 4-6c** lanes 7 and 9, respectively). This is consistent with my initial speculation that lower band corresponded to the disulfide-bonded species. Wild type (TC) and diCys (TC) had the same profile as wild type and diCys in disulfide bond formation, respectively, in the absence of thrombin treatment (**Figure 4-6b-e** lanes 6-10). These results showed that the disulfide-bonded species migrated faster than the unmodified species. By following the formation of the lower

band on SDS-gel, I can monitor the rate of the disulfide bond formation over time. Moreover, native c-CBL can adopt the closed RING conformation in solution.

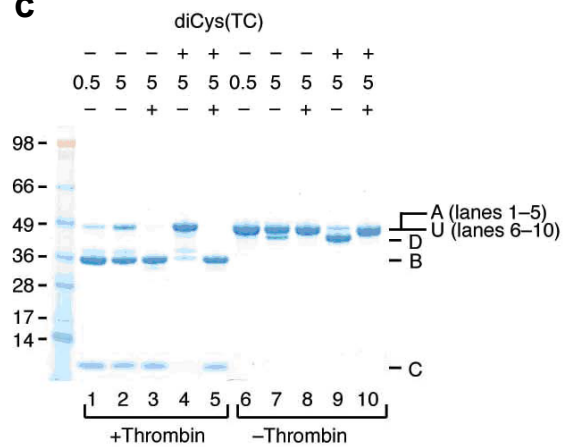
a



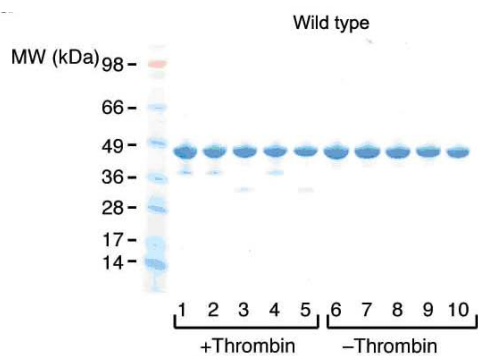
b



c



d



e

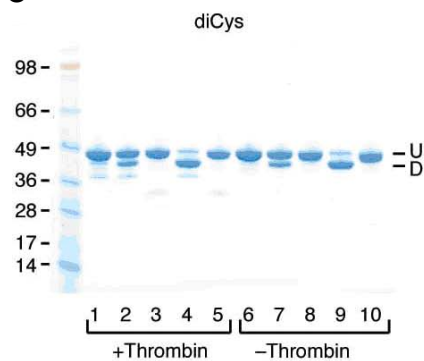


Figure 4-6. CBL variants disulfide bond formation tested by thrombin cleavage.

(a) Strategy for visualization of intramolecular disulfide bond formation.

(b) Disulfide bond formation with wild type (TC) in the absence or presence of NaTT or DTT as indicated.

(c) Same in **b** but with diCys (TC). Lanes 1-5 and 6-10 were treated with and without thrombin, respectively. For lanes 1-5 in **b** and **c**, bands A, B and C refer to fragments predicted in **a**. For lanes 6-10, the slow migrating (upper) band corresponds to uncleaved wild type (TC) or diCys (TC) that did not form a disulfide bond labelled as U (Unmodified); the fast migrating (lower) band corresponds to uncleaved wild type (TC) or diCys (TC) that formed a disulfide bond labelled as D (Disulfide).

(d, e) Same in **b** but with wild type and diCys respectively. Wild type and diCys lacking an inserted TC sequence yield slow and fast migrating bands, which correspond to unmodified (U) and disulfide-bonded species (D), respectively. The disulfide-bonded species is readily reduced to the unmodified species in the presence of DTT. Molecular weight standards are indicated.

4.2.4 Interactions in the closed RING conformation

In c-CBL structure, the RING domain interacts with the TKBD, the LH and the LL2, burying about 980 Å² of surface area. This closed RING conformation is maintained by hydrophobic and hydrophilic interactions. Hydrophobic interactions occur between Ile383, Trp408, Phe418 from the RING domain and Leu219, Met22 from the TKBD. Hydrogen bonds are formed between the side chains of LH's Glu373 and RING's Lys389, between the side chains of LL2's Thr377 and TKBD's Asn150, between the backbone oxygen of Thr377 and the side chain of RING's Lys382, between the backbone oxygen of LL2's Phe378 and the side chain of RING's Lys389, between the side chains of LL2's Gln379 and TKBD's Gln146, and between the backbone oxygen of Gln379 and the backbone amide nitrogen of RING's Lys389 (**Figure 4-7**). These interactions are unique and not observed in previous structure.

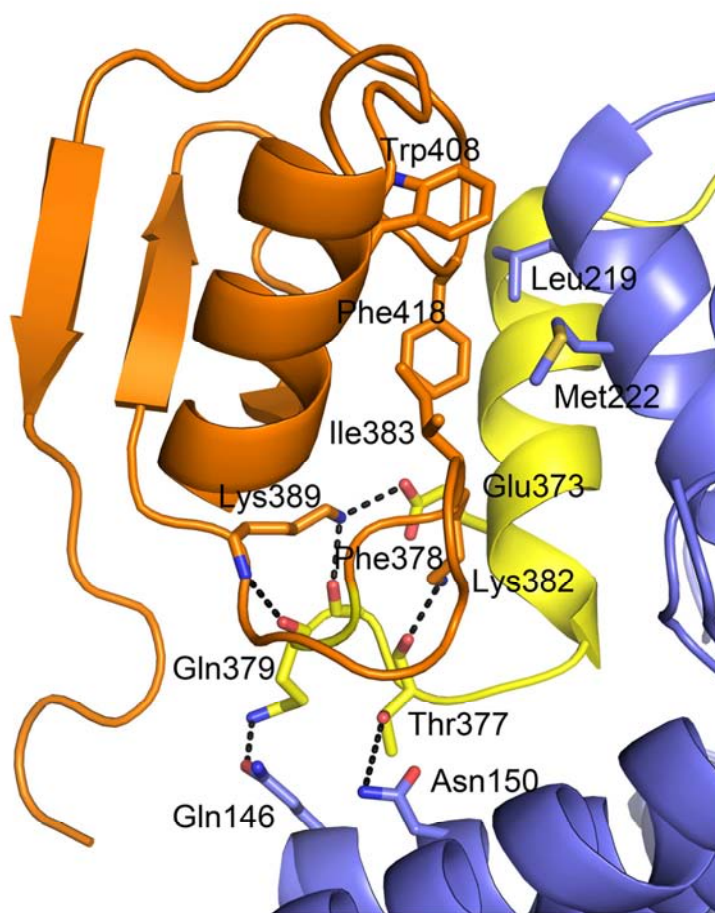


Figure 4-7. Detailed interactions to stabilize the closed RING conformation.

Close up view of the closed RING conformation. Colouring is as described in **Figure 4-3**. Key residues are shown as sticks with N atoms blue, O atoms red, and S atom yellow. Putative hydrogen bonds are shown as dashed lines.

Interestingly, the RING domain uses its E2 binding surface to contact the TKBD, thus the same residues on the RING domain's E2 binding surface are involved in establishing both the closed and open RING conformations (**Figure 4-8a and b**). This suggests that c-CBL encodes dual-functional residues that maintain the closed RING conformation and participate in E2 binding. Superposition of the RING domain onto the RING domain portion in c-CBL-Ubch7-ZAP-70 peptide structure reveals that Met222 contacts Ile383 of the RING domain in a similar manner to Ubch7's Ala98, suggesting that the RING-Met222 interaction may compete against E2 binding (**Figure 4-8c**).

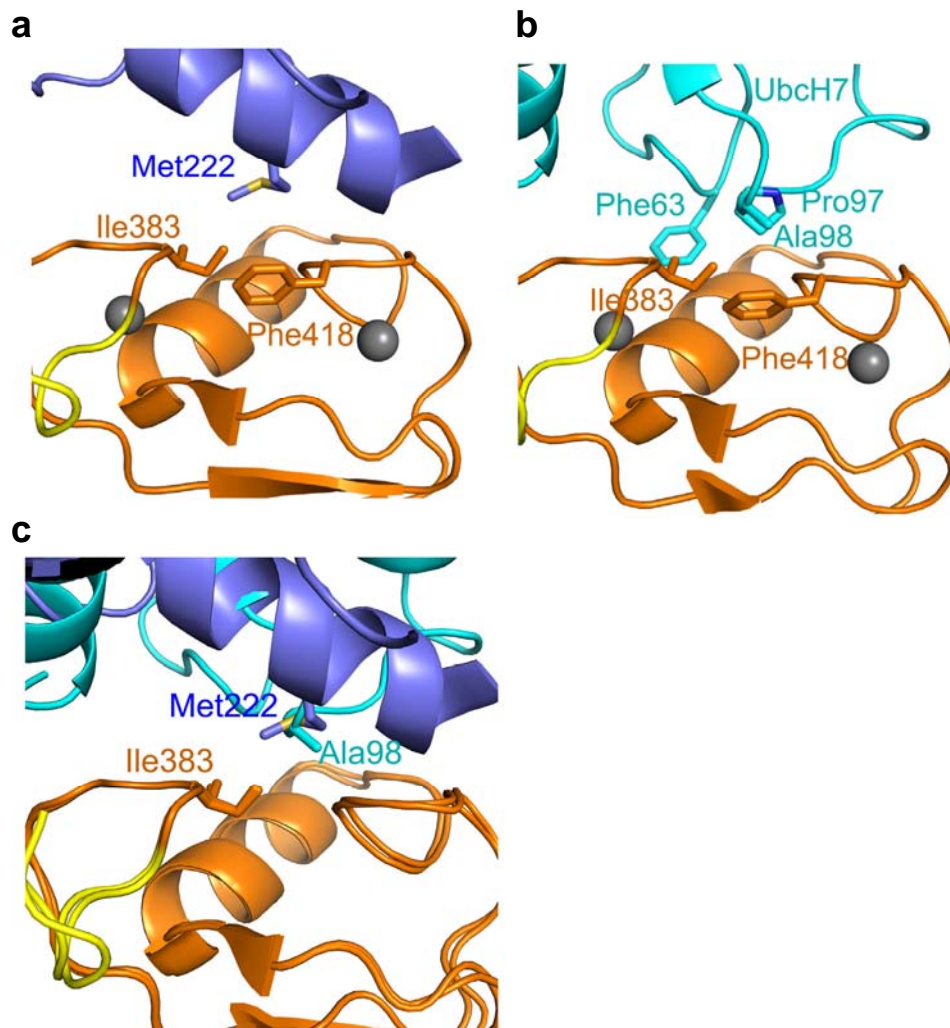


Figure 4-8. Superposition of RING domains from the structures of c-CBL fragment and c-CBL-UbcH7-ZAP70 peptide complex.

(a) Hydrophobic interactions between residues Ile383 and Phe418 from the RING domain and Met222 from the TKBD of c-CBL fragment structure.

(b) The same residues from the RING domain of c-CBL-UbcH7-ZAP-70 peptide [52] contact residues from E2 UbcH7.

(c) Superposition of the RING domains in a and b. Ile383 contacts TKBD's Met222 in the closed RING conformation and E2's Ala98 in the open RING conformation.

Sequence alignment of CBL proteins from different species suggests that c-CBL Met222 is conserved across higher eukaryotes and in CBL-B. In CBL-C, the corresponding residue is leucine in human but appears more divergent in other species (Figure 4-9).

| | | | | | | |
|-----|----------------|---|----------|-----|------------------------|---------------|
| 209 | HEVHPISSG-LEAM | A | LKSTIDL | 230 | <i>H. sapiens</i> |] c-CBL |
| 207 | HEVHPISSG-LEAM | A | LKSTIDL | 228 | <i>M. musculus</i> | |
| 193 | HEFHPISSG-LEAM | A | LKSTIDL | 214 | <i>D. rerio</i> | |
| 201 | HEVHQISSS-LEAM | A | LKSTIDL | 222 | <i>H. sapiens</i> |] CBL-B |
| 201 | HEVHQISSG-LEAM | A | LKSTIDL | 222 | <i>M. musculus</i> | |
| 196 | HDVHPISSG-LEAM | A | LKSTIDL | 217 | <i>D. rerio</i> | |
| 179 | GTCHPVEPG-CTAL | L | ALRSTIDL | 200 | <i>H. sapiens</i> |] CBL-C |
| 178 | CACHPVEPG-PTM | Q | ALRSTIDL | 199 | <i>M. musculus</i> | |
| 178 | CICHPVEPG-STAL | L | ALRSTIDL | 199 | <i>B. taurus</i> | |
| 197 | NKVHPIISG-LEAM | A | LKTTIDL | 218 | <i>D. melanogaster</i> |] CBL homolog |
| 217 | EKHHGSTIGKMEA | A | ELKATIDL | 239 | <i>C. elegans</i> | |
| 267 | QKFFNKEIL-AYE | S | SLRYTLDF | 288 | <i>D. discoideum</i> | |

Figure 4-9. Sequence alignment of CBL protein or CBL homolog from different species. Proteins sequences were aligned by Clustal W method in MegAlign software. The conserved methionine residues or corresponding residues are coloured in red.

4.2.4.1 Probing RING-TKBD interactions

To probe the RING-TKBD interaction, several mutations were introduced to diCys mutant. Wild type and individual mutations did not form disulfide over time at room temperature (**Figure 4-10**). Met222 appears to be the primary contributor to maintain the closed RING conformation via the intramolecular hydrophobic interaction. I predict that mutation of Met222 to phenylalanine or glutamate would enhance or disrupt this interaction, respectively. To test this hypothesis, I incorporate M222F or M222E into diCys and monitor the rate of disulfide bond formation. Indeed, diCys M222F mutant increased the disulfide bond formation while M222E mutation reduced the disulfide bond formation (**Figure 4-10**). The structure of c-CBL-UbcH7-ZAP-70 peptide complex suggests that addition of E2 and ZAP-70 peptide would change the RING domain conformation, and therefore reduce disulfide bond formation in diCys. Indeed, addition of E2 and/or ZAP-70 peptide reduced disulfide bond formation (**Figure 4-10**; Note: c-CBL-ZAP-70 peptide structure showed that the RING domain also undergoes rotation explaining why addition of ZAP-70 peptide alone also reduced diCys disulfide bond formation, see **Section 4.3.1**). Together, these data indicate that c-CBL can adopt the closed RING conformation in solution and the

RING domain may sample different conformations upon binding to E2 and/or ZAP-70 peptide.

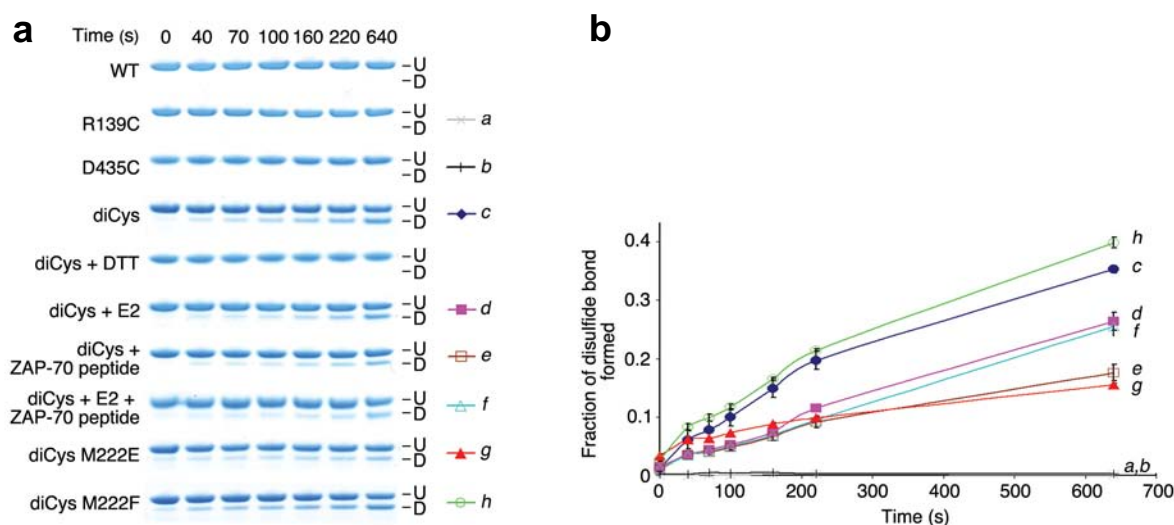


Figure 4-10. Probing RING-TKBD interaction with disulfide crosslinking assay.

(a) Disulfide bond formation for c-CBL variants in the absence or presence of E2, ZAP-70 peptide or both on SDS-PAGE. The upper band is the unmodified (U) species and lower band is the disulfide-bonded (D) are indicated. The colour symbols on the right panel with italic letters (*a-h*) correspond to the chart legend in **b**.

(b) Fraction of disulfide bond formed (F) was expressed as $F = D / (D + U)$ and plotted against time corresponding to variants in **a**. Triplicate reactions were performed and the standard errors are shown as error bars.

4.2.4.2 The RING-TKBD interaction competes against E2 binding

Based on the structure, Met222 is the key residue on the TKBD to contact the RING domain in the closed RING conformation. To assess the effects of Met222 on E2 binding, I purified c-CBL fragment constructs with N-terminal GST tag and Ubch5B for SPR experiments. Binding experiments were conducted by my colleague Gary Sibbet. GST tagged c-CBL wild type, M222E and M222F were individually captured by anti-GST antibody that was coupled onto the chip. Ubch5B was serially titrated in running buffer and floated onto the chip. Purified GST protein was used as a control.

His results showed that c-CBL M222E displays about 3 fold higher E2 binding affinity than wild type; whereas M222F mutant has a weaker binding to E2 than wild

type, suggesting that the RING-TKBD interactions compete against E2 binding (Table 4-2).

Table 4-2. The RING-Met222 interaction competes against E2 binding by SPR analysis.

| E3 variants | E2 | K_d (μ M) |
|-----------------|--------|------------------|
| c-CBL wild type | UbcH5B | 330 ± 45 |
| c-CBL M222E | UbcH5B | 112 ± 14 |
| c-CBL M222F | UbcH5B | 416 ± 55 |

4.2.4.3 The RING-TKBD interaction reduces E3 activity

Non-RTK Syk was reported to be ubiquitinated by CBL family proteins [167, 179]. The N-terminal fragment of c-CBL has been shown to be sufficient to function as an E3 [52, 216]. To determine whether the RING-TKBD interaction plays an inhibitory role in substrate ubiquitination, I assayed the effect of M222E mutant on Syk ubiquitination using c-CBL fragment (residue 47-435). My results showed that M222E exhibits greater activity than c-CBL wild type, suggesting disruption of the RING-TKBD interaction enhances E3 activity (Figure 4-11a). The RING-TKBD interaction also affects the E3 activity as demonstrated by autoubiquitination assay using purified full-length c-CBL variants and 32 P-labelled Ub (Appendix 4. The purity of full-length c-CBL variants). Similarly, M222E mutant displayed high activity than wild type whereas M222F mutant showed a similar activity as the wild-type c-CBL (Figure 4-11b). These results suggested that the RING-Met222 interactions compete against E2 binding and reduce E3 activity.

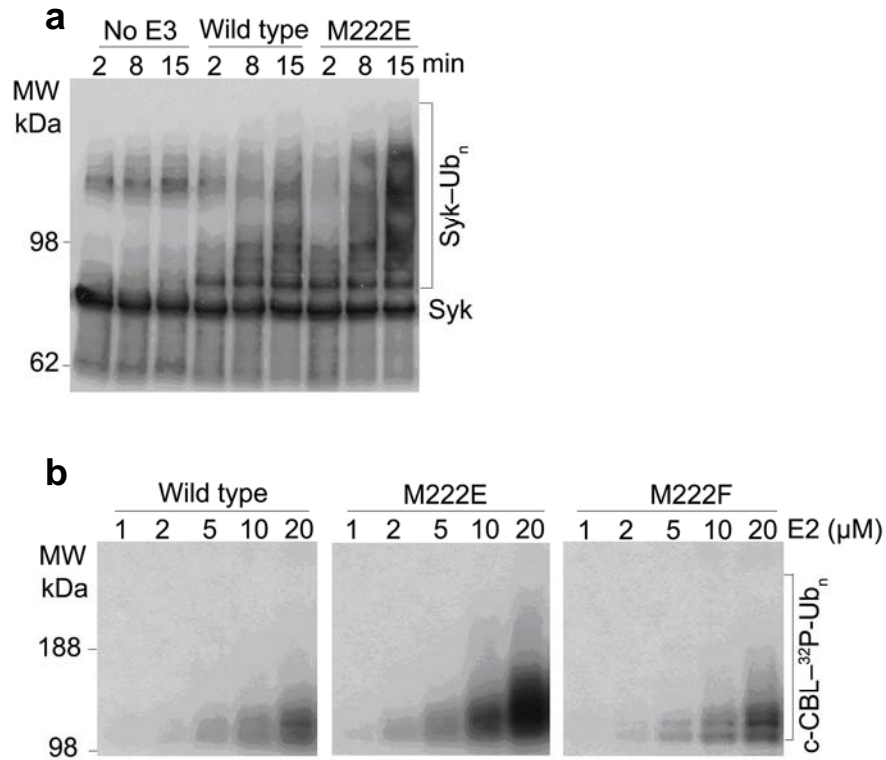


Figure 4-11. The RING-Met222 interaction plays an inhibitory role in the E3 activity of c-CBL.

(a) Western blots show *in vitro* Syk ubiquitination mediated by c-CBL (47-435) variants (0.1 μM) over time at 30 °C using anti-Syk antibody.

(b) Reduced autoradiograms show the autoubiquitination of full-length c-CBL variants (3 μM) with an increasing concentration of UbcH5B at 30 °C for 15 min.

4.3 Discussion

4.3.1 Autoinhibition of c-CBL

RING E3s recruit E2s and substrates to promote substrate ubiquitination and decide the fates of substrates, thus precise control of E3s' activity is important for regulating diverse cellular processes. My structure and biochemical results reveal a novel autoinhibitory mechanism in modulating c-CBL's E3 activity via blocking the E2-binding surface of the RING domain in a competitive manner. The E2-binding surface on the RING domain of c-CBL participates in forming the closed RING conformation. In the absence of E2 or TKBD ligand, c-CBL's RING domain contacts the TKBD, where the E2-binding surface on the RING domain is blocked (**Figure 4-12a**). The RING-TKBD interaction competes against E2 binding and reduces E2 binding affinity and CBL activity [200].

The RING domain undergoes conformational changes in the presence of E2 and/or ZAP-70 peptide. The structure of c-CBL bound to the ZAP-70 peptide (c-CBL-ZAP-70 peptide, PDB 2Y1N) solved in our lab showed that ZAP-70 peptide binding induces the RING domain rotation resulting in a half-open RING conformation [200]. This RING domain conformation is maintained by novel hydrophobic interactions with the TKBD and LHR (**Figure 4-12b**). Addition of E2 further induces RING domain rotation leading to the open RING conformation (**Figure 4-12c**). In disulfide bond cross-linking reactions, E2 and/or ZAP-70 peptide were not saturated, therefore c-CBL's RING domain is likely to toggle between the open and closed conformations, and hence reduced disulfide bond formation was observed. Recently, Fuyuhiko Inagaki's group showed that CBL-B fragment (residue 39-426) is in dynamic equilibrium between a closed and partially open state [199]. The partially open state may be considered an ensemble of multiple states, one of which may be similar to the open RING conformation. They hypothesised that both the LHR and the RING domain may be released from the TKBD to expose the conserved tyrosine for phosphorylation [199].

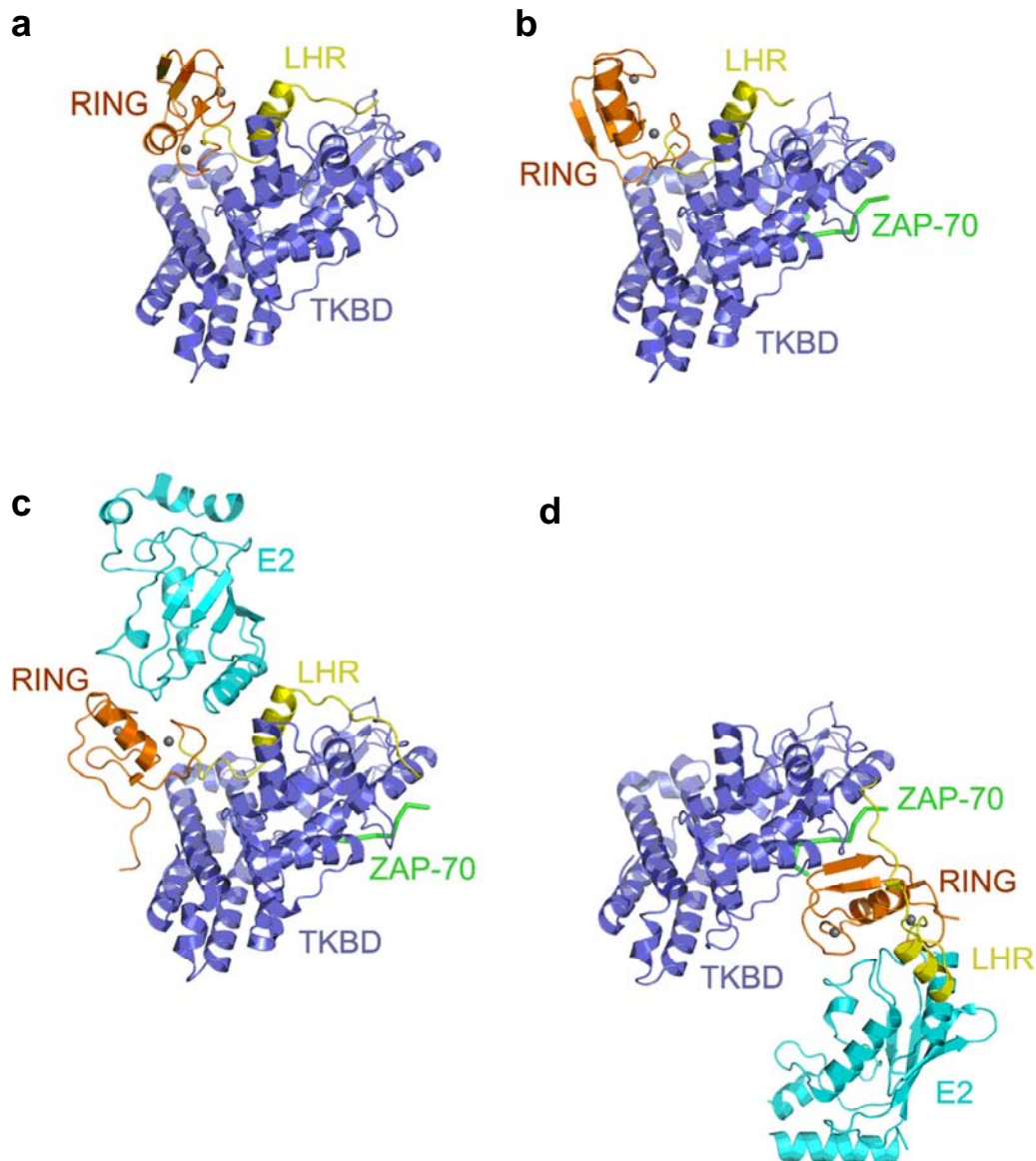


Figure 4-12. Four states of c-CBL's RING domain.

(a) The structure of c-CBL in closed RING conformation.

(b) The structure of c-CBL–ZAP-70 peptide (PDB 2Y1N [200]) in half-open RING conformation. The RING domain rotates about 70° compared to **a**.

(c) The structure of c-CBL–UbcH5B–ZAP-70 peptide (PDB 1FBV [52]) in open RING conformation. The RING domain rotates about 90° compared to **a**.

(d) The structure of pTyr371-c-CBL–UbcH7–ZAP-70 peptide (PDB 4A4C [200]) in active RING conformation. The LH flips about 180° compared to **c** and brings the RING domain bound E2 onto the substrate binding side of the TKBD. In four RING conformations, the TKBD remains unchanged. Colouring is as described in **Figure 4-3**.

CBL proteins can function as both E3s and adaptor proteins in diverse signalling pathways [135]. The RING-mediated autoinhibition mechanism I present here indicates that autoinhibition may prevent inappropriate substrate ubiquitination and presumably make CBL a worse E3 enzyme but a better adaptor protein. For example,

in the RTK Met signalling pathway, c-CBL activates MAP kinases downstream of Met signalling, but at the same time c-CBL ubiquitinates Met and promotes Met degradation [174, 175, 217]. Thus, autoinhibited c-CBL may function as a scaffold to apply positive effects on the downstream of Met. Upon removal of autoinhibition, c-CBL may rapidly ubiquitinate Met, thereby attenuating the signals. Future studies are required to reveal how c-CBL switches between its dual functions.

4.3.2 Phosphorylation-dependent activation of c-CBL

c-CBL undergoes Tyr371-phosphorylation upon EGF stimulation, which is verified by mass spectrometry [218]. In addition to unphosphorylated c-CBL structures, my colleagues determined the structure of c-CBL phosphorylated at Tyr371 (pTyr371-c-CBL) in complex with UbcH5B and ZAP-70 peptide (pTyr371-c-CBL-UbcH5B-ZAP-70 peptide, PDB 4A4C) [200] (**Figure 4-12d**). This structure reveals dramatic conformational changes upon Tyr371 phosphorylation explaining how phosphorylation activates c-CBL's activity.

In unphosphorylated c-CBL structures, Tyr371 is buried in a hydrophobic pocket formed by residues from the TKBD, thereby fastening the LHR to the TKBD (**Figure 1-11c and Figure 4-12a to c**). However, upon phosphorylation, pTyr371 containing a phosphate group can no longer accommodate in the hydrophobic pocket on the TKBD and this causes the release of LHR from the TKBD. The LHR flips 180° compared to the one in the open RING conformation (**Figure 4-12c**) and brings the RING domain and E2 adjacent to the substrate-binding site (**Figure 4-12d**). pTyr371-c-CBL can no longer adopt the closed RING conformation and this is supported by disulfide bond crosslinking assays, where incorporation of pTyr371 in to diCys abolished disulfide bond formation [200]. Thus, phosphorylation activates c-CBL by abolishing the autoinhibition and promoting LHR flexibility such that E2 and RING domain are able to reach the substrate-binding site.

Furthermore, pTyr371 also initiates direct interactions with the RING domain to form a new LHR-RING conformation that is distinct from that in the unphosphorylated

state (**Figure 4-13**). SPR experiments showed that the E2-binding affinity of c-CBL fragment was enhanced by about 11-fold upon Tyr371 phosphorylation [200]. This improvement in E2 binding is due to disruption of autoinhibition and the formation of the LHR-RING conformation, called the pTyr371-binding surface (**Figure 4-13**). Mutational analyses of the key residues to maintain this interface (K389A and V431A) reduced E2 binding affinity and E3 activity, suggesting that this pTyr371-binding surface contributes to E2 binding and catalysis [200].

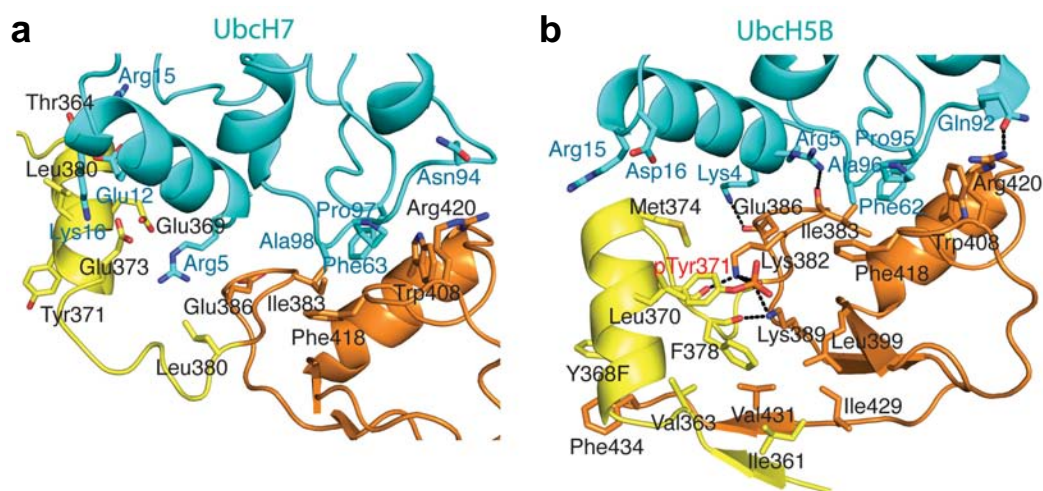


Figure 4-13. Novel LHR-RING interactions in pTyr371-c-CBL-UbcH5B-ZAP-70 peptide.

(a) Close-up view of the interactions between UbcH7 and from c-CBL-UbcH7-ZAP-70 peptide (PDB 1FBV [52]).

(b) Close-up view of the interactions between UbcH5B, the pTyr371-LHR-RING portion in E2-pCBL-LHR-RING. pTyr371 alters LHR conformation and creates new LHR interactions with the RING domain. All colouring is as described in **Figure 4-3**. pTyr371 is labelled red.

Phosphorylation activates CBL and this activation is required for receptor tyrosine kinase (RTK) ubiquitination [48] but it is not clear whether phosphorylation is required for ubiquitination of every substrate. In the unphosphorylated state, c-CBL recruits targets through different substrate-binding domains (such as TKBD or proline-rich region), and hence the locations of substrate relative to the RING domain may differ from the ones in the phosphorylated state. It remains to be investigated whether different RING states have preferences for substrate ubiquitination.

4.3.3 Model for autoinhibition and phosphorylation-dependent activation of c-CBL

To summarize, unphosphorylated c-CBL exists in equilibrium between the closed RING (autoinhibited) conformation and the open RING (E2-bound) conformation. Phosphorylation of the LHR Tyr371 releases the LHR from the TKBD, prevents c-CBL from adopting the closed RING conformation, establishing pTyr371-binding surface to enhance E2 binding, and therefore leads to the activation of c-CBL (**Figure 4-14**).

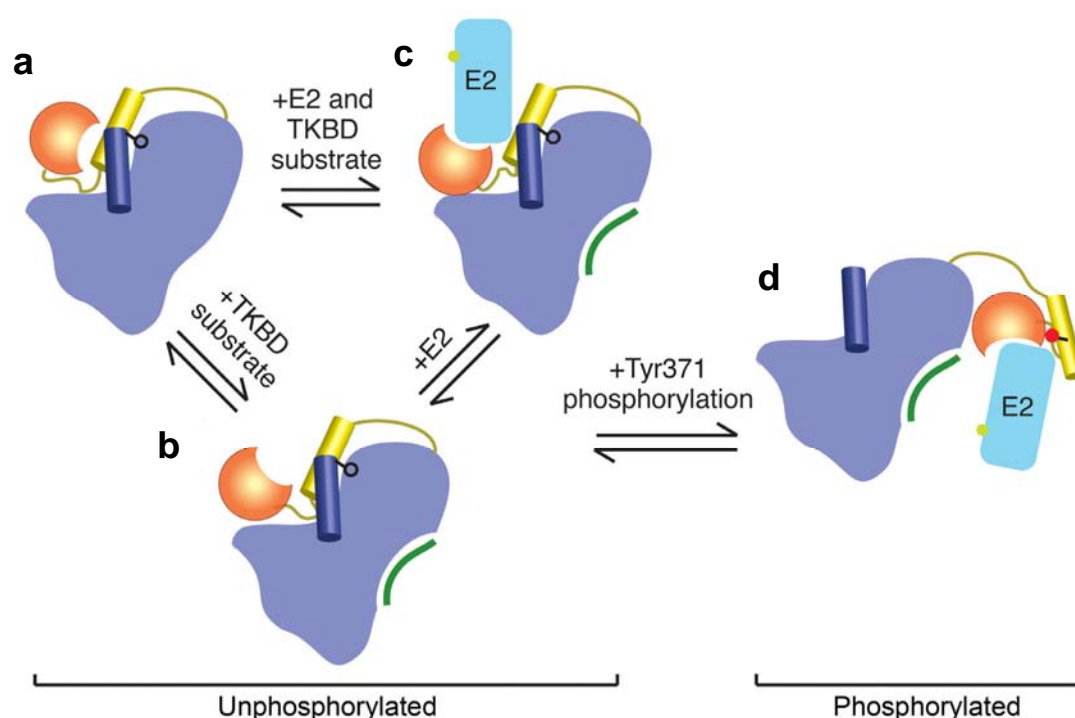


Figure 4-14. Model for autoinhibition and phosphorylation-dependent activation of c-CBL.

(a) In the native state, c-CBL adopts the closed RING conformation, in which the E2-binding surface of the RING domain interacts with the TKBD. Colouring of c-CBL, E2, and substrate peptide is as described in **Figure 4-3**.

(b) In the presence of substrate peptide, c-CBL adopts the half-open RING conformation.

(c) Additional E2 binding causes the RING domain to adopt the open RING conformation.

(a-c) In unphosphorylated c-CBL, Tyr371 (black ball-and-stick) secures the LHR to the TKBD and limits the RING domain rotation. The TKBD-RING interaction competes with E2 binding and reduces c-CBL activity.

(d) Upon phosphorylation, pTyr371 (red ball-and-stick) activates c-CBL by releasing the LHR from the TKBD, thereby abolishing autoinhibition and establishing pTyr371-binding surface to improve E2 binding.

Chapter 5
Mechanism of Ub transfer by a monomeric RING
E3, pTyr363-CBL-B

5 Mechanism of Ub transfer by a monomeric RING E3, pTyr363-CBL-B

5.1 Aims and objectives

In **Chapter 3**, I demonstrate the mechanism of Ub transfer by dimeric RING E3s, where the cross-dimer arrangement plays an essential role in stabilizing donor Ub. Monomeric RING E3s (also called single-subunit or simple RING E3s) function without a dimeric partner; therefore, it is unclear how monomeric RING E3s facilitate Ub transfer. The aim of this project is to obtain a complex structure of a monomeric RING E3 bound to E2~Ub.

As I mentioned in **Chapter 4** discussion section, our previous pTyr371-c-CBL-UbcH5B-ZAP-70 peptide structure reveals that phosphorylation activates CBL by disrupting autoinhibition, freeing up RING domain, and improving E2 binding. However, it does not fully explain the massive activation (about 1,400-fold enhancement) induced by phosphorylation in enzyme catalysis. By crystallizing tyrosine phosphorylated CBL proteins with E2~Ub, I hope to figure out the role of phosphorylation in CBL-catalysed Ub transfer.

In this chapter, I report the crystal structure of pCBL-B fragment bound to stabilized UbcH5B_{RK}~Ub and ZAP-70 peptide, which is the first complex structure of a monomeric RING E3 bound to E2~Ub. Based on this structure, I describe the novel interactions between pTyr and donor Ub, and the known donor Ub interactions demonstrated in **Chapter 3**. I also present biochemical and kinetic data to validate crucial interfaces observed in this structure and investigate the role of pTyr in catalysis. Lastly, I compare my structure with the existing structures of dimeric RING E3s bound to E2~Ub. Together, we can gain more insights into the molecular mechanism of Ub transfer catalysed by RING E3s.

5.2 Results

5.2.1 Strategies

Sequence alignments show that the N-terminal fragments of CBL proteins are highly conserved in c-CBL and CBL-B with sequence identity of 84.6% (**Figure 5-1**). CBL-C N-terminal fragment has sequence identity of 50%.



Figure 5-1. Sequence alignment of N-terminal fragments from CBL family.

Proteins sequences of c-CBL, CBL-B, and CBL-C N-terminal fragments containing the TKBD, the LHR and the RING domain were aligned by Clustal W method in MegAlign software. Conserved residues are highlighted in yellow.

To generate homogeneous tyrosine (Tyr371 in c-CBL, Tyr363 in CBL-B and Tyr341 in CBL-C) phosphorylated CBL proteins, the other tyrosine on the LHR (Tyr368 in c-CBL and Tyr360 in CBL-B) was mutated to phenylalanine. This tyrosine is a leucine in CBL-C. Based on our previous study, Y368F mutation did not affect CBL's activity or structure [200]. Based on the structure of pTyr363-CBL-B LHR-RING domain, Y360F substitution should not have an impact on the structure [199]. Several tyrosine-phosphorylated CBL proteins containing N-terminal fragment or just LHR-RING domain were cloned, co-expressed with Src, and purified by me, Danny Huang and Lori Buetow (**Chapter 2**). Based on the structural study of RNF4-UbcH5A-Ub complex, an isopeptide-linked UbcH5B-Ub was also engineered by mutating UbcH5B's Cys85 to lysine, and Ser22 to arginine (UbcH5B_{RK}-Ub) [212]. The UbcH5B_{RK}-Ub complex was purified by Danny Huang (**Chapter 2**).

Purified phosphorylated CBL proteins were mixed with stabilized UbcH5B_{RAS}~Ub or UbcH5B_{RK}-Ub with or without ZAP-70 peptide at 1:1:1 molar ratio for crystallization trials at 4 °C. After screening several phosphorylated constructs of c-CBL, CBL-B and CBL-C, I successfully obtained crystals for a complex structure using Tyr363-phosphorylated CBL-B fragment (residue 38-427, termed as pCBL-B). Crystals of pCBL-B-UbcH5B_{RK}-Ub-ZAP-70 peptide grew into a stick shape with thickness (**Figure 5-2**). To verify all components are present in the crystals, crystals were harvested, washed, and loaded onto SDS-PAGE (**Chapter 2**). The bands on the gel suggest that crystals contain pCBL-B and UbcH5B_{RK}-Ub at around 1:1 molar ratio. ZAP-70 peptide runs off the gel (**Figure 5-2**).

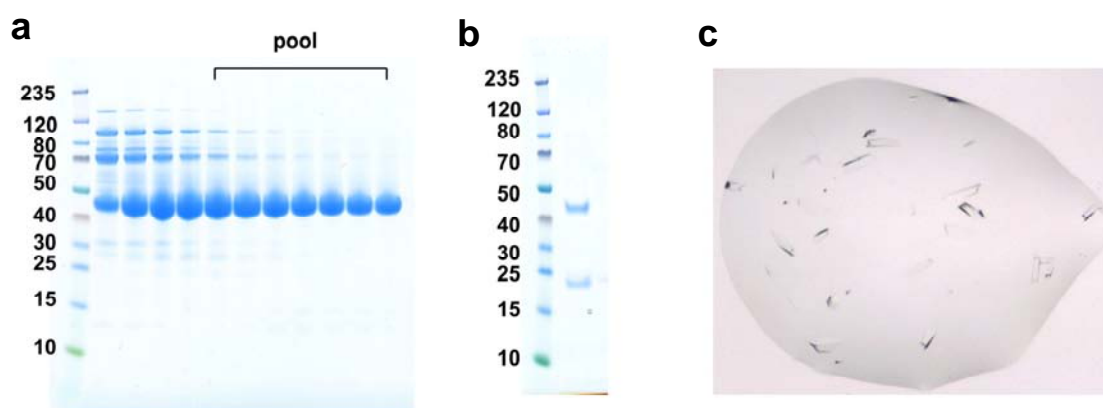


Figure 5-2. The purity of pCBL-B and crystals of pCBL-B-Ubch5B_{RK}-Ub complex.

(a) pCBL-B was purified by series of chromatography described in **Chapter 2**. The gel shows the purity of the protein after the final step, size-exclusion chromatography (SD75 GE). Fractions were pooled as indicated and concentrated to about 3.5 mg/ml for crystallization trials.

(b) The complex crystals were confirmed to contain pCBL-B (higher band) and Ubch5B_{RK}-Ub (lower band).

(c) The crystals of pCBL-B-Ubch5B_{RK}-Ub-ZAP-70 peptide complex.

5.2.2 Structure of pCBL-B-Ubch5B_{RK}-Ub-ZAP-70 peptide complex

The crystal of pCBL-B bound to Ubch5B_{RK}-Ub and ZAP-70 peptide diffracts to 2.21Å [219]. The complex crystallized in space group P 1 2₁ 1 with four copies of pCBL-B-Ubch5B_{RK}-Ub-ZAP-70 peptide tetramer per asymmetric unit. The four copies of tetramers are similar with r.m.s.d ranging from 0.41-0.57 Å for C α atoms. Data collection and refinement statistics are shown in **Table 5-1**. My discussion focuses on the complex with the best-defined model at the E3-Ub interface (Chains E-H).

Table 5-1. Data collection and refinement statistics

| pCBL-B-UbcH5B _{RK} -Ub-ZAP-70 peptide | |
|--|------------------------|
| Data Collection | |
| Space group | P 1 2 ₁ 1 |
| Cell dimensions | |
| a, b, c (Å) | 95.0, 131.8, 122.0 |
| α , β , γ (°) | 90.0, 91.9, 90.0 |
| Resolution (Å) | 30.54-2.21 (2.27-2.21) |
| R_{merge} (%) | 0.058 (0.688) |
| I/σ | 14.2 (2.1) |
| Completeness (%) | 99.6 (99.9) |
| Redundancy | 3.4 (3.5) |
| Wilson B factor | 43.3 |
| Refinement | |
| Resolution (Å) | 30.5-2.21 |
| No. reflections | 149,230 |
| $R_{\text{work}}/R_{\text{free}}$ | 0.175/0.211 |
| No. atoms | |
| Protein | 19,758 |
| Ions | 12 |
| Solvent | 776 |
| B -factors (Å ²) | |
| Protein | 48.1 |
| Ions | 44.1 |
| Solvent | 41.0 |
| R.m.s. deviations | |
| Bond length (Å) | 0.004 |
| Bond angles (°) | 0.811 |

Note: Highest-resolution shell is shown in parenthesis.

The structure of pCBL-B-UbcH5B_{RK}-Ub-ZAP-70 peptide complex reveals extensive contacts between pCBL-B's LHR-RING domain and UbcH5B_{RK}-Ub (**Figure 5-3**). The structures of UbcH5B_{RK} and Ub resemble previously published UbcH5B and Ub structures (PDB 3A33 [195]) with r.m.s.d of 0.685 and 0.511 for C α atoms respectively. The structure of pCBL-B is similar to pTyr371-c-CBL portion from the pTyr371-c-CBL-UbcH5B-ZAP-70 peptide complex [200] with r.m.s.d of 1.43 for C α atoms (**Figure 5-4**). Like in pTyr371 c-CBL, pCBL-B's LHR-RING domain undergoes remarkable conformational changes and brings E2 (in this case UbcH5B_{RK}-Ub) adjacent to the TKBD substrate-binding site (**See section 4.3**). In this structure, Ub's C-terminal tail is conjugated to UbcH5B's active site via an isopeptide linkage and UbcH5B_{RK}-Ub is facing the ZAP-70 peptide (**Figure 5-3**). The mode of

ZAP-70 peptide binding is analogous to other CBL TKBD-peptide complexes [52, 139].

pCBL-B RING-UbcH5B interactions resemble other E2-CBLs complexes [52, 200]. Upon binding to UbcH5B, Ub's globular body is stabilized by numerous interactions between UbcH5B's $\alpha 3$ helix and Ub's Ile44 patch, and between pCBL-B RING domain and Ub's Ile36 surface. These interactions are nearly identical to those observed in dimeric RING E3-E2-Ub complexes [201, 212]. Notably, pCBL-B LHR also packs against Ub's Ile36 patch and pTyr363 directly contacts Ub (Figure 5-3).

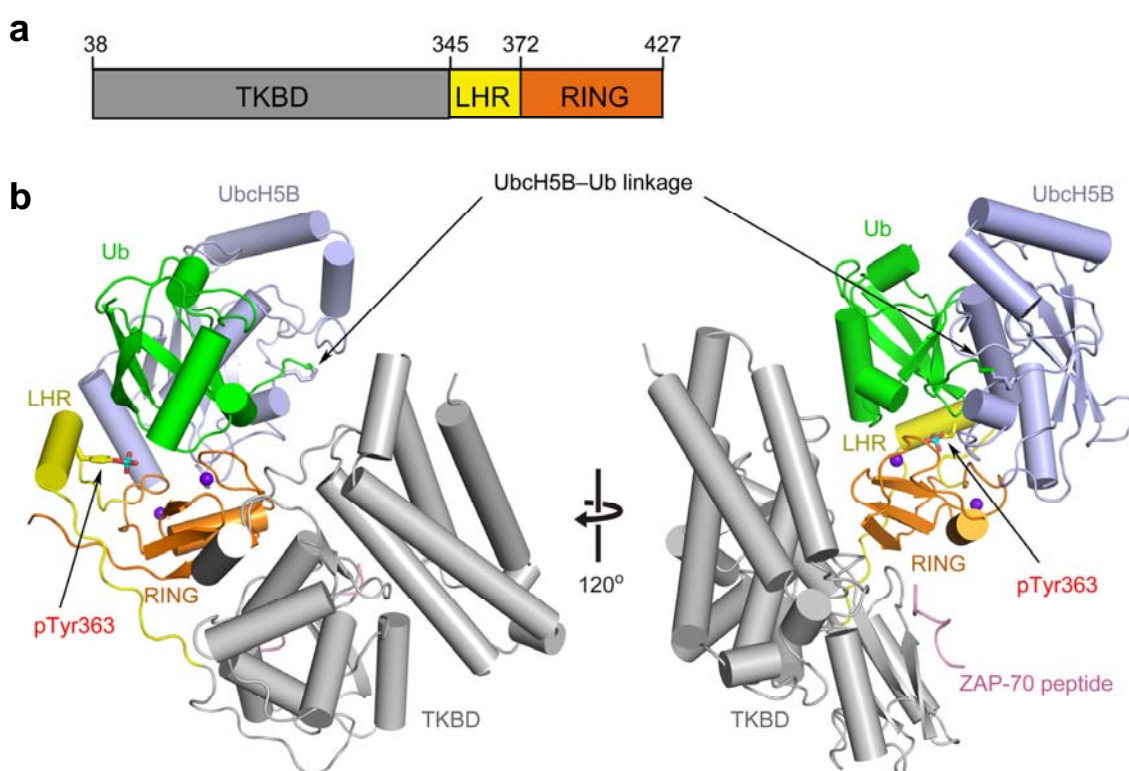


Figure 5-3. Overall structure of pCBL-B-UbcH5B_{RK}-Ub-ZAP-70 peptide.

(a) Diagram of the crystallized pCBL-B: TKBD in gray, LHR in yellow and RING domain in orange. Residues encompassing each domain are indicated.

(b) Cartoon representation of the complex. Left and right panels are related by 120° rotation about the y-axis. pCBL-B domains are coloured as in a. Ub is coloured green; UbcH5B, light blue; ZAP-70 peptide, pink; pTyr363 side chain is shown as sticks and phosphorus is coloured cyan. Zn²⁺ atoms are demonstrated as purple spheres.

5.2.3 pCBL-B adopts an active RING conformation

Our earlier study on c-CBL suggested that, upon phosphorylation, pTyr releases the LHR, frees up the RING domain, and induces an active RING conformation (Chapter 4) [200]. In the pCBL-B–UbcH5B_{RK}–Ub–ZAP-70 peptide structure, pCBL-B adopts a similar conformation as the active RING conformation of pTyr371-c-CBL (Figure 5-4). The region containing LHR and RING domain, termed as pCBL-B_{LRR}, resembles the NMR model of phosphorylated CBL-B (residues 353-426) with r.m.s.d of 1.03 Å for C α atoms [199].

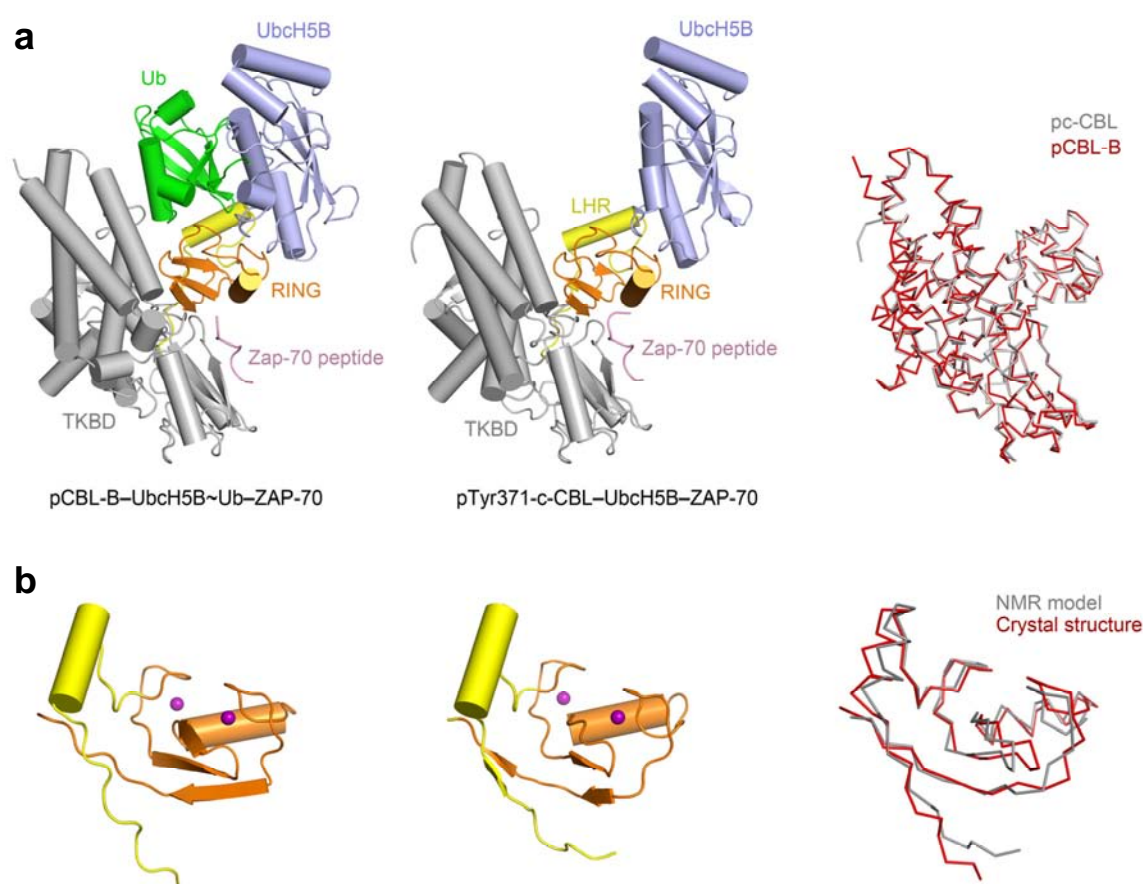


Figure 5-4. pCBL-B adopts an active RING conformation.

(a) Left panel: structure of pCBL-B–UbcH5B_{RK}–Ub–ZAP-70 peptide complex. Middle panel: structure of pTyr371-c-CBL–UbcH5B–ZAP-70 peptide complex (PDB 4A4C [200]). Right panel: superposition of pCBL-B (red) and pTyr371-c-CBL (gray) (r.m.s.d of 0.65 Å for all C α atoms).

(b) Left panel: the pCBL-B_{LRR} portion of pCBL-B–UbcH5B_{RK}–Ub–ZAP-70 peptide complex. Middle panel: NMR model of phosphorylated CBL-B (residue 345-426) (PDB 2LDR [199]). Right panel: superposition of the pCBL-B_{LRR} from my structure (left panel, coloured red) and the NMR model (middle panel, coloured gray) (r.m.s.d of 1.03 Å for all C α atoms). Colouring is as described in Figure 5-3. Zn²⁺ atoms are shown as purple spheres.

In my structure, pCBL-B's RING domain faces the substrate-binding site of the TKBD, and the LHR is adjacent to the RING domain, which appears to extend the E2-binding surface (**Figure 5-5a**). Notably, pTyr363 of pCBL-B does not directly contact E2 but interacts directly with the RING domain as observed in pTyr371-c-CBL-UbcH5B-ZAP-70 peptide structure [200]. pTyr363's phosphate moiety is stabilized by RING domain's Lys374 and Lys381 side chains. The aromatic side chain of pTyr363 is stabilized by hydrophobic interactions involving LHR's Leu362, Met366 and Phe370 and RING domain's Leu391, Ile421 and Val423 (**Figure 5-5b**). These interactions make up the new LHR configuration that is different from the LHR conformation in the unphosphorylated state (**See section 4.3.2**). This new LHR configuration is called the pTyr363-induced element in CBL-B.

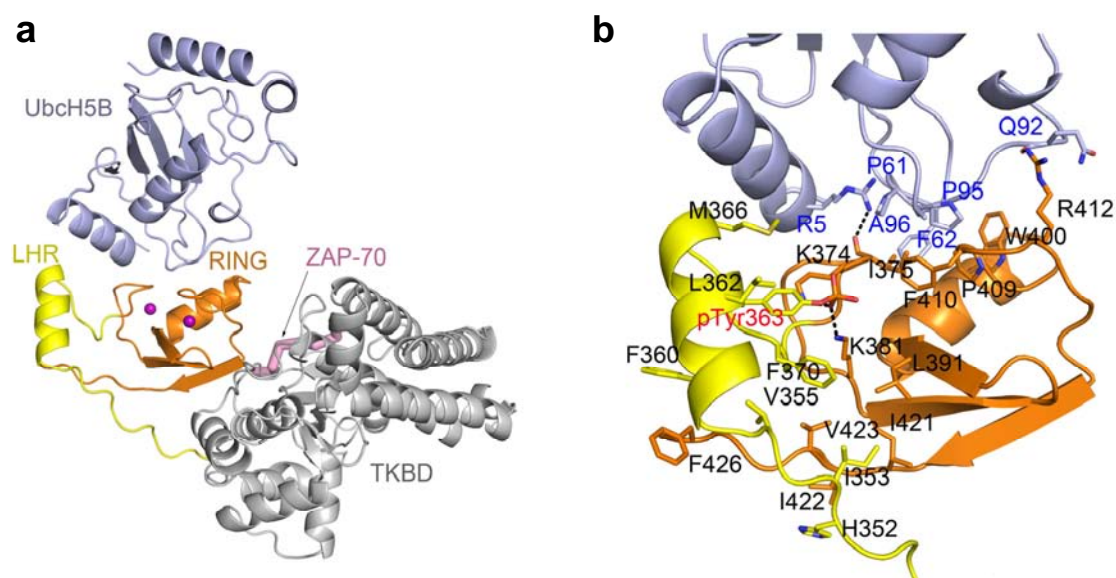


Figure 5-5. The LHR-binding surface in pCBL-B-UbcH5B_{RK}-Ub-ZAP-70 peptide structure.

(a) The portion of pCBL-B-UbcH5B_{RK}-Ub-ZAP-70 peptide from the structure of pCBL-B-UbcH5B_{RK}-Ub-ZAP-70 peptide demonstrates that the RING domain is adjacent to the ZAP-70 peptide binding site of TKBD. Colouring is as described in **Figure 5-3**.

(b) Close-up view of the LHR-binding surface in pCBL-B. Key residues are shown as sticks with N atoms blue, O atoms red and S atom yellow. Putative hydrogen bonds are shown as dashed lines. pTyr363 is labelled red.

Our earlier study with pTyr371 c-CBL fragment showed that pTyr371 activates E3 activity by 1,400-fold [200]. This is partly due to disruption of autoinhibition and increased LHR flexibility thereby allowing the RING domain to sample different lysine site. To investigate the direct effect of pTyr363 in Ub transfer, I assayed CBL-

B constructs containing the LHR and the RING domain in both phosphorylated and unphosphorylated forms (termed as pCBL-B_{LRR} and CBL-B_{LRR}), thereby eliminating other contributions. Using lysine-discharge reactions, I showed that in the presence of CBL-B_{LRR}, UbcH5B~Ub was completely discharged to free UbcH5B and Ub after 10 min; whereas in the presence of pCBL-B_{LRR}, UbcH5B~Ub discharged much faster (**Figure 5-6**). In addition, Y360F substitution used for structural determination, does not affect enzyme activity in both unphosphorylated and phosphorylated states. This result suggested that pTyr363 directly contributes to the enhancement in activity.

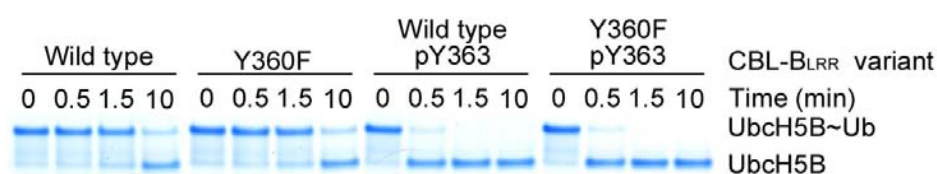


Figure 5-6. Lysine-discharge reactions on unphosphorylated and phosphorylated CBL-B variants.

Non-reduced SDS-PAGE shows the disappearance of UbcH5B~Ub with CBL-B_{LRR} variants (120 nM) in the presence of L-lysine over time.

5.2.4 Detailed interactions and validation

Numerous donor Ub interactions with UbcH5B and pCBL-B are observed in this structure. UbcH5B's $\alpha 3$ interacts with Ub's Ile44 patch (**Figure 5-7a**) and UbcH5B's $\alpha 2$ interacts with Ub's tail (**Figure 5-7b**). pCBL-B's RING contacts Ub's Ile36 patch, establishing the RING-Ub interface. This interface is formed by hydrophobic interactions between pCBL-B's Phe410, His390, and Cys411 and Ub's Thr9, Ile36, and Pro37. Hydrogen bonds occur between the side chains of pCBL-B's Arg412 and Ub's Gln40; and between pCBL-B's His390 and the backbone oxygen of Ub's Glu34 (**Figure 5-7c**). These Ub interactions strongly resemble those observed in the dimeric RING E3s-UbcH5-Ub complexes [201, 212] (**Chapter 3**).

In place of the dimer tail in dimeric RING E3s, the pTyr363-induced element directly interacts with donor Ub's Ile36 surface (**Figure 5-7c and d**). The phosphate moiety from pCBL-B's pTyr363 forms a hydrogen bond with the side chain of Ub's Thr9. In

addition, pCBL-B's Leu362, pTyr363, and Met366 from the LHR form hydrophobic interactions with the hydrophobic side chain of Ub's Lys11 (**Figure 5-7c**).

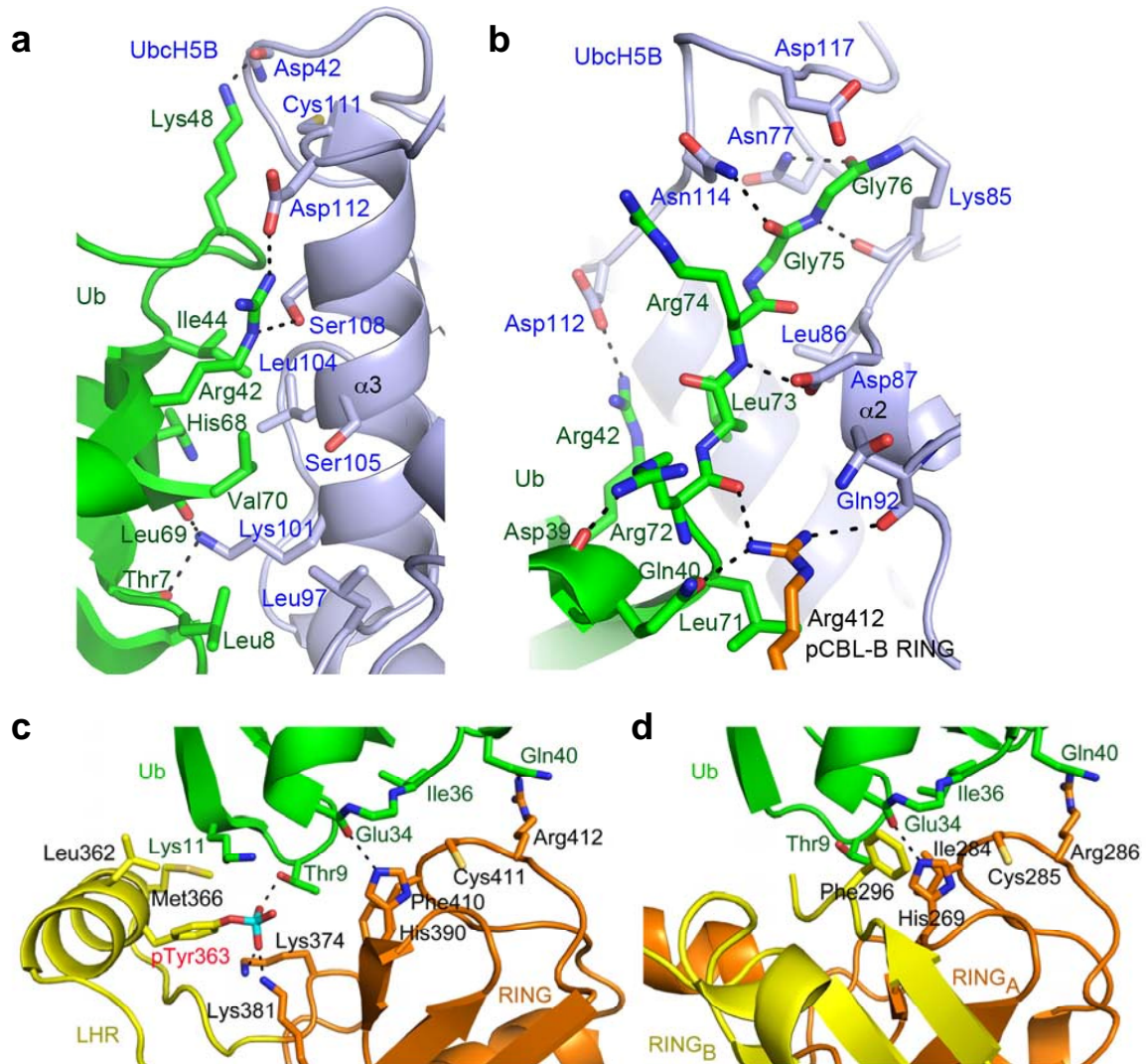


Figure 5-7. Detailed donor Ub interactions.

(a) Detailed interactions between Ub's Ile44 surface and UbcH5B's $\alpha 3$. Colouring is as described in **Figure 5-3** with N atoms blue, O atoms red, and S atoms yellow. Putative hydrogen bonds are shown as dashed lines.

(b) Detailed interactions between Ub's tail and UbcH5B's $\alpha 2$.

(c) Detailed interactions between Ub's Ile36 surface and pCBL-B.

(d) Close-up view of the BIRC7-Ub's Ile36 patch (PDB 4AUQ [201]). RING_A coloured orange is in the same orientation as the pCBL-B RING domain in **a**. The second subunit of the dimer is coloured yellow. Ub and UbcH5B are coloured as in **Figure 5-3**.

To verify these interactions, key residues of UbcH5B and Ub were mutated and tested in single-turnover lysine-discharge assays. My results showed that mutations on the E2-Ub's Ile44 patch or E2-Ub's tail caused defects in Ub transfer. Ub D58A that is distal to any donor Ub interface had similar activity to wild type. UbcH5B S22R that sits on the backside of E2 displayed similar activity to wild type in lysine-discharge assay (**Figure 5-8**). Disrupting the pTyr363-RING domain interaction (K381A) or mutating a key CBL-B residue that sits at the junction of RING, UbcH5B, and Ub (R412A) caused defects in Ub transfer (**Figure 5-8c**).

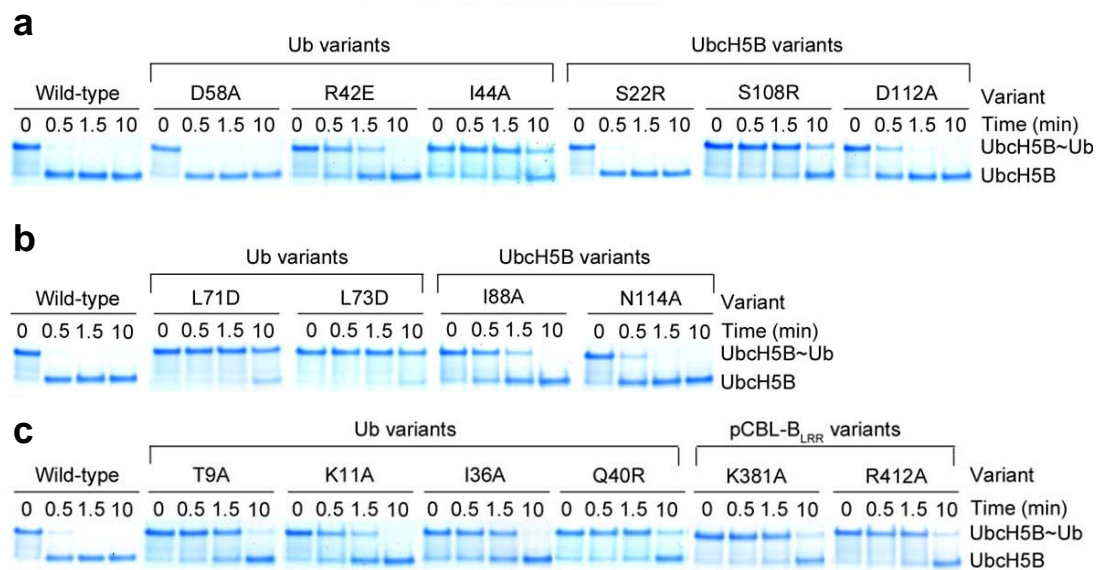


Figure 5-8. Effects of UbcH5B and Ub mutations on Ub transfer by pCBL-B_{LRR}.
(a) Non-reduced SDS-PAGE of pulse-chase lysine-discharge reactions show the disappearance of UbcH5B~Ub with UbcH5B and Ub variants in the presence of L-lysine over time. Selected mutations on residues from the E2-Ub's Ile44 patch were tested.
(b) Same as in **a**, but with mutants from the E2-Ub's tail.
(c) Same as in **a**, but with mutants from the E3-Ub.

5.2.5 Kinetics validation

5.2.5.1 Kinetic assay design

Based on the preliminary SPR data done by Gary Sibbet, we estimate that pCBL-B_{LRR} binds UbcH5B~Ub with K_d of less than 1 μ M. At this concentration ranges, the pulse-chase kinetic experiment described in **Chapter 3** is not suitable due to the detection sensitivity problem (here I am working in UbcH5B~Ub concentration range that is 10 times less than that reported for BIRC3 in **Section 3.2.6** and hence 10-fold less detection sensitivity). To overcome this problem, I decided to perform the kinetic analyses by continuously regenerating UbcH5B~Ub with saturated E1 concentration. In this system, UbcH5B was pre-charged with ³²P-Ub, and then the reaction was initiated by addition of a mixture of CBL-B_{LRR} variants and acceptor Ub. The acceptor Ub has a C-terminal deletion of Gly75 and Gly76 and an N-terminal His tag (His-Ub Δ GG), which cannot be activated by E1. Under this condition UbcH5B~³²P-Ub was continuously charged by saturated E1 and this was confirmed by monitoring UbcH5B~³²P-Ub formation over UbcH5B concentration range in the presence of E3 and His-Ub Δ GG (**Figure 5-9a and b**). The linear relationship between UbcH5B~³²P-Ub over UbcH5B concentration range indicated that UbcH5B~³²P-Ub was continuously recharged by saturated E1. By quantifying the amount of DiUb formation over UbcH5B concentration range, I can plot rate of DiUb formation over UbcH5B concentration to determine the kinetic constants for the reaction (**Figure 5-9c and d**). Like in **Section 3.2.6**, the reactions were performed under initial rate condition. In this case less than 0.2% of His-Ub Δ GG was modified by ³²P-Ub, thus the acceptor Ub concentration is not altered significantly during the reactions. In addition, there was no observable autoubiquitination of CBL-B_{LRR} or pCBL-B_{LRR}. Kinetic data process and original autoradiogram representation are shown in **Appendix 3**.

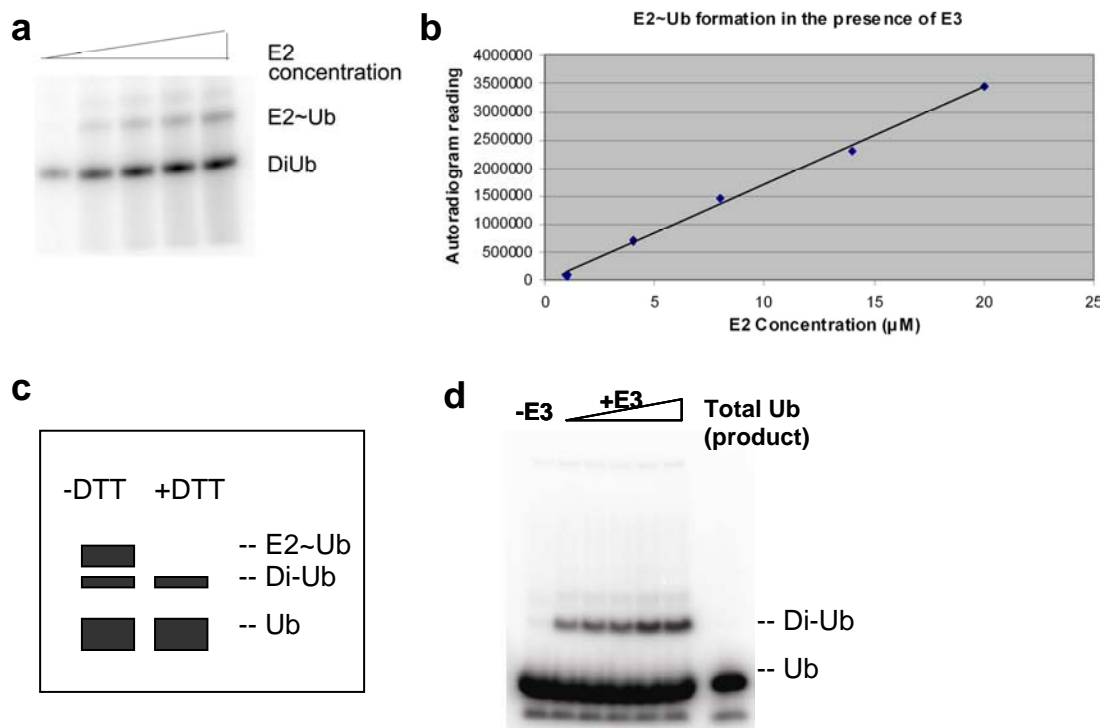


Figure 5-9. Kinetic reactions within initial rate under certain conditions.

(a) Non-reduced autoradiogram shows the formation of DiUb with increasing concentrations of E2~Ub and pCBL-B_{LRR} (450 nM).

(b) The autoradiogram reading of E2~Ub formed in a was plotted against E2 concentration. The linear curve suggests that E3-catalysed Ub transfer does not affect E2~Ub formation.

(c) Strategy for visualization of DiUb formation with or without DTT.

(d) Reduced autoradiogram shows the formation of DiUb in the absence or presence of E3 at 2 min. The reaction is enhanced with increasing concentrations of E3. Total product is visualized by total donor ³²P-Ub. The E3 concentration is selected by forming less than 15% of total product.

5.2.5.2 Kinetic validation using CBL-B_{LRR}

The kinetic analyses on CBL-B_{LRR} and pCBL-B_{LRR} were first performed with wild-type Ub and UbcH5B. The kinetic data suggested that phosphorylation activates CBL-B_{LRR} by reducing K_m and increasing k_{cat} (Figure 5-10a and b).

According to the structural alignment (Figure 5-7c and d), pTyr363-induced element seems to functionally replace the dimer tail in BIRC7 that plays an essential role in priming Ub for transfer (Chapter 3). In dimeric RING E3s, mutations on the E2-Ub or E3-Ub interfaces increase K_m and decrease k_{cat} in DiUb formation reactions

(Chapter 3). If pTyr363-induced element and the dimer tail have similar functions in Ub transfer, disrupting the pTyr363-Ub interface or perturbing the LHR-binding surface will likewise affect both K_m and k_{cat} . Therefore, I assayed mutational effects from pCBL-B_{LRR}'s K381A and Ub's T9A in DiUb formation assays. These mutations resulted in increased K_m and reduced k_{cat} as compared to pCBL-B_{LRR} (Figure 5-10). Thus, pTyr363-induced element plays a similar role as the dimeric BIRC7 tail in stabilizing donor Ub globular body, thereby allowing optimal positioning of Ub'C-terminal tail and hence the thioester bond for catalysis.

Our previous kinetic data on autoubiquitination suggest that phosphorylation activates c-CBL fragment (~ 1,400- fold enhancement) by disrupting autoinhibition, enhancing E2 binding, and inducing conformational changes [200]. By using CBL-B_{LRR} variants, I showed that the pTyr363-induce element alone enhances the activity of CBL-B by ~ 180-fold (Table 5-2).

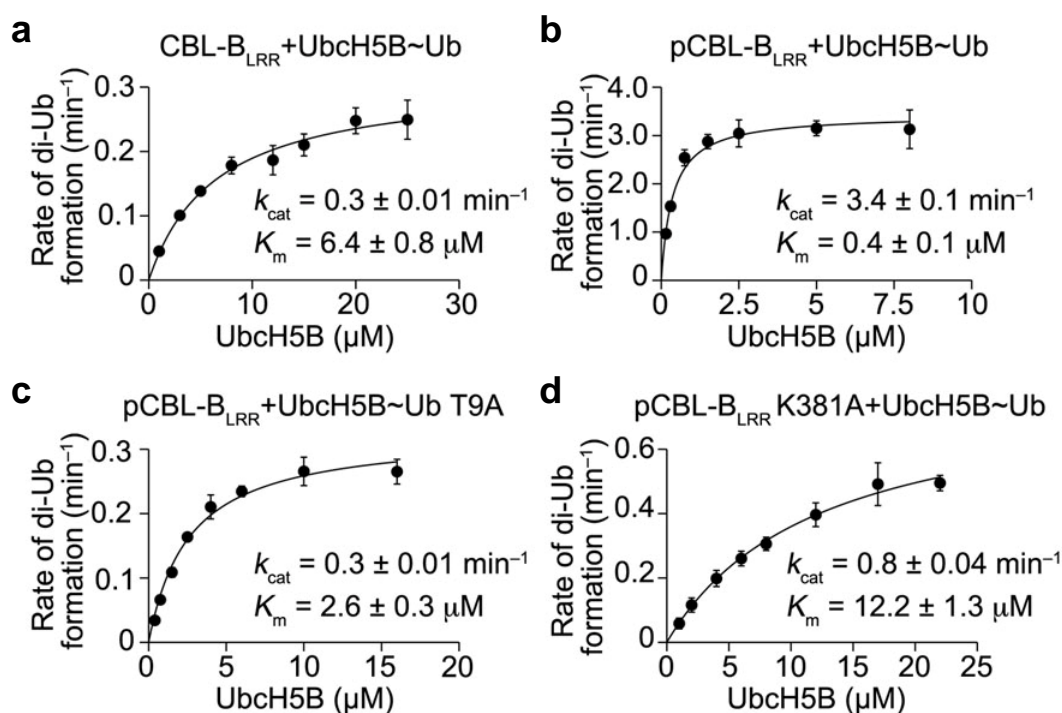


Figure 5-10. Effects of pTyr363-Ub interface on the Ub transfer kinetics.

(a) Kinetics of DiUb formation catalysed by CBL-B_{LRR}. The rate of DiUb formation was plotted against Ubch5B concentration for wild-type Ubch5B and ³²P-Ub.
 (b) As in a but performed with pCBL-B_{LRR} and wild-type ³²P-Ub.
 (c) As in a but with pCBL-B_{LRR} and ³²P-Ub T9A
 (d) As in a but with pCBL-B_{LRR} K381A and wild-type ³²P-Ub. All reactions were performed in triplicate. Kinetic parameters are indicated. Error bars, s.d.

Table 5-2. CBL-B_{LRR} kinetics of DiUb formation assay.

| CBL-B_{LRR} variants (μM) | k_{cat} (min^{-1}) | K_{m} (μM) | $k_{\text{cat}}/K_{\text{m}}$ ($10^3 \text{ min}^{-1}\text{M}^{-1}$) | Effect of pTyr363 |
|---|---|---|---|---------------------------|
| CBL-B _{LRR} (2 μM) | 0.3 \pm 0.01 | 6.4 \pm 0.8 | 47 | |
| pCBL-B _{LRR} (0.15 μM) | 3.4 \pm 0.1 | 0.4 \pm 0.1 | 8500 | 180-fold enhancement |
| E3 or Ub variants (μM) | k_{cat} (min^{-1}) | K_{m} (μM) | $k_{\text{cat}}/K_{\text{m}}$ ($10^3 \text{ min}^{-1}\text{M}^{-1}$) | Mutational effects |
| pCBL-B _{LRR} (0.15 μM) with Ub wild-type | 3.4 \pm 0.1 | 0.4 \pm 0.1 | 8500 | |
| pCBL-B _{LRR} (1.5 μM) with Ub T9A | 0.3 \pm 0.01 | 2.6 \pm 0.3 | 115 | 75-fold defective |
| pCBL-B _{LRR} K381A (1.2 μM) with Ub wild-type | 0.8 \pm 0.04 | 12.2 \pm 1.3 | 66 | 130-fold defective |

5.2.6 The model of unphosphorylated CBL_{LRR}-UbcH5B_{RK}-Ub

Kinetic analyses suggest that the pTyr363-induced element is crucial for Ub transfer catalysed by pCBL-B_{LRR}. Unphosphorylated CBL-B_{LRR} lacking the pTyr363-induced element is less active but retains E3 activity. It questions whether CBL-B_{LRR} uses similar mechanism to facilitate Ub transfer. Based on a model of c-CBL_{LRR}-UbcH5B_{RK}-Ub, it appears that most donor Ub interactions are present expect the LHR-Ub (**Figure 5-11a**). To verify these interactions, same sets of UbcH5B, Ub mutants were tested in single-turnover lysine-discharge assays using CBL-B_{LRR} variants. To make sure the reaction is completed for wild type, 10-fold amount of CBL-B_{LRR} variants were used here compared to **Figure 5-6**. The results suggest that mutations on the UbcH5B-Ub's Ile44 patch and RING-Ub's Ile36 patch caused defect in Ub transfer. These mutants include Ub's T9A, I36A, I44A, L73D, and UbcH5B's D87A, S108R, D112A. CBL-B_{LRR}'s Arg412 corresponds to c-CBL_{LRR}'s Arg420 that contacts both UbcH5B and Ub in the model. Mutation on this residue also caused defect in Ub transfer (**Figure 5-11b**).

Based on the structure of pCBL-B-UbcH5B_{RK}-Ub-ZAP-70 peptide, both Lys11 of Ub and Lys381 of pCBL-B interact with pTyr363 to maintain the pTyr363-Ub

interaction. However, in the model of c-CBL_{LRR}-UbcH5B_{RK}-Ub, Ub's Lys11 and c-CBL_{LRR}'s Lys389 that corresponds to CBL-B_{LRR}'s Lys381 are not involved in any interactions. Biochemical results suggest that mutations on these two residues displayed similar activity to wild type. Y360F substitution in CBL-B_{LRR} (Y368F in c-CBL_{LRR}) used for structural determination should not affect structure and enzyme activity of CBL-B_{LRR} [199, 200], thus cooperation of Y360F had no effect in lysine-discharge reactions catalysed by CBL-B_{LRR} variants (**Figure 5-11b**). According to modelling and biochemical data, unphosphorylated CBL-B_{LRR} likely promotes Ub transfer by stabilizing donor Ub in a similar manner. However, it is important to note that in the absence of Tyr363-induced element, unphosphorylated CBL-B_{LRR}'s catalytic efficiency is reduced by ~180-fold (**Table 5-2**) and this may have a significant implication for its activity *in vivo*.

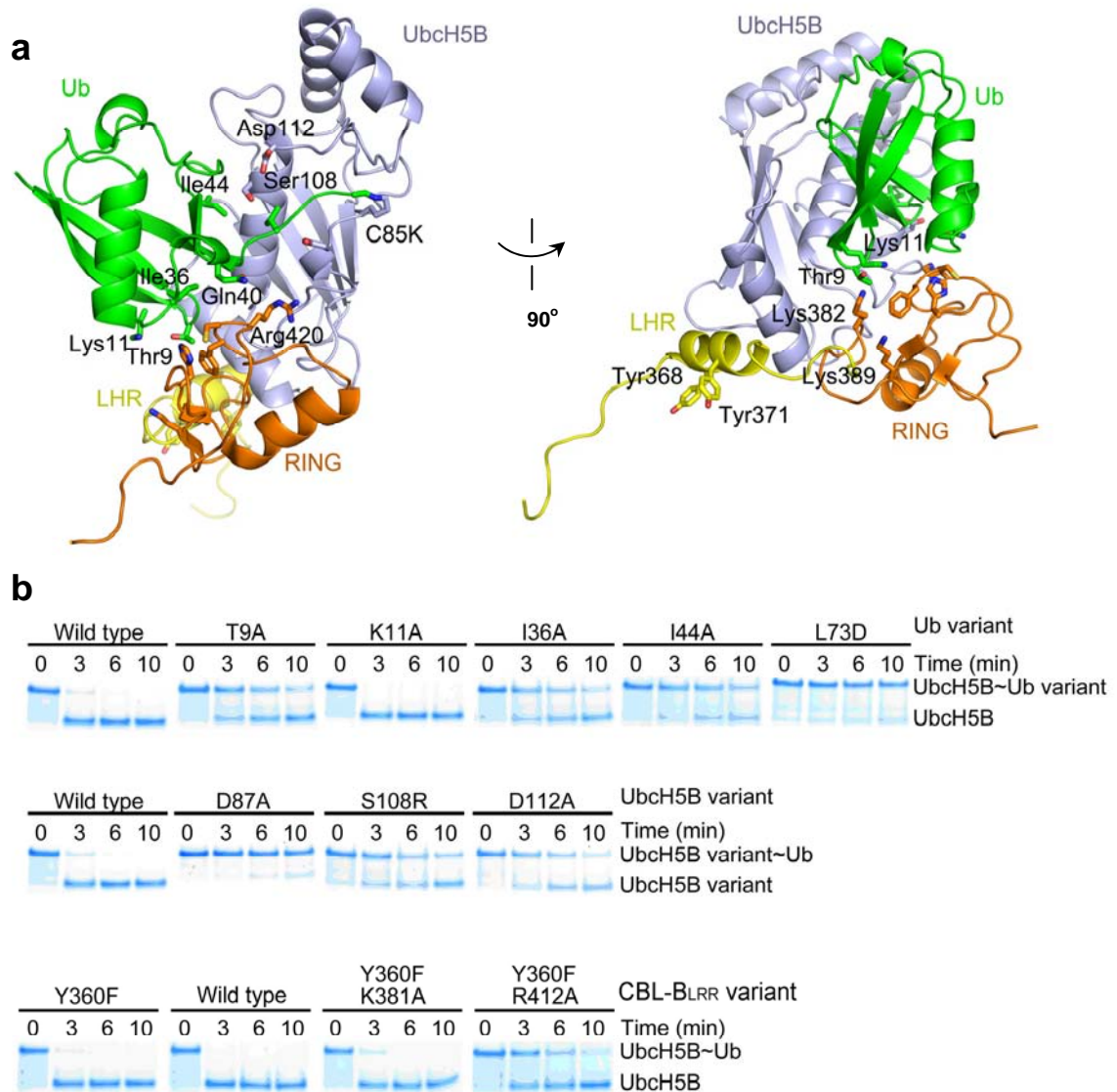


Figure 5-11. Lysine-discharge assay on unphosphorylated CBL-B_{LRR}.

(a) The model of c-CBL_{LRR}-UbcH5B_{RK}-Ub generated by superposing the RING domain of c-CBL_{LRR} from PDB 1FBV [52] onto pCBL-B-UbcH5B_{RK}-Ub-ZAP-70 peptide. Colouring is as described in **Figure 5-3**. Residues Tyr368, Tyr371, Lys382, Lys389, and Arg420 in c-CBL_{LRR} correspond to Tyr360, Tyr363, Lys374, Lys381, and Arg412 in CBL-B_{LRR}, respectively.

(b) Lysine-discharge reactions were performed under pulse-chase conditions with unphosphorylated CBL-B_{LRR} variants (1.2 μM). The same sets of Ub or UbcH5B mutants were assayed as in the pCBL-B assays. Non-reduced SDS-PAGE shows the disappearance of UbcH5B~Ub over time. The results indicate that the RING-Ub's Ile36 and the E2-Ub's Ile44 are crucial for Ub transfer mediated by CBL-B_{LRR}. Whether the LHR in the unphosphorylated state adopts in the pTyr-LHR conformation and plays a similar role in stabilizing donor Ub remains unclear.

5.3 Discussion

5.3.1 The donor Ub configuration poised for transfer

In **Chapter 3**, I showed that the C-terminal tails of donor Ub in the BIRC7_{239-C}-UbcH5B_{RAS}-Ub and RNF4-UbcH5A-Ub structures [212] are clamped by the E2s' active site residues. By locking the C-terminal tail of Ub, the thioester bond is optimized for nucleophilic attack by the substrate's lysine. To achieve this optimal Ub's C-terminal tail configuration, numerous interactions are essential to stabilize the globular Ub body including E2-Ub, RING-Ub, and dimer tail-Ub interactions.

CBL-B adopts a similar strategy as the dimeric RING E3s BIRC7 and RNF4. The Ub's C-terminal tail locking mechanism is observed in the pCBL-B-UbcH5B_{RK}-Ub-ZAP-70 peptide structure (**Figure 5-12a to c**). The E2-Ub's Ile44 patch and RING-Ub interactions observed in dimeric E3 complexes are conserved in this structure. The pTyr-induced element in pCBL-B seemingly replaces the dimer tail by contacting Ub's Ile36 surface. Thus, the mode of Ub-stabilizing mechanism observed in this structure is similar to that observed in dimeric E3 complexes. These structural observations are further confirmed by my biochemical and kinetic analyses.

Interestingly, similar Ub's C-terminal tail configuration was found in a non-RING SUMO E3 RanBP2 complex structure [220]. The C-terminal tail of SUMO is locked by Ubc9's active site residues and the globular body of SUMO is stabilized via contacts from the E2-binding domain of RanBP2 and an N-terminal extension that contains a SUMO-interacting motif [220] (**Figure 5-12d**). For the SUMO RING E3 Siz/PIAS, it remains unknown how it promotes SUMO transfer. Biochemical assays suggested that acidic patch on the α -helix outside of the RING domain may play a role in positioning SUMO [221]. This observation is consistent with a model of Siz1-Ubc9-SUMO (**Figure 5-12e**). Recently, an Ub-loaded HECT complex structure reveals a similar Ub tail locking mechanism required for Ub transfer by a HECT E3 [222] (**Figure 5-12f**).

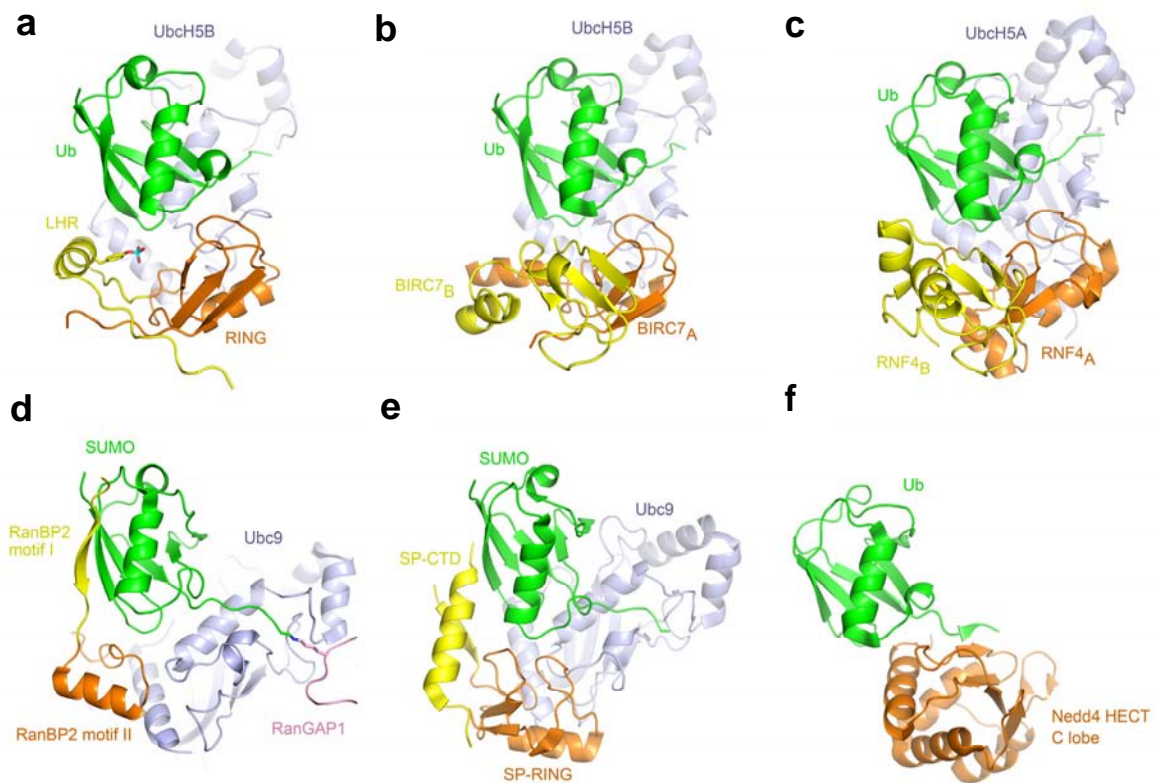


Figure 5-12. Comparison of E3–E2–Ub/SUMO complexes.

(a) A portion of pCBL-B–Ubch5B_{RK}–Ub–ZAP-70 peptide structure lacking the TKBD. Colouring is as described in **Figure 5-3**.

(b) A portion of BIRC7_{239-C}–Ubch5B_{RAS}~Ub structure lacking one copy of Ubch5B~Ub is displayed by aligning the BIRC7_A to the RING domain of pCBL-B in **a**. BIRC7_A is coloured orange and BIRC7_B yellow.

(c) A portion of RNF4–Ubch5A–Ub structure lacking one copy of Ubch5A–Ub (PDB 4AP4 [212]) is displayed as in **b**. The RING domain of RNF4 that binds Ubch5A in the portion is labelled as RNF4_A and coloured orange. The other subunit is labelled RNF4_B and coloured yellow.

(d) Structure of RanBP2–Ubc9–SUMO–RanGAP1 complex (PDB 1Z5S [220]) is displayed by aligning SUMO to Ub in **a**. The E2-binding domain is coloured orange, E2 light blue, SUMO green and the SUMO-interacting component yellow.

(e) Model of a portion of Siz1 RING E3 (PDB 3I2D [221]) bound to Ubc9 and SUMO generated by aligning Siz-1 RING domain to pCBL-B RING domain in **a**, and by superposing Ubc9 with SUMO from PDB 1Z5S [220] onto Ubch5B in **a**. The E2-binding domain is coloured orange, E2 light blue, SUMO green and the potential SUMO-interacting component yellow.

(f) A portion of Nedd4 HECT~Ub (PDB 4BBN [222]) is displayed by aligning to Ub in **a**. The C-lobe Nedd4 is coloured orange and Ub green.

5.3.2 Additional element outside the RING domain may be required for other monomeric RING E3 activity

In all three RING E3–UbcH5–Ub structures (**Figure 5-12a to c**), the donor Ub's Ile36 patch is stabilized by the RING domain and additional component outside the RING domain. In dimeric E3s, the tail acts as this additional Ub-binding component. In CBL-B, the pTyr363-induced element seemingly replaces the dimer tail and stabilizes the donor Ub. Biochemical results suggest that removing the dimeric partner or phosphorylation-induced element cause defects in Ub transfer reactions (**Chapter 3 and 5**). These results suggested that RING domain alone is not sufficient for optimal Ub transfer and an additional Ub-binding element outside the RING domain is required in these three RING E3s.

Notably, key residues on the RING domain that are involved in binding Ub (His390, Phe410, and Arg412 in pCBL-B) are highly conserved in CBL family proteins. This His-Cys-Arg-Phe/Ile/Thr arrangement is also found in other E3s (**Figure 5-13**). Biochemical studies on other dimeric RING E3s suggested that mutations at the C-terminal dimer tail also caused defects in Ub transfer catalysed by BIRC3 (**Chapter 3**) and XIAP [128]. It seems that the RING domain with the His-Cys-Arg-Phe/Ile/Thr arrangement is not sufficient to stabilize donor Ub configuration, thus these E3s may require an additional Ub-binding surface for Ub transfer. Future studies are required to support this hypothesis.

However, some E3s such as RBX1, CHIP, and E4B do not share the His-Cys-Arg-Phe/Ile/Thr arrangement (**Figure 5-13**). The molecular mechanism of Ub transfer by these E3s remains unclear. Recently, dimeric U-box E3 CHIP and RNF4 were suggested to use a similar mechanism to catalyse Ub transfer [212], indicating that an additional element outside the RING domain (the dimer tail) may also be required in CHIP. However, available structures of full-length Ufd2p (a yeast homolog of E4B) and RBX1 in CRL complexes do not reveal obvious element outside the canonical RING/U-box domain that has potential to bind donor Ub [223-225]. Previous NMR studies indicated that RBX1 and E4B may not require an additional Ub-binding element for Ub transfer. RBX1 was shown to bind CDC34~Ub with about 50-fold higher affinity than CDC34 [226]. E4B was suggested to promote the UbcH5C~Ub to adopt a closed conformation, which is more reactive for Ub transfer [214, 215]. More

studies are needed to investigate whether additional element outside the RING/U-box domain is crucial for other E3s to catalyse Ub transfer.

| | | | | | | | | | | | | | | |
|--------|------|---------------------------|-----|-------|-----|---------|-----|----------------|---|--------------------|----------------------------|-----|-------------------------|------|
| | | | * * | | | * * * * | | * * | | | | | | |
| CBL-B | 371 | QLCKICAE | --- | NDKDV | --- | KIEPC | --- | GHLM | - | CTSCLTAWQESDGGQGCP | FCR CEIKGTEPIIVDPFD | 427 | | |
| c-CBL | 379 | QLCKICAE | --- | NDKDV | --- | KIEPC | --- | GHLM | - | CTSCLTSWQESDGGQGCP | FCR CEIKGTEPIIVDPFD | 435 | | |
| CBL-c | 349 | ELCKICAE | --- | SNKDV | --- | KIEPC | --- | GHLI | - | CSCCLAAWQHSDSQTCP | FCR CEIKGWEAVSIYQFH | 405 | | |
| BIRC7 | 250 | RTCKVCLD | --- | RAVSI | --- | VFVPC | --- | GHLV | - | CAECAPG-IQ | --- | LCP | ICR APVRSRVRTFLS | 298 |
| BIRC3 | 555 | RTCKVCLD | --- | KEVSI | --- | VFVPC | --- | GHLV | - | VCKDCAPS-LR | --- | KCP | ICR STIKGTVRTFLS | 604 |
| RNF4 | 134 | VSCPICMDGYSEIVQNGRLIVSTEC | --- | G | --- | HVF | - | CSQCLRDSLKNAN | - | TCPT | CR KKINHKRYHPIYI | 194 | | |
| RNF168 | 14 | OQCGICME | --- | ILVE | --- | PVTIPC | --- | NHTL | - | CKPCFQSTVEKASLCCP | FCR RRVSS | 60 | | |
| MDM2 | 436 | EPCVICQG | --- | RPKNG | --- | CIVHGKT | --- | GHLMACFTCAKK | - | LKRNKPCP | VCR QPIQMIIVLYFP | 491 | | |
| RBX1 | 51 | DLCEIQANQASATSEECTVAWGVC | --- | N | --- | HAF | - | HFHCISRWLKTRQV | - | CPL | LDN REWEFQKYGH | 108 | | |
| CHIP | 239 | ISFELMRE | --- | PCI | --- | TPS | --- | GITY | - | DRKDIEEHLQRVGHFDP | VTR SPLTQEQILIPNL | 284 | | |
| E4B | 1107 | LMDTLMTD | --- | PVR | --- | LPS | --- | GTIM | - | DRSII LRHLINSPT | - | DP | FN RQTLTESMLEPVP | 1155 |

Figure 5-13. Sequence alignment of RING or U-box domains.

Protein sequences were aligned by Clustal W method in MegAlign software. Conserved residues that are potentially involved in Ub binding are coloured in red. Asterisks indicate the Zn-binding ligands on the RING domains. Upper panel: RING domains. Lower panel: U-box domains.

5.3.3 Implications for cancer-linked mutations

RTKs play critical roles in the regulation of cell proliferation, differentiation, and survival [227]. CBL proteins ubiquitinate RTKs toward degradation and function as negative regulators of the RTK signal transduction [228]. Recently, CBL mutations have been identified in human myeloid malignancies, including juvenile myelomonocytic leukemia (JMML), chronic myelomonocytic leukemias (CML), acute myeloid leukemia (AML), myelodysplastic syndromes, and myeloproliferative neoplasms [143]. c-CBL is also reportedly highly altered in non-small cell lung cancer (NSCLC) [229]. Most CBL mutations are likely to function in a dominant-negative manner. However, CBL mutations may also display a gain-of-function activity to activate aberrant signalling pathways, such as JAK-STAT and PI3K-AKT pathways [230, 231]. Previous studies showed that some cancer mutations found in CBL proteins induce cell transforming [142, 230] (**Table 5-3**). A combined CBL and CBL-B deficiency in hematopoietic stem cells reportedly leads to early-onset myeloid malignancies in mice [232].

Mapping c-CBL mutations from myeloid malignancies and NSCLC onto the structure of c-CBL-UbcH7-ZAP-70 peptide and a model of Tyr371-c-CBL-UbcH5B-ZAP-70

peptide indicates that these mutations probably affect CBL's E3 activity (**Figure 5-14**). Mutations within the TKBD may affect the TKBD folding, substrate binding and autoinhibition. Mutations within the LHR may affect the flexibility of the RING domain. Mutations on the LHR Tyr371 in c-CBL would prevent the phosphorylation-dependent activation of c-CBL. Mutations within the RING domains may affect RING domain folding, E2 binding, and Ub binding. More research is needed to understand how CBL mutations are related to cancers.

Table 5-3. Selected cancer mutations in c-CBL.

| Cancer mutations | Detected in cancers and validated <i>in vivo</i> | Possible structural effects |
|-------------------------|--|---|
| C419R (1255T>C) | Juvenile myelomonocytic leukemia (JML) [233] | Disrupts the RING domain folding, Ub binding |
| F418S (1253T>C) | Acute myeloid leukemia (AML) [234], JML [235], CML [236] | Reduces E2 binding |
| G375P (unknown) | AML [237]. | Reduces the RING domain flexibility |
| H320D (1096C>G) | Squamous cell lung cancer (SCC) [238]. | Disrupts substrate binding |
| H398R (1193A>G) | Chronic myelomonocytic leukemia (CML) [236]. | Disrupts RING domain folding, Ub binding |
| H94Y (280C>T) | Non-small cell lung cancer (NSCLC) [229]. | Disrupts TKBD folding |
| K382E (1144A>G) | AML [239]. | Disrupts the active RING conformation, autoinhibition, Ub binding |
| M374V (1120A>G) | Infant acute lymphoblastic leukaemia (ALL) [240]. | Disrupts Ub binding |
| Q249E (745C>G) | NSCLC. Increased cell viability and cell motility in NSCLC cells [229]. | Disrupts the active RING conformation |
| R420Q (1259G>A) | CML [236, 241]. Lost E3 activity and cell transformation in 32Ds cell [242]. | Affects E2 binding, Ub binding |
| Y371H (1111T>C) | JML [233, 235, 243], AML [244]. | Prevents phosphorylation, disrupts autoinhibition |
| Y371D (1111T>G) | JML [235], CML [236] | Prevents phosphorylation, disrupts autoinhibition |

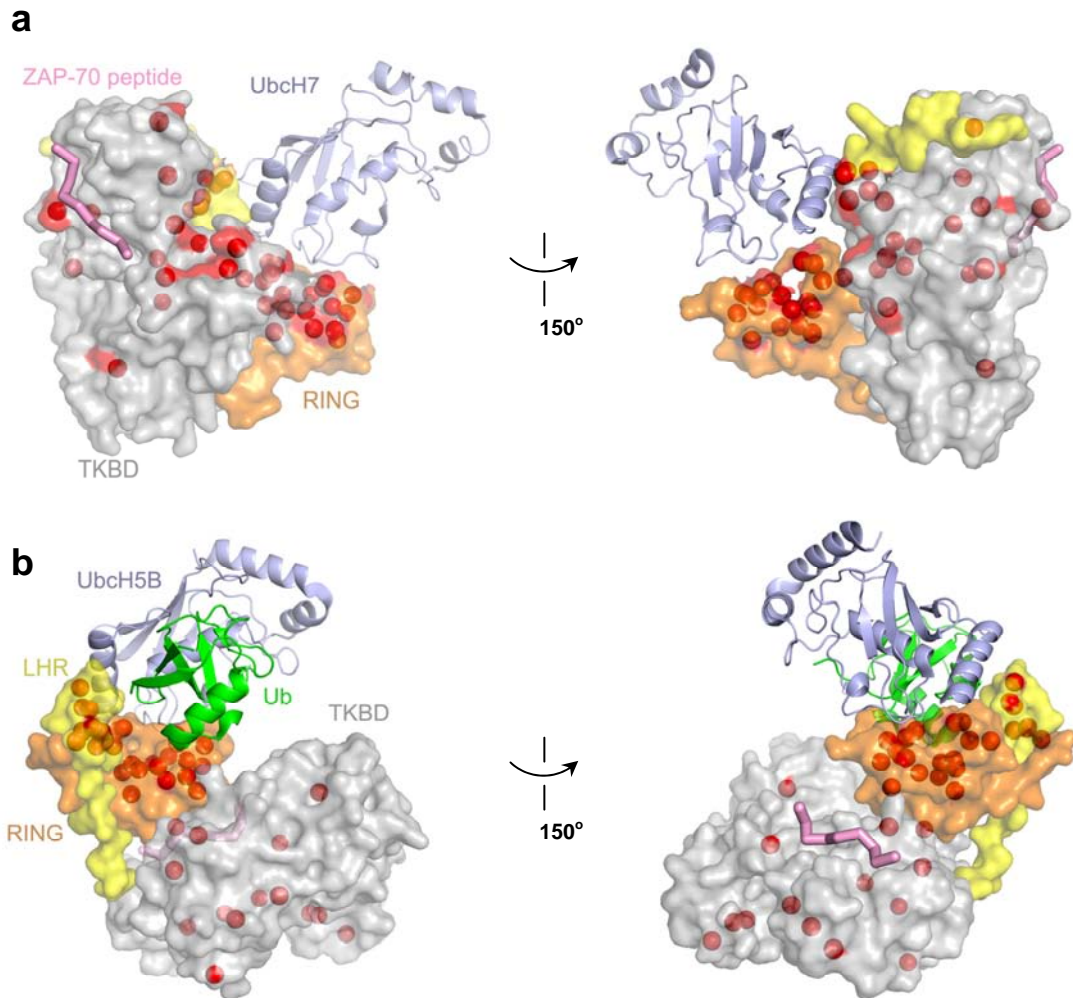


Figure 5-14. Locations of cancer mutations on c-CBL structures.

(a) Left panel: In the structure of c-CBL-UbcH7-ZAP-70 peptide complex (PDB 1FBV [52]), c-CBL domains are shown in surface representation, UbcH7 cartoon, and ZAP-70 peptide ribbon. Colouring is described as in **Figure 5-3**. Based on COSMIC database [245], sites of c-CBL mutations in human patients with myeloproliferative diseases and lung cancer are displayed as red spheres. Right panel is same as left panel but is rotated by 150° about the y-axis.

(b) Left panel: Same as in **a**, but with the model of pTyr371-c-CBL-UbcH5B_{RK}-Ub. c-CBL domains are shown in surface representation, UbcH7 cartoon, ZAP-70 peptide ribbon, Ub cartoon. The model is generated by superposing pTyr371-c-CBL onto the pCBL-B portion from the pCBL-B-UbcH5B_{RK}-Ub-ZAP-70 peptide complex structure. UbcH5B is in the same orientation as in **a** (left panel). Right panel is same as left panel but is rotated by 150° about the y-axis.

Chapter 6

Conclusion and Future directions

6 Conclusion and Future directions

6.1 Mechanisms of Ub transfer by RING E3s

It is now evident that RING E3s not only function as scaffold to bind E2 and substrate, but also catalytically mediate Ub transfer from E2's active site to substrate's lysine. Certain RING E3s function as a dimer, some of which display higher affinity against E2~Ub than free E2. Crystal structures of dimeric RING E3s (BIRC7 and RNF4) bound to E2~Ub complex both reveal a locked Ub C-terminal tail configuration poised for Ub transfer, where the tail of Ub is locked by the E2's active site residues [201, 212] (**Chapter 3**). To achieve the optimal configuration, numerous donor Ub interactions occur between Ub's Ile44 patch and E2's $\alpha 3$, between Ub's tail and E2's $\alpha 2$, and between Ub's Ile36 patch and both subunits of dimeric E3 – the RING domain of one subunit and the tail of the other. These interactions contribute to the optimization of the donor Ub for transfer, thus making E2~Ub thioester more reactive for transfer. Furthermore, NMR studies suggest that E2~Ub samples a large range of conformations in the absence of an E3, however, the presence of an RING E3 makes the donor Ub adopt more 'closed' (active) conformation [215]. Modelling and biochemical assays suggest that this Ub-priming mechanism probably exists in other dimeric E3s that have a similar cross-dimer arrangement to BIRC7 and RNF4, such as BIRC3, Mdm2/MdmX, XIAP, and CHIP [128, 201, 212].

Interestingly, the Ub-priming mechanism is also conserved in a monomeric RING E3. In CBL-B, tyrosine-phosphorylation induces conformational changes and establishes a novel Ub-priming element, pTyr-induced element. This element seems to functionally replace the dimer tail via similar interactions with the donor Ub's Ile36 patch (**Chapter 5**). Since the N-terminal fragment of CBL proteins is highly conserved, this Ub-priming mechanism would apply to c-CBL and CBL-C.

However, some dimeric E3s do not have similar cross-dimer arrangement as BIRC7 or RNF4 and some monomeric RING E3s may not have an additional Ub-binding component, hence it remains unclear how other RING E3s, including BRCA1/BARD1, RNF2/BMI1, E4B and RBX1 stabilize the donor Ub for transfer or whether the RING domain alone is sufficient for them, such as E4B [215]. Further

studies on full-length RING E3s are needed for better understanding how they promote Ub transfer. It will also be interesting to investigate the mechanism of Ub transfer in the presence of a substrate. Crystal structures or NMR models are required to illustrate any conformational changes in E2, E3, or donor Ub upon nucleophilic attack by substrate lysine.

6.2 Regulations of RING E3 activity

RING E3s mediate substrate ubiquitination and decide the fates of substrates. Cellular roles of RING E3s are mostly related to their E3 activity. On the other hand, RING E3s usually contain diverse substrate binding domains, thus they can potentially function as adaptor proteins. When they serve as an adaptor, their E3 activity is not required.

There are several ways to regulate RING E3s activity. Some proteins were reported to bind to the RING domain of E3s via blocking the E2 binding surface. Examples are Spouty2 binds to the RING domain of c-CBL [147] and glomulin interacts with RBX1 in CRLs [246]. Interestingly, several RING E3s execute their own domains to function as the inhibitory factors. In c-CBL, the TKBD interacts with the RING domain and competes against E2 binding, illustrating an autoinhibitory mechanism in single-subunit RING E3s (**Chapter 4**). In cIAPs, the CARD domain blocks the E2 binding surface and prevents dimerization of the RING domain [105]. A recent study of RBR also demonstrates that a helical element of parkin binds to the E2-binding surface of RING1, thus keeps RBR autoinhibited [247]. In some cases, autoinhibition can be released by competent binding of antagonist, such as active E2~Ub or substrate.

A second way to inhibit RING E3s is through autoubiquitination. Many RING E3s reportedly ubiquitinate themselves *in vivo* and promote their degradation by proteasomes. For example, the expression level of IAPs can be regulated by autoubiquitination for proteasomal degradation [95]. Enhanced autoubiquitination of RING E3s correlates with reduced degradation of substrates. Ubiquitination by RING E3s can be reversed by DUBs [26].

Some RING E3s also have other post-translational modifications to regulate their E3 activity or substrate recognition. CBL proteins are activated by phosphorylation on the conserved tyrosine residue. Studies by my colleagues and me demonstrated that phosphorylation induces remarkable conformational changes in the LHR and the RING domain (**Chapter 4**). These changes fully expose the E2 binding surface, abolish autoinhibition, and orientate the RING domain adjacent to the substrate-binding site of the TKBD. Later on, my work suggested that the pTyr-induced element plays a catalytic role in promoting Ub transfer via direct interactions with donor Ub (**Chapter 5**). For APC/C^{Cdc20}, both phosphorylation on the RING subunit and dephosphorylation of Cdc20 are crucial in activating APC/C^{Cdc20} [248]. In addition, neddylation stimulates CRLs by inducing significant conformational changes [224]. Further investigations are required to understand the regulations of RING E3s in cellular functions.

6.3 Characterization of CBL and BIRC family proteins

The E3 activity of CBL proteins is carried out through the RING domain and corresponding substrate-binding domains, such as the TKBD or the proline-rich region. EGFR is well-studied substrate of CBL proteins. Upon phosphorylation by EGFR, CBL binds to EGFR, mediates EGFR ubiquitination toward degradation, and thereby negatively regulates EGFR signalling pathways [49, 155, 156]. So far, structural and biochemical studies have provided us with better understanding of the N-terminus of CBL proteins, containing the TKBD, the LHR and the RING domain [52, 139, 200]. Those structures reveal multiple RING conformations in CBL proteins (**Chapter 4**). They also demonstrate that phosphorylation activates CBL proteins via enhancing E2-binding affinity and improving the catalysis of Ub transfer (**Chapter 5**). However, existing structures failed to explain how CBL proteins become phosphorylated since the conserve tyrosine appears inaccessible for burying within the TKBD.

Furthermore, CBL proteins also functions as scaffold to recruit signal proteins, resulting in prolonging signal transduction [149]. It will be interesting to investigate how CBL proteins switch functions between E3 ligase and adaptor proteins. Currently,

our knowledge of CBL proteins is mostly limited to the N-terminus. Although individual domains or motifs at the C-terminus have been solved subsequently, the entire structures are not available.

Mutated CBL proteins were found in patients with leukaemia and lung cancer [143, 229]. So far, most mutations found in cancers are related to the lost of E3 activity. Mutations of the conserved tyrosine in c-CBL that prevent phosphorylation-dependent activation are frequently found in patients with leukaemia [235]. To rescue this kind of lost E3 activity, drugs that mimic the phosphorylated tyrosine may provide new therapeutic strategies. On the other hand, failures to inhibit E3 activity in CBL proteins may also be related to diseases. In this case, drugs are required to prolong CBL's adaptor activity by either keeping CBL autoinhibited or blocking the RING-E2 interface. With characterization of CBL's roles in human diseases, the CBL family proteins may be considered as promising therapeutic targets in the future.

The BIRC family proteins (IAPs) not only function as anti-apoptosis proteins to control cell death, but also influence other signalling pathways, such as NF- κ B pathways [115]. Structures of the full-length BIRCs are not available, and many aspects of IAPs functions remain to be discovered. So far, the longest fragment is from c-IAP1. It contains the BIR3, the UBA domain, the CARD domain and the RING domain, but lacks the N-terminal BIR1 and BIR2 domains. This structure reveals the autoinhibition of c-IAPs through blocking the E2-binding surface by the CARD domain, thus c-IAPs remain as monomer until stimulation of SMAC or caspase binding [105]. However, this autoinhibitory mechanism may not exist in those IAPs that lack the CARD domain. For example, XIAP stay as dimer and do not require SMAC stimulation to become active [103]. How these IAPs are regulated remains unclear.

Overexpression of IAPs is found in many kinds of cancers and has been related to poor prognosis and chemo-resistance [249]. SMAC mimetic are small compounds that suppress IAPs and specifically reactivate apoptosis in tumour cells. To date, several SMAC mimetics have entered clinic with good anti-tumour activity [250, 251]. Anti-apoptotic protein IAPs are now acknowledged as promising therapeutic targets but their other cellular functions remains to be exploited in the future.

Chapter 7

Appendix

7 Appendix

7.1 Appendix 1. Construct list

| Constructs | Template | Primers | Restriction Sites | Vector |
|----------------------------------|-------------------------|--|----------------------|----------------|
| UbcH5B | cDNA | 5'- cgGGATCCatggetctgaagagaatccac 3'- cgGAATTCttacatcgatacttctgagtc | 5' BamH1 3' EcoR1 | pRSFDuet |
| UbcH5B S22R | UbcH5B | 5'-ccagcacagatgCGCgcaggtcctgttg 3'-caacaggacctgcGCGacactgtgctgg | 5' BamH1 3' EcoR1 | pRSFDuet |
| UbcH5B N77A | UbcH5B | 5'-caagaatttatcccaGCGattaacagtaatggcag 3'-ctgccattactgttaacCGCtgatgataaattcttg | 5' BamH1 3' EcoR1 | pRSFDuet |
| UbcH5B D87A | UbcH5B | 5'-cagcatttctgtgCtattctacgatcac 3'-gtgatcgtagaataGcaagacaaatgctg | 5' BamH1 3' EcoR1 | pRSFDuet |
| UbcH5B D117A | UbcH5B | 5'-cccaatccagatgCtcttttagtgcc 3'-ggcactaaagggaGcatctggattggg | 5' BamH1 3' EcoR1 | pRSFDuet |
| UbcH5B D112A | UbcH5B | 5'-tctctgtgtgtgCtcccaatccagat 3'-atctggattgggaGcacacaacagaga | 5' BamH1 3' EcoR1 | pRSFDuet |
| UbcH5B N114A | UbcH5B | 5'-ctgttctgtgatcccGCTccagatgatcctt 3'-aaggatcatctggaGCGggatcacacaacag | 5' BamH1 3' EcoR1 | pRSFDuet |
| UbcH5B S108R | UbcH5B | 5'-ctcttgcactctgTCGctgtgtgtgatc 3'-gatcacacaacagaCGacagatggacaagag | 5' BamH1 3' EcoR1 | pRSFDuet |
| UbcH5B I88A | UbcH5B | 5'-agcatttctgtgatGCTctacgatcacagt 3'-actgtgatcgtagaGCatcaagacaaatgct | 5' BamH1 3' EcoR1 | pRSFDuet |
| UbcH5B C85S | UbcH5B | 5'-gatcgtagaatatcaagaGaaatgctgccattac 3'-gtaatggcagcatttCcttगतattctacgatc | 5' Nco1 3' EcoR1 | pRSFDuet |
| Ub | cDNA | 5'-cgGGATCCggtggctctatgcagatttctgtaaaacc 3'-ccgCTCGAGttaaccaccacgaagtctcaacac | 5' BamH1 3' Xho1 | pGEX4T1 2TK |
| Ub I44A | Ub | 5'-cagcagagactgGCctttgtgccaag 3'-cttgccagcaagGCcagctctctctg | 5' BamH1 3' Xho1 | pGEX4T1 2TK |
| Ub H68A/V70A | Ub | 5'-gagtctactcttGCTcttgCgttgagactctg 3'-cgaagtctcaacGcaagaGCaagagtagactc | 5' BamH1 3' Xho1 | pGEX4T1 2TK |
| Ub L73D | Ub | 5'- cgGGATCCggtggctctatgcagatttctgtaaaacc 3'-ccgCTCGAGtcaaccaccacgaTCtctcaacaagatg | 5' BamH1 3' Xho1 | pGEX4T1 2TK |
| Ub R42E | Ub | 5'-ctctgatcagcagGAactgatcttctgctg 3'-cagcaaatgacagTCTctgctgatcaggag | 5' BamH1 3' Xho1 | pGEX4T1 2TK |
| Ub Q49E | Ub | 5'-cttctgtgcaagGagctggaagatgg 3'-ccatctccagctCcttgcagcaaaag | 5' BamH1 3' Xho1 | pGEX4T1 2TK |
| Ub L8D | Ub | 5'-cgGGATCCggtggctctatgcagatttctgtaaaacc gaaaaccGAtacgggaagacc 3'- ccgCTCGAGttaaccaccacgaagtctcaacac | 5' BamH1 3' Xho1 | pGEX4T1 2TK |
| Ub Q40R | Ub | 5'-attcctctgatcGTcagagactgatctttg 3'-caaagatcagctctctgACgatcaggaggaat | 5' BamH1 3' Xho1 | pGEX4T1 2TK |
| Ub G47E | Ub | 5'-actgatcttctgAAaagcagctggaagat 3'-atctccagctgcttTCagcaaatgacagt | 5' BamH1 3' Xho1 | pGEX4T1 2TK |
| Ub L71D | Ub | 5'-actctcatctgtgGATagacttctgtgtgtg 3'-accaccacgaagtctATCcaaatggaagat | 5' BamH1 3' Xho1 | pGEX4T1 2TK |
| Ub G35E | Ub | 5'-aggataaggaagAaattcctctctgatca 3'-tgatcaggaggaattTcttcttctct | 5' BamH1 3' Xho1 | pGEX4T1 2TK |
| Ub K11A | Ub | 5'-acccttacggggGCAaccatcacctc 3'-gagggtgatggtTGCccccgtaagggt | 5' BamH1 3' Xho1 | pGEX4T1 2TK |
| Ub I36A | Ub | 5'-gataaggaaggaGCTcctctctgatcag 3'-ctgatcaggaggaGCTcctctcttct | 5' BamH1 3' Xho1 | pGEX4T1 2TK |
| Ub D58A | Ub | 5'-acgtacttctgctgCctacaatattcaaaag 3'-ctttgaaatatttagGcagacaagtacgt | 5' BamH1 3' Xho1 | pGEX4T1 2TK |
| Ub ΔGG | Ub | 5'- cgGGATCCggtggctctatgcagatttctgtaaaacc 3'- atagttaGCGGCCGCTcaacgaagtctcaacaagaatgaag | 5' BamH1 3' Xho1 | pGEX4T1 2TK |
| c-CBL ₄₇₋₄₃₅ | cDNA | 5'- cgGGATCCccgcccgggacggtggacaagaag 3'- ccgCTCGAGttaatcaaacggatctaccacgatggg | 5' BamH1 3' Xho1 | pGEX4T1 |
| c-CBL ₄₇₋₄₃₅ R139C | c-CBL ₄₇₋₄₃₅ | 5'- caaggagggaagaaTgCatgtatgaggagaattc 3'- gaattctctcatacatGcAttctttccctcttg | 5' BamH1 3' Xho1 | pGEX4T1 |
| c-CBL ₄₇₋₄₃₅ | cDNA | 5'- cgGGATCCccgcccgggacggtggacaagaag | 5' BamH1 | pGEX4T1 |

| | | | | |
|--|-------------------------|---|-----------------------|----------|
| D435C | | 3'- ccgCTCGAGttaGCAaaacggatctaccacgatggg | 3' XhoI | |
| c-CBL ₄₇₋₄₃₅ M222F | c-CBL ₄₇₋₄₃₅ | 5'-gttctggctggaggccTtTgctctgaaatccacta 3'-tagtggatttcagagcAaAggctccagcccagaac | 5' BamHI 3' XhoI | pGEX4T1 |
| c-CBL ₄₇₋₄₃₅ M222E | c-CBL ₄₇₋₄₃₅ | 5'-gttctggctggaggccGAAGctctgaaatccacta 3'-tagtggatttcagagcTTCggctccagcccagaac | 5' BamHI 3' XhoI | pGEX4T1 |
| c-CBL ₄₇₋₄₃₅ K389A | c-CBL ₄₇₋₄₃₅ | 5'-atgtgctgaaaatgatGCggatgtaaagattg 3'-caatctttacatccGCatcattttcagcacat | 5' BamHI 3' XhoI | pGEX4T1 |
| c-CBL ₄₇₋₄₃₅ V431A | c-CBL ₄₇₋₄₃₅ | 5'-aacccatcgtggCagatccgtttgat 3'-atcaaacggatctGccacgatgggtt | 5' BamHI 3' XhoI | pGEX4T1 |
| c-CBL full-length | cDNA | 5'-cgGGATCCatgcccggcaacgtgaagaagagc 3'-ccgCTCGAGctaggtagctacatggcaggagaag | 5' BamHI 3' XhoI | pGEX4T1 |
| c-CBL ₄₇₋₄₃₅ ggsLVPrggs insertion | c-CBL ₄₇₋₄₃₅ | 5'-GGTTCTCTGGTTCCGCGTGGCGGTTCTcc aactccccaaagaccatataca 3'-GCCACGCGGAACCCAGAGAACCGCctcac ataagccagtcagatcagg | 5' BamHI 3' XhoI | pGEX4T1 |
| BIRC2 full-length | cDNA | 5'-gaAGATCTatgcacaaaactgcctcccaaag 3'-cgGAATTCttaagagagaatgtacgaacagtacc | 5' Bgl II 3' EcoRI | pGEX4T1 |
| BIRC2 _{555-C} | BIRC2 full-length | 5'- gaAGATCTggtctgtcactggaagaacaattg 3'- cgGAATTCttaagagagaaatgtacgaacagtacc | 5' Bgl II 3' EcoRI | pGEX4T1 |
| BIRC3 full-length | cDNA | 5'-cgGGATCCatgaacatagtagaaaacagcatattc 3'-cgGAATTCcatgaagaatgtacgaactgtacc | 5' BamHI 3' EcoRI | pGEX4T1 |
| BIRC3 _{541-C} | BIRC3 full-length | 5'-cgGGATCCgatctaccagtggagaacaattgc 3'- cgGAATTCcatgaagaatgtacgaactgtacc | 5' BamHI 3' EcoRI | pGEX4T1 |
| BIRC3 _{541-C} F602H | BIRC3 _{541-C} | 5'-cgGGATCCgatctaccagtggagaacaattgc 3'- cgGAATTCcatgaagaTGgtacgaactgtaccctg | 5' BamHI 3' EcoRI | pGEX4T1 |
| BIRC4 full-length | cDNA | 5'- cgGGATCCatgacttttaacagttttgaaggatc 3'-cgGAATTCttaagacataaaaaattttgcttgaagtaag | 5' BamHI 3' EcoRI | pGEX4T1 |
| BIRC4 _{434-C} | BIRC4 full-length | 5'-cgGGATCCgagattagtaggaagcagctaag 3'- cgGAATTCttaagacataaaaaattttgcttgaagtaag | 5' BamHI 3' EcoRI | pGEX4T1 |
| BIRC7 full-length | cDNA | 5'- cgGGATCCatgggacctaaagacagtccaag 3'- cgGAATTCtaggacaggaaggtcgcac | 5' BamHI 3' EcoRI | pGEX4T1 |
| BIRC7 _{239-C} | BIRC7 full-length | 5'- cgGGATCCgtggaggcgcagctgcggcg 3'- cgGAATTCctaggacaggaaggtcgcac | 5' BamHI 3' EcoRI | pGEX4T1 |
| BIRC7 _{239-C} F296A | BIRC7 full-length | 5'- cgGGATCCgtggaggcgcagctgcggcg 3'- cgGAATTCctaggacagTGCggtgcgcacgcg | 5' BamHI 3' EcoRI | pGEX4T1 |
| BIRC7 _{239-C} F296H | BIRC7 full-length | 5'- cgGGATCCgtggaggcgcagctgcggcg 3'- cgGAATTCctaggacagATGggtgcgcacgcg | 5' BamHI 3' EcoRI | pGEX4T1 |
| BIRC7 _{239-C} V263R | BIRC7 full-length | 5'- ccgtgtccatcCGCtttgtgccgtgc 3'- gcacggcacaaaGCGgatggacacgg | 5' BamHI 3' EcoRI | pGEX4T1 |
| BIRC7 _{239-C} Δ296-298 | BIRC7 full-length | 5'- cgGGATCCgtggaggcgcagctgcggcg 3'- cgGAATTCctaggacagcgcgctgcggac | 5' BamHI 3' EcoRI | pGEX4T1 |
| BIRC8 full-length | cDNA | 5'- cgGGATCCatgacgggttatgaagcccgg 3'- ccgCTCGAGttaagacataaaaacttttcttgaatc | 5' BamHI 3' EcoRI | pGEX4T1 |
| BIRC8 _{173-C} | BIRC8 full-length | 5'- cgGGATCCgaaatcagccctgaagaccg 3'- ccgCTCGAGttaagacataaaaacttttcttgaatc | 5' BamHI 3' EcoRI | pGEX4T1 |
| SMAC _{56-C} | cDNA | 5'-catgCCATGGcggttcctattgcacagaaatcag 3'-ccgCTCGAGatcctcagcaggtaggcctcctg | 5' NcoI 3' XhoI | pET23d |
| SMAC _{56-C} -2TK (gsRRASV)-His | cDNA | 5'-catgCCATGGcggttcctattgcacagaaatcag 3'-ccgCTCGAGACCGCTTGCGGACG GCTGCCatcctcagcaggtaggcctcctg | 5' NcoI 3' XhoI | pET23d |
| Mouse Src ₈₄₋₆₂₆ | cDNA | 5'-cgGGATCCgggggtaccacctttgtggc 3'-cgGAATTCctactcagtgacgtaagtagtcttc | 5' BamHI 3' EcoRI | pRSFDuet |
| CBL-B ₃₆₋₄₂₇ | cDNA | 5'- gaAGATCTcctaagcaagctgccgcagatc 3'- ccgCTCGAGctaatcaaggatccacgattatgg | 5' Bgl II 3' XhoI | pGEX4T1 |
| CBL-B ₃₆₋₄₂₇ Y360F | CBL-B ₃₆₋₄₂₇ | 5'- agttacacaggaacaatTtgaattatattgtga 3'- tcacaatataattcaAattgtcctgtgtaact | 5' Bgl II 3' XhoI | pGEX4T1 |
| Mdm2 _{428-C} | cDNA | 5'- cgGGATCCtctagttggccccttaagccattg 3'- cgGAATTCctagggaaataagttagcacaatc | 5' BamHI 3' EcoRI | pGEX4T1 |
| MdmX _{428-C} | cDNA | 5'-cgGGATCCgaggattgccagaatctctgaag 3'-cgGAATTCtatgctataaaaaccttaataaccagctg | 5' BamHI 3' EcoRI | pGEX4T1 |

7.2 Appendix 2. Contribution list

| Projects | Cloning | Purification | Crystallization | Data collection | Data process | Structure refinement | Validation |
|----------|---------|--------------|-----------------|-----------------|--------------|----------------------|------------|
| BIRC7 | JD | JD/DH* | JD | JD | JD/DH | JD/DH/LB | JD/LB |
| c-CBL | JD | JD | JD | JD | JD/DH | JD/DH | JD |
| pCBL-B | JD | JD/DH* | JD | JD | JD | JD/DH/LB | JD/LB |

Note: JD: Hao (Julia) Dou; DH: Danny Huang; LB: Lori Buetow.

- DH purified stabilized Ub_{CH5B}~Ub, both S22R/C85S/N77A mutant and S22R/C85K mutant.
- Data process was done by JD under supervision of DH.
- Structure refinement was conducted by JD. Last few cycles of refinement were done by JD, DH and LB to achieve better model building.
- Structural validations were done by JD with help of LB in two projects. For BIRC7 project, JD investigated mutational effects of Ub variants and E3 variants, whereas LB studied the ones of E2 variants. During the paper revision, JD and LB performed *in vitro* ubiquitination assays together. JD performed the kinetic analyses under supervision of DH. For pCBL-B project, JD and LB performed lysine discharge reactions together. JD performed the kinetic analyses.

7.3 Appendix 3. Enzyme kinetics

7.3.1 Brief introduction

Enzyme catalysis refers to the catalysis of chemical reactions by enzymes, resulting in a great enhancement in reaction rate and high specificity of substrate. Building on the work of Victor Henri, Leonor Michaelis and Maud L. Menten proposed a mechanism to describe how the initial rate of enzyme-catalysed reactions depends on substrate binding equilibrium and catalytic constant k_2 in 1913 [252]. They considered the following scheme, in which E is enzyme, S is substrate, ES is the enzyme–substrate complex and P is product:



Steady-State kinetics was first proposed by George Briggs and John Haldane in 1925 [253]. They assumed that after enzyme and substrate are mixed (the initial substrate concentration is much larger than the enzyme concentration), the concentration of the enzyme–substrate complex will reach a constant value [253, 254]. In this case, Michaelis-Menten Kinetics equation can be written with the steady-state approximation to as follows:

$$v_0 = \frac{V_{\max}[\text{S}]}{K_m + [\text{S}]}$$

v_0 is the initial rate of a reaction; V_{\max} is the velocity of the reaction where the enzyme is operating at maximum capacity; K_m is the Michaelis constant, is defined as

$$K_m = \frac{k_{-1} + k_2}{k_1}$$

The plot of v versus $[\text{S}]$ is not linear; although initially linear at low $[\text{S}]$, it bends over to saturate at high $[\text{S}]$ (**Figure S 1a**). In the past, it was difficult to estimate K_m and V_{\max} accurately based on nonlinear curves. The lineweaver-Burk plot or double reciprocal plot is a common way to illustrate kinetic data [255]. It is produced by taking the reciprocal of both sides of the Michaelis-Menten equation. As shown in **Figure S 1b**, this is a linear form of the Michaelis-Menten equation and produces a straight line with the equation $y = mx + c$ with a y -intercept equivalent to $1/V_{\max}$ and

an x-intercept of the graph representing $-1/K_m$. Linear representations are useful for visualizing data, but computer softwares are used for accurate determination.

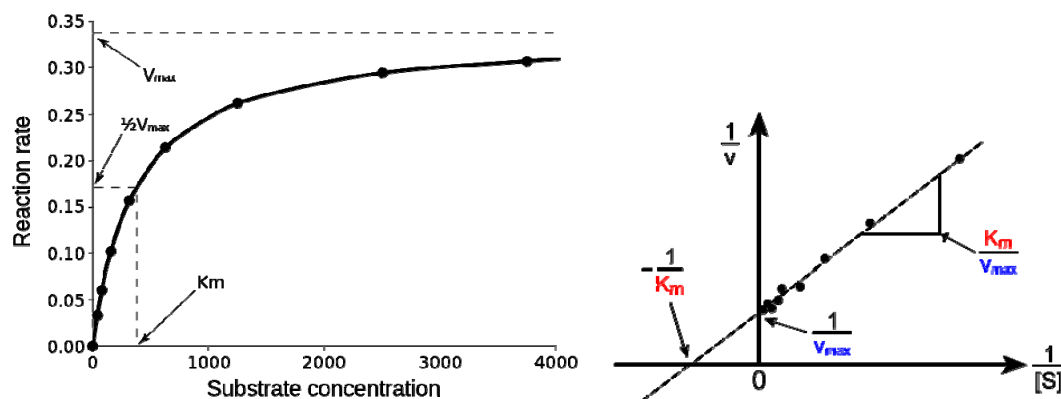


Figure S 1. Michaelis-Menten kinetics.

(a) An example of a saturation curve demonstrates the relationship between the substrate concentration and reaction rate with implication of kinetics parameters [256].

(b) The lineweaver-Burk plot illustrates the significance of the axis intercepts and gradient [257].

7.3.2 Kinetic data process

For kinetics assay, it is crucial to subtract a correct background. Normally, we just run the assay and use a blank lane as a control for analysis. However, in my case, the main background is the E2-catalysed Ub transfer reaction in the absence of E3. Thus, I assayed the same scale of E2~Ub with or without adding E3s. The reactions without E3 at each E2 concentration was used as control for background subtraction (**Figure S 2**).

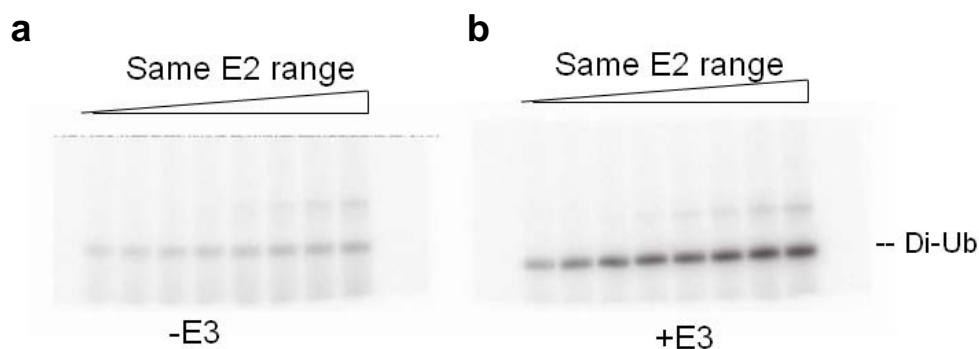


Figure S 2. DiUb formation in the absence and presence of E3.

The E2-mediated DiUb formation is at low catalytic efficiency. The addition of E3 massively enhances the reaction rate. Under the same E2 concentration, E2-catalysed Ub transfer is considered as a control for subtracting to determine E3 kinetics.

To quantify the reaction, an Ub standard was used to convert radioactive reading to pmol. This standard is obtained by titrating known amount of ^{32}P -Ub (demonstrated as pmol). According to the curve of autoradiogram reading against pmol of Ub, an equation is obtained (**Figure S 3a and b**). In addition to subtracting the control reactions (E2-catalysed Ub transfer), pmol of E3 used in the assay (and actually loaded onto the gel) is calculated and therefore the reaction rate is determined as the pmol of product (DiUb formed) per minute per pmol of E3. An example of data processing is shown in **Figure S 3c**. At least two independent datasets were fitted to the Michaelis-Menten equation using SigmaPlot 8.0 (Systat Software Inc.).

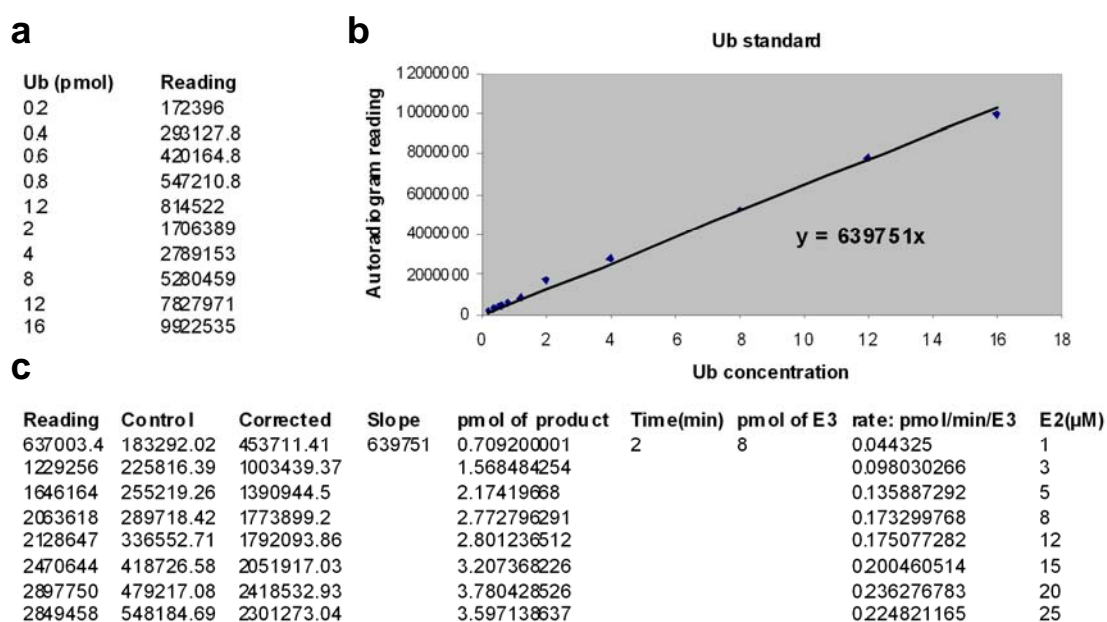


Figure S 3. Examples of kinetic data process.

(a) Autoradiogram reading for various amount of ^{32}P -Ub.

(b) An equation to convert radioactive reading to pmol is gained by plotting the autoradiogram reading against pmol of ^{32}P -Ub.

(c) An example of the kinetic data process. Reading refers to the autoradiogram reading of the DiUb formation in the presence of an E3; Control refers to the autoradiogram reading of the DiUb formation catalysed by E2 only; Corrected refers to the value of Reading minus Control; Slope is gained by the linear curve in **b**; pmol of product is calculated by Corrected over Slope; The reaction rate is calculated by pmol of product over Time over pmol of E3. The kinetics curve is plotted by the reaction rate against E2 concentration.

7.3.3 Autoradiogram representation

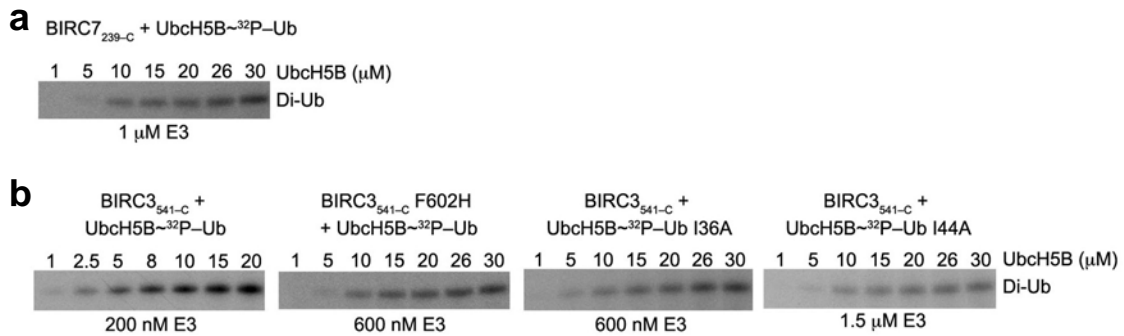


Figure S 4. Single turnover kinetics of DiUb formation catalysed by BIRC RING domains.

(a) Representative reduced autoradiogram of DiUb formation catalysed by wild-type BIRC7_{239-C}. Various concentrations of UbcH5B~³²P-Ub were chased with acceptor Ub (His-Ub, 820 μM) in the presence of BIRC7_{239-C}.

(b) Reactions were performed as in a, but catalysed by BIRC3_{541-C} or Ub variants. E3 Final UbcH5B and E3 concentrations are indicated.

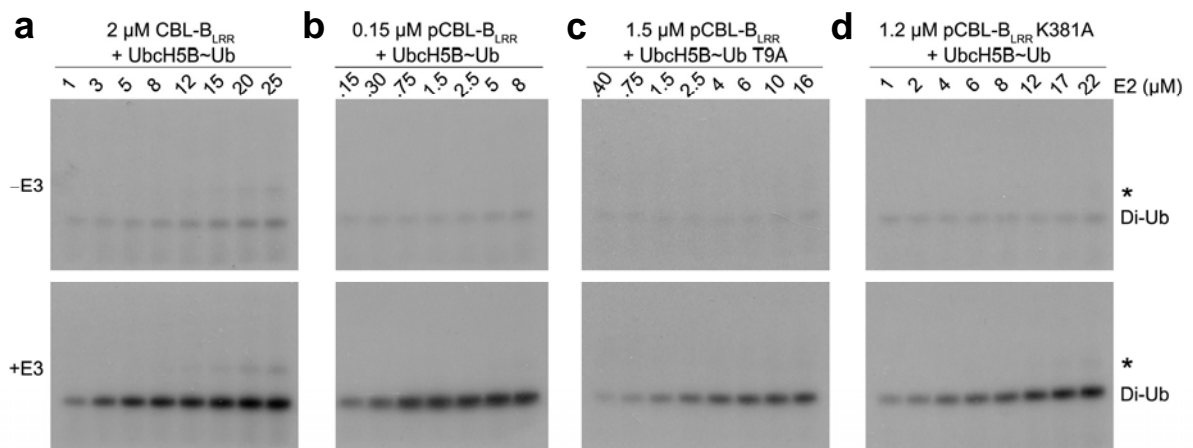


Figure S 5. Single turnover kinetics of DiUb formation catalysed by CBL-B_{LRR} variants.

(a) Representative reduced autoradiograms of DiUb kinetic assays. Reactions were performed in the absence (upper panel) or in the presence of CBL-B_{LRR} (lower panel). Reactions performed in the absence of E3 were used for background subtraction during quantification.

(b-d) Reactions were performed as in a, but with CBL-B_{LRR} or Ub variants. Final UbcH5B and E3 concentrations are shown. Asterisks refer to non-reducible E2-Ub bands.

7.4 Appendix 4. The purity of full-length c-CBL variants

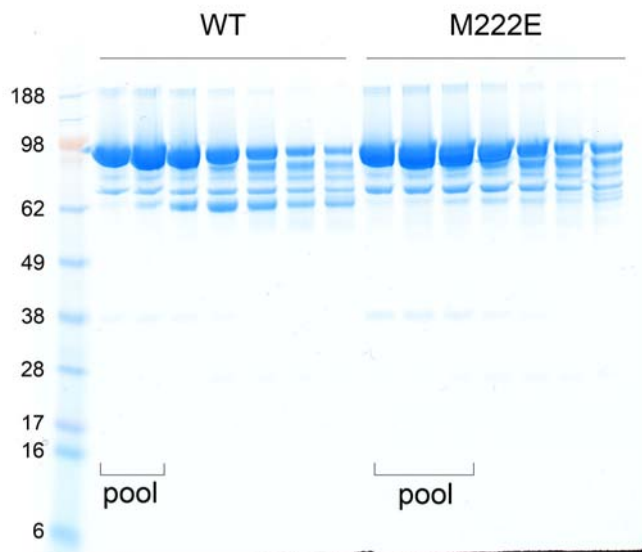


Figure S 6. The purity of full-length c-CBL variants.

Full-length c-CBL variants were purified by series of chromatography as described in **Chapter 2**. The gel shows the purity of the protein after the final step, size-exclusion chromatography (SD200, GE). Fractions were pooled as indicated for biochemical assays.

7.5 Appendix 5. Published papers and structures

Dou, H., Buetow, L. Hock, A. Sibbet, G. J. Vousden, K. H. Huang, D. T., Structural basis for autoinhibition and phosphorylation-dependent activation of c-Cbl. *Nat Struct Mol Biol*, 2012. 19(2): p. 184-92.

c-CBL₄₇₋₄₃₅: PDB 2Y1M

c-CBL₄₇₋₄₃₅ bound to ZAP-70 peptide: PDB 2Y1N

Phosphorylated c-CBL₄₇₋₄₃₅ bound to UbcH5B and ZAP-70 peptide: PDB 4A4C

Phosphorylated c-CBL₄₇₋₄₃₅ (Y368F) bound to UbcH5B and ZAP-70 peptide: PDB 4A4B

Phosphorylated c-CBL₃₅₄₋₄₃₅ (Y368F) bound to UbcH5B: PDB 4A49

Dou, H., Buetow, L. Sibbet, G. J. Cameron, K. Huang, D. T., BIRC7-E2 ubiquitin conjugate structure reveals the mechanism of ubiquitin transfer by a RING dimer. *Nat Struct Mol Biol*, 2012. 19(9): p. 876-83.

BIRC7_{239-C} bound to UbcH5B_{RAS}~Ub: PDB 4AUQ

Dou, H., Buetow, L., Sibbet, G.J., Cameron, K., and Huang, D.T., Essentiality of a non-RING element in priming donor ubiquitin for catalysis by a monomeric E3. *Nat Struct Mol Biol*.

Phosphorylated CBL-B₃₈₋₄₂₇ bound to UbcH5B_{RK}-Ub and ZAP-70 peptide: PDB 3ZNI

8 Bibliography

1. Hershko, A., Ciechanover, A., Heller, H., Haas, A.L., and Rose, I.A. (1980). Proposed role of ATP in protein breakdown: conjugation of protein with multiple chains of the polypeptide of ATP-dependent proteolysis. *Proc Natl Acad Sci U S A* 77, 1783-1786.
2. Ciechanover, A., Heller, H., Elias, S., Haas, A.L., and Hershko, A. (1980). ATP-dependent conjugation of reticulocyte proteins with the polypeptide required for protein degradation. *Proc Natl Acad Sci U S A* 77, 1365-1368.
3. Piper, R.C., and Lehner, P.J. (2011). Endosomal transport via ubiquitination. *Trends Cell Biol* 21, 647-655.
4. Nakayama, K.I., and Nakayama, K. (2006). Ubiquitin ligases: cell-cycle control and cancer. *Nat Rev Cancer* 6, 369-381.
5. Chen, Z.J. (2005). Ubiquitin signalling in the NF-kappaB pathway. *Nat Cell Biol* 7, 758-765.
6. Jackson, S.P., and Durocher, D (2013). Regulation of DNA damage responses by ubiquitin and SUMO. *Mol Cell* 49, 795-807.
7. Sakamoto, K.M. (2002). Ubiquitin-dependent proteolysis: its role in human diseases and the design of therapeutic strategies. *Mol Genet Metab* 77, 44-56.
8. van der Veen, A.G., and Ploegh, H.L. (2012). Ubiquitin-like proteins. *Annu Rev Biochem* 81, 323-357.
9. Tateishi, K., Omata, M., Tanaka, K., and Chiba, T. (2001). The NEDD8 system is essential for cell cycle progression and morphogenetic pathway in mice. *J Cell Biol* 155, 571-579.
10. Rabut, G., and Peter, M. (2008). Function and regulation of protein neddylation. 'Protein modifications: beyond the usual suspects' review series. *EMBO Rep* 9, 969-976.
11. Deshaies, R.J., and Joazeiro, C.A. (2009). RING domain E3 ubiquitin ligases. *Annu Rev Biochem* 78, 399-434.
12. Ikeda, F., and Dikic, I. (2008). Atypical ubiquitin chains: new molecular signals. 'Protein Modifications: Beyond the Usual Suspects' review series. *EMBO Rep* 9, 536-542.
13. Terrell, J., Shih, S., Dunn, R., and Hicke, L. (1998). A function for monoubiquitination in the internalization of a G protein-coupled receptor. *Mol Cell* 1, 193-202.
14. Tanaka, Y., Tanaka, N., Saeki, Y., Tanaka, K., Murakami, M., Hirano, T., Ishii, N., and Sugamura, K. (2008). c-Cbl-dependent monoubiquitination and lysosomal degradation of gp130. *Mol Cell Biol* 28, 4805-4818.
15. Pavri, R., Zhu, B., Li, G., Trojer, P., Mandal, S., Shilatifard, A., and Reinberg, D. (2006). Histone H2B monoubiquitination functions cooperatively with FACT to regulate elongation by RNA polymerase II. *Cell* 125, 703-717.
16. van Delft, S., Govers, R., Strous, G.J., Verkleij, A.J., and van Bergen en Henegouwen, P.M. (1997). Epidermal growth factor induces ubiquitination of Eps15. *J Biol Chem* 272, 14013-14016.
17. Woelk, T., Oldrini, B., Maspero, E., Confalonieri, S., Cavallaro, E., Di Fiore, P.P., and Polo, S. (2006). Molecular mechanisms of coupled monoubiquitination. *Nat Cell Biol* 8, 1246-1254.
18. Fallon, L., Belanger, C.M., Corera, A.T., Kontogianna, M., Regan-Klapisz, E., Moreau, F., Voortman, J., Haber, M., Rouleau, G., Thorarinsdottir, T., et

- al. (2006). A regulated interaction with the UIM protein Eps15 implicates parkin in EGF receptor trafficking and PI(3)K-Akt signalling. *Nat Cell Biol* 8, 834-842.
19. Husnjak, K., and Dikic, I. (2006). EGFR trafficking: parkin' in a jam. *Nat Cell Biol* 8, 787-788.
 20. Thrower, J.S., Hoffman, L., Rechsteiner, M., and Pickart, C.M. (2000). Recognition of the polyubiquitin proteolytic signal. *EMBO J* 19, 94-102.
 21. Wang, B., and Elledge, S.J. (2007). Ubc13/Rnf8 ubiquitin ligases control foci formation of the Rap80/Abraxas/Brc1/Brcc36 complex in response to DNA damage. *Proc Natl Acad Sci U S A* 104, 20759-20763.
 22. Nathan, J.A., Kim, H.T., Ting, L., Gygi, S.P., and Goldberg, A.L. (2013). Why do cellular proteins linked to K63-polyubiquitin chains not associate with proteasomes? *EMBO J* 32, 552-565.
 23. Christensen, D.E., Brzovic, P.S., and Klevit, R.E. (2007). E2-BRCA1 RING interactions dictate synthesis of mono- or specific polyubiquitin chain linkages. *Nat Struct Mol Biol* 14, 941-948.
 24. Kim, H.T., Kim, K.P., Lledias, F., Kisselev, A.F., Scaglione, K.M., Skowyra, D., Gygi, S.P., and Goldberg, A.L. (2007). Certain pairs of ubiquitin-conjugating enzymes (E2s) and ubiquitin-protein ligases (E3s) synthesize nondegradable forked ubiquitin chains containing all possible isopeptide linkages. *J Biol Chem* 282, 17375-17386.
 25. Glickman, M.H., and Ciechanover, A. (2002). The ubiquitin-proteasome proteolytic pathway: destruction for the sake of construction. *Physiol Rev* 82, 373-428.
 26. Nijman, S.M., Luna-Vargas, M.P., Velds, A., Brummelkamp, T.R., Dirac, A.M., Sixma, T.K., and Bernards, R. (2005). A genomic and functional inventory of deubiquitinating enzymes. *Cell* 123, 773-786.
 27. Komander, D., Clague, M.J., and Urbe, S. (2009). Breaking the chains: structure and function of the deubiquitinases. *Nat Rev Mol Cell Biol* 10, 550-563.
 28. Walden, H., Podgorski, M.S., and Schulman, B.A. (2003). Insights into the ubiquitin transfer cascade from the structure of the activating enzyme for NEDD8. *Nature* 422, 330-334.
 29. Lois, L.M., and Lima, C.D. (2005). Structures of the SUMO E1 provide mechanistic insights into SUMO activation and E2 recruitment to E1. *EMBO J* 24, 439-451.
 30. Lee, I., and Schindelin, H. (2008). Structural insights into E1-catalyzed ubiquitin activation and transfer to conjugating enzymes. *Cell* 134, 268-278.
 31. Huang, D.T., Hunt, H.W., Zhuang, M., Ohi, M.D., Holton, J.M., and Schulman, B.A. (2007). Basis for a ubiquitin-like protein thioester switch toggling E1-E2 affinity. *Nature* 445, 394-398.
 32. Olsen, S.K., Capili, A.D., Lu, X., Tan, D.S., and Lima, C.D. (2010) Active site remodelling accompanies thioester bond formation in the SUMO E1. *Nature* 463, 906-912.
 33. Olsen, S.K., and Lima, C.D. (2013). Structure of a ubiquitin E1-E2 complex: insights to E1-E2 thioester transfer. *Mol Cell* 49, 884-896.
 34. Wenzel, D.M., Stoll, K.E., and Klevit, R.E. (2011). E2s: structurally economical and functionally replete. *Biochem J* 433, 31-42.
 35. Eletr, Z.M., Huang, D.T., Duda, D.M., Schulman, B.A., and Kuhlman, B. (2005). E2 conjugating enzymes must disengage from their E1 enzymes

- before E3-dependent ubiquitin and ubiquitin-like transfer. *Nat Struct Mol Biol* *12*, 933-934.
36. Wu, P.Y., Hanlon, M., Eddins, M., Tsui, C., Rogers, R.S., Jensen, J.P., Matunis, M.J., Weissman, A.M., Wolberger, C., and Pickart, C.M. (2003). A conserved catalytic residue in the ubiquitin-conjugating enzyme family. *EMBO J* *22*, 5241-5250.
 37. Mace, P.D., Linke, K., Feltham, R., Schumacher, F.R., Smith, C.A., Vaux, D.L., Silke, J., and Day, C.L. (2008). Structures of the cIAP2 RING domain reveal conformational changes associated with ubiquitin-conjugating enzyme (E2) recruitment. *J Biol Chem* *283*, 31633-31640.
 38. Hibbert, R.G., Huang, A., Boelens, R., and Sixma, T.K. (2011). E3 ligase Rad18 promotes monoubiquitination rather than ubiquitin chain formation by E2 enzyme Rad6. *Proc Natl Acad Sci U S A* *108*, 5590-5595.
 39. Brzovic, P.S., Lissounov, A., Christensen, D.E., Hoyt, D.W., and Klevit, R.E. (2006). A UbcH5/ubiquitin noncovalent complex is required for processive BRCA1-directed ubiquitination. *Mol Cell* *21*, 873-880.
 40. Husnjak, K., and Dikic, I. (2012). Ubiquitin-binding proteins: decoders of ubiquitin-mediated cellular functions. *Annu Rev Biochem* *81*, 291-322.
 41. Stoll, K.E., Brzovic, P.S., Davis, T.N., and Klevit, R.E. (2011). The essential Ubc4/Ubc5 function in yeast is HECT E3-dependent, and RING E3-dependent pathways require only monoubiquitin transfer by Ubc4. *J Biol Chem* *286*, 15165-15170.
 42. Das, R., Mariano, J., Tsai, Y.C., Kalathur, R.C., Kostova, Z., Li, J., Tarasov, S.G., McFeeters, R.L., Altieri, A.S., Ji, X., et al. (2009). Allosteric activation of E2-RING finger-mediated ubiquitylation by a structurally defined specific E2-binding region of gp78. *Mol Cell* *34*, 674-685.
 43. Metzger, M.B., Liang, Y.H., Das, R., Mariano, J., Li, S., Li, J., Kostova, Z., Byrd, R.A., Ji, X., and Weissman, A.M. (2013). A structurally unique E2-binding domain activates ubiquitination by the ERAD E2, Ubc7p, through multiple mechanisms. *Mol Cell* *50*, 516-527.
 44. Freemont, P.S., Hanson, I.M., and Trowsdale, J. (1991). A novel cysteine-rich sequence motif. *Cell* *64*, 483-484.
 45. Lovering, R., Hanson, I.M., Borden, K.L., Martin, S., O'Reilly, N.J., Evan, G.I., Rahman, D., Pappin, D.J., Trowsdale, J., and Freemont, P.S. (1993). Identification and preliminary characterization of a protein motif related to the zinc finger. *Proc Natl Acad Sci U S A* *90*, 2112-2116.
 46. Saurin, A.J., Borden, K.L.B., Boddy, M.N., and Freemont, P.S. (1996). Does this have a familiar RING? *Trends in Biochemical Sciences* *21*, 208-214.
 47. Yokouchi, M., Kondo, T., Houghton, A., Bartkiewicz, M., Horne, W.C., Zhang, H., Yoshimura, A., and Baron, R. (1999). Ligand-induced ubiquitination of the epidermal growth factor receptor involves the interaction of the c-Cbl RING finger and UbcH7. *J Biol Chem* *274*, 31707-31712.
 48. Levkowitz, G., Waterman, H., Ettenberg, S.A., Katz, M., Tsygankov, A.Y., Alroy, I., Lavi, S., Iwai, K., Reiss, Y., Ciechanover, A., et al. (1999). Ubiquitin ligase activity and tyrosine phosphorylation underlie suppression of growth factor signaling by c-Cbl/Sli-1. *Mol Cell* *4*, 1029-1040.
 49. Joazeiro, C.A., Wing, S.S., Huang, H., Leverson, J.D., Hunter, T., and Liu, Y.C. (1999). The tyrosine kinase negative regulator c-Cbl as a RING-type, E2-dependent ubiquitin-protein ligase. *Science* *286*, 309-312.

50. Xie, Y., and Varshavsky, A. (1999). The E2-E3 interaction in the N-end rule pathway: the RING-H2 finger of E3 is required for the synthesis of multiubiquitin chain. *EMBO J* 18, 6832-6844.
51. Kosarev, P., Mayer, K.F., and Hardtke, C.S. (2002). Evaluation and classification of RING-finger domains encoded by the Arabidopsis genome. *Genome Biol* 3, RESEARCH0016.
52. Zheng, N., Wang, P., Jeffrey, P.D., and Pavletich, N.P. (2000). Structure of a c-Cbl-UbcH7 complex: RING domain function in ubiquitin-protein ligases. *Cell* 102, 533-539.
53. de Melker, A.A., van der Horst, G., Calafat, J., Jansen, H., and Borst, J. (2001). c-Cbl ubiquitinates the EGF receptor at the plasma membrane and remains receptor associated throughout the endocytic route. *J Cell Sci* 114, 2167-2178.
54. Liew, C.W., Sun, H., Hunter, T., and Day, C.L. (2010). RING domain dimerization is essential for RNF4 function. *Biochem J* 431, 23-29.
55. Linke, K., Mace, P.D., Smith, C.A., Vaux, D.L., Silke, J., and Day, C.L. (2008). Structure of the MDM2/MDMX RING domain heterodimer reveals dimerization is required for their ubiquitylation in trans. *Cell Death Differ* 15, 841-848.
56. Brzovic, P.S., Rajagopal, P., Hoyt, D.W., King, M.C., and Klevit, R.E. (2001). Structure of a BRCA1-BARD1 heterodimeric RING-RING complex. *Nat Struct Biol* 8, 833-837.
57. Buchwald, G., van der Stoop, P., Weichenrieder, O., Perrakis, A., van Lohuizen, M., and Sixma, T.K. (2006). Structure and E3-ligase activity of the Ring-Ring complex of polycomb proteins Bmi1 and Ring1b. *EMBO J* 25, 2465-2474.
58. Uldrijan, S., Pannekoek, W.J., and Vousden, K.H. (2007). An essential function of the extreme C-terminus of MDM2 can be provided by MDMX. *EMBO J* 26, 102-112.
59. Cao, R., Tsukada, Y., and Zhang, Y. (2005). Role of Bmi-1 and Ring1A in H2A ubiquitylation and Hox gene silencing. *Mol Cell* 20, 845-854.
60. Petroski, M.D., and Deshaies, R.J. (2005). Function and regulation of cullin-RING ubiquitin ligases. *Nat Rev Mol Cell Biol* 6, 9-20.
61. Ang, X.L., and Wade Harper, J. (2005). SCF-mediated protein degradation and cell cycle control. *Oncogene* 24, 2860-2870.
62. Cardozo, T., and Pagano, M. (2004). The SCF ubiquitin ligase: insights into a molecular machine. *Nat Rev Mol Cell Biol* 5, 739-751.
63. Schreiber, A., Stengel, F., Zhang, Z., Enchev, R.I., Kong, E.H., Morris, E.P., Robinson, C.V., da Fonseca, P.C., and Barford, D. (2011). Structural basis for the subunit assembly of the anaphase-promoting complex. *Nature* 470, 227-232.
64. Vodermaier, H.C. (2004). APC/C and SCF: controlling each other and the cell cycle. *Curr Biol* 14, R787-796.
65. Xu, Z., Kohli, E., Devlin, K.I., Bold, M., Nix, J.C., and Misra, S. (2008). Interactions between the quality control ubiquitin ligase CHIP and ubiquitin conjugating enzymes. *BMC Struct Biol* 8, 26.
66. Vander Kooi, C.W., Ohi, M.D., Rosenberg, J.A., Oldham, M.L., Newcomer, M.E., Gould, K.L., and Chazin, W.J. (2006). The Prp19 U-box crystal structure suggests a common dimeric architecture for a class of oligomeric E3 ubiquitin ligases. *Biochemistry* 45, 121-130.

67. Goto, E., Ishido, S., Sato, Y., Ohgimoto, S., Ohgimoto, K., Nagano-Fujii, M., and Hotta, H. (2003). c-MIR, a human E3 ubiquitin ligase, is a functional homolog of herpesvirus proteins MIR1 and MIR2 and has similar activity. *J Biol Chem* 278, 14657-14668.
68. Ivanov, A.V., Peng, H., Yurchenko, V., Yap, K.L., Negorev, D.G., Schultz, D.C., Psulkowski, E., Fredericks, W.J., White, D.E., Maul, G.G., et al. (2007). PHD domain-mediated E3 ligase activity directs intramolecular sumoylation of an adjacent bromodomain required for gene silencing. *Mol Cell* 28, 823-837.
69. Wenzel, D.M., Lissounov, A., Brzovic, P.S., and Klevit, R.E. (2011). UBCH7 reactivity profile reveals parkin and HHARI to be RING/HECT hybrids. *Nature* 474, 105-108.
70. Kitada, T., Asakawa, S., Hattori, N., Matsumine, H., Yamamura, Y., Minoshima, S., Yokochi, M., Mizuno, Y., and Shimizu, N. (1998). Mutations in the parkin gene cause autosomal recessive juvenile parkinsonism. *Nature* 392, 605-608.
71. Campbell, S.J., Edwards, R.A., Leung, C.C., Neculai, D., Hodge, C.D., Dhe-Paganon, S., and Glover, J.N. (2012). Molecular insights into the function of RING finger (RNF)-containing proteins hRNF8 and hRNF168 in Ubc13/Mms2-dependent ubiquitylation. *J Biol Chem* 287, 23900-23910.
72. Suzuki, Y., Nakabayashi, Y., and Takahashi, R. (2001). Ubiquitin-protein ligase activity of X-linked inhibitor of apoptosis protein promotes proteasomal degradation of caspase-3 and enhances its anti-apoptotic effect in Fas-induced cell death. *Proc Natl Acad Sci U S A* 98, 8662-8667.
73. Morizane, Y., Honda, R., Fukami, K., and Yasuda, H. (2005). X-linked inhibitor of apoptosis functions as ubiquitin ligase toward mature caspase-9 and cytosolic Smac/DIABLO. *J Biochem* 137, 125-132.
74. Skaar, J.R., D'Angiolella, V., Pagan, J.K., and Pagano, M. (2009). SnapShot: F Box Proteins II. *Cell* 137, 1358, 1358 e1351.
75. Wickliffe, K.E., Lorenz, S., Wemmer, D.E., Kuriyan, J., and Rape, M. (2011). The mechanism of linkage-specific ubiquitin chain elongation by a single-subunit E2. *Cell* 144, 769-781.
76. Saha, A., Lewis, S., Kleiger, G., Kuhlman, B., and Deshaies, R.J. (2011). Essential role for ubiquitin-ubiquitin-conjugating enzyme interaction in ubiquitin discharge from Cdc34 to substrate. *Mol Cell* 42, 75-83.
77. Yin, Q., Lin, S.C., Lamothe, B., Lu, M., Lo, Y.C., Hura, G., Zheng, L., Rich, R.L., Campos, A.D., Myszka, D.G., et al. (2009). E2 interaction and dimerization in the crystal structure of TRAF6. *Nat Struct Mol Biol* 16, 658-666.
78. Kerr, J.F., Wyllie, A.H., and Currie, A.R. (1972). Apoptosis: a basic biological phenomenon with wide-ranging implications in tissue kinetics. *Br J Cancer* 26, 239-257.
79. Elmore, S. (2007). Apoptosis: a review of programmed cell death. *Toxicol Pathol* 35, 495-516.
80. Horvitz, H.R. (2003). Nobel lecture. Worms, life and death. *Biosci Rep* 23, 239-303.
81. Chaabane, W., User, S.D., El-Gazzah, M., Jaksik, R., Sajjadi, E., Rzeszowska-Wolny, J., and Los, M.J. (2013). Autophagy, apoptosis, mitoptosis and necrosis: interdependence between those pathways and effects on cancer. *Arch Immunol Ther Exp (Warsz)* 61, 43-58.

82. Bursch, W., Ellinger, A., Gerner, C., Frohwein, U., and Schulte-Hermann, R. (2000). Programmed cell death (PCD). Apoptosis, autophagic PCD, or others? *Ann N Y Acad Sci* 926, 1-12.
83. Sprick, M.R., and Walczak, H. (2004). The interplay between the Bcl-2 family and death receptor-mediated apoptosis. *Biochim Biophys Acta* 1644, 125-132.
84. Scorrano, L., and Korsmeyer, S.J. (2003). Mechanisms of cytochrome c release by proapoptotic BCL-2 family members. *Biochem Biophys Res Commun* 304, 437-444.
85. Brunelle, J.K., and Letai, A. (2009). Control of mitochondrial apoptosis by the Bcl-2 family. *J Cell Sci* 122, 437-441.
86. Lawen, A. (2003). Apoptosis - an introduction. *Bioessays* 25, 888-896.
87. Sjostrom, J., and Bergh, J. (2001). How apoptosis is regulated, and what goes wrong in cancer. *BMJ* 322, 1538-1539.
88. Deveraux, Q.L., and Reed, J.C. (1999). IAP family proteins--suppressors of apoptosis. *Genes Dev* 13, 239-252.
89. Crook, N.E., Clem, R.J., and Miller, L.K. (1993). An apoptosis-inhibiting baculovirus gene with a zinc finger-like motif. *J Virol* 67, 2168-2174.
90. Birnbaum, M.J., Clem, R.J., and Miller, L.K. (1994). An apoptosis-inhibiting gene from a nuclear polyhedrosis virus encoding a polypeptide with Cys/His sequence motifs. *J Virol* 68, 2521-2528.
91. Shi, Y. (2002). Mechanisms of caspase activation and inhibition during apoptosis. *Mol Cell* 9, 459-470.
92. Roy, N., Mahadevan, M.S., McLean, M., Shutler, G., Yaraghi, Z., Farahani, R., Baird, S., Besner-Johnston, A., Lefebvre, C., Kang, X., et al. (1995). The gene for neuronal apoptosis inhibitory protein is partially deleted in individuals with spinal muscular atrophy. *Cell* 80, 167-178.
93. Liston, P., Roy, N., Tamai, K., Lefebvre, C., Baird, S., Cherton-Horvat, G., Farahani, R., McLean, M., Ikeda, J.E., MacKenzie, A., et al. (1996). Suppression of apoptosis in mammalian cells by NAIP and a related family of IAP genes. *Nature* 379, 349-353.
94. Srinivasula, S.M., and Ashwell, J.D. (2008). IAPs: what's in a name? *Mol Cell* 30, 123-135.
95. Yang, Y., Fang, S., Jensen, J.P., Weissman, A.M., and Ashwell, J.D. (2000). Ubiquitin protein ligase activity of IAPs and their degradation in proteasomes in response to apoptotic stimuli. *Science* 288, 874-877.
96. Vaux, D.L., and Silke, J. (2005). IAPs, RINGs and ubiquitylation. *Nat Rev Mol Cell Biol* 6, 287-297.
97. Lopez, J., John, S.W., Tenev, T., Rautureau, G.J., Hinds, M.G., Francalanci, F., Wilson, R., Broemer, M., Santoro, M.M., Day, C.L., et al. (2011). CARD-mediated autoinhibition of cIAP1's E3 ligase activity suppresses cell proliferation and migration. *Mol Cell* 42, 569-583.
98. Gyrd-Hansen, M., Darding, M., Miasari, M., Santoro, M.M., Zender, L., Xue, W., Tenev, T., da Fonseca, P.C., Zvelebil, M., Bujnicki, J.M., et al. (2008). IAPs contain an evolutionarily conserved ubiquitin-binding domain that regulates NF-kappaB as well as cell survival and oncogenesis. *Nat Cell Biol* 10, 1309-1317.
99. Blankenship, J.W., Varfolomeev, E., Goncharov, T., Fedorova, A.V., Kirkpatrick, D.S., Izrael-Tomasevic, A., Phu, L., Arnott, D., Aghajan, M., Zobel, K., et al. (2009). Ubiquitin binding modulates IAP antagonist-

- stimulated proteasomal degradation of c-IAP1 and c-IAP2(1). *Biochem J* 417, 149-160.
100. Choi, Y.E., Butterworth, M., Malladi, S., Duckett, C.S., Cohen, G.M., and Bratton, S.B. (2009). The E3 ubiquitin ligase cIAP1 binds and ubiquitinates caspase-3 and -7 via unique mechanisms at distinct steps in their processing. *J Biol Chem* 284, 12772-12782.
 101. MacFarlane, M., Merrison, W., Bratton, S.B., and Cohen, G.M. (2002). Proteasome-mediated degradation of Smac during apoptosis: XIAP promotes Smac ubiquitination in vitro. *J Biol Chem* 277, 36611-36616.
 102. Silke, J., Hawkins, C.J., Ekert, P.G., Chew, J., Day, C.L., Pakusch, M., Verhagen, A.M., and Vaux, D.L. (2002). The anti-apoptotic activity of XIAP is retained upon mutation of both the caspase 3- and caspase 9-interacting sites. *J Cell Biol* 157, 115-124.
 103. Nakatani, Y., Kleffmann, T., Linke, K., Condon, S.M., Hinds, M.G., and Day, C.L. (2012). Regulation of ubiquitin transfer by XIAP, a dimeric RING E3 ligase. *Biochem J* 450, 629-638.
 104. Silke, J., Kratina, T., Chu, D., Ekert, P.G., Day, C.L., Pakusch, M., Huang, D.C., and Vaux, D.L. (2005). Determination of cell survival by RING-mediated regulation of inhibitor of apoptosis (IAP) protein abundance. *Proc Natl Acad Sci U S A* 102, 16182-16187.
 105. Dueber, E.C., Schoeffler, A.J., Lingel, A., Elliott, J.M., Fedorova, A.V., Giannetti, A.M., Zobel, K., Maurer, B., Varfolomeev, E., Wu, P., et al. (2011). Antagonists induce a conformational change in cIAP1 that promotes autoubiquitination. *Science* 334, 376-380.
 106. Huang, Y., Park, Y.C., Rich, R.L., Segal, D., Myszka, D.G., and Wu, H. (2001). Structural basis of caspase inhibition by XIAP: differential roles of the linker versus the BIR domain. *Cell* 104, 781-790.
 107. Riedl, S.J., Renatus, M., Schwarzenbacher, R., Zhou, Q., Sun, C., Fesik, S.W., Liddington, R.C., and Salvesen, G.S. (2001). Structural basis for the inhibition of caspase-3 by XIAP. *Cell* 104, 791-800.
 108. Scott, F.L., Denault, J.B., Riedl, S.J., Shin, H., Renatus, M., and Salvesen, G.S. (2005). XIAP inhibits caspase-3 and -7 using two binding sites: evolutionarily conserved mechanism of IAPs. *EMBO J* 24, 645-655.
 109. Shiozaki, E.N., Chai, J., Rigotti, D.J., Riedl, S.J., Li, P., Srinivasula, S.M., Alnemri, E.S., Fairman, R., and Shi, Y. (2003). Mechanism of XIAP-mediated inhibition of caspase-9. *Mol Cell* 11, 519-527.
 110. Wu, G., Chai, J., Suber, T.L., Wu, J.W., Du, C., Wang, X., and Shi, Y. (2000). Structural basis of IAP recognition by Smac/DIABLO. *Nature* 408, 1008-1012.
 111. Srinivasula, S.M., Hegde, R., Saleh, A., Datta, P., Shiozaki, E., Chai, J., Lee, R.A., Robbins, P.D., Fernandes-Alnemri, T., Shi, Y., et al. (2001). A conserved XIAP-interaction motif in caspase-9 and Smac/DIABLO regulates caspase activity and apoptosis. *Nature* 410, 112-116.
 112. Verhagen, A.M., and Vaux, D.L. (2002). Cell death regulation by the mammalian IAP antagonist Diablo/Smac. *Apoptosis* 7, 163-166.
 113. Eckelman, B.P., Salvesen, G.S., and Scott, F.L. (2006). Human inhibitor of apoptosis proteins: why XIAP is the black sheep of the family. *EMBO Rep* 7, 988-994.
 114. Vucic, D., Franklin, M.C., Wallweber, H.J., Das, K., Eckelman, B.P., Shin, H., Elliott, L.O., Kadkhodayan, S., Deshayes, K., Salvesen, G.S., et al. (2005).

- Engineering ML-IAP to produce an extraordinarily potent caspase 9 inhibitor: implications for Smac-dependent anti-apoptotic activity of ML-IAP. *Biochem J* 385, 11-20.
115. Gyrd-Hansen, M., and Meier, P. (2010). IAPs: from caspase inhibitors to modulators of NF-kappaB, inflammation and cancer. *Nat Rev Cancer* 10, 561-574.
 116. Bertrand, M.J., Milutinovic, S., Dickson, K.M., Ho, W.C., Boudreault, A., Durkin, J., Gillard, J.W., Jaquith, J.B., Morris, S.J., and Barker, P.A. (2008). cIAP1 and cIAP2 facilitate cancer cell survival by functioning as E3 ligases that promote RIP1 ubiquitination. *Mol Cell* 30, 689-700.
 117. Vandenabeele, P., and Bertrand, M.J. (2012). The role of the IAP E3 ubiquitin ligases in regulating pattern-recognition receptor signalling. *Nat Rev Immunol* 12, 833-844.
 118. Kluger, H.M., McCarthy, M.M., Alvero, A.B., Sznol, M., Ariyan, S., Camp, R.L., Rimm, D.L., and Mor, G. (2007). The X-linked inhibitor of apoptosis protein (XIAP) is up-regulated in metastatic melanoma, and XIAP cleavage by Phenoxodiol is associated with Carboplatin sensitization. *J Transl Med* 5, 6.
 119. Shi, Y.H., Ding, W.X., Zhou, J., He, J.Y., Xu, Y., Gambotto, A.A., Rabinowich, H., Fan, J., and Yin, X.M. (2008). Expression of X-linked inhibitor-of-apoptosis protein in hepatocellular carcinoma promotes metastasis and tumor recurrence. *Hepatology* 48, 497-507.
 120. Vucic, D., Stennicke, H.R., Pisabarro, M.T., Salvesen, G.S., and Dixit, V.M. (2000). ML-IAP, a novel inhibitor of apoptosis that is preferentially expressed in human melanomas. *Curr Biol* 10, 1359-1366.
 121. Gazzaniga, P., Gradilone, A., Giuliani, L., Gandini, O., Silvestri, I., Nofroni, I., Sacconi, G., Frati, L., and Agliano, A.M. (2003). Expression and prognostic significance of LIVIN, SURVIVIN and other apoptosis-related genes in the progression of superficial bladder cancer. *Ann Oncol* 14, 85-90.
 122. Zender, L., Spector, M.S., Xue, W., Flemming, P., Cordon-Cardo, C., Silke, J., Fan, S.T., Luk, J.M., Wigler, M., Hannon, G.J., et al. (2006). Identification and validation of oncogenes in liver cancer using an integrative oncogenomic approach. *Cell* 125, 1253-1267.
 123. Augello, C., Caruso, L., Maggioni, M., Donadon, M., Montorsi, M., Santambrogio, R., Torzilli, G., Vaira, V., Pellegrini, C., Roncalli, M., et al. (2009). Inhibitors of apoptosis proteins (IAPs) expression and their prognostic significance in hepatocellular carcinoma. *BMC Cancer* 9, 125.
 124. Herman, M.D., Moche, M., Flodin, S., Welin, M., Tresaugues, L., Johansson, I., Nilsson, M., Nordlund, P., and Nyman, T. (2009). Structures of BIR domains from human NAIP and cIAP2. *Acta Crystallogr Sect F Struct Biol Cryst Commun* 65, 1091-1096.
 125. Lu, M., Lin, S.C., Huang, Y., Kang, Y.J., Rich, R., Lo, Y.C., Myszka, D., Han, J., and Wu, H. (2007). XIAP induces NF-kappaB activation via the BIR1/TAB1 interaction and BIR1 dimerization. *Mol Cell* 26, 689-702.
 126. Wist, A.D., Gu, L., Riedl, S.J., Shi, Y., and McLendon, G.L. (2007). Structure-activity based study of the Smac-binding pocket within the BIR3 domain of XIAP. *Bioorg Med Chem* 15, 2935-2943.
 127. Hui, S.K., Tse, M.K., Yang, Y., Wong, B.C., and Sze, K.H. (2010). Backbone and side-chain 1H, 13C and 15N assignments of the ubiquitin-associated domain of human X-linked inhibitor of apoptosis protein. *Biomol NMR Assign* 4, 13-15.

128. Nakatani, Y., Kleffmann, T., Linke, K., Condon, S.M., Hinds, M.G., and Day, C.L. (2012). Regulation of ubiquitin transfer by XIAP, a dimeric RING E3 ligase. *Biochem J* 450, 629-638.
129. Zheng, C., Kabaleeswaran, V., Wang, Y., Cheng, G., and Wu, H. (2010). Crystal structures of the TRAF2: cIAP2 and the TRAF1: TRAF2: cIAP2 complexes: affinity, specificity, and regulation. *Mol Cell* 38, 101-113.
130. Kulathila, R., Vash, B., Sage, D., Cornell-Kennon, S., Wright, K., Koehn, J., Stams, T., Clark, K., and Price, A. (2009). The structure of the BIR3 domain of cIAP1 in complex with the N-terminal peptides of SMAC and caspase-9. *Acta Crystallogr D Biol Crystallogr* 65, 58-66.
131. Cossu, F., Malvezzi, F., Canevari, G., Mastrangelo, E., Lecis, D., Delia, D., Seneci, P., Scolastico, C., Bolognesi, M., and Milani, M. (2010). Recognition of Smac-mimetic compounds by the BIR domain of cIAP1. *Protein Sci* 19, 2418-2429.
132. Flygare, J.A., Beresini, M., Budha, N., Chan, H., Chan, I.T., Cheeti, S., Cohen, F., Deshayes, K., Doerner, K., Eckhardt, S.G., et al. (2012). Discovery of a potent small-molecule antagonist of inhibitor of apoptosis (IAP) proteins and clinical candidate for the treatment of cancer (GDC-0152). *J Med Chem* 55, 4101-4113.
133. Shin, H., Renatus, M., Eckelman, B.P., Nunes, V.A., Sampaio, C.A., and Salvesen, G.S. (2005). The BIR domain of IAP-like protein 2 is conformationally unstable: implications for caspase inhibition. *Biochem J* 385, 1-10.
134. Langdon, W.Y., Hartley, J.W., Klinken, S.P., Ruscetti, S.K., and Morse, H.C., 3rd (1989). v-cbl, an oncogene from a dual-recombinant murine retrovirus that induces early B-lineage lymphomas. *Proc Natl Acad Sci U S A* 86, 1168-1172.
135. Tsygankov, A.Y., Teckchandani, A.M., Feshchenko, E.A., and Swaminathan, G. (2001). Beyond the RING: CBL proteins as multivalent adapters. *Oncogene* 20, 6382-6402.
136. Griffiths, E.K., Sanchez, O., Mill, P., Krawczyk, C., Hojilla, C.V., Rubin, E., Nau, M.M., Khokha, R., Lipkowitz, S., Hui, C.C., et al. (2003). Cbl-3-deficient mice exhibit normal epithelial development. *Mol Cell Biol* 23, 7708-7718.
137. Hime, G.R., Dhungat, M.P., Ng, A., and Bowtell, D.D. (1997). D-Cbl, the *Drosophila* homologue of the c-Cbl proto-oncogene, interacts with the *Drosophila* EGF receptor in vivo, despite lacking C-terminal adaptor binding sites. *Oncogene* 14, 2709-2719.
138. Yoon, C.H., Chang, C., Hopper, N.A., Lesa, G.M., and Sternberg, P.W. (2000). Requirements of multiple domains of SLI-1, a *Caenorhabditis elegans* homologue of c-Cbl, and an inhibitory tyrosine in LET-23 in regulating vulval differentiation. *Mol Biol Cell* 11, 4019-4031.
139. Meng, W., Sawadikosol, S., Burakoff, S.J., and Eck, M.J. (1999). Structure of the amino-terminal domain of Cbl complexed to its binding site on ZAP-70 kinase. *Nature* 398, 84-90.
140. Bonita, D.P., Miyake, S., Lupher, M.L., Jr., Langdon, W.Y., and Band, H. (1997). Phosphotyrosine binding domain-dependent upregulation of the platelet-derived growth factor receptor alpha signaling cascade by transforming mutants of Cbl: implications for Cbl's function and oncogenicity. *Mol Cell Biol* 17, 4597-4610.

141. Lupher, M.L., Jr., Reedquist, K.A., Miyake, S., Langdon, W.Y., and Band, H. (1996). A novel phosphotyrosine-binding domain in the N-terminal transforming region of Cbl interacts directly and selectively with ZAP-70 in T cells. *J Biol Chem* 271, 24063-24068.
142. Thien, C.B., Walker, F., and Langdon, W.Y. (2001). RING finger mutations that abolish c-Cbl-directed polyubiquitination and downregulation of the EGF receptor are insufficient for cell transformation. *Mol Cell* 7, 355-365.
143. Kales, S.C., Ryan, P.E., Nau, M.M., and Lipkowitz, S. (2010). Cbl and human myeloid neoplasms: the Cbl oncogene comes of age. *Cancer Res* 70, 4789-4794.
144. Waterman, H., Levkowitz, G., Alroy, I., and Yarden, Y. (1999). The RING finger of c-Cbl mediates desensitization of the epidermal growth factor receptor. *J Biol Chem* 274, 22151-22154.
145. Shtiegman, K., and Yarden, Y. (2003). The role of ubiquitylation in signaling by growth factors: implications to cancer. *Semin Cancer Biol* 13, 29-40.
146. Rao, N., Dodge, I., and Band, H. (2002). The Cbl family of ubiquitin ligases: critical negative regulators of tyrosine kinase signaling in the immune system. *J Leukoc Biol* 71, 753-763.
147. Wong, E.S., Lim, J., Low, B.C., Chen, Q., and Guy, G.R. (2001). Evidence for direct interaction between Sprouty and Cbl. *J Biol Chem* 276, 5866-5875.
148. Hall, A.B., Jura, N., DaSilva, J., Jang, Y.J., Gong, D., and Bar-Sagi, D. (2003). hSpry2 is targeted to the ubiquitin-dependent proteasome pathway by c-Cbl. *Curr Biol* 13, 308-314.
149. Schmidt, M.H., and Dikic, I. (2005). The Cbl interactome and its functions. *Nat Rev Mol Cell Biol* 6, 907-918.
150. Sanjay, A., Miyazaki, T., Itzstein, C., Purev, E., Horne, W.C., and Baron, R. (2006). Identification and functional characterization of an Src homology domain 3 domain-binding site on Cbl. *FEBS J* 273, 5442-5456.
151. Fang, D., Wang, H.Y., Fang, N., Altman, Y., Elly, C., and Liu, Y.C. (2001). Cbl-b, a RING-type E3 ubiquitin ligase, targets phosphatidylinositol 3-kinase for ubiquitination in T cells. *J Biol Chem* 276, 4872-4878.
152. Feshchenko, E.A., Langdon, W.Y., and Tsygankov, A.Y. (1998). Fyn, Yes, and Syk phosphorylation sites in c-Cbl map to the same tyrosine residues that become phosphorylated in activated T cells. *J Biol Chem* 273, 8323-8331.
153. Tsygankov, A.Y., Mahajan, S., Fincke, J.E., and Bolen, J.B. (1996). Specific association of tyrosine-phosphorylated c-Cbl with Fyn tyrosine kinase in T cells. *J Biol Chem* 271, 27130-27137.
154. Davies, G.C., Ettenberg, S.A., Coats, A.O., Mussante, M., Ravichandran, S., Collins, J., Nau, M.M., and Lipkowitz, S. (2004). Cbl-b interacts with ubiquitinated proteins; differential functions of the UBA domains of c-Cbl and Cbl-b. *Oncogene* 23, 7104-7115.
155. Levkowitz, G., Waterman, H., Zamir, E., Kam, Z., Oved, S., Langdon, W.Y., Beguinot, L., Geiger, B., and Yarden, Y. (1998). c-Cbl/Sli-1 regulates endocytic sorting and ubiquitination of the epidermal growth factor receptor. *Genes Dev* 12, 3663-3674.
156. Miyake, S., Lupher, M.L., Jr., Druker, B., and Band, H. (1998). The tyrosine kinase regulator Cbl enhances the ubiquitination and degradation of the platelet-derived growth factor receptor alpha. *Proc Natl Acad Sci U S A* 95, 7927-7932.

157. Fukazawa, T., Miyake, S., Band, V., and Band, H. (1996). Tyrosine phosphorylation of Cbl upon epidermal growth factor (EGF) stimulation and its association with EGF receptor and downstream signaling proteins. *J Biol Chem* 271, 14554-14559.
158. Huang, F., Kirkpatrick, D., Jiang, X., Gygi, S., and Sorkin, A. (2006). Differential regulation of EGF receptor internalization and degradation by multiubiquitination within the kinase domain. *Mol Cell* 21, 737-748.
159. Haglund, K., Sigismund, S., Polo, S., Szymkiewicz, I., Di Fiore, P.P., and Dikic, I. (2003). Multiple monoubiquitination of RTKs is sufficient for their endocytosis and degradation. *Nat Cell Biol* 5, 461-466.
160. Pennock, S., and Wang, Z. (2008). A tale of two Cbls: interplay of c-Cbl and Cbl-b in epidermal growth factor receptor downregulation. *Mol Cell Biol* 28, 3020-3037.
161. Meijer, I.M., van Rotterdam, W., van Zoelen, E.J., and van Leeuwen, J.E. (2012). Cbl and Itch binding sites in ERBB4 CYT-1 and CYT-2 mediate K48- and K63-polyubiquitination, respectively. *Cell Signal* 25, 470-478.
162. Longva, K.E., Blystad, F.D., Stang, E., Larsen, A.M., Johannessen, L.E., and Madshus, I.H. (2002). Ubiquitination and proteasomal activity is required for transport of the EGF receptor to inner membranes of multivesicular bodies. *J Cell Biol* 156, 843-854.
163. Umabayashi, K., Stenmark, H., and Yoshimori, T. (2008). Ubc4/5 and c-Cbl continue to ubiquitinate EGF receptor after internalization to facilitate polyubiquitination and degradation. *Mol Biol Cell* 19, 3454-3462.
164. Yokouchi, M., Kondo, T., Sanjay, A., Houghton, A., Yoshimura, A., Komiya, S., Zhang, H., and Baron, R. (2001). Src-catalyzed phosphorylation of c-Cbl leads to the interdependent ubiquitination of both proteins. *J Biol Chem* 276, 35185-35193.
165. Rao, N., Miyake, S., Reddi, A.L., Douillard, P., Ghosh, A.K., Dodge, I.L., Zhou, P., Fernandes, N.D., and Band, H. (2002). Negative regulation of Lck by Cbl ubiquitin ligase. *Proc Natl Acad Sci U S A* 99, 3794-3799.
166. Kyo, S., Sada, K., Qu, X., Maeno, K., Miah, S.M., Kawauchi-Kamata, K., and Yamamura, H. (2003). Negative regulation of Lyn protein-tyrosine kinase by c-Cbl ubiquitin-protein ligase in Fc epsilon RI-mediated mast cell activation. *Genes Cells* 8, 825-836.
167. Zou, W., Reeve, J.L., Zhao, H., Ross, F.P., and Teitelbaum, S.L. (2009). Syk tyrosine 317 negatively regulates osteoclast function via the ubiquitin-protein isopeptidase activity of Cbl. *J Biol Chem* 284, 18833-18839.
168. Guenou, H., Kaabeche, K., Dufour, C., Miraoui, H., and Marie, P.J. (2006). Down-regulation of ubiquitin ligase Cbl induced by twist haploinsufficiency in Saethre-Chotzen syndrome results in increased PI3K/Akt signaling and osteoblast proliferation. *Am J Pathol* 169, 1303-1311.
169. Soubeyran, P., Barac, A., Szymkiewicz, I., and Dikic, I. (2003). Cbl-ArgBP2 complex mediates ubiquitination and degradation of c-Abl. *Biochem J* 370, 29-34.
170. Ettenberg, S.A., Magnifico, A., Cuello, M., Nau, M.M., Rubinstein, Y.R., Yarden, Y., Weissman, A.M., and Lipkowitz, S. (2001). Cbl-b-dependent coordinated degradation of the epidermal growth factor receptor signaling complex. *J Biol Chem* 276, 27677-27684.

171. Bao, J., Gur, G., and Yarden, Y. (2003). Src promotes destruction of c-Cbl: implications for oncogenic synergy between Src and growth factor receptors. *Proc Natl Acad Sci U S A* *100*, 2438-2443.
172. Dikic, I. (2002). CIN85/CMS family of adaptor molecules. *FEBS Lett* *529*, 110-115.
173. Soubeyran, P., Kowanetz, K., Szymkiewicz, I., Langdon, W.Y., and Dikic, I. (2002). Cbl-CIN85-endophilin complex mediates ligand-induced downregulation of EGF receptors. *Nature* *416*, 183-187.
174. Petrelli, A., Gilestro, G.F., Lanzardo, S., Comoglio, P.M., Migone, N., and Giordano, S. (2002). The endophilin-CIN85-Cbl complex mediates ligand-dependent downregulation of c-Met. *Nature* *416*, 187-190.
175. Garcia-Guzman, M., Larsen, E., and Vuori, K. (2000). The proto-oncogene c-Cbl is a positive regulator of Met-induced MAP kinase activation: a role for the adaptor protein Crk. *Oncogene* *19*, 4058-4065.
176. Chiang, S.H., Baumann, C.A., Kanzaki, M., Thurmond, D.C., Watson, R.T., Neudauer, C.L., Macara, I.G., Pessin, J.E., and Saltiel, A.R. (2001). Insulin-stimulated GLUT4 translocation requires the CAP-dependent activation of TC10. *Nature* *410*, 944-948.
177. Liu, Y.C., and Gu, H. (2002). Cbl and Cbl-b in T-cell regulation. *Trends Immunol* *23*, 140-143.
178. Wang, H.Y., Altman, Y., Fang, D., Elly, C., Dai, Y., Shao, Y., and Liu, Y.C. (2001). Cbl promotes ubiquitination of the T cell receptor zeta through an adaptor function of Zap-70. *J Biol Chem* *276*, 26004-26011.
179. Sohn, H.W., Gu, H., and Pierce, S.K. (2003). Cbl-b negatively regulates B cell antigen receptor signaling in mature B cells through ubiquitination of the tyrosine kinase Syk. *J Exp Med* *197*, 1511-1524.
180. Yang, B., Gay, D.L., MacLeod, M.K., Cao, X., Hala, T., Sweezer, E.M., Kappler, J., Marrack, P., and Oliver, P.M. (2008). Nedd4 augments the adaptive immune response by promoting ubiquitin-mediated degradation of Cbl-b in activated T cells. *Nat Immunol* *9*, 1356-1363.
181. Kassenbrock, C.K., and Anderson, S.M. (2004). Regulation of ubiquitin protein ligase activity in c-Cbl by phosphorylation-induced conformational change and constitutive activation by tyrosine to glutamate point mutations. *J Biol Chem* *279*, 28017-28027.
182. Williamson, M.P. (1994). The structure and function of proline-rich regions in proteins. *Biochem J* *297 (Pt 2)*, 249-260.
183. Jozic, D., Cardenas, N., Deribe, Y.L., Moncalian, G., Hoeller, D., Groemping, Y., Dikic, I., Rittinger, K., and Bravo, J. (2005). Cbl promotes clustering of endocytic adaptor proteins. *Nat Struct Mol Biol* *12*, 972-979.
184. Zhou, Z.R., Gao, H.C., Zhou, C.J., Chang, Y.G., Hong, J., Song, A.X., Lin, D.H., and Hu, H.Y. (2008). Differential ubiquitin binding of the UBA domains from human c-Cbl and Cbl-b: NMR structural and biochemical insights. *Protein Sci* *17*, 1805-1814.
185. Peschard, P., Kozlov, G., Lin, T., Mirza, I.A., Berghuis, A.M., Lipkowitz, S., Park, M., and Gehring, K. (2007). Structural basis for ubiquitin-mediated dimerization and activation of the ubiquitin protein ligase Cbl-b. *Mol Cell* *27*, 474-485.
186. Ryan, P.E., Sivadasan-Nair, N., Nau, M.M., Nicholas, S., and Lipkowitz, S. (2010). The N terminus of Cbl-c regulates ubiquitin ligase activity by

- modulating affinity for the ubiquitin-conjugating enzyme. *J Biol Chem* 285, 23687-23698.
187. Bradford, M.M. (1976). A rapid and sensitive method for the quantitation of microgram quantities of protein utilizing the principle of protein-dye binding. *Analytical biochemistry* 72, 248-254.
 188. Haas, A.L., and Wilkinson, K.D. (1985). The large scale purification of ubiquitin from human erythrocytes. *Prep Biochem* 15, 49-60.
 189. Pickart, C.M., and Raasi, S. (2005). Controlled synthesis of polyubiquitin chains. *Methods Enzymol* 399, 21-36.
 190. Otwinowski, Z., Minor, W., and Charles W. Carter, Jr. (1997). Processing of X-ray diffraction data collected in oscillation mode. In *Methods in Enzymology*, Volume Volume 276. (Academic Press), pp. 307-326.
 191. Leslie, A.G.W. (1992). Recent changes to the MOSFLM package for processing film and image plate data. *oint CCP4 + ESF-EAMCB Newsletter on Protein Crystallography* 26.
 192. Kabsch, W. (2010). XDS. *Acta Crystallogr D Biol Crystallogr* 66, 125-132.
 193. COLLABORATIVE COMPUTATIONAL PROJECT, NUMBER 4. (1994). The CCP4 suite: programs for protein crystallography. *Acta Crystallogr D Biol Crystallogr* 50, 760-763.
 194. Storoni, L.C., McCoy, A.J., and Read, R.J. (2004). Likelihood-enhanced fast rotation functions. *Acta Crystallogr D Biol Crystallogr* 60, 432-438.
 195. Sakata, E., Satoh, T., Yamamoto, S., Yamaguchi, Y., Yagi-Utsumi, M., Kurimoto, E., Tanaka, K., Wakatsuki, S., and Kato, K. (2010). Crystal structure of UbcH5b~ubiquitin intermediate: insight into the formation of the self-assembled E2~Ub conjugates. *Structure* 18, 138-147.
 196. Emsley, P., and Cowtan, K. (2004). Coot: model-building tools for molecular graphics. *Acta Crystallogr D Biol Crystallogr* 60, 2126-2132.
 197. Brunger, A.T., Adams, P.D., Clore, G.M., DeLano, W.L., Gros, P., Grosse-Kunstleve, R.W., Jiang, J.S., Kuszewski, J., Nilges, M., Pannu, N.S., et al. (1998). Crystallography & NMR system: A new software suite for macromolecular structure determination. *Acta Crystallogr D Biol Crystallogr* 54, 905-921.
 198. Adams, P.D., Grosse-Kunstleve, R.W., Hung, L.W., Ioerger, T.R., McCoy, A.J., Moriarty, N.W., Read, R.J., Sacchettini, J.C., Sauter, N.K., and Terwilliger, T.C. (2002). PHENIX: building new software for automated crystallographic structure determination. *Acta Crystallogr D Biol Crystallogr* 58, 1948-1954.
 199. Kobashigawa, Y., Tomitaka, A., Kumeta, H., Noda, N.N., Yamaguchi, M., and Inagaki, F. (2012). Autoinhibition and phosphorylation-induced activation mechanisms of human cancer and autoimmune disease-related E3 protein Cbl-b. *Proc Natl Acad Sci U S A* 108, 20579-20584.
 200. Dou, H., Buetow, L., Hock, A., Sibbet, G.J., Vousden, K.H., and Huang, D.T. (2012). Structural basis for autoinhibition and phosphorylation-dependent activation of c-Cbl. *Nat Struct Mol Biol* 19, 184-192.
 201. Dou, H., Buetow, L., Sibbet, G.J., Cameron, K., and Huang, D.T. (2012). BIRC7-E2 ubiquitin conjugate structure reveals the mechanism of ubiquitin transfer by a RING dimer. *Nat Struct Mol Biol* 19, 876-883.
 202. Ozkan, E., Yu, H., and Deisenhofer, J. (2005). Mechanistic insight into the allosteric activation of a ubiquitin-conjugating enzyme by RING-type ubiquitin ligases. *Proc Natl Acad Sci U S A* 102, 18890-18895.

203. Plechanovova, A., Jaffray, E.G., McMahon, S.A., Johnson, K.A., Navratilova, I., Naismith, J.H., and Hay, R.T. (2011). Mechanism of ubiquitylation by dimeric RING ligase RNF4. *Nat Struct Mol Biol* 18, 1052-1059.
204. Feltham, R., Bettjeman, B., Budhidarmo, R., Mace, P.D., Shirley, S., Condon, S.M., Chunduru, S.K., McKinlay, M.A., Vaux, D.L., Silke, J., et al. (2011). Smac mimetics activate the E3 ligase activity of cIAP1 protein by promoting RING domain dimerization. *J Biol Chem* 286, 17015-17028.
205. Pickart, C.M. (2001). Mechanisms underlying ubiquitination. *Annu Rev Biochem* 70, 503-533.
206. Eddins, M.J., Carlile, C.M., Gomez, K.M., Pickart, C.M., and Wolberger, C. (2006). Mms2-Ubc13 covalently bound to ubiquitin reveals the structural basis of linkage-specific polyubiquitin chain formation. *Nat Struct Mol Biol* 13, 915-920.
207. Page, R.C., Pruneda, J.N., Amick, J., Klevit, R.E., and Misra, S. (2012). Structural insights into the conformation and oligomerization of E2~ubiquitin conjugates. *Biochemistry* 51, 4175-4187.
208. Hamilton, K.S., Ellison, M.J., Barber, K.R., Williams, R.S., Huzil, J.T., McKenna, S., Ptak, C., Glover, M., and Shaw, G.S. (2001). Structure of a conjugating enzyme-ubiquitin thiolester intermediate reveals a novel role for the ubiquitin tail. *Structure* 9, 897-904.
209. Kamadurai, H.B., Souphron, J., Scott, D.C., Duda, D.M., Miller, D.J., Stringer, D., Piper, R.C., and Schulman, B.A. (2009). Insights into ubiquitin transfer cascades from a structure of a UbcH5B approximately ubiquitin-HECT(NEDD4L) complex. *Mol Cell* 36, 1095-1102.
210. Pickart, C.M., and Rose, I.A. (1985). Functional heterogeneity of ubiquitin carrier proteins. *J Biol Chem* 260, 1573-1581.
211. Amemiya, Y., Azmi, P., and Seth, A. (2008). Autoubiquitination of BCA2 RING E3 ligase regulates its own stability and affects cell migration. *Mol Cancer Res* 6, 1385-1396.
212. Plechanovova, A., Jaffray, E.G., Tatham, M.H., Naismith, J.H., and Hay, R.T. (2012). Structure of a RING E3 ligase and ubiquitin-loaded E2 primed for catalysis. *Nature* 489, 115-120.
213. Pruneda, J.N., Stoll, K.E., Bolton, L.J., Brzovic, P.S., and Klevit, R.E. (2011). Ubiquitin in motion: structural studies of the ubiquitin-conjugating enzyme approximately ubiquitin conjugate. *Biochemistry* 50, 1624-1633.
214. Soss, S.E., Klevit, R.E., and Chazin, W.J. (2013). Activation of UbcH5c~Ub is the result of a shift in interdomain motions of the conjugate bound to U-box E3 ligase E4B. *Biochemistry* 52, 2991-2999.
215. Pruneda, J.N., Littlefield, P.J., Soss, S.E., Nordquist, K.A., Chazin, W.J., Brzovic, P.S., and Klevit, R.E. (2012). Structure of an E3:E2~Ub complex reveals an allosteric mechanism shared among RING/U-box ligases. *Mol Cell* 47, 933-942.
216. Lill, N.L., Douillard, P., Awwad, R.A., Ota, S., Lupher, M.L., Jr., Miyake, S., Meissner-Lula, N., Hsu, V.W., and Band, H. (2000). The evolutionarily conserved N-terminal region of Cbl is sufficient to enhance down-regulation of the epidermal growth factor receptor. *J Biol Chem* 275, 367-377.
217. Taher, T.E., Tjin, E.P., Beuling, E.A., Borst, J., Spaargaren, M., and Pals, S.T. (2002). c-Cbl is involved in Met signaling in B cells and mediates hepatocyte growth factor-induced receptor ubiquitination. *J Immunol* 169, 3793-3800.

218. Zhang, Y., Wolf-Yadlin, A., Ross, P.L., Pappin, D.J., Rush, J., Lauffenburger, D.A., and White, F.M. (2005). Time-resolved mass spectrometry of tyrosine phosphorylation sites in the epidermal growth factor receptor signaling network reveals dynamic modules. *Mol Cell Proteomics* 4, 1240-1250.
219. Dou, H., Buetow, L., Sibbet, G.J., Cameron, K., and Huang, D.T. (2013). Essentiality of a non-RING element in priming donor ubiquitin for catalysis by a monomeric E3. *Nat Struct Mol Biol*.
220. Reverter, D., and Lima, C.D. (2005). Insights into E3 ligase activity revealed by a SUMO-RanGAP1-Ubc9-Nup358 complex. *Nature* 435, 687-692.
221. Yunus, A.A., and Lima, C.D. (2009). Structure of the Siz/PIAS SUMO E3 ligase Siz1 and determinants required for SUMO modification of PCNA. *Mol Cell* 35, 669-682.
222. Maspero, E., Valentini, E., Mari, S., Cecatiello, V., Soffientini, P., Pasqualato, S., and Polo, S. (2013). Structure of a ubiquitin-loaded HECT ligase reveals the molecular basis for catalytic priming. *Nat Struct Mol Biol* 20, 696-701.
223. Tu, D., Li, W., Ye, Y., and Brunger, A.T. (2007). Structure and function of the yeast U-box-containing ubiquitin ligase Ufd2p. *Proc Natl Acad Sci U S A* 104, 15599-15606.
224. Duda, D.M., Borg, L.A., Scott, D.C., Hunt, H.W., Hammel, M., and Schulman, B.A. (2008). Structural insights into NEDD8 activation of cullin-RING ligases: conformational control of conjugation. *Cell* 134, 995-1006.
225. Calabrese, M.F., Scott, D.C., Duda, D.M., Grace, C.R., Kurinov, I., Kriwacki, R.W., and Schulman, B.A. (2011). A RING E3-substrate complex poised for ubiquitin-like protein transfer: structural insights into cullin-RING ligases. *Nat Struct Mol Biol* 18, 947-949.
226. Spratt, D.E., Wu, K., Kovacev, J., Pan, Z.Q., and Shaw, G.S. (2012). Selective recruitment of an E2~ubiquitin complex by an E3 ubiquitin ligase. *J Biol Chem* 287, 17374-17385.
227. Lemmon, M.A., and Schlessinger, J. (2010). Cell signaling by receptor tyrosine kinases. *Cell* 141, 1117-1134.
228. Dikic, I., Szymkiewicz, I., and Soubeyran, P. (2003). Cbl signaling networks in the regulation of cell function. *Cell Mol Life Sci* 60, 1805-1827.
229. Tan, Y.H., Krishnaswamy, S., Nandi, S., Kanteti, R., Vora, S., Onel, K., Hasina, R., Lo, F.Y., El-Hashani, E., Cervantes, G., et al. (2010). CBL is frequently altered in lung cancers: its relationship to mutations in MET and EGFR tyrosine kinases. *PLoS One* 5, e8972.
230. Sanada, M., Suzuki, T., Shih, L.Y., Otsu, M., Kato, M., Yamazaki, S., Tamura, A., Honda, H., Sakata-Yanagimoto, M., Kumano, K., et al. (2009). Gain-of-function of mutated C-CBL tumour suppressor in myeloid neoplasms. *Nature* 460, 904-908.
231. Lipkowitz, S., and Weissman, A.M. (2011). RINGs of good and evil: RING finger ubiquitin ligases at the crossroads of tumour suppression and oncogenesis. *Nat Rev Cancer* 11, 629-643.
232. Naramura, M., Nandwani, N., Gu, H., Band, V., and Band, H. (2010). Rapidly fatal myeloproliferative disorders in mice with deletion of Casitas B-cell lymphoma (Cbl) and Cbl-b in hematopoietic stem cells. *Proc Natl Acad Sci U S A* 107, 16274-16279.
233. Shiba, N., Kato, M., Park, M.J., Sanada, M., Ito, E., Fukushima, K., Sako, M., Arakawa, H., Ogawa, S., and Hayashi, Y. (2010). CBL mutations in juvenile

- myelomonocytic leukemia and pediatric myelodysplastic syndrome. *Leukemia* 24, 1090-1092.
234. Kao, H.W., Sanada, M., Liang, D.C., Lai, C.L., Lee, E.H., Kuo, M.C., Lin, T.L., Shih, Y.S., Wu, J.H., Huang, C.F., et al. (2011). A high occurrence of acquisition and/or expansion of C-CBL mutant clones in the progression of high-risk myelodysplastic syndrome to acute myeloid leukemia. *Neoplasia* 13, 1035-1042.
 235. Loh, M.L., Sakai, D.S., Flotho, C., Kang, M., Fliegau, M., Archambeault, S., Mullighan, C.G., Chen, L., Bergstraesser, E., Bueso-Ramos, C.E., et al. (2009). Mutations in CBL occur frequently in juvenile myelomonocytic leukemia. *Blood* 114, 1859-1863.
 236. Kohlmann, A., Grossmann, V., Klein, H.U., Schindela, S., Weiss, T., Kazak, B., Dicker, F., Schnittger, S., Dugas, M., Kern, W., et al. (2010). Next-generation sequencing technology reveals a characteristic pattern of molecular mutations in 72.8% of chronic myelomonocytic leukemia by detecting frequent alterations in TET2, CBL, RAS, and RUNX1. *J Clin Oncol* 28, 3858-3865.
 237. Caligiuri, M.A., Briesewitz, R., Yu, J., Wang, L., Wei, M., Arnoczky, K.J., Marburger, T.B., Wen, J., Perrotti, D., Bloomfield, C.D., et al. (2007). Novel c-CBL and CBL-b ubiquitin ligase mutations in human acute myeloid leukemia. *Blood* 110, 1022-1024.
 238. Kan, Z., Jaiswal, B.S., Stinson, J., Janakiraman, V., Bhatt, D., Stern, H.M., Yue, P., Haverty, P.M., Bourgon, R., Zheng, J., et al. (2010). Diverse somatic mutation patterns and pathway alterations in human cancers. *Nature* 466, 869-873.
 239. Barresi, V., Palumbo, G.A., Musso, N., Consoli, C., Capizzi, C., Meli, C.R., Romano, A., Di Raimondo, F., and Condorelli, D.F. (2010). Clonal selection of 11q CN-LOH and CBL gene mutation in a serially studied patient during MDS progression to AML. *Leukemia Research* 34, 1539-1542.
 240. Shiba, N., Park, M.J., Taki, T., Takita, J., Hiwatari, M., Kanazawa, T., Sotomatsu, M., Ishii, E., Arakawa, H., Ogawa, S., et al. (2012). CBL mutations in infant acute lymphoblastic leukaemia. *Br J Haematol* 156, 672-674.
 241. Grand, F.H., Hidalgo-Curtis, C.E., Ernst, T., Zoi, K., Zoi, C., McGuire, C., Kreil, S., Jones, A., Score, J., Metzgeroth, G., et al. (2009). Frequent CBL mutations associated with 11q acquired uniparental disomy in myeloproliferative neoplasms. *Blood* 113, 6182-6192.
 242. Sargin, B., Choudhary, C., Crosetto, N., Schmidt, M.H., Grundler, R., Rensinghoff, M., Thiessen, C., Tickenbrock, L., Schwable, J., Brandts, C., et al. (2007). Flt3-dependent transformation by inactivating c-Cbl mutations in AML. *Blood* 110, 1004-1012.
 243. Muramatsu, H., Makishima, H., Jankowska, A.M., Cazzolli, H., O'Keefe, C., Yoshida, N., Xu, Y., Nishio, N., Hama, A., Yagasaki, H., et al. (2010). Mutations of an E3 ubiquitin ligase c-Cbl but not TET2 mutations are pathogenic in juvenile myelomonocytic leukemia. *Blood* 115, 1969-1975.
 244. Fernandes, M.S., Reddy, M.M., Croteau, N.J., Walz, C., Weisbach, H., Podar, K., Band, H., Carroll, M., Reiter, A., Larson, R.A., et al. (2010). Novel oncogenic mutations of CBL in human acute myeloid leukemia that activate growth and survival pathways depend on increased metabolism. *J Biol Chem* 285, 32596-32605.

245. Forbes, S.A., Bhamra, G., Bamford, S., Dawson, E., Kok, C., Clements, J., Menzies, A., Teague, J.W., Futreal, P.A., and Stratton, M.R. (2008). The Catalogue of Somatic Mutations in Cancer (COSMIC). *Curr Protoc Hum Genet Chapter 10*, Unit 10 11.
246. Duda, D.M., Olszewski, J.L., Tron, A.E., Hammel, M., Lambert, L.J., Waddell, M.B., Mittag, T., DeCaprio, J.A., and Schulman, B.A. (2012). Structure of a glomulin-RBX1-CUL1 complex: inhibition of a RING E3 ligase through masking of its E2-binding surface. *Mol Cell* 47, 371-382.
247. Trempe, J.F., Sauve, V., Grenier, K., Seirafi, M., Tang, M.Y., Menade, M., Al-Abdul-Wahid, S., Krett, J., Wong, K., Kozlov, G., et al. (2013). Structure of parkin reveals mechanisms for ubiquitin ligase activation. *Science* 340, 1451-1455.
248. Labit, H., Fujimitsu, K., Bayin, N.S., Takaki, T., Gannon, J., and Yamano, H. (2012). Dephosphorylation of Cdc20 is required for its C-box-dependent activation of the APC/C. *EMBO J* 31, 3351-3362.
249. Tamm, I., Kornblau, S.M., Segall, H., Krajewski, S., Welsh, K., Kitada, S., Scudiero, D.A., Tudor, G., Qui, Y.H., Monks, A., et al. (2000). Expression and prognostic significance of IAP-family genes in human cancers and myeloid leukemias. *Clin Cancer Res* 6, 1796-1803.
250. LaCasse, E.C., Mahoney, D.J., Cheung, H.H., Plenchette, S., Baird, S., and Korneluk, R.G. (2008). IAP-targeted therapies for cancer. *Oncogene* 27, 6252-6275.
251. Chen, D.J., and Huerta, S. (2009). Smac mimetics as new cancer therapeutics. *Anticancer Drugs* 20, 646-658.
252. Johnson, K.A., and Goody, R.S. (2013). The Original Michaelis Constant: Translation of the 1913 MichaelisMenten Paper. *Biochemistry* 50, 8264-8269.
253. Briggs, G.E., and Haldane, J.B. (1925). A Note on the Kinetics of Enzyme Action. *Biochem J* 19, 338-339.
254. Briggs, G.E. (1925). A Further Note on the Kinetics of Enzyme Action. *Biochem J* 19, 1037-1038.
255. Lineweaver, H., and Burk, D. (1934). The Determination of Enzyme Dissociation Constants. *Journal of the American Chemical Society* 56, 658-666.
256. fullofstars. (2007). Michaelis-Menten saturation curve of an enzyme reaction. en.wikipedia.org.
<http://upload.wikimedia.org/wikipedia/commons/9/99/Michaelis-Menten_saturation_curve_of_an_enzyme_reaction.svg>.
257. Catcher, P.b. (2007). lineweaverBurk plot. en.wikipedia.org.
<http://upload.wikimedia.org/wikipedia/commons/7/70/Lineweaver-Burke_plot.svg>.